Investigation of the mechanical behaviour of fine/coarse soil mixture

Yu Su

THÈSE DE DOCTORAT

de l'École des Ponts ParisTech

Investigation of the mechanical behavior of fine/coarse soil mixture

École doctorale N°531 - SIE (Sciences, Ingénierie, Environnement)

Specialty: Geotechnical Engineering

Laboratoire Navier/CERMES

Date : 02 September 2021

by

Yu SU

Composition du jury :

Prof. Antonio Gomes Correia (University of Minho)	Président
Prof. Cyrille Chazallon (INSA de Strasbourg)	Rapporteur
Prof. Pierre Breul (Université Clermont Auvergne)	Rapporteur
Dr. Pierre Hornych (Université Gustave Eiffel)	Examinateur
Dr. Nicolas Calon (Société Nationale des Chemins de fer Français)	Examinateur
Dr. Jean-Claude Dupla (Ecole des Ponts ParisTech)	Examinateur
Dr. Jean Canou (Ecole des Ponts ParisTech)	Examinateur
Prof. Yu-Jun Cui (Ecole des Ponts ParisTech)	Directeur de thèse

ACKNOWLEDGEMENTS

This dissertaiton is the result of four years work in Laboratoire Navier of Ecole des Ponts ParisTech. This work was financed by the China Scholarship Council (CSC) and Ecole des Ponts ParisTech (ENPC). I would like to take this opportunity to address my thanks to all persons who give me support to the accomplishment of this dissertation.

First, I would like to address my deepest gratitude to my supervisor Prof. Yu-Jun Cui. His guidance, patience and encouragement are crucial elements in the course of my PhD work. It is my honor to have such a responsible and outstanding supervisor. What he taught me is not only helpful to my PhD work, but also beneficial for my future career.

I wish to acknowledge my co-supervisors Dr. Jean-Claude Dupla and Dr. Jean Canou, who accompany me to finish the whole PhD work. Thanks for their excellent guidance and constructive suggestions to help me finish the experimental tests.

I am grateful to all other Jury members: Prof. Cyrille Chazallon, Prof. Pierre Breul, Prof. Antonio Gomes Correia, Dr. Pierre Hornych and Dr. Nicolas Calon. Thanks to them for examining this dissertation and giving constructive comments and suggestions.

I also wish to address my thanks to my friends and colleagues in Ecole des Ponts ParisTech, especially those who came to France together and almost graduated in the same time: Zi, Hao, Zhi-Xiong, Yang-Zi and so on. I am also grateful to the technical team: Emmanuel De Laure, Marine Lemaire, Xavier Boulay, Baptiste Chabot and Loïc Lesueur. Without their help, it is impossible for me to finish my experimental tests.

For the early 29 years of the whole life, one of the luckiest things happened on me is to meet Uncle Yang, the founder of Guohua Memory Middle School and the company of Country Garden Holdings. They have supported me economically and mentally for fourteen years. They taught me how to be a better person and devote myself to the society.

Finally, I am so lucky to have my fiancée Jing Xiong and family standing with me forever. No matter what difficulties I face and what decisions I make, they choose to trust me and support me.

RESUME

Dans les voies ferrées conventionnelles françaises, au cours des décennies de trafic, une couche intermédiaire a été créée par l'interpénétration de grains de ballast et de sous-sols fins. Compte tenu de sa densité sèche élevée (2,4 Mg/m^3) et donc de sa capacité portante élevée, la Société Nationale des Chemins de Fer (SNCF) a décidé de la conserver dans le cadre du programme de rénovation. Comme le sol intermédiaire correspond à un mélange de grains de ballast et de sol fin, le comportement mécanique d'un tel mélange a été étudié dans cette étude.

Les propriétés de rétention d'eau ont été étudiée pour différentes teneurs en grains grossiers et différentes densités sèches du sol fin. La méthode du papier filtre a été adoptée pour mesurer la succion matricielle. Des essais de porosimétrie par intrusion de mercure ont été réalisés pour l'observation de la microstructure des sols fins. Les résultats ont montré que la courbe de rétention du mélange de sols est indépendante de la teneur en grains grossiers et ne dépend que de la densité sèche du sol fin. De plus, la courbe de rétention est régie par les macro-pores du sol fin dans la plage de basse succion, et par les micro-pores du sol fin dans la plage de succion élevée.

L'effet de la microstructure du sol fin sur le comportement mécanique du mélange de sols a été étudié. La microstructure du sol fin a été mesurée par la porosimétrie par intrusion de mercure, et son effet sur le comportement mécanique du mélange a été examiné par des essais triaxiaux monotones. Les résultats ont montré que l'approche de préparation des échantillons développée, qui consistait à compacter le sol à l'optimum proctor du sol fin et à amener à la teneur en eau voulue par séchange ou par humidification, permettait de minimiser l'effet de la microstructure du sol fin sur le comportement mécanique du mélange. En utilisant cette approche de préparation d'échantillons, l'effet de la teneur en eau sur le comportement mécanique du mélange avec différentes teneurs en grains grossiers a été étudié par des tests triaxiaux monotones. Une teneur en gros grains caractéristique a été identifiée, séparant la structure du mélange en deux zones : une microstructure à matrice fine lorsque la teneur en grains grossiers est inférieure à la valeur caractéristique, et une microstructure en squelette de grains grossier lorsque la teneur en grains grossiers est supérieure à la valeur caractéristique. De plus, la teneur en gros grains caractéristique augmentait avec la diminution de la teneur en eau, ce qui s'expliquait par la propriété de gonflement sous humidification ou de rétraction sous séchage du sol fin.

L'effet de la teneur en eau sur la déformation permanente, le module réversible et le coefficient d'amortissement du mélange de sols a été étudié par des essais triaxiaux cycliques. Une procédure de chargement en plusieurs étapes à long terme a été adoptée pour étudier la déformation permanente, et une procédure de chargement en plusieurs étapes à court terme a été adoptée pour étudier le module réversible et le coefficient d'amortissement. Les résultats ont montré qu'une augmentation de la teneur en eau entraînait une augmentation de la déformation permanente et une diminution du module réversible en raison de la diminution de la succion matricielle, et une augmentation du coefficient d'amortissement en raison de l'augmentation de la viscosité du sol.

Une loi de comportement a été proposée pour la déformation permanente, permettant de tenir compte des effets du nombre des cycles de chargement, de la contrainte déviatorique et de la teneur en gros grains. De plus, l'effet de la succion matricielle était également pris en compte en incorborant les propriétes de rétention d'eau. Une autre loi de comportement a été également proposée pour le module réversible, permettant la description de la variation du module réversible avec les variations de la contrainte déviatorique, de la succion matricielle et de la teneur en gros grains.

Mots clés : mélange de sol fin / grossier; comportement mécanique; microstructure; teneur en eau; teneur en grains grossiers; loi de comportement

ABSTRACT

In the French conventional railway tracks, under the decades of traffic loadings, an interlayer was created by the interpenetration of ballast grains and subgrade fine soil. Considering the high bearing capacity related to its high dry density (2.4 Mg /m^3), the French national railway company (SNCF) decided to keep it as one part of the substructure during the renewal program. As the interlayer soil corresponded to a mixture of ballast grains and fine soil, the mechanical behaviour of such fine/coarse soil mixture was investigated in this study.

The water retention properties of soil mixture were investigated under varying coarse grain contents and dry densities of fine soil. The filter paper method was adopted to measure the matric suction. The mercury intrusion porosimetry tests were performed for the microstructure observation of fine soil. Results showed that the soil-water retention curve of soil mixture was independent of coarse grain content, and only dependent on the dry density of fine soil. Moreover, the soil-water retention curve in low suction range was governed by macro-pores of fine soil, while in high suction range by micro-pores of fine soil.

The effect of microstructure of fine soil on the mechanical behaviour of soil mixture was studied. The microstructure of fine soil was measured by mercury intrusion porosimetry tests, and its effect on the mechanical behaviour of mixture was examined by monotonic triaxial tests. Results showed that the developed sample preparation approach, which is to compact the soil at the optimum water content and then modify it to the desired value by either wetting or drying, allowed the effect of microstructure of fine soil on the mechanical behaviour of mixture to be minimized. Using this sample preparation approach, the effect of water content on the mechanical behaviour of mixture with varying coarse grain contents was investigated by monotonic triaxial tests. A characteristic coarse grain content was identified, separating the fabric of mixture into two zones: a fine matrix macrostructure when the coarse grain content was smaller than the characteristic value, and a coarse grian skeleton fabric when the coarse grain content was larger than the characteristic value. Moreover, the characteristic coarse grain content increased with the decrease of water content, which was explained by the shrinkage property of fine soil.

The effect of water content on the permanent strain, the resilient modulus and the damping ratio of soil mixture was investigated by cyclic triaxial tests. A long-term multi-stage loading procedure was performed for studying permanent strain, and a shor-term multi-stage loading

procedure for studying resilient modulus and damping ratio. Results showed that increasing water content led to an increase of permanent strain and a decrease of resilient modulus owing to the decrease of matric suction, and an increase of damping ratio owing to the increase of soil viscosity.

A constitutive model was proposed for the permanent strain, allowing the effects of the number of loading cycles, deviator stress and coarse grain content to be accounted for. Furthermore, the effect of matric suction was taken into account by incorporating soil-water retention curve. Another constitutive model was developed for the resilient modulus, allowing the description of the resilient modulus variation with changes in deviator stress, matric suction and coarse grain content.

Keywords: fine/coarse soil mixture; mechanical behaviour; microstructure; water content; coarse grain content; constitutive model

PUBLICATIONS

1. Su, Y., Cui, Y. J., Dupla, J. C., Canou, J., & Qi, S. 2021. Developing a Sample Preparation Approach to Study the Mechanical Behavior of Unsaturated Fine/Coarse Soil Mixture. Geotechnical Testing Journal, 44(4), 912-928.

2. Su, Y., Cui, Y. J., Dupla, J. C., Canou, J., & Qi, S. 2020. A fatigue model for track-bed materials with consideration of the effect of coarse grain content. Transportation Geotechnics, 23, 100353.

3. Su, Y., Cui, Y. J., Dupla, J. C., & Canou, J. 2020. Investigation of the effect of water content on the mechanical behavior of track-bed materials under various coarse grain contents. Construction and Building Materials, 263, 120206.

4. Su, Y., Cui, Y. J., Dupla, J. C., & Canou, J. 2021. Effect of water content on resilient modulus and damping ratio of fine/coarse soil mixtures with varying coarse grain contents. Transportation Geotechnics, 26, 100452.

5. Su, Y., Cui, Y. J., Dupla, J. C., & Canou, J. 2021. Soil-water retention behaviour of fine/coarse soil mixture with varying coarse grain contents and fine soil dry densities. Canadian Geotechnical Journal. (Accepted)

6. Su, Y., Cui, Y. J., Dupla, J. C., & Canou, J. Effect of water content on permanent deformation of fine/coarse soil mixtures with varying coarse grain contents and subjected to multi-stage cyclic loading. Under review in Acta Geotechnica.

7. Su, Y., Cui, Y. J., Dupla, J. C., & Canou, J. Modelling the suction- and deviator stress-dependent resilient modulus of unsaturated fine/coarse soil mixture by considering soil-water retention curve. Under review in Acta Geotechnica.

8. Su, Y., Cui, Y. J., Dupla, J. C., & Canou, J. A fatigue model for fine/coarse soil mixture with consideration of the effects of coarse grain content and suction. Under review in Canadian Geotechnical Journal.

CONTENTS

GENERAL INTRODUCTION

General context

The French railway network started to be constructed in 1850s. Up to now, the French national railway company (SNCF) operates a total of 30000 km lines, which consists of new railway lines and conventional ones, with the conventional railway lines representing 94% of the total network. Figure 1 shows a comparion between the new railway tracks and the conventional ones. It can be observed that for the new railway tracks, a transition of sub-ballast layer and capping layer existe between the ballast layer and the subgrade, while an interlayer was created in the conventional tracks. Such interlayer was formed because the ballast was directly putting on the subgrade for conventional tracks. Over decades of traffic loadings, the interpenetration of ballast grains and subgrade soil has been taking place, creating the interlayer.

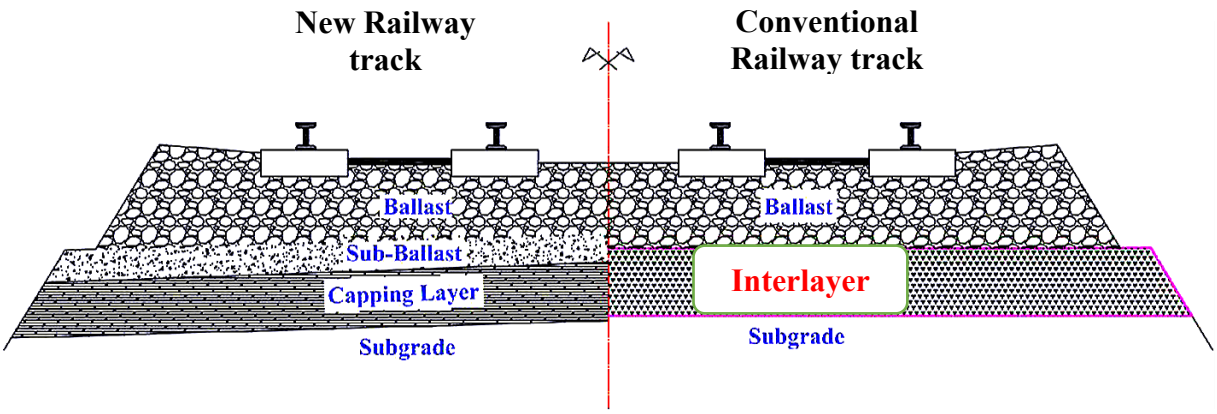

Figure 1. Comparison between new and conventional railway tracks (after Cui et al. 2014)

Since the problems related to the stability of railway tracks were frequently recorded for the conventional railway tracks, in spite of the frequent maintenance, recently, the French national railway company (SNCF) decided to renew the conventional lines. As the interlayer soil has a dry density as high as 2.4 Mg/m^3, its bearing capacity is expected to be high and its deformability is expected to be low. (Trinh 2011). Therefore, in the renewal program, it was decided to be remained in the substructure. The grain size distribution of the interlayer soil ranged from ballast grain (a maximum diameter d = 60 mm) to clay particle (smaller than 2 mm). The thickness of interlayer soil was dependent on the ballast grains, subgrade soil and the traffic loadings in the filed. In general, the thickness ranges from 30 to 50 cm. Figure 2 shows a photograph of interlayer soil at Sénissiat (north-west of Lyon, France). Over depth, the ballast

grain content decreased. Roughly, the interlayer could be divided into two parts: an upper part which was dominated by ballast grains, with subgrade soil filling their voids, and a lower part which was dominated by subgrade soil, with ballast grains dispersed in it. As a component of conventional railway tracks, the interlayer soil must fullfill three major functions, as follows:

(i) Spreading static and dynamic traffic loadings from ballast to subgrade, avoiding excessive permanent deformation.
(ii) Ensuring grain size transition between ballast grains and subgrade fine soil.
(iii) Protecting the subgrade from rainwater seepage.

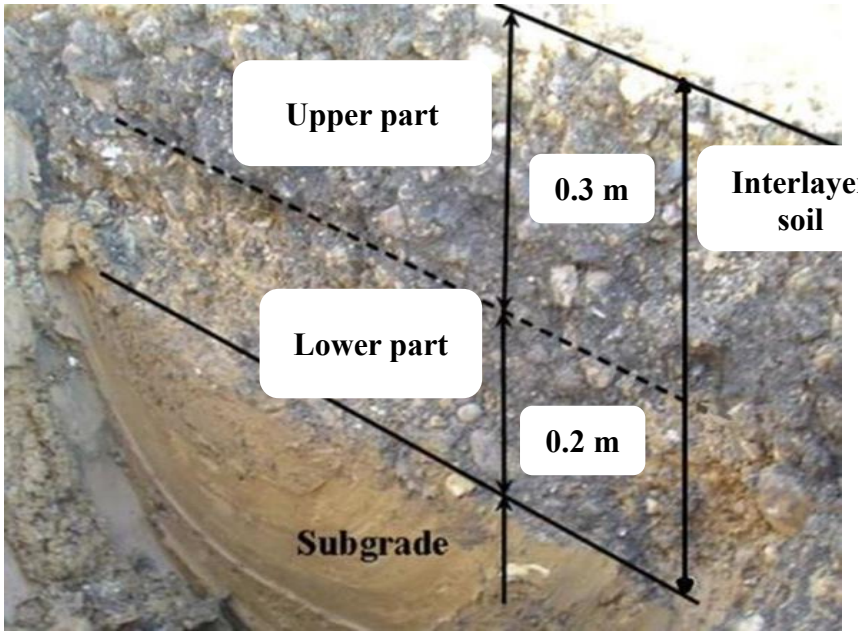

Figure 2. A photograph of interlayer soil (after Trinh et al. 2012)

For the upper part of interlayer soil, different studies have been carried out. Trinh (2011) and Trinh et al. (2012) studied the mechanical behaviour of fouled ballast by large-scale triaxial tests, and found that a decrease of water content led to an increase of shear strength and a decrease of permanent deformation. Duong et al. (2013, 2014a, 2014b, 2016) investigated the combined effects of fine soil content and water content on the hydro-mechanical behaviour of interlayer soil by large-scale triaxial tests. They reported that increasing fine soil content induced a decrease of stiffness and shear strength under saturated state, while an opposite trend was observed under unsaturated state. Lamas-Lopez (2016) performed field and laboratory tests on the dynamic behavior of interlayer soil, and concluded that increasing water content led to a decrease of resilient modulus and an increase of damping ratio. When it comes to the lower part,

Wang et al. (2017, 2018a, 2018b) investigated the effect of coarse grain content f_v on its static and dynamic behaviors. They identified a characteristic coarse grain content $f_{v\text{-}cha}$, which separated the fabric of interlayer soil into two parts: a fine matrix macrostructure at $f_v < f_{v\text{-}cha}$, and a coarse grain skeleton fabric at $f_v > f_{v\text{-}cha}$. Qi et al. (2020a, 2020b) studied the effect of grain size distribution of coarse grains on the mechanical behavior of interlayer soil with both fabrics. They found that a decrease of coefficient of uniformity C_u induced an increase of stiffness and shear strength for the coarse grain skeleton fabric, while an opposite trend was observed for the fine matrix macrostructure. However, the effect of water content on the mechanical behavior of interlayer soil with both fabrics has not been investigated.

Objectives

In this study, the effects of water content and coarse grain content on the mechanical behaviour of the reconstituted interlayer soil were investigated. The main objectives include:

(i) Studying the water retention behaviour of soil mixture with varying coarse grain contents and fine soil dry densities.
(ii) Investigating the effect of microstructure of fine soil on the mechanical behaviour of soil mixture.
(iii) Investigating the effect of water content on the mechanical behaviour of soil mixture under monotonic loading, such as shear strength, cohesion, friction angle and so on.
(iv) Investigating the effect of water content on permanent deformation of soil mixture under long-term multi-stage cyclic loading.
(v) Investigating the effect of water content on resilient modulus and damping ratio of soil mixture under shor-term multi-stage cyclic loading.
(vi) Modelling the effects of water content and coarse grain content on the permanent deformation and the resilient modulus of soil mixture by incorporating the soil-water retention curve.

Outline

The dissertation is organized in five chapters.

The first chapter is devoted to the literature review. Firstly, a comparison was made between the intact interlayer soil and the reconstituted soil mixture. A good agreement between these two soils was obtained. Secondly, the water retention behavior of soil mixture was presented.

Thirdly, the mechanical behaviors of soil mixture were reported, in terms of static behavior and dynamic behavior. Different factors affecting these mechanical behaviors were discussed. Finally, the constitutive models describing variations of permanent deformation and resilient modulus with changes in different factors were reviewed.

The second chapter is dedicated to the water retention behavior of soil mixture. The effects of coarse grain content and dry density of fine soil on the soil-water retention curve (SWRC) of mixture were investigated. The filter paper method was applied to measure the matric suction. Mercury intrusion porosimetry tests were performed for the microstructure observation of fine soil under varying dry densities. The SWRC of mixture was found to be only dependent on the dry density of fine soil and independent of coarse grain content. These obtained results were presented in a paper published in Canadian Geotechnical Journal.

The third chapter is devoted to the mechanical behaviour of fine/coarse soil mixture under monotonic loading, which corresponded to two published papers. The first paper, published in Geotechnical Testing Journal, developed a sample preparation approach for unsaturated soil mixture, allowing the effect of microstructure of fine soil on the mechanical behaviour of mixture to be minimized. The second paper, published in Construction and Building Materials, addressed the effect of water content on mechanical behaviour of soil mixture with varying coarse grain contents. A series of monotonic triaxial tests were conducted. The variations of mechanical parameters with water content and coarse grain content were analysed.

The fourth chapter depicts the mechanical behaviour of soil mixture under cyclic loading, which was presented in two papers. In the first paper submitted to Acta Geotechnica, the effects of water content and coarse grain content on the permanent deformation of soil mixture were investigated by cyclic triaxial tests. A long-term cyclic loading was performed for this purpose. In the second paper published in Transportation Geotechnics, the effects of water content and coarse grain content on dynamic properties of soil mixture were investigated, which included resilient modulus and damping ratio. A shor-term cyclic loading was adopted.

The fifth chapter is devoted to the modeling of the mechanical bahavior of soil mixture incorporating the soil-water retention curve, which were presented in three papers. The first paper, published in Transportation Geotechnics, presents a fatigue model describing the variation of permanent strain with the number of loading cycles, deviator stress and coarse grain content. In the second paper submitted to Canadian Geotechnical Journal, a new fatigue model

incorporating matric suction was developed based on the previously developed fatigue model. This model was validated using the experimental data from literature. Comparisons with existing models showed the performance of the proposed model in describing the permanent strain variation with changes in number of loading cycles, deviator stress, coarse grain content and matric suction. In the third paper submitted to Acta Geotechnica, a constitutive model was proposed for the resilient modulus of unsaturated soil mixtures, allowing the effects of matric suction, deviator stress and coarse grain content to be accounted for. The proposed model was validated by experimental results from literature. Comparisons with representative existing models showed that the proposed model was capable to well describe the variations of resilient modulus with changes in matric suction, deviator stress and coarse grain content.

The general conclusions were presented at the end, together with some perspectives for the future study.

CHAPTER I. LITERATURE REVIEW

I.1 Introduction

In this chapter, a comparison between intact interlayer soil and reconstituted soil mixture was made (Section I.2). Then, the water retention behavior of soil mixture was presented (Section I.3), with discussion of the effects of coarse grain content and dry density of fine soil fraction. Afterwards, the mechanical behaviors of soil mixture including the static behavior and the dynamic behavior were described (Section I.4). Factors such as coarse grain content, matric suction (or water content), stress state, etc, were discussed. Finally, the constitutive models of permanent deformation and resilient modulus were presented (Section I.5), allowing the aforementioned factors to be described.

I.2 Comparison between intact interlayer soil and reconstituted soil mixture

In-situ investigation shows that the interlayer soil was created mainly by the interpenetration of ballast grains and subgrade soil (Trinh 2011). The size of ballast grains ranged from 20 to 63 mm, and that of subgrade soil from 0 to 2 mm. The subgade soil was considered as fine soil in the interlayer (Duong et al. 2013). Considering the difficulty of obtaining intact interlayer soil from the field, a mixture of micro-ballast and reconstituted fines was fabricated in the laboratory as a substitute in the previous studies. Comparisons of grain size distribution and plasticity between subgrade fines and reconstituted fine soil were made, while that of grain size distribution between ballast grains and micro-ballast was conducted.

To obtain a similar grain size distribution of subgrade fines, nine different commercial soils were mixed with the calculated mass proportions (Table I-1, Qi et al. 2020a). The details of calculations and mixing procedure could be found in Lamas-Lopez (2016). Figure I-1 shows a good agreement of grain size distribution between reconstituted fine soil (Wang et al. 2018a) and subgrade fine soil (Trinh 2011). Figure I-2 compares the plasticity of reconstituted fine soil (Wang et al. 2018a) with that of subgrade fines from Senissiat site (Trinh 2011) and Vierzon site (Lamas-Lopez 2016). It indicates that the plasticity of reconstituted fine soil was quite similar to that of subgrade fine soil.

Table I-1. Mass proportions and grain size ranges of nine different commercial soils (Qi et al. 2020a)

Category	Soil Symbol	Mass proportion (%)	Grain size range (mm)
Clay	Bentonite	6.7	0.001–0.01 (20% of the particles)
	Kaolinite	23.3	0.0003–0.01 (80% of the particles)
Fine sand	C-10	20.0	0.0009–0.25
	C-4	16.7	0.0009–0.50
Medium sand	HN 34	3.3	0.063–0.50
	HN 31	3.3	0.16–0.63
	HN 0.4–0.8	6.7	0.25–1
	HN 0.6–1.6	6.7	0.32–2
	HN 1–2.5	13.3	0.32–3.20

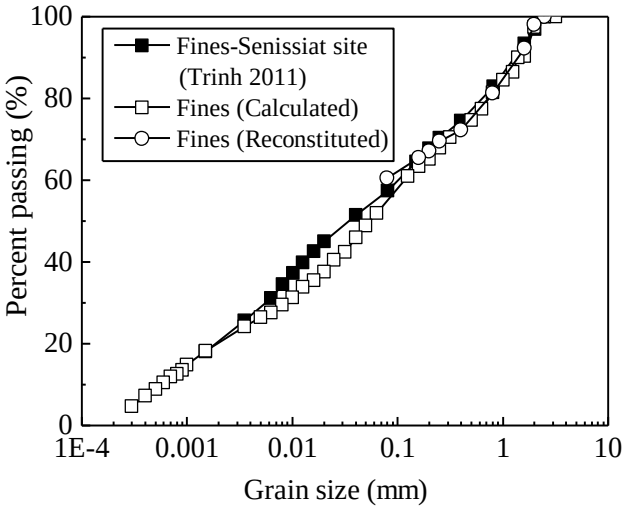

Figure I-1. Comparison of grain size distribution between reconstituted fine soil and subgrade fine soil (Wang et al. 2018a)

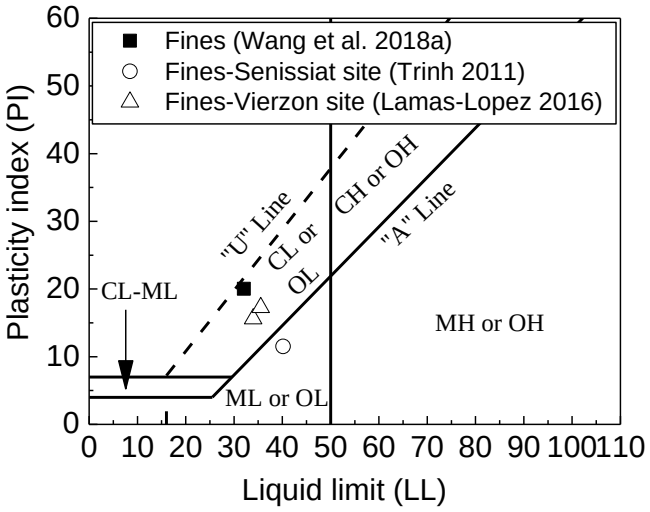

Figure I-2. Comparison of plasticity between reconstituted fine soil and subgrade fine soil (Wang et al. 2018a)

Since testing ballast grains with a maximum diameter d = 63 mm is very difficult with the common laboratory equipment, micro-ballast with a maximum d = 20 mm was adopted. The value of d = 20 mm was determined by considering the size effect of sample with a diameter d = 100 mm and a height h = 200 mm. The parallel gradation method was applied by Wang et al. (2017, 2018a and 2018b) and Qi et al. (2020a, 2020b) for this purpose. Figure I-3 shows the grain size distribution of ballast with that of mico-ballast following the similitude method. The micro-ballast was obtained by mixing three coarse materials (G10-20, G4-10 and HN2-4) with their mass proportions in Table I-2.

Table I-2. Mass proportions and grain size ranges of three coarse soils (after Lamas-Lopez 2016)

Soil Symbol	Mass proportion (%)	Gran size range (mm)
G 10-20	34	4 - 20
G 4-10	58	2 - 20
HN 2-4	8	2 - 6

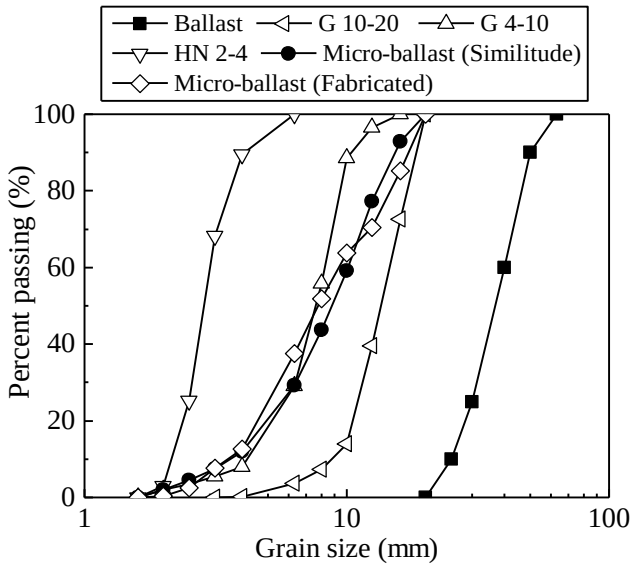

Figure I-3. Comparison of grain size distribution between micro-ballast and ballast (Wang et al. 2018a)

The validity of this paralle gradation method was verified by Qi et al. (2020a) through comparisons of permanent strain and resilient modulus between micro-ballast and ballast. Figure I-4 shows the variations of end-stage permanent strains with coarse grain content f_v (the ratio of the volume of coarse grains – ballast or microballast to that of mixture) under varying deviator stresses Δq for ballast samples and micro-ballast samples. Note that the same reconstituted fine soil was adopted in the ballast and micro-ballast samples. Six f_v values (0%, 5%, 10%, 20%, 35% and 45%) and five Δq values (10, 15, 20, 25 and 30 kPa) were considered by Qi et al. (2020b). It is worth noting that Wang et al. (2018a) found a characteristic coarse grain content $f_{v\text{-}cha} \approx 27\%$ separating the fabric of fine/coarse mixture into two zones: a fine matrix macrostructure at $f_v \leq f_{v\text{-}cha}$, and a coarse grain skeleton structure at $f_v \geq f_{v\text{-}cha}$. Comparisons of permanent strain between ballast samples and micro-ballast samples show a good agreement for these two fabrics.

Figure I-5 shows that the variations of resilient modulus with loading cycles for micro-ballast samples were consistent with those for ballast samples at f_v = 0% - 20%, which corresponded to the fine matrix macrostructure. On the contrary, Figure I-6 shows that the resilient modulus of ballast sample was slightly larger than that of micro-ballast sample at f_v = 35% - 45%, corresponding to the coarse grain skeleton structure. The slight difference between ballast sample and micro-ballast sample was explained by the irregular grain sliding and the

heterogeneity of the distribution of fine soil. This indicates the validity of the parallel gradation method.

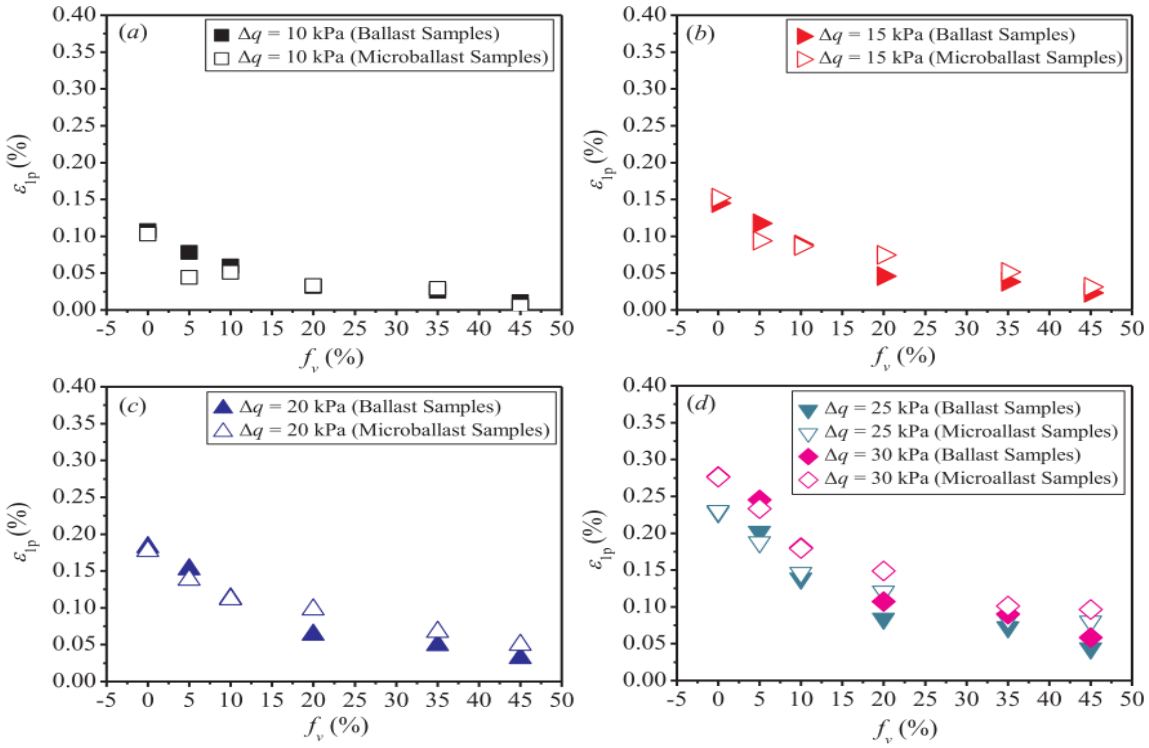

Figure I-4. Comparisons of variations of end-stage permanent strain with f_v at varying Δq between ballast samples and micro-ballast samples: (a) Δq = 10 kPa; (b) Δq = 15 kPa; (c) Δq = 20 kPa; (d) Δq = 25 and 30 kPa (Qi et al. 2020b)

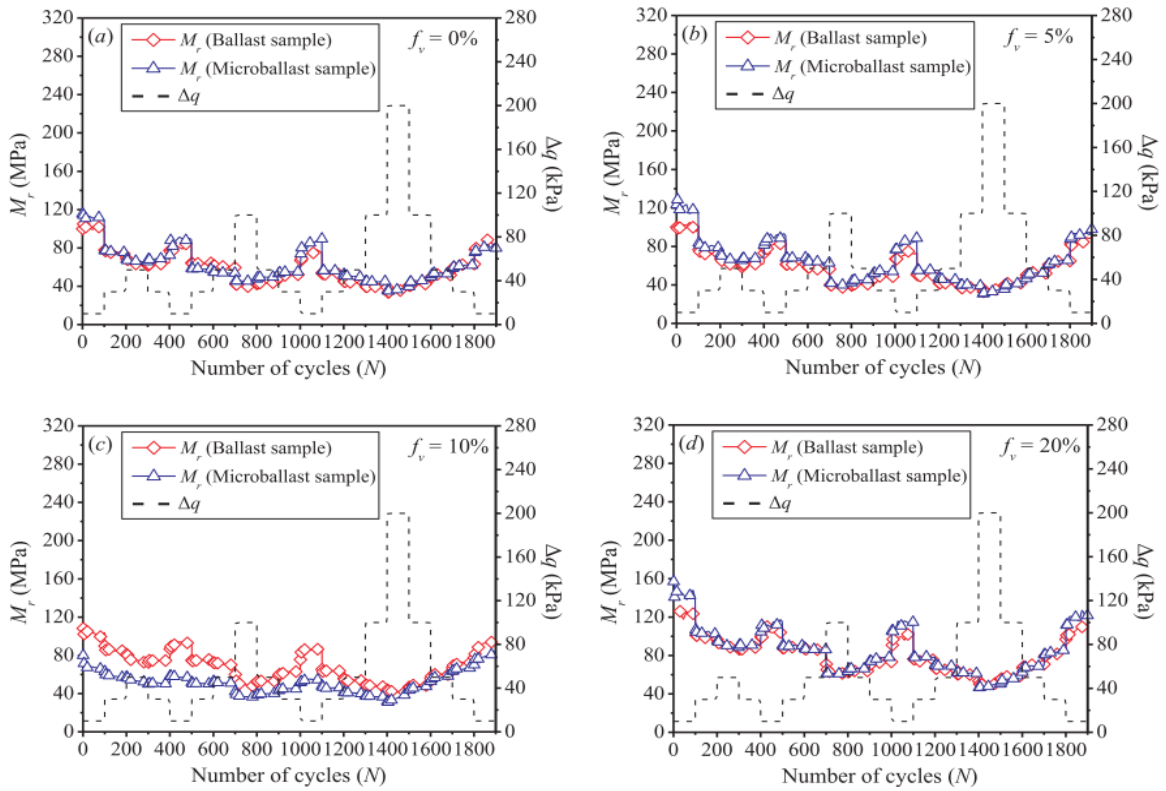

Figure I-5. Comparisons of variations of resilient modulus with N at f_v = 0% - 20% between ballast samples and micro-ballast samples: (a) f_v = 0%; (b) f_v = 5%; (c) f_v = 10%; (d) f_v = 20% (Qi et al. 2020b)

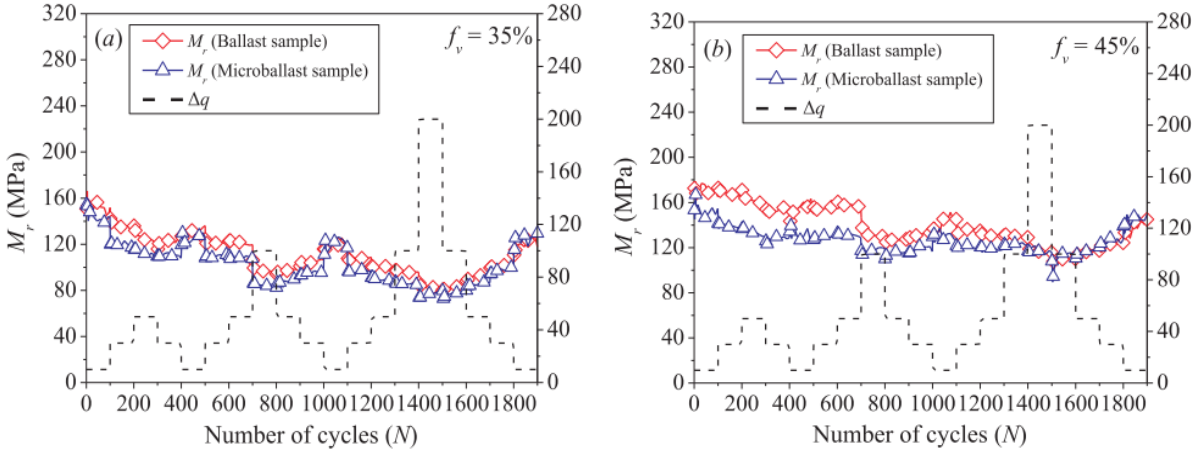

Figure I-6. Comparisons of variations of resilient modulus with N at f_v = 35% - 45% between ballast samples and micro-ballast samples: (a) f_v = 35%; (b) f_v = 45% (Qi et al. 2020b)

I.3 Water retention behavior of soil mixture

The water retention property plays an important role for the permanent deformation, stiffness and shear strength of unsaturated soil mixture. The soil-water retention curve (SWRC) describes the soil's capacity to store and release water under vaying suctions, which was generally expressed in terms of the suction as a function of the degree of saturation or the gravimetric water content. Figure I-7 depicts a typical main drying SWRC. The SWRC was divided into three zones by Vanapalli et al. (1996): the boundary effect zone, the transition zone (including primary and secondary transition zones) and residual zone. Figure I-8 shows the variation of water area with desaturation in different zones of SWRC. In the boundary effect zone, all voids were filled with water, leading to continuous water menisci in contact with soil particles. In the transition zone, water content decreased significantly with increasing suction, resulting in uncontinuous water menisci. In the residual zone, a small decrease of water content led to a significant increase of suction. Note that the boundary effect zone and the transition zone was separated by the air-entry value (AEV), while the transition zone and the residual zone was separated by residual suction, corresponding to the residual water content.

The water retention behavior of soil mixture was affected by many factors, in particular the dry density and coarse grain content.

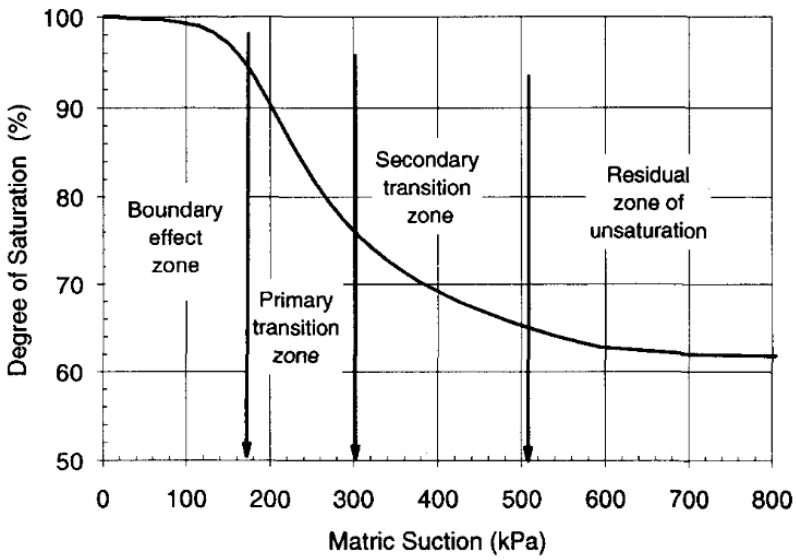

Figure I-7. A typical main drying SWRC for porous medium (Vanapalli et al. 1996)

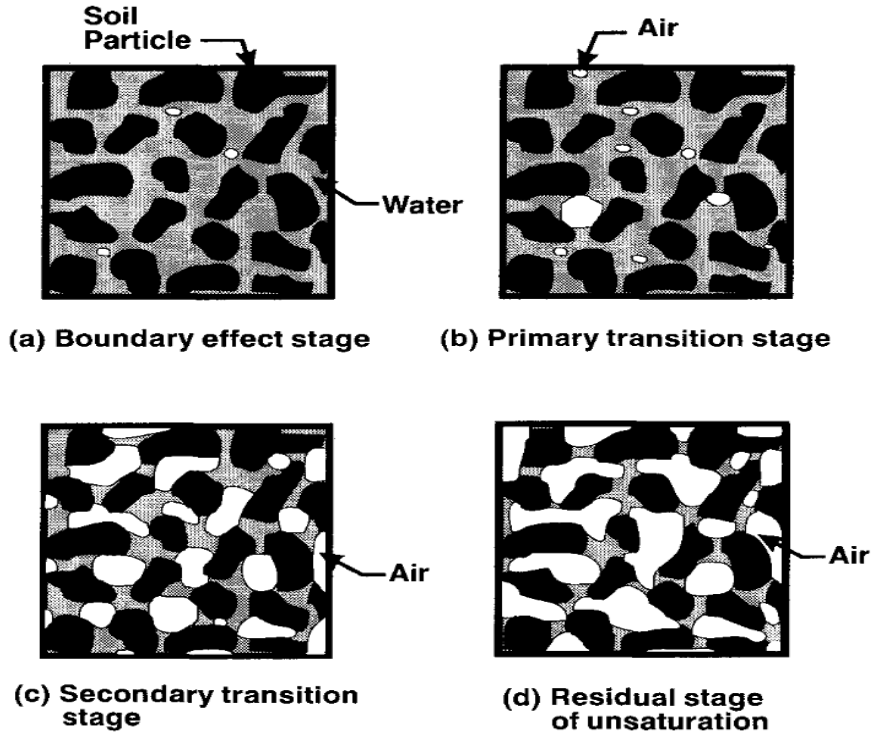

Figure I-8. Variation of water area with desaturation in different zones of SWRC (Vanapalli et al. 1996)

I.3.1 Effect of dry density

Romero et al. (1999) studied the effect of dry density on the water retention behavior of compacted Boom clay. The main wetting/drying SWRCs of Boom clay were measured under two different dry densities, and its corresponding microstructure was examined by mercury intrusion porosimetry tests. They found that the increase of dry density induced a decrease of volume of inter-aggregate voids, without significantly affecting the intra-aggregate voids. Accordingly, the SWRC was divided into two zones: an inter-aggregate governing suction zone and an intra-aggregate governing suction zone.

Birle et al. (2008) investigated the effects of initial water content and dry density on the water retention behavior of compacted clay. While plotted in terms of gravimetric water content with suction, the similar drying SWRCs were obtained for soils compacted at the same unsaturated water content and varying dry densities. Meanwhile, the similar intra-aggregate pores and different inter-aggregate pores were found. This was explained by that the similar drying SWRCs were the consequence of similar intra-aggregate pores.

Salager et al. (2013) investigated the effect of dry density on water retention behavior of deformable soils. The main drying path of SWRC was measured for a clayey soil in a wide range of suction. Figure I-9 shows that when the SWRC was expressed in terms of degree of saturation versus suction, the increase of dry density led to a higher water retention capacity. On the contrary, when expressed in terms of gravimetric wate content versus suction, the SWRCs for different dry densities converged into the same one beyond the suction value of 5000 kPa. In addition, with increasing suction, the void ratio of soil slightly decreased in the boundary effect zone, significantly decreased in the transition zone, and almost kept constant in the residual zone.

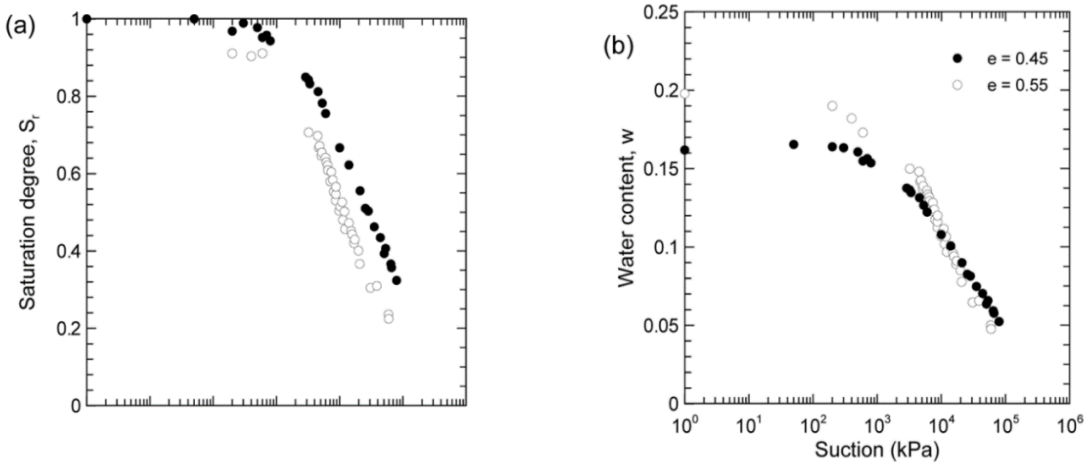

Figure I-9. Soil-water retention curves of compacted clayey soil: (a) degree of saturation versus suction; (b) water content versus suction (Salager et al. 2013)

Gao and Sun (2017) studied the water retention behavior of clayey silt under varying dry densities. They reported that the main drying SWRC expressed in terms of gravimetric water content with suction was independent of dry density when the suction was beyond the value of 200 kPa. This threshold suction corresponded to that obtained at the delimiting pore diameter of inter-aggregate and intra-aggregate voids.

I.3.2 Effect of coarse grain content

Spomer (1980) investigated the effect of sand content on porosity and water retention property of sand/fine soil mixture. At low sand content, the SWRC of mixture kept the same shape as that of fine soil. That was because sand was dispersed in the fine soil, without creating macro-

pores among sand. Conversely, at high sand content, the shape of SWRC of mixture resembled that of sand.

Ravina and Magier (1984) studied the water retention behavior of mixture of clay soil and coarse grains. They found that an increase of coarse grain content gave rise to an increase of mixture's resistance to compaction. During the compaction of mixture, some macro-pores among coarse grains was conserved. As a result, the volume of macro-pores increased with increasing coarse grain content.

Fies et al. (2002) investigated the water retention property of mixture at varying glass fragments. The increase of glass content led to a decrease of water content in the mixture. The macro-pores could retain water when suction was lower than 10 kPa. The formation of these macro-pores was determined by two mechanisms: incomplete filling between glass and fine soil, and shrinkage of fine soil during drying.

Baetens et al. (2009) studied the effect of rock fragments on the water retention property of stony soil. They found that increasing rock fragments significantly affected the water retention property of mixture when matric sution was lower than 30 kPa, which was attributed to the effect of rock fragment on pore size distribution of mixture.

Gargiulo et al. (2016) investigated the effect of rock fragment on soil porosity. The soil-pore imaging technique was adopted to quantify the development of pore structure of mixture under varying rock fragments. With increasing rock fragments, the porosity of mixture exhibited a decreasing trend, followed by an increasing trend (Figure I-10). A threshold rock fragment was identified. This threshold value depended on the combined effects of two mechanisms: i) the substitution of fine soil with rock fragment induced a reduction of porosity, ii) the shrinkage of fine soil contributed to an increase of porosity.

Jing (2017) studied the effect of fine soil content on soil-water retention curve of sand/fine soil mixture. They reported that an increase of fine content resulted in an increase of water retention capacity.

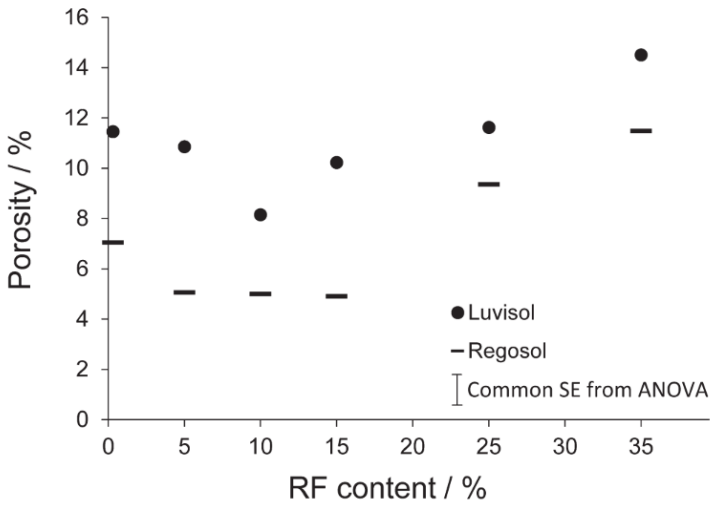

Figure I-10. Variations of porosity of mixture with rock fragment content (Gargiulo et al. 2016)

I.4 Mechanical behavior of soil mixture

The mechanical behavior of soil mixture was presented in this section, including the static behaviour and the dynamic behaviour.

I.4.1 Static behavior

The static behavior of soil mixture such as shear strength was affected by many factors, in particular the coarse grain content and water content.

I.4.1.1 Effect of coarse grain content

Vallejo (2001) investigated the shear strength of binary granular mixture. Two glass beads at different sizes (5 and 0.4 mm) were adopted as substitutes for coarse/fine grains. A coarse grain supported structure was identified when the proportion of large glass beads was more than 70%; a transition structure (including transitional coarse/fine grain supported structure) was found when the proportion ranged from 40% to 70%; a fine grain supported structure was found when the proportion was less than 40%. This was consistent with the findings of previous studies on gravel/sand mixture shown in Table I-3.

Table I-3. Variations of shear strength of gravel/sand mixture with gravel content in different studies (Vallejo 2001)

	Percentage of gravel in the mixture			
	Mixture shear strength ≈ frictional resistance of the gravel	Mixture shear strength ≈ frictional resistance of the gravel and sand	Mixture shear strength ≈ frictional resistance of the sand	Reference
	>65	65–40	<40	Fragaszy et al. 1992
	>70	70–50	<50	Marsal and Fuentes de la Rosa 1976
	>80	80–55	<55	Vasileva et al. 1971
	>70	70–50	<50	Doddiah et al. 1969
	>65	65–50	<50	Holtz and Gibbs 1956
Average	>70	70–49	<49	

Seif EI Dine et al. (2010) studied the mechanical behaviour of a mixture of sandy matrix and gravels. The volumetric fraction of gravel ranging from 0% to 35% was considered. In this range, the mechanical behaviour of mixture was primarily governed by the sandy matrix. As a result, an increasing gravel content led to a slight increase of shear strength of mixture.

Duong et al. (2013) studied the effect of fine soil content on the mechanical behaviour of interlayer soil. The legend ITL_0 and ITL_{10} refer to adding 0% and 10% of fine soil into the interlayer soil, respectively. 'ITL_0w12s100' represents ITL_0 at a water content of 12% and a confining pressure of 100 kPa. Figure I-11 shows that an increase of fine soil content induced a decreasing peak deviator stress under saturated water content (w = 12%). On the contrary, Figure I-12 shows that an increase of fine soil content led to an increasing peak deviator stress under unsaturated water content (w = 4%). This was attributed to the effect of suction which was developed inside the fines.

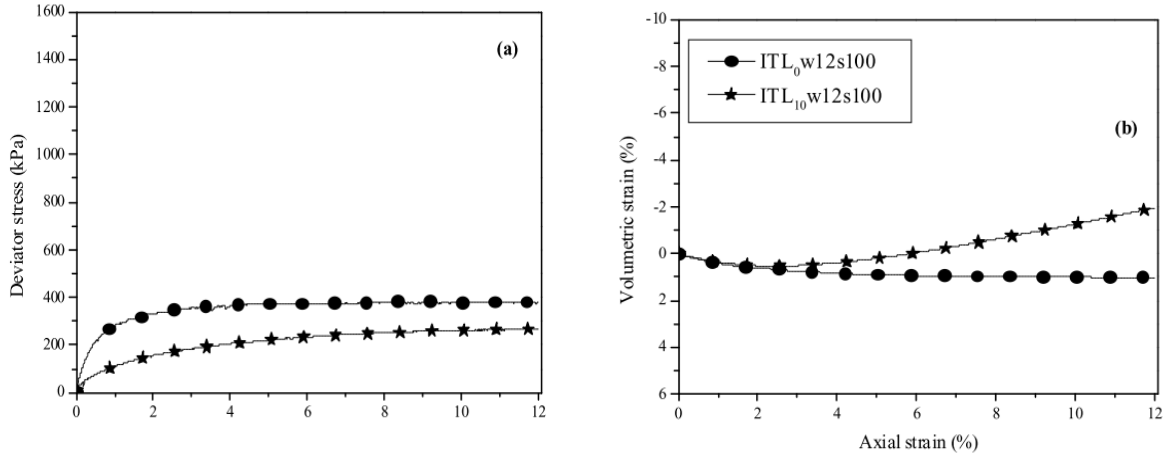

Figure I-11. Effect of fine soil content on mechanical behavior of soil mixture under saturated state: (a) deviator stress – axial strain curves; (b) volumetric strain – axial strain curves (Duong et al. 2013)

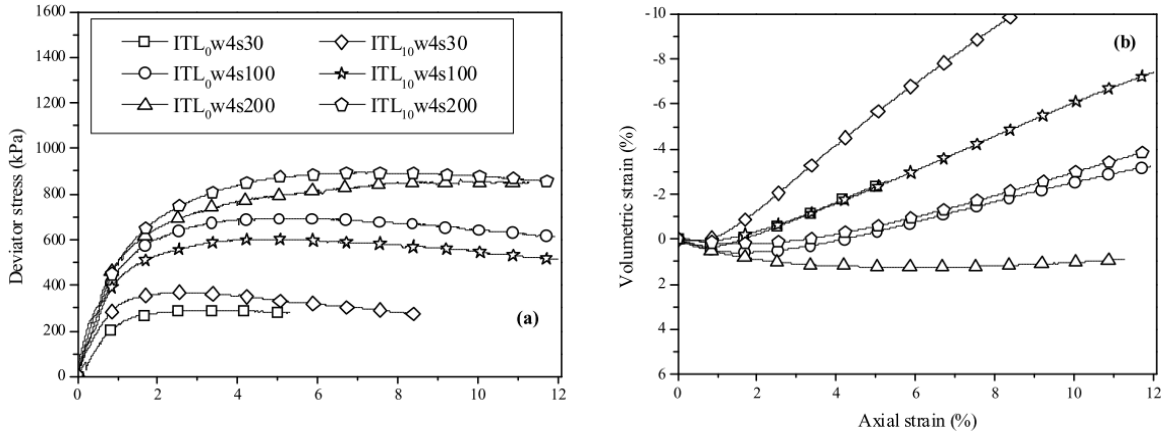

Figure I-12. Effect of fine soil content on mechanical behavior of soil mixture under unsaturated state: (a) deviator stress – axial strain curves; (b) volumetric strain – axial strain curves (Duong et al. 2013)

de Frias Lopez et al. (2016) analysed the effect of fines content on the fabric development of binary granular mixture using discrete-element method. Figure I-13 depicts the variations of fabric of mixture with increasing fines content. Four load-bearing fabrics were identified: underfilled (coarse grains fully contributing to the load-bearing skeleton); interactive-underfilled (coarse grains as the main skleton); interactive-overfilled (fine grains starting to form a skeleton); overfilled (fine grains as the skeleton). The four fabrics corresponded to those defined by Vallejo (2001), respectively: a coarse grain supported structure, a transitional coarse

grain supported structure, a transitional fine grain supported structure, and a fine grain supported structure.

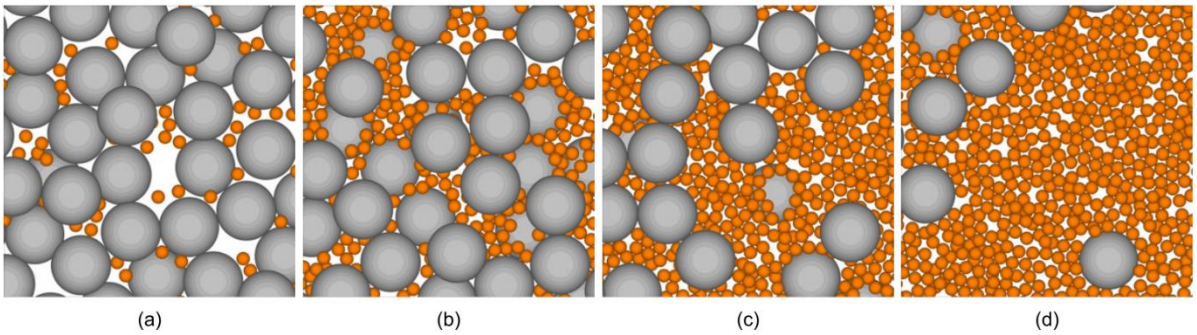

Figure I-13. Four load-bearing fabrics of soil mixture with varying fines content: (a) underfilled; (b) interactive-underfilled; (c) interactive-overfilled; (d) overfilled (de Frias Lopez et al. 2016)

Wang et al. (2018a) studied the effect of coarse grain content f_v (the ratio of the volume of coarse grains to that of soil mixture) on the mechanical behavior of fine/coarse soil mixture. The mechanical behavior of mixture was investigated by monotonic triaxial tests, and its fabric was examined by CT tests. Figure I-14 shows the variation of peak deviator stress with coarse grain content f_v. A fine matrix macrostructure was found at f_v = 0% ~ 20%, while a coarse grain skeleton fabric at f_v = 35% ~ 45%. A characteristic coarse grain content $f_{v\text{-}cha}$ was identified around 27%, which was consistent with the observation by CT tests (Figure I-15).

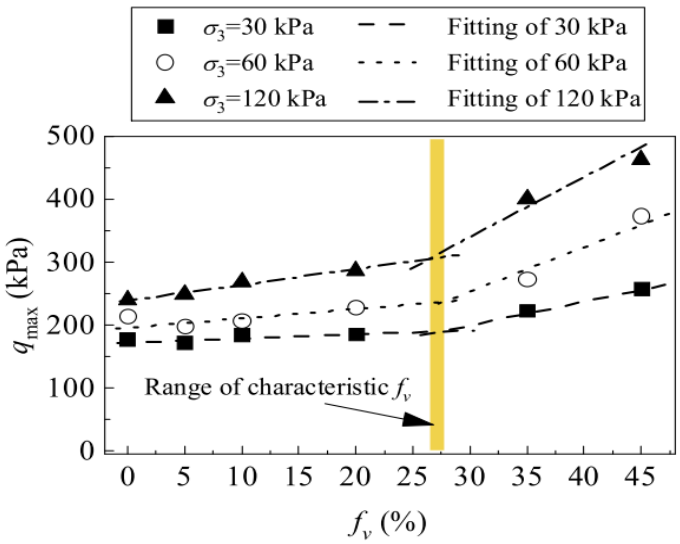

Figure I-14. Variation of peak deviator stress of soil mixture with coarse grain content (Wang et al. 2018a)

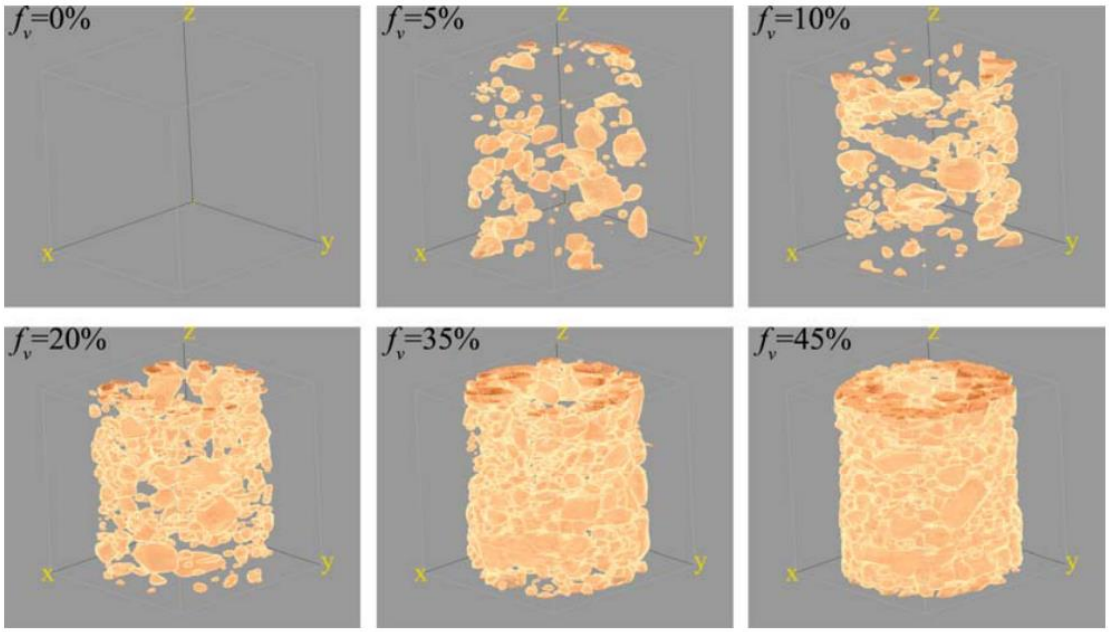

Figure I-15. 3D views of coarse grain distribution in compacted soil mixture (Wang et al. 2018a)

I.4.1.2 Effect of water content

Delage et al. (1996) investigated the effect of compaction water content on microstructure of silt by scanning electron microscopy and mercury intrusion porosimetry tests. Figure I-16 shows a bi-modal porosity microstructure of silt compacted on the dry side of optimum, while a uni-modal porosity microstructure of silt on the wet side. This was attributed to a fine aggregate structure of silt formed on the dry side, while a fine matrix structure on the wet side.

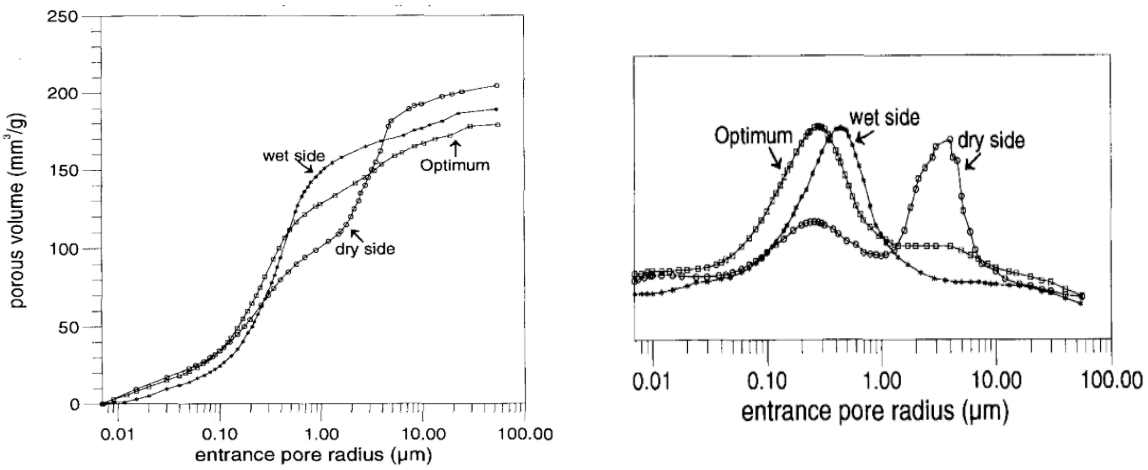

Figure I-16. Pore size distributions of silt compacted at three different water contents: (a) cumulative curves; (b) differential curves (Delage et al. 1996)

Li and Zhang (2009) studied the effects of compaction, wetting and drying on the microstructure of mixture of clay and sand. They found that the inter-aggregate pores were significantly affected by the compaction, while the intra-aggregate porere notably influenced by the wetting and drying processes.

Zhang and Li (2010) studied the microstructure of soil mixture at varying coarse grain contents by mass. When the coarse grain content was smaller than 70%, a fines-controlled microstructure was identified, while when the coarse grain content was larger than 70%, a coarse grain dominated fabric was found. For both fabrics, a bi-modal porosity was obtained when compacting the mixture at optimum moisture content. In the case of fines-controlled microstructure, saturation of the mixture led to a change from bi-modal to uni-modal microstructure, and drying of the mixture resulted in a reduction of total volume. On the contrary, in the case of coarse grain dominated fabric, the bi-modal porosity structure remained stable, whatever the water content change.

Zhang et al. (2018a) investigated the effect of water content on the shear modulus of fine soil. Figure I-17 shows that with increasing water content, the shear modulus increased when the water content was smaller than the optimum value, while decreased when the water content was larger than the optimum one. This was explained as follows: on the dry side, the aggregates governed the stiffness. With increasing water content, the inter-aggregate contact surface increased, leading to an increase of shear modulus. On the contrary, on the wet side, suction started to govern the stiffness. Increasing water content led to a decrease of shear modulus.

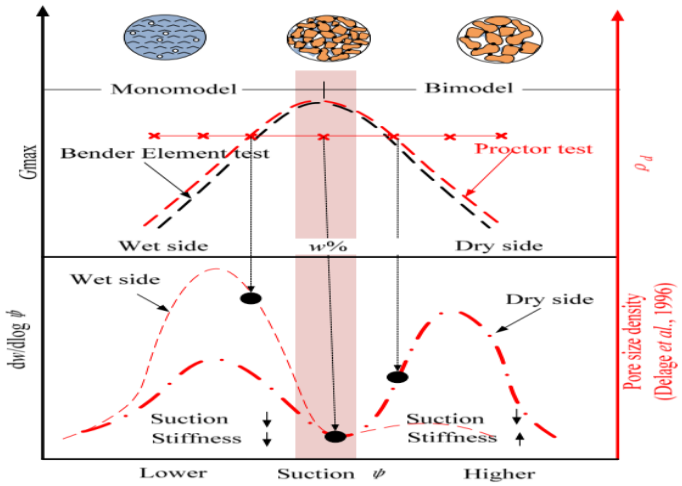

Figure I-17. Variations of shear modulus, fabric and suction with water content (Zhang et al. 2018a)

Trinh et al. (2012) studied the effect of water content on the shear strength of fouled ballast. They found that the lower the water content, the higher the shear strength.

Duong et al. (2013) investigated the effect of water content on the mechanical behavior of interlayer soil. The legend 'ITL$_{10}$w4s30' refers to the interlayer soil with addition of 10% of fines at a water content of 4% and a confining pressure of 30 kPa. Figure I-18 shows that a decrease of water content gave rise to increases of shear strength and dilatancy angle. This was attributed to the suction effect inside the fines.

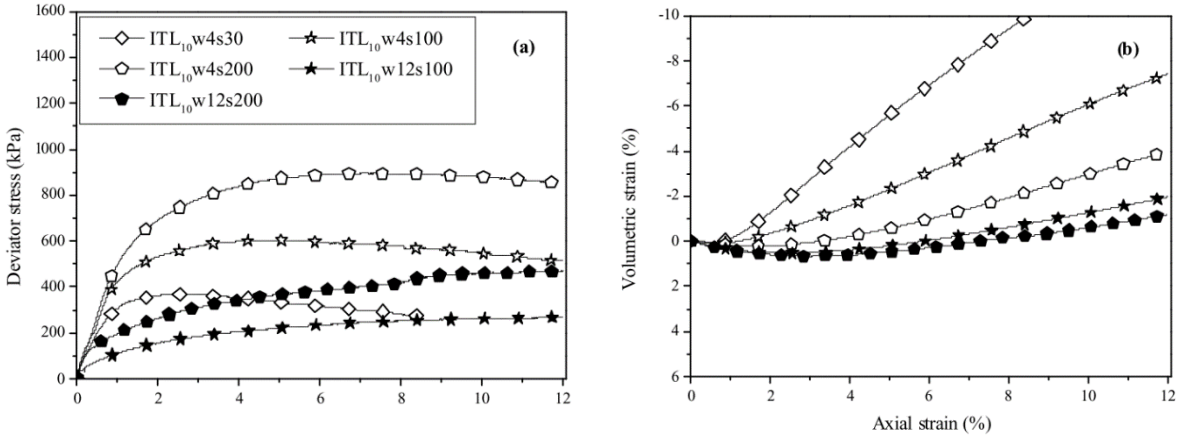

Figure I-18. Effect of water content on the mechanical behavior of interlayer soil: (a) deviator stress – axial strain; (b) volumetric strain – axial strain (Duong et al. 2013)

I.4.2 Permanent deformation behavior

The permanent deformation of fine/coarse soil mixture was affected by many factors, such as the loading cycles, stress level, stress history, coarse grain content, and water content (or suction).

I.4.2.1 Effect of loading cycles

The number of loading cycles is one of the most important factor for the permanent strain of soil mixture. The permanent strain can be determined by cyclic triaxial tests. AFNOR (2004) recommends a test procedure to determine the evolution of permanent strain with loading cycles. The loading cycles are performed under constant stress amplitudes. Figure I-19 shows that under a given loading cycle, the total strain can be separated into the resilient strain and the permanent strain.

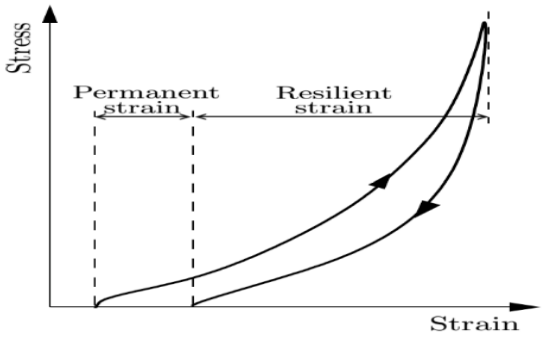

Figure I-19. Determination of permanent strain and resilient strain in a loading cycle (Varandas 2013)

The permanent strain increased with the increase of loading cycles, and tended to stabilize. Figure I-20 shows that under a constant deviator stress, the permanent strain increased rapidly at the first loading cycles, and gradually stabilized. Up to now, there was no consensus on the number of loading cycles required for the stabilization of permanent strain. This was because the stabilization of permanent strain was highly dependent on the stress level, coarse grain content, water content, etc. For instance, Stewart (1982) found that 1000 loading cycles were needed for the stabilization of permanent strain for the ballast, while Allen and Thompson (1974) found that 50 – 100 cycles were enough for granular materials.

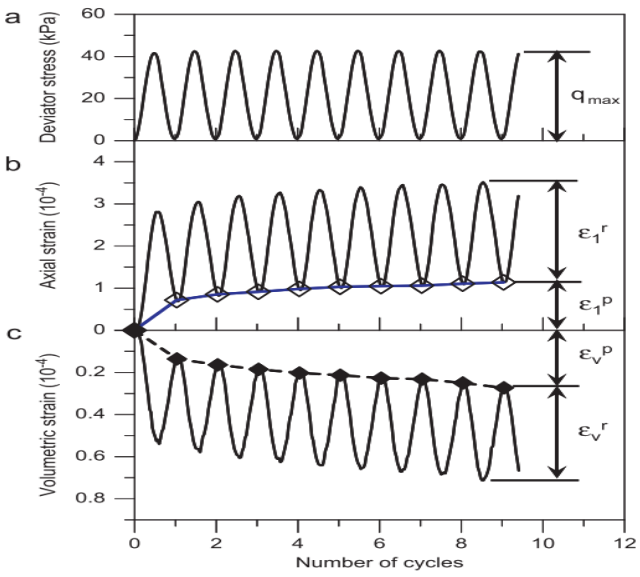

Figure I-20. Evolutions of permanent and resilient strains with loading cycles (Trinh et al. 2012)

I.4.2.2 Effect of stress level and stress history

The cyclic stress ratio n_{cyclic} was defined as the ratio of cyclic deviator stress amplitude Δq_{cycle} to the maximum deviator stress determined by monotonic triaxial test. This was adopted to reflect the effect of stress level on permanent strain. Figure I-21 shows that the higher the n_{cyclic}, the larger the permanent strain.

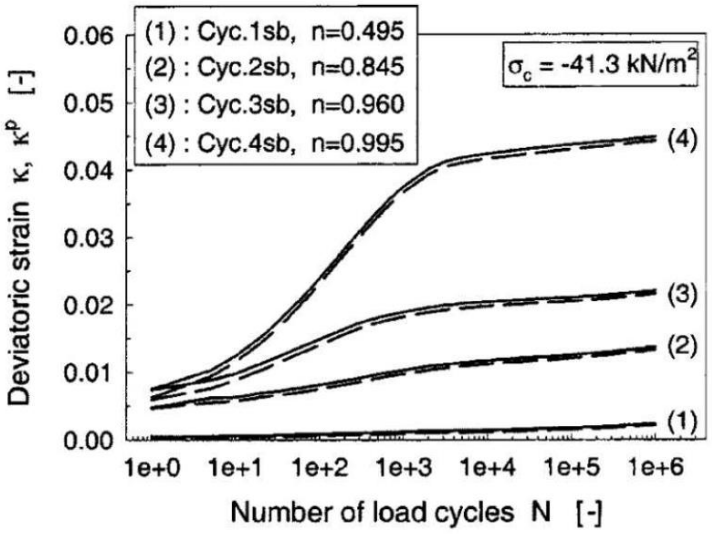

Figure I-21. Variations of permanent strain with loading cycles under varying n_{cyclic} (Suiker 2005)

Brown and Hyde (1975) investigated the effect of stress history on permanent strain of granular materials by comparison of two different tests. In the first test, a target deviator stress of 650 kPa was directly applied. On the contrary, in the second test, the deviator stress increased in steps until the target value. The results showed that the permanent strain in the former case was much higher than that in the latter case. This was attributed to the gradual material hardening in the latter case.

Gidel et al. (2001) proposed a multi-stage loading procedure to study the permanent strain of unbound granular materials. Figure I-22(a) shows that the reference curves was obtained by cyclic tests under a constant stress level, and then the model curve corresponding to multi-stage stress levels was derived from a combination of these reference curves. Figure I-22(b) shows a good agreement between the model curve and the corresponding experimental measurements.

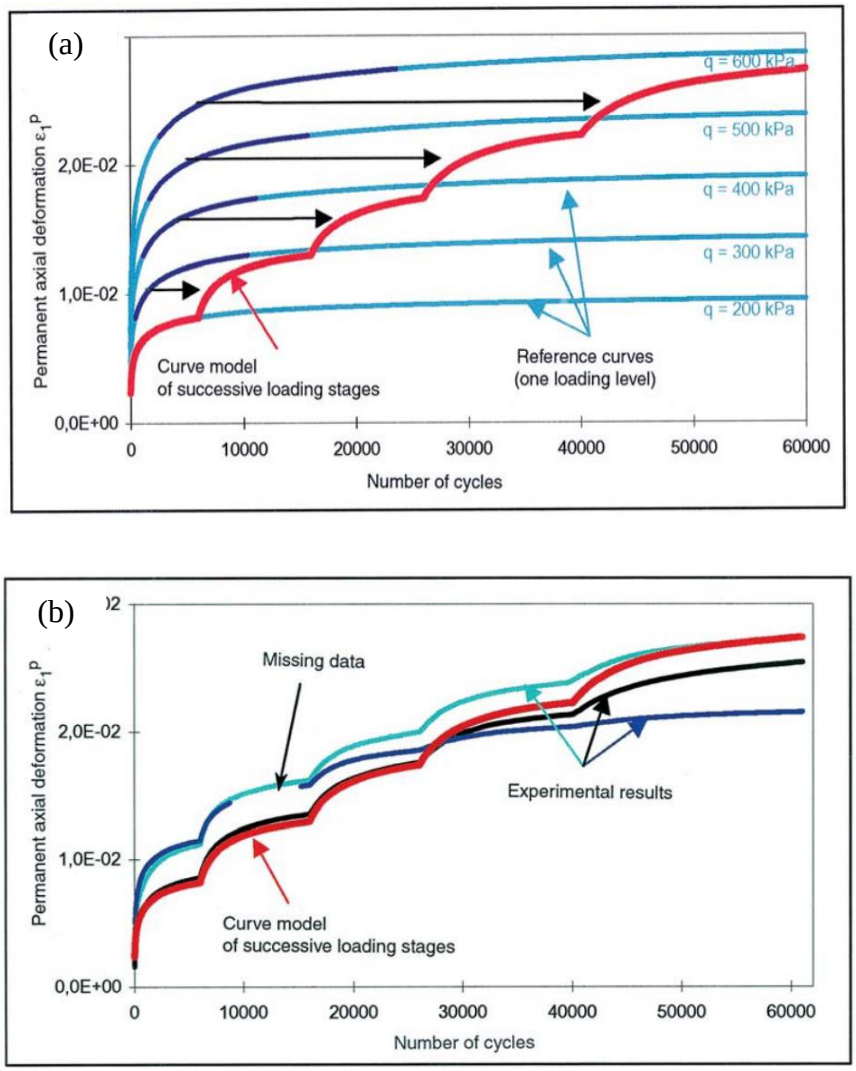

Figure I-22. (a) Construction of the model curve and (b) comparisons of the model curve with the corresponding experimental measurements (Gidel et al. 2001)

I.4.2.3 Effect of coarse grain content

Duong et al. (2013) studied the effect of fine soil content on permanent strain of interlayer soil under varying water contents. The legend was defined as follows: $ITL_{10}w12C$ refers to the interlayer soil with addition of 10% fine soil at a water content of 12%. Figure I-23 shows that increasing fine soil content induced an increase of permanent stain under saturated condition (w = 12%), while an opposite trend was observed under unsaturated conditions (w = 4% and 6%). This was because increasing fines content led to an increase of suction under unsaturated condition, and thus a decrease of permanent strain. This phenomenon was confirmed by Jing (2017) on granular materials.

Wang et al. (2018b) studied the effect of coarse grain content f_v (the ratio of the volume of coarse grains to that of soil mixture) on permanent strain of fine/coarse soil mixture. A series of multi-stage loading cyclic tests were performed. They found that an increase of coarse grain content led to a decrease of permanent strain. Figure I-24 shows that a characteristic coarse grain content $f_{v\text{-}cha}$ was identified, below which the permanent strain decreased with increasing f_v quickly, while beyond which decreased slowly.

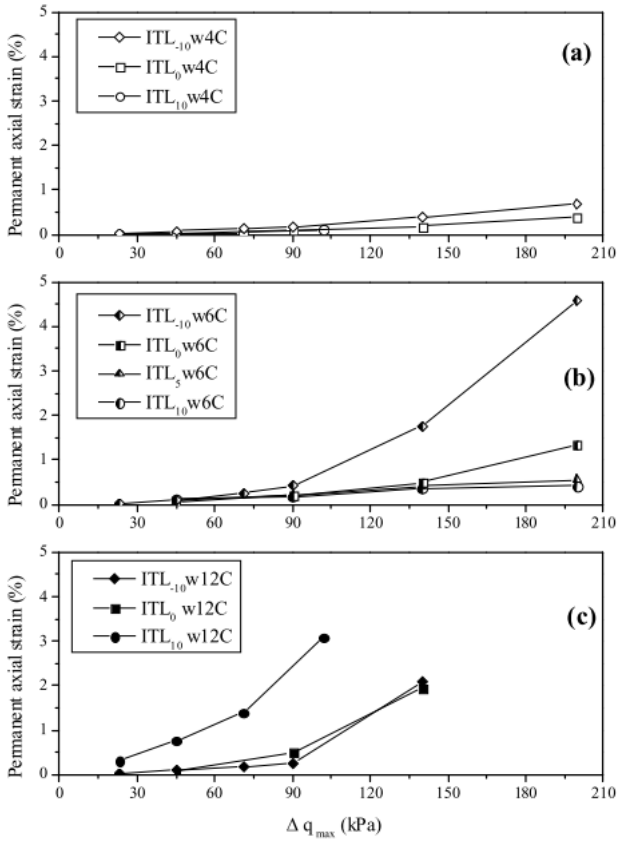

Figure I-23. Effect of fine soil content on permanent strain of interlayer soil under varying water contents: (a) w = 4%; (b) w = 6%; (c) w = 12% (Duong et al. 2013)

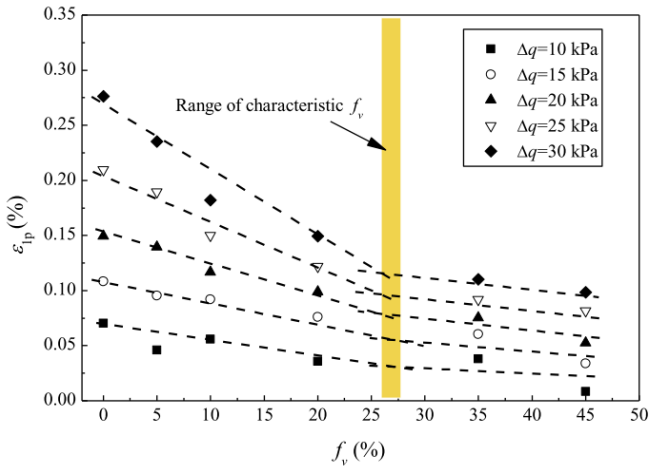

Figure I-24. Variations of permanent strain of soil mixture with f_v under varying deviator stresses (Wang et al. 2018b)

I.4.2.4 Effect of water content

Changes in water content can significantly affect the permanent strain of soil mixture. Under saturated state, the traffic loadings induced an accummulation of pore water pressure and thus a decrease of effective stress. As a result, the permanent strain increased. On the contrary, under unsaturated state, the decrease of water content led to a decrease of permanent strain, which was attributed to the suction effect (Gidel et al. 2001; Werkmeister et al. 2001, 2004a; Jing 2017).

Trinh et al. (2012) studied the effect of water content on the permanent strain of fouled ballast by large-scale cyclic triaxial tests. They reported that increasing water content resulted in an increase of permanent strain.

Azam et al. (2015) investigated the permanent strain of mixture of clay masonry and concrete aggregate under varying water contents. The legend 'RMC' refers to the ratio of water content to optimum water content. Figure I-25 shows that the permanent strain of mixture increased with increasing RMC. Moreover, a power relation was found between the permanent strain and RMC.

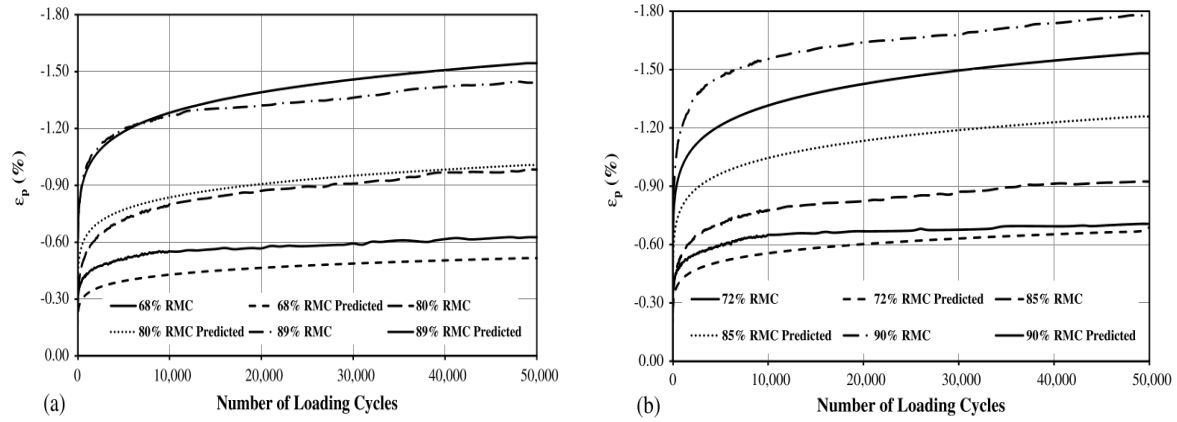

Figure I-25. Variation of permanent strain with the number of loading cycles under varying water contents

I.4.2.5 Shakedown theory

Under the combined effects of the number of loading cycles, deviator stress, coarse grain content and water content in cyclic triaxial tests, the soil mixture either reaches a stable state, or fails due to excessive accumulated permanent strain. The shakedown theory can be used to describe such permanent strain behaviors.

Werkmeister et al. (2001) adopted the shakedown concept for describing the permanent strain of unbound granular material subjected to cyclic loadings. Figure I-26 shows three ranges of permanent strain behavior: range A (plastic shakedown) – permanent stran approaches a constant value with increasing loading cycles; range B (plastic creep) – soil fails at a large number of loading cycles; range C (incremental collapse) – soil fails at a small number of loading cycles. Song and Ooi (2010) summarized three approaches to distinguish these different permanent strain behaviors (Figure I-27): permanent strain versus the loading cycles; resilient strain versus the loading cycles; permanent strain rate versus permanent strain. The last approach was commonly used.

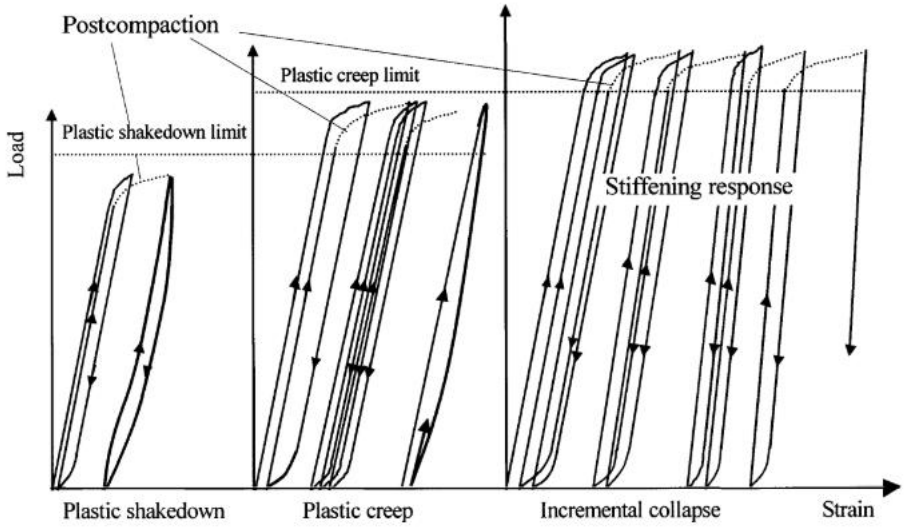

Figure I-26. Three permanent strain behaviors of granular material under cyclic loading (Werkmeister et al. 2001)

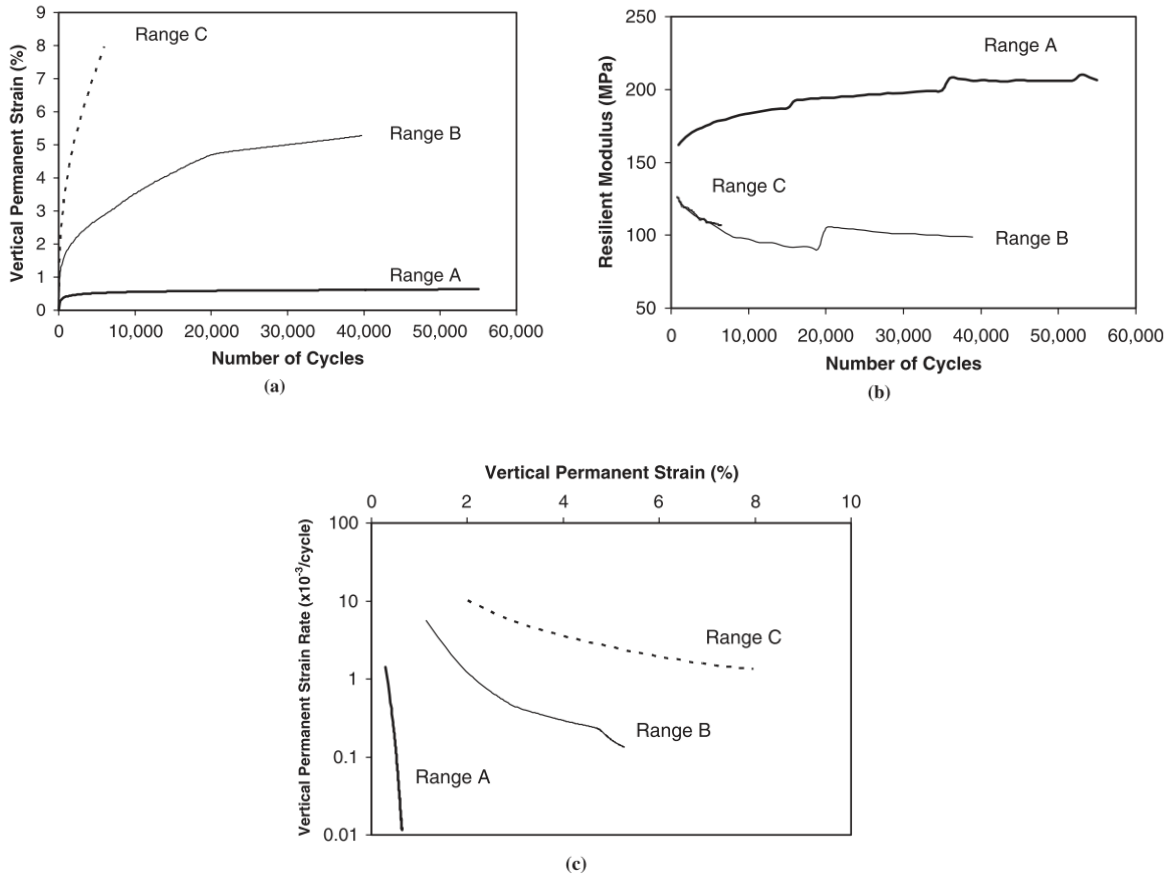

Figure I-27. Three approaches to distinguish different permanent strain behaviors: (a) permanent strain versus the loading cycles; (b) resilient strain versus the loading cycles; (c) permanent strain rate versus permanent strain (Song and Ooi 2010)

Yang and Huang (2007) investigated the effect of water content on the permanent strain behavior of subgrade soil by cyclic tests. They found that the critical stress between range A and B decreased with the increasing water content.

Tao et al. (2010) studied the permanent strain behavior of pavement base materials under cyclic loading. Two responses of permanent strain were identified - stable and unstable. This was found to be highly dependent on the loading levels and type of materials.

I.4.3 Dynamic characteristics

The dynamic properties of soil mixture were generally expressed in terms of resilient modulus and damping ratio, which can be determined by cyclic triaxial tests (Menq 2003). Figure I-28 shows the variation of axial strain with the loading cycles. The axial strain was separated into resilient and permanent strain. Figure I-29 shows the definitions of resilient modulus and damping ratio. Under a given hysteresis loop, the resilient modulus was defined as the ratio of deviator stress amplitude to resilient strain, and the damping ratio was defined as the ratio of dissipated energy to the total energy.

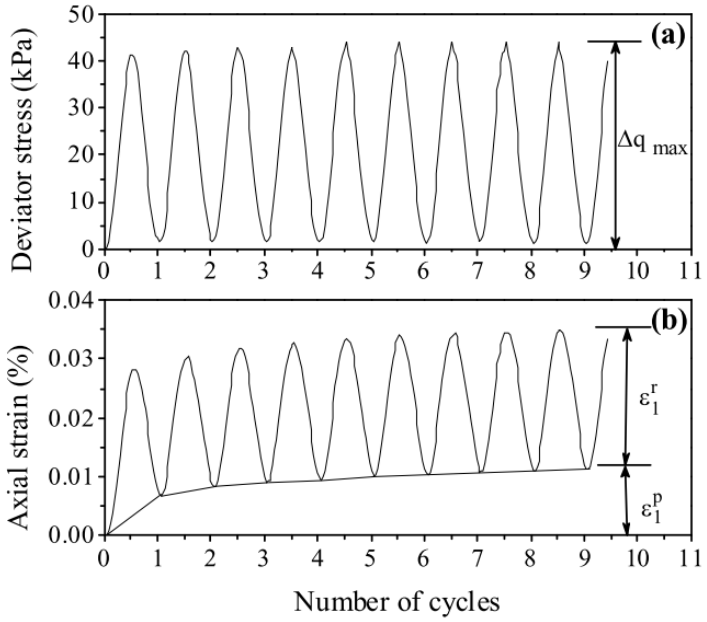

Figure I-28. Variation of axial strain with the loading cycles under constant deviator stress (Duong et al. 2016)

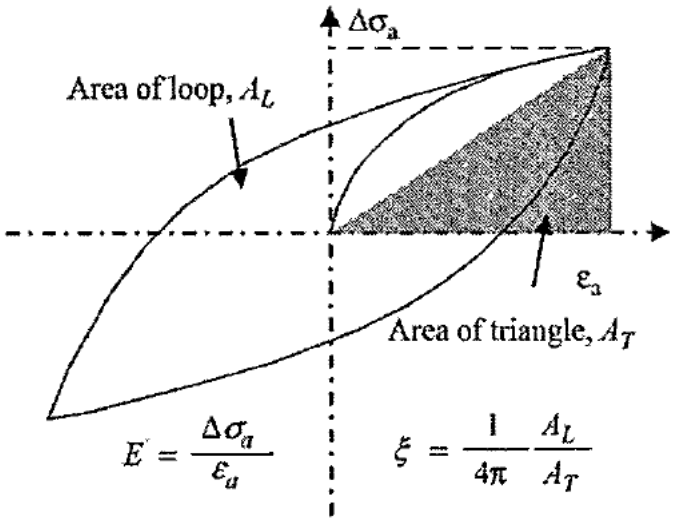

Figure I-29. Definitions of resilient modulus and damping ratio (Khan et al. 2011)

I.4.3.1 Effect of coarse grain content

Lin et al. (2000) investigated the dynamic properties of gravelly cobble deposits mixed with fine soil by cyclic triaxial tests. They found that the gravel content can greatly affect the nonlinear shear modulus-shear strain and damping ratio-shear strain relations.

Tennakoon and Indraratna (2014) studied the dynamic characteristics of clay-fouled ballast by performing large-scale cyclic triaxial tests, and reported that increasing fouling magnitude resulted in a decrease of resilient modulus.

Wang et al. (2017) studied the effect of coarse grain content f_v (the ratio of the volume of coarse grains to that of soil mixture) on the dynamic characteristicss of fine/coarse soil mixture by cyclic triaxial tests, and found that increasing the coarse grain content led to an increase of resilient modulus and a decrease of damping ratio. Figure I-30 shows the comparisons of resilient modulus and damping ratio between Wang et al. (2017), Duong et al. (2016) and Lamas-Lopez (2016). A characteristic coarse grain content $f_{v\text{-}cha}$ was identified, separating the fabric of soil mixture into two zones: a fine matrix macrostructure at $f_v < f_{v\text{-}cha}$, and a coarse grain skeleton fabric at $f_v > f_{v\text{-}cha}$.

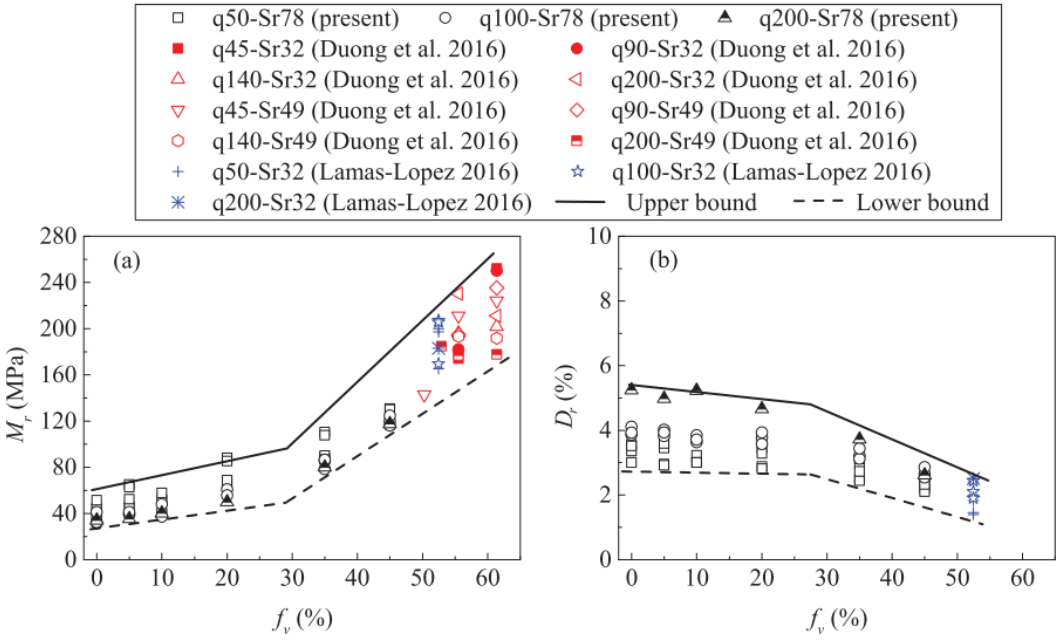

Figure I-30. Comparisons of resilient modulus and damping ratio in different studies (Wang et al. 2017)

Duong et al. (2016) investigated the effect of fine soil content on the resilient modulus of the upper part interlayer soil by cyclic tests (Figure I-31). ITL-$_{10}$, ITL$_0$, ITL$_5$ and ITL$_{10}$ refer to decrease 10% and increase 0%, 5% and 10% of fine soil content in interlayer soil, respectively. It was found that increasing fine soil content led to a decrease of resilient modulus under saturated condition (w = 12%), while an increase of that under unsaturated condition (w = 4% and 6%). That was explained by the increase of suction due to the increase of fine soil content under unsaturated condition.

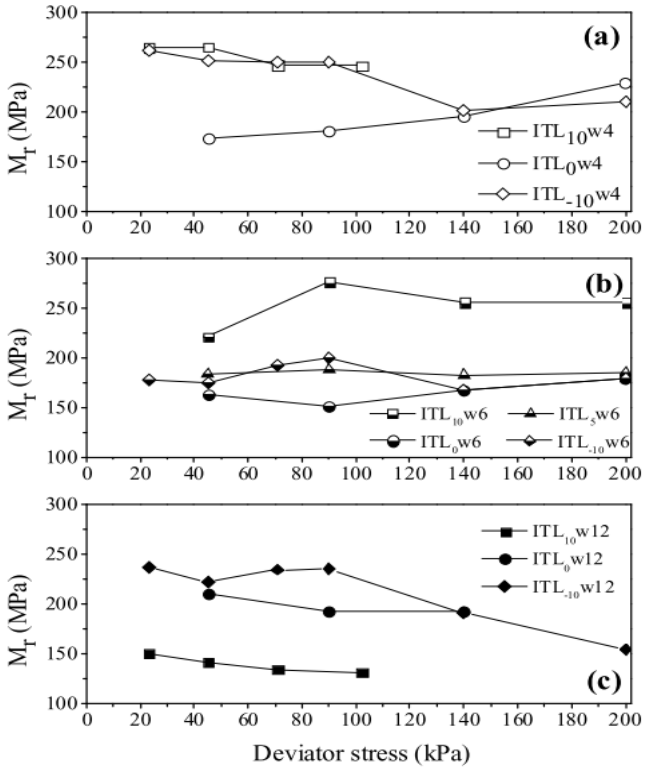

Figure I-31. Variations of resilient modulus with deviator stress under varying fine soil contents and water contents: (a) *w* = 4%; (b) *w* = 6%; (c) *w* = 12% (Duong et al. 2016)

I.4.3.2 Effect of water content

Lamas-Lopez (2016) studied the effect of water content on the dynamic properties of the upper part interlayer soil. A multi-stage loading procedure was adopted, with a number of loading cycles of 100 for each stage (Figure I-32). The legend 'B3S4' refers to sine shape loading and water content of 4%. It can be observed that increasing wate content gave rise to a decrease of resilient modulus and an increase of damping ratio.

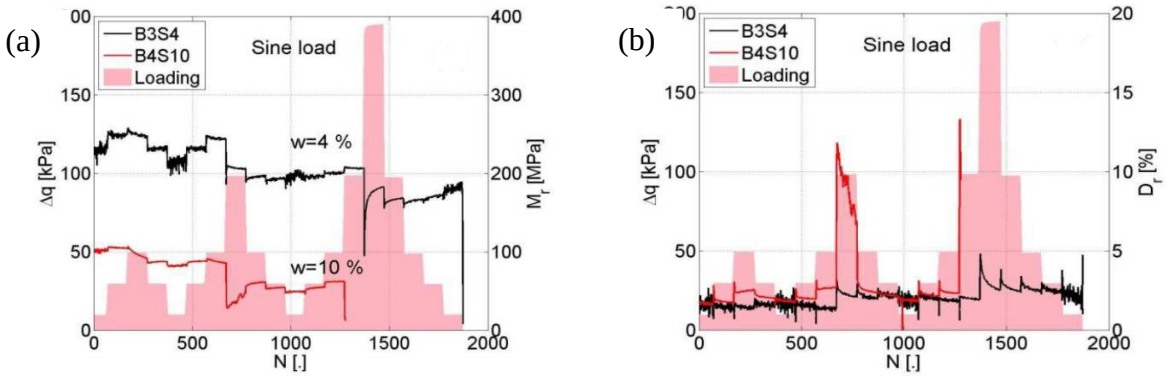

Figure I-32. Effect of water content on (a) resilient modulus and (b) damping ratio

Khasawneh and Al- jamal (2019) adopted different approaches to describe the resilient modulus of fine-grained materials based on data from 3709 tests collected. Different parameters were considered, including optimum moisture content, confining pressure, liquid limit, plasticity indes, dry density, etc. The results showed that among all parameters the optimum moisture content affected the resilient modulus the most.

Jibon et al. (2020) investigated the resilient modulus of subgrade soil by cyclic triaxial tests. They found that the water content significantly affected the resilient modulus of plastic soil. An increase of water content led to a large reduction of resilient modulus for plastic soil, while a slight reduction for non-plastic soil.

I.5 Constitutive models for soil mixture

The constitutive models for soil mixtures were reviewed in this section, mainly in terms of permanent deformation and resilient modulus. It is worth noting that the model parameters with the same notations (e.g. a and b; k_1, k_2 and k_3) are adopted in different models. These parameters in different models can have different physical meanings.

I.5.1 Permanent deformation

The permanent deformation of soil mixture was significantly affected by the loading cycles, stress state, coarse grain content and suction (or water content). Accordingly, different models were proposed.

I.5.1.1 Effect of loading cycles

Barksdale (1972) studied the permanent deformation of unstabilized base course materials by cyclic triaxial tests, and found a linear relationship between the permanent strain ε_1^p and the number of loading cycles *N* on a logarithmic scale:

$$\varepsilon_1^p = a + b \log N \tag{I-1}$$

where a and b are model parameters.

Khedr (1985) investigated the permanent strain of granular crushed limestone by cyclic tests, and reported a power relation between ε_1^p and *N*:

$$\frac{\varepsilon_1^p}{N} = aN^{-b} \quad \text{(I-2)}$$

where a and b are model parameters.

Sweere (1990) proposed Eq. (I-3) to describe the variation of ε_1^p with *N* for unbound granular materials:

$$\varepsilon_1^p = aN^b \quad \text{(I-3)}$$

where a and b are model parameters.

Hornych et al. (1993) proposed Eq. (I-4) to describe the effect of *N* on ε_1^p of unbound granular materials, which has been adopted in French standard for cyclic triaxial tests (AFNOR 1995):

$$\varepsilon_1^p = f(N) = A \cdot [1 - (\frac{N}{100})^{-B}] \quad \text{(I-4)}$$

where *A* and *B* are model parameters; *A* represents the maximum permanent strain when the number of loading cycles approaches infinity; B controls the evolution of permanent strain with the increase of loading cycles.

Bonaquist and Witczak (1997) developed Eq. (I-5) for granular materials, allowing the effect of strain hardening to be accounted for:

$$\varepsilon_1^p = \sum \frac{1}{N^h} \varepsilon_1 \quad \text{(I-5)}$$

where ε_1 is the permanent strain at the first loading cycle; *h* is the hardening parameter.

I.5.1.2 Effect of stress state

Lashine et al. (1971) found a linear relationship between the permanent strain and the ratio of deviator stress σ_d to confining pressure σ_3:

$$\varepsilon_1^p = a\frac{\sigma_\mathrm{d}}{\sigma_3} \quad \text{(I-6)}$$

where a is model parameter.

Barksdale (1972) proposed Eq. (I-7) to describe the variation of ε_1^p for base course materials, with changes in the ratio of σ_d to σ_3, cohesion *c* and friction angle φ:

$$\varepsilon_1^p = \frac{\frac{\sigma_d}{a\sigma_3^n}}{1-[\frac{(R_f \cdot \sigma_d)(1-\sin\varphi)}{2(c\cdot\cos\varphi+\sigma_3\sin\varphi)}]} \quad \text{(I-7)}$$

where a, n and R_f are model parameters.

Lekarp and Dawson (1998) proposed Eq. (I-8) for describing ε_1^p of unbound granular materials under the combined effects of the ratio of deviator stress σ_d to mean stress p and the length of stress path:

$$\frac{\varepsilon_1^p\,(N_{ref})}{(L/p_0)} = a(\frac{\sigma_d}{p})^b_{max} \quad \text{(I-8)}$$

where $\varepsilon_1^p\ (N_{ref})$ is the accumulated permanent strain after a given number of loading cycles N_{ref}; L is the length of stress path, equal to $(\sigma_d^2 + p^2)^{1/2}$; p_0 is the reference stress; a and b are model parameters.

Gidel et al. (2001) developed Eq. (I-9) for unbound granular materials, allowing the effects of N and stress state on ε_1^p to be accounted for:

$$\varepsilon_1^p = f(N) \cdot g(p_{max}, \sigma_d) \quad \text{(I-9)}$$

with

$$f(N) = A \cdot [1 - (\frac{N}{100})^{-B}] \quad \text{(I-10)}$$

$$g(p_{max}, \sigma_d) = \varepsilon_1^{p_1}(\frac{l_{max}}{p_a})^{n_1} \frac{1}{(m_1 + \frac{s_1}{p_{max}} - \frac{\sigma_d}{p_{max}})} \quad \text{(I-11)}$$

where $f(N)$ is derived from Eq. (I-4) (Hornych et al. 1993); $l_{max} = (\sigma_d^2 + p_{max}^2)^{1/2}$, σ_d and p_{max} are maximum deviator stress and mean stress, respectively; $\varepsilon_1^{p_1}$, n_1, m_1, s_1, A and B are model parameters; p_a is the atmospheric pressure.

Korkiala-Tanttu (2005) proposed Eq. (I-12) for unbound materials, taking the effects of N and deviator stress ratio R on ε_1^p into account:

$$\varepsilon_1^p = cN^b \frac{R}{A-R} \quad \text{(I-12)}$$

where c and b are model parameters; R is the deviator stress ratio, equal to $\sigma_{\mathrm{d}}/\sigma_{\mathrm{d-f}}$, $\sigma_{\mathrm{d-f}}$ is the deviator stress at failure; A is the theoretical maximum deviator stress ratio ($A = R_{\max} = 1.0$); $A = 1.02 – 1.05$ was recommended to avoid numerical problems.

I.5.1.3 Effect of coarse grain content, water content and suction

Trinh et al. (2012) studied the effect of water content on ε_1^p of interlayer soil by large-scale cyclic triaxial tests, and developed Eq. (I-13) allowing the description of ε_1^p variation under the combined effects of loading cycles N, deviator stress σ_{d} and water content:

$$\varepsilon_1^p = f(N) \cdot t(w, \sigma_{\mathrm{d}}) \tag{I-13}$$

with

$$f(N) = A \cdot [1 - (\frac{N}{100})^{-B}] \tag{I-14}$$

$$t(w, \sigma_{\mathrm{d}}) = \varepsilon_1^{p_0} \cdot (w + a) \cdot (\frac{\sigma_{\mathrm{d}}}{p_{\mathrm{a}}})^{b} \tag{I-15}$$

where $f(N)$ is derived from Eq. (I-4) (Hornych et al. 1993); $\varepsilon_1^{p_0}$, a and b are model parameters; p_{a} is the atmospheric pressure.

Azam et al. (2015) investigated the effects of coarse grain content and suction on ε_1^p of soil mixture, and proposed Eq. (I-16) to describe the variation of ε_1^p with loading cycles N, coarse grain content RCM (percent of coarse grain in mixture) and suction ψ:

$$\varepsilon_1^p = aN^b \left(\frac{\psi+1}{p_{\mathrm{a}}}\right)^c (\frac{\mathrm{DDR}}{1+\mathrm{wPI}+\mathrm{RCM}})^d \tag{I-16}$$

where a, b, c and d are model parameters; wPI is the weighted plasticity index, equal to PI × (percent passing 200 sieve/100); PI is the plasticity index (%); 200 sieve refers to 0.075 mm; DDR is the ratio of dry density to the maximum dry density corresponding to optimum moisture content.

Jing et al. (2018) studied the effects of fine soil content and water content on ε_1^p of sand, and developed Eq. (I-17) taking the effects of fines content f_c (the ratio of the mass of fine soil to that of mixture), deviator stress σ_d and water content on ε_1^p into account:

$$\varepsilon_1^p = R[1 - \left(\frac{N}{100}\right)^{\left(\frac{k'}{w}+o'*f_c\right)}] \cdot g(f_c, \sigma_d, w) \tag{I-17}$$

with

$$g(f_c, \sigma_d, w)=[a \cdot (\frac{w}{k})^{o \cdot f_c{}^u}] \cdot [\frac{l_{max}}{p_a}]^n \cdot \frac{1}{m+\frac{s}{p_{max}}-\frac{\sigma_d}{p_{max}}} \tag{I-18}$$

where R, k', o', a, k, o, u, n, m and s are model parameters; $l_{max} = (\sigma_d^2 + p_{max}^2)^{1/2}$, σ_d and p_{max} are maximum deviator stress and mean stress, respectively.

Furthermore, the effects of fines content f_c and water content on ε_1^p in Eq. (I-17) were substituted by that of suction ψ in Eq. (I-19):

$$\varepsilon_1^p = T[1 - \left(\frac{N}{100}\right)^{e \cdot \ln(\frac{\psi}{\psi_a})+f}] \cdot b \cdot \left(\frac{\psi}{\psi^*}\right)^d \cdot (\frac{l_{max}}{p_a})^n \cdot \frac{1}{m+\frac{s}{p_{max}}-\frac{\sigma_d}{p_{max}}} \tag{I-19}$$

where ψ^* is the suction value corresponding to the intersection point of wetting and drying paths of SWRC; ψ_a = 100 kPa; T, e, f, b, d, n, m and s are model parameters.

I.5.2 Resilient modulus

The resilient modulus is a fundamental parameter to describe the stiffness of soil mixture under cyclic loading. The resilient modulus of soil mixture was highly dependent on stress state, coarse grain content and suction (or water content). The constitutive models of resilient modulus were developed by incorporating these factors.

I.5.2.1 Effect of stress state

Seed et al. (1967) studied the resilient modulus of subgrade soil, and described the resilient modulus as a function of bulk stress:

$$M_{\mathrm{r}} = k_1(\frac{\theta}{p_{\mathrm{a}}})^{k_2} \quad \text{(I-20)}$$

where k_1 and k_2 are model parameters; θ is the bulk stress, equal to the sum of three principal stresses σ_1, σ_2 and σ_3.

Thompson and Robnett (1979) investigated the resilient properties of 50 Illinois fine-grained soil, and proposed bilinear models of stress – dependent resilient modulus for cohesive soil:

$$M_{\mathrm{r}} = k_2 + k_3(k_1 - \sigma_{\mathrm{d}}) \text{ , } k_1 > \sigma_{\mathrm{d}} \quad \text{(I-21)}$$

$$M_{\mathrm{r}} = k_2 + k_4(\sigma_{\mathrm{d}} - k_1) \text{ , } k_1 < \sigma_{\mathrm{d}} \quad \text{(I-22)}$$

where k_1, k_2, k_3 and k_4 are model parameters; σ_{d} is the deviator stress.

Moossazadeh and Witczak (1981) proposed a deviator stress model for cohesive soil, which was widely used:

$$M_{\mathrm{r}} = k_1(\frac{\sigma_{\mathrm{d}}}{p_{\mathrm{a}}})^{k_2} \quad \text{(I-23)}$$

where k_1 and k_2 are model parameters.

The Mechanistic-Empirical Pavement Design Guide (MEPDG 2004) (ARA, Inc., ERES Consultants Division 2004) recommended Eq. (I-24) to estimate the resilient modulus:

$$M_{\mathrm{r}} = k_1 p_{\mathrm{a}}(\frac{\theta}{p_{\mathrm{a}}})^{k_2}(\frac{\tau_{\mathrm{oct}}}{p_{\mathrm{a}}} + 1)^{k_3} \quad \text{(I-24)}$$

where k_1, k_2, and k_3 are model parameters; τ_{oct} is the octahedral shear stress.

I.5.2.2 Effect of coarse grain content

The coarse grain content significantly affected the resilient modulus of soil mixture, as shown by Duong et al. (2016) and Wang et al. (2017). However, very few models have been proposed to describe such coarse grain content effect.

The MEPDG (2004) adopted Eq. (I-25) to predict the resilient modulus of coarse-grained and fine-grained materials, with varying values of model parameters *a*, *b* and k_{m} (Table I-4):

$$\log\frac{M_{\mathrm{r}}}{M_{\mathrm{r-opt}}} = a + \frac{b-a}{1+\exp(\ln\frac{-b}{a} + k_m\cdot(S_{\mathrm{r}} - S_{\mathrm{r-opt}}))} \quad \text{(I-25)}$$

where M_r/M_{r-opt} is the resilient modulus ratio; M_r is the resilient modulus at a given degree of saturation S_r; M_{r-opt} is the resilient modulus at a degree of saturation corresponding to the optimum moisture content S_{r-opt}; *a*, *b* and k_m are model parameters.

Table I-4. Model parameters *a*, *b* and k_m for coarse-grained and fine-grained materials (MEPDG 2004)

Parameter	Coarse-grained materials	Fine-grained materials
a	-0.3123	-0.5934
b	0.3	0.4
k_m	6.8157	6.1324

I.5.2.3 Effect of suction

Empirical relationships between resilient modulus M_r and matric suction ψ were developed by some investigators. Some of such models were summarized below.

Johnson et al. (1986) proposed an empirical model for sandy soil:

$$M_r = 1.35 \times 10^6 \times (101.36 - \psi)^{2.36}(J_1)^{3.25}(\rho_d)^{3.06} \quad \text{(I-26)}$$

where J_1 is the first stress invariant; ρ_d is the dry density.

Parreira and Gonçalves (2000) studied the effect of ψ on M_r for the lateritic soil from Brazil under cyclic triaxial tests, and established a relationship between M_r, deviator stress σ_d and ψ:

$$M_r = 14.10(\sigma_d)^{0.782}(\psi)^{0.076} \quad \text{(I-27)}$$

Doucet and Doré (2004) proposed Eq. (I-28) for crushed granular materials from Canada:

$$M_r = 1060\theta - 8700\psi + 5700 \quad \text{(I-28)}$$

Sawangsuriya et al. (2009) investigated the effect of ψ on M_r for four compacted subgrade soils, and proposed Eqs. (I-29) and (I-30) by considering two reference M_r values - M_{r-sat} and M_{r-opt}, respectively:

$$\frac{M_r}{M_{r-sat}} = -5.61 + 4.54\log(\psi) \quad \text{(I-29)}$$

$$\frac{M_r}{M_{r-opt}} = -0.24 + 0.25\log(\psi) \quad \text{(I-30)}$$

where $M_{\mathrm{r-sat}}$ and $M_{\mathrm{r-opt}}$ are M_{r} under saturated and optimum moisture content conditions, respectively.

Ba et al. (2013) proposed Eq. (I-31) to describe the variation of resilient modulus ratio $M_r/M_{\mathrm{r-opt}}$ with ψ for four unbound granular materials:

$$\frac{M_{\mathrm{r}}}{M_{\mathrm{r-opt}}} = 0.385 + 0.267\log(\psi) \tag{I-31}$$

These empirical models were developed based on limited experimental results using regression analysis, which were difficult to be generalized to other materials. The constitutive models considering stress state above (e.g. I-23 and I-24) can be revised, by either incorporating the suction into the stress state, or adding the suction as an independent term. Compared with empirical models, these revised constitutive models were more generalizable.

Loach (1987) investigated the resilient response of three clays under varying deviator stresses and suctions, and proprosed Eq. (I-32):

$$M_{\mathrm{r}} = \frac{\sigma_{\mathrm{d}}}{k_1}\left(\frac{c\sigma_{\mathrm{c}}+\psi}{\sigma_{\mathrm{d}}}\right)^{k_2} \tag{I-32}$$

where k_1 and k_2 are model parameters; c is the compressibility factor; σ_{c} is the confining stress.

Heath et al. (2004) proposed Eq. (I-33) for granular base materials, allowing the combined effects of ψ, stress state and pore air pressure to be accounted for:

$$M_{\mathrm{r}} = k_1 p_{\mathrm{a}}\left(\frac{\frac{\theta}{3}-u_{\mathrm{a}}+\chi\psi}{p_{\mathrm{a}}}\right)^{k_2}\left(\frac{\sigma_{\mathrm{d}}}{p_{\mathrm{a}}}\right)^{k_3} \tag{I-33}$$

where k_1, k_2 and k_3 are model parameters; u_{a} is the pore air pressure; χ is the Bishop's effective stress parameter.

Yang et al. (2005) investigated the variation of resilient modulus with ψ for compacted subgrade soil, and incorporated ψ into σ_{d} in Eq. (I-34):

$$M_{\mathrm{r}} = k_1(\sigma_{\mathrm{d}} + \chi\psi)^{k_2} \tag{I-34}$$

where k_1 and k_2 are model parameters.

Gupta et al. (2007) studied the effect of ψ on resilient modulus for four fine-grained subgrade soils, and found a power relationship between resilient modulus and ψ:

$$M_{\mathrm{r}} = k_1 p_{\mathrm{a}} \left(\frac{\theta - 3k_4}{p_{\mathrm{a}}}\right)^{k_2} \left(\frac{\tau_{\mathrm{oct}}}{p_{\mathrm{a}}} + k_5\right)^{k_3} + \alpha_1 \psi^{\beta_1} \quad \text{(I-35)}$$

where k_1-k_5, α_1 and β_1 are model parameters.

Liang et al. (2008) studied the effects of stress state and water content on the resilient modulus of cohesive soil, and incorporated the ψ into θ in Eq. (I-36):

$$M_{\mathrm{r}} = k_1 p_{\mathrm{a}} \left(\frac{\theta + \chi\psi}{p_{\mathrm{a}}}\right)^{k_2} \left(\frac{\tau_{\mathrm{oct}}}{p_{\mathrm{a}}} + 1\right)^{k_3} \quad \text{(I-36)}$$

where k_1, k_2 and k_3 are model parameters.

Khoury et al. (2009) investigated the effect of ψ on the resilient modulus of 18 undisturbed subgrade soil specimens, and proposed Eq. (I-37):

$$M_{\mathrm{r}} = k_1 p_{\mathrm{a}} \left(\frac{\theta}{p_{\mathrm{a}}}\right)^{k_2} \left(\frac{\tau_{\mathrm{oct}}}{p_{\mathrm{a}}} + k_4\right)^{k_3} + \alpha_1 \psi^{\beta_1} \quad \text{(I-37)}$$

where k_1-k_4, α_1 and β_1 are model parameters.

Caicedo et al. (2009) performed small strain cyclic triaxial tests on non-standard granular materials, and developed Eq. (I-38):

$$M_{\mathrm{r}} = k_1 p_{\mathrm{a}} \left(1 + k_2 \frac{\sigma_{\mathrm{d}}}{p_{\mathrm{a}}}\right) \left(\frac{\psi}{p_{\mathrm{a}}}\right)^{k_3} \frac{f(e)}{f(0.33)} \quad \text{(I-38)}$$

where k_1, k_2 and k_3 are model parameters; $f(e) = (1.93 - e)^2/(1 + e)$, e is void ratio.

Khoury et al. (2011) incorporated the effect of hysteresis on the resilient modulus of reconstituted silty soil:

$$M_{\mathrm{r}} = \left[k_1 p_{\mathrm{a}} \left(\frac{\theta}{p_{\mathrm{a}}}\right)^{k_2} \left(\frac{\tau_{\mathrm{oct}}}{p_{\mathrm{a}}} + 1\right)^{k_3} + (\psi - \psi_0)\left(\frac{\theta_{\mathrm{d}}}{\theta_{\mathrm{s}}}\right)^{\frac{1}{n}}\right] \times \frac{\theta_{\mathrm{d}}}{\theta_{\mathrm{w}}} \quad \text{(I-39)}$$

where k_1, k_2 and k_3 are model parameters; n is the model parameter obtained from the Fredlund and Xing (1994) soil-water retention curve (SWRC) model; θ_{s} is the saturated volumetric water content; θ_{d} and θ_{w} are the volumetric water content along the drying and wetting SWRC curves, respectively.

Cary and Zapata (2011) proposed Eq. (I-40) for a granular soil and a clayey sand, by incorporating the positive pore water pressure under saturated condition $\Delta u_{\mathrm{w-sat}}$ and the matric suction variation under unsaturated condition $\Delta\psi$:

$$M_{\mathrm{r}} = k_1 p_{\mathrm{a}} \left(\frac{\theta_{\mathrm{net}} - 3\Delta u_{\mathrm{w-sat}}}{p_{\mathrm{a}}}\right)^{k_2} \left(\frac{\tau_{\mathrm{oct}}}{p_{\mathrm{a}}} + 1\right)^{k_3} \left(\frac{\psi - \Delta\psi}{p_{\mathrm{a}}} + 1\right)^{k_4} \quad \text{(I-40)}$$

where k_1-k_4 are model parameters; θ_{net} is net bulk stress.

Oh et al. (2012) considered in-situ water content in Eq. (I-41) for granular base and subgrade soils:

$$M_{\mathrm{r}} = k_1 p_{\mathrm{a}} \left(\frac{\theta + 3k_4\psi\theta_1}{p_{\mathrm{a}}}\right)^{k_2} \left(\frac{\tau_{\mathrm{oct}}}{p_{\mathrm{a}}} + 1\right)^{k_3} \quad \text{(I-41)}$$

where k_1, k_2, k_3 and k_4 are model parameters; θ_1 is the volumetric water content.

Ng et al. (2013) investigated the resilient modulus of subgrade soil under varying deviator stresses and suctions by suction-controlled cyclic tests, and proposed Eq. (I-42):

$$M_{\mathrm{r}} = M_0 \left(\frac{p}{p_{\mathrm{r}}}\right)^{k_1} \left(\frac{\sigma_{\mathrm{d}}}{p_{\mathrm{r}}} + 1\right)^{k_2} \left(\frac{\psi}{p} + 1\right)^{k_3} \quad \text{(I-42)}$$

where k_1, k_2 and k_3 are model parameters; p is the net mean stress; p_{r} is the reference pressure; M_0 is the M_{r} value at reference stress state when ψ = 0, $p = p_{\mathrm{r}}$ and $\sigma_{\mathrm{d}} = p_{\mathrm{r}}$.

Han and Vanapalli (2015) proposed Eq. (I-43) to predict the variation of resilient modulus with suction for 11 different compacted subgrade soils. The soil-water retention curve was incorporated.

$$\frac{M_{\mathrm{r}} - M_{\mathrm{r-sat}}}{M_{\mathrm{r-opt}} - M_{\mathrm{r-sat}}} = \frac{\psi}{\psi_{\mathrm{opt}}} \left(\frac{S_{\mathrm{r}}}{S_{\mathrm{r-opt}}}\right)^{\xi} \quad \text{(I-43)}$$

where $M_{\mathrm{r-sat}}$ is the resilient modulus under saturated condition; $M_{\mathrm{r-opt}}$ and ψ_{opt} are resilient modulus and matric suction under optimum moisture content condition; S_{r} is the degree of saturation; $S_{\mathrm{r-opt}}$ is the degree of saturation corresponding to the optimum moisture content; ξ is model parameter.

I.6 Conclusions

This chapter firstly shows a comparison between the intact interlayer soil from the field and the reconstituted soil mixture prepared in the laboratory, showing a good agreement in terms of grain size distribution and plasticity of fine soil fraction. Then, the water retention behavior of soil mixture was reviewed. The mechanical behaviors of soil mixture including static behavior and dynamic characteristics were also presented. Finally, the constitutive models of permanent strain and resilient modulus were summarized. The following conclusions can be drawn:

Considering the difficulty of obtaining intact interlayer soil, the reconstituted soil mixture was adopted in previous studies. The effect of coarse grain content on the mechanical behavior of soil mixture was investigated. They assumed that under a given water content, the matric suction of mixture kept constant at the same dry density of fine soil fraction, whatever the coarse grain content. Up to now, this point has not been experimentally examined yet.

Previous studies show the effect of coarse grain content on the static behavior of soil mixture. However, the effect of water content was not investigated. Compacted under different water contents, the fine soil fraction can exhibite different microstructures, which significantly affected the mechanical behavior. This aspect has not been investigated. In addition, the fabric of soil mixture was separated into two zones by a characteristic value of coarse grain content: a fine matrix macrostructure when the coarse grain content is smaller than this value, and a coarse grain skeleton fabric when the coarse grain content is larger than this value. No studies addressed the effect of water content on the characteristic value of coarse grain content.

The effect of coarse grain content on the long-term permanent deformation of soil mixture was investigated. However, the effect of water content has not been considered. Moreover, in most studies, the dry density of soil mixture was constant, leading to a decrease of dry density of fine soil fraction with increasing coarse grain content. In that case, both coase grain content and matric suction affected the permanent strain behavior, making the analysis difficult.

The effect of coarse grain content on the short-term dynamic behavior of mixture was studied. However, the effect of water content was not investigated. In particular, the difference of the characteristic coarse grain content under monotonic and cyclic loadings was not analyzed.

Some constitutive models were proposed for the permanent strain, taking the effects of loading cycles and stress state into account. However, the effect of coarse grain content has not been

incorporated. Furthermore, no existing constitutive models have been developed to describe the variation of permanent strain of soil mixture with changes in loading cycles, stress state, coarse grain content and matric suction.

Some constitutive models were proposed for the resilient modulus, allowing the stress state and matric suction to be taken into consideration. However, no existing constitutive models described the coupled effects of stress state and matric suction. In addition, the effect of coarse grain content on resilient modulus has not been incorporated.

CHAPTER II. WATER RETENTION BEHAVIOR OF SOIL MIXTURE

The water retention property can greatly affect the mechanical behaviour of unsaturated fine/coarse soil mixture. In-situ investigation showed that for the interlayer soil, the coarse grain content decreased over depth. Besides, the dry density of fine soil varied, due to different vertical stresses at different depths. Thus, it appears essential to investigate the effects of coarse grain content f_v and dry density of fine soil $\rho_{d\text{-}f}$ on the water retention behaviour of soil mixture.

Three f_v values under the same $\rho_{d\text{-}f}$ and three $\rho_{d\text{-}f}$ values under the same f_v were considered. The filter paper method was adopted to measure the matric suction ψ. Mercury intrusion porosimetry tests were performed for microstructure observation of fine soil. Results showed that when plotted in terms of gravimetric water content with ψ, the soil-water retention curve (SWRC) was significantly affected by $\rho_{d\text{-}f}$ at ψ < 715 kPa, while independent of $\rho_{d\text{-}f}$ at ψ > 715 kPa. This threshold matric suction corresponded to the delimiting pore diameter of bi-modal microstructure of fine soil, which separated the micro-pores from macro-pores. When plotted in terms of degree of saturation with ψ, the SWRC was affected by $\rho_{d\text{-}f}$ in the full suction range, while independent of f_v. These findings indicated that the decrease of f_v induced no change in water retention property of interlayer soil, when the $\rho_{d\text{-}f}$ kept constant. In addition, the SWRC could be incorporated into the constitutive model for unsaturated soil mixture, allowing the description of permanent strain with change in ψ under the effect of cyclic loading. All these results were presented in a paper published in Canadian Geotechnical Journal.

Su, Y., Cui, Y. J., Dupla, J. C., & Canou, J. 2021. Canadian Geotechnical Journal.

Soil-water retention behaviour of fine/coarse soil mixture with varying coarse grain contents and fine soil dry densities

Yu Su, Yu-Jun Cui, Jean-Claude Dupla, Jean Canou

Abstract: An interlayer soil identified in the French conventional rail track corresponded to a mixture of fine soil and coarse grains. To investigate the role of fines in the soil-water retention property of such mixture, different coarse grain contents f_v and dry densities of fine soil $\rho_{d\text{-}f}$ were considered. The filter paper method was applied to measure the matric suction. Mercury intrusion porosimetry tests were performed for the microstructure observation of fine soil. In terms of gravimetric water content of fine soil w_f with matric suction ψ, the soil-water retention curve (SWRC) was significantly affected by $\rho_{d\text{-}f}$ for ψ < 715 kPa, while independent of $\rho_{d\text{-}f}$ for ψ > 715 kPa. Interestingly, this threshold ψ corresponded to a delimiting pore diameter of bi-modal microstructure of fine soil, which separated micro-pores from macro-pores. In terms of degree of saturation S_r with ψ, the SWRC was significantly affected by $\rho_{d\text{-}f}$ in the full suction range, while independent of f_v. These findings help better understand the results on samples with the dry density of mixture ρ_d kept constant: an increase of f_v resulted in a decrease of $\rho_{d\text{-}f}$ and the suction changed accordingly. In that case, both f_v and ψ affected the mechanical behavior.

Keywords: soil-water retention; matric suction; pore size distribution; dry density; coarse grain content

Introduction

In the French conventional rail track, an interlayer was naturally created in the substructure under the long-term traffic loading, which corresponded to a mixture of ballast grains and subgrade fine soil. As its suction can greatly affect its mechanical behavior (see details in Su et al. 2020a and Wang et al. 2018), it appears important to investigate its water retention property in-depth.

In-situ investigations showed a decrease of ballast grain content with the increasing depth of interlayer soil (Trinh 2011, Cui et al. 2013). Globally, the interlayer soil was separated into two parts: the upper part was characterized by a coarse grain skeleton fabric, and the lower part by a fine matric macrostructure with dispersed coarse grains. In addition, due to the different vertical stresses over depths, the dry density of fine soil $\rho_{d\text{-}f}$ was different. Wang et al. (2017, 2018), Cui (2018) and Qi et al. (2020a) studied the effect of coarse grain content f_v (the ratio of

Ecole des Ponts ParisTech, Laboratoire Navier/CERMES, 6 – 8 av. Blaise Pascal, Cité Descartes, Champs-sur-Marne, 77455 Marne – la – Vallée cedex 2, France

the volume of coarse grains V_c to the volume of total sample V) on the mechanical behavior of interlayer soil at a constant $\rho_{d\text{-}f}$ = 1.82 Mg/m^3. They assumed that under a given water content, the matric suction of mixture was the same at a constant $\rho_{d\text{-}f}$ = 1.82 Mg/m^3. Up to now, this point has not been experimentally examined yet. It seems necessary to verify this point by investigating the effects of coarse grain content f_v and dry density of fine soil $\rho_{d\text{-}f}$ on the soil-water retention property of fine/coarse soil mixture.

The effects of dry density and coarse grain content on soil-water retention property were investigated previously in some studies. The filter paper method (ASTM D5298-10, 2010) was usually adopted for the measurement of suction (Muñoz-Castelblanco et al. 2010; Kim et al. 2015; Jing 2017). It appeared that the effect of dry density on soil-water retention behavior was strongly dependent on the microstructure (Simms and Yanful 2002; Romero et al. 2011). Romero et al. (1999) studied the effect of dry density on water retention and microstructure of Boom clay by vapor equilibrium technique and mercury intrusion porosimetry tests, respectively. The results showed that the soil-water retention curve (SWRC) in the low suction range was governed by the inter-aggregate pores, while that in high suction range was governed by intra-aggregate pores. Similarly, Salager et al. (2013) and Gao and Sun (2017) investigated the water retention capacity of clayey soil and found that the SWRCs for different dry densities was independent of dry density beyond a certain matric suction. It is worth noting that these studies only involved the effect of dry density without the effect of coarse grain content. Fiès et al. (2002) studied the soil-water retention property of fine soil/glass fragments mixture, and found that increasing glass content led to a reduction of the amount of water stored in the mixture. Baetens et al. (2009) investigated the effect of rock fragments on the water retention property of stony soil, and reported that rock fragments could affect the SWRC when the matric suction was smaller than 30 kPa. Duong et al. (2014) studied the hydraulic behavior of interlayer soil by infiltration column, and observed that increasing coarse grain content resulted in a lower SWRC or a lower water retention capacity. Note that in most of these studies, the effect of coarse grain content on soil-water retention property of mixture was investigated with a large quantity of coarse grains, which corresponded to the coarse grain skeleton structure of mixture, without considering the fine matric macrostructure. In addition, the dry density of mixture ρ_d was taken constant, leading to a decrease of dry density of fine soil $\rho_{d\text{-}f}$ with the increase of coarse grain content. That would increase the difficulty of analysis while studying the effect of suction.

This study aims to investigate the effects of coarse grain content f_v and dry density of fine soil $\rho_{d\text{-}f}$ on soil-water retention property of fine/coarse soil mixture. Three f_v = 0%, 20% and 35% were adopted at the same $\rho_{d\text{-}f}$ = 1.82 Mg/m^3 for studying the effect of f_v, and three $\rho_{d\text{-}f}$ =1.82, 1.67 and 1.52 Mg/m^3 were adopted at the same f_v = 0% for studying the effect of $\rho_{d\text{-}f}$. The filter paper method was applied to measure the matric suction of soil mixture. The microstructure of fine soil under varying $\rho_{d\text{-}f}$ values was determined by mercury intrusion porosimetry tests. The results obtained allowed the effects of f_v and $\rho_{d\text{-}f}$ on soil-water retention property of soil mixture to be clarified.

Materials and methods

Fine soil and coarse grains

Considering the difficulty of extracting intact interlayer soil from the field, the reconstituted fine soil and coarse grains were fabricated in the laboratory. For the fine soil fraction, to obtain a similar grain size distribution of fines from 'Senissiat site' (Trinh 2011) (Fig. 1), nine different mass proportions of commercial soils were mixed (Table 1; see details in Lamas-Lopez 2016). The liquid limit and plasticity index of the reconstituted fine soil were 32% and 20%, respectively. Consequently, a good agreement between in-situ fine soil and reconstituted fine soil was observed in terms of grain size distribution, plasticity index and liquid limit (see details in Wang et al. 2017). Fig. 2 presents the standard Proctor compaction curve of the reconstituted fine soil, defining an optimum water content $w_{opt\text{-}f}$ = 13.7% and a maximum dry density $\rho_{dmax\text{-}f}$ = 1.82 Mg/m^3. Note that the $\rho_{dmax\text{-}f}$ = 1.82 Mg/m^3 of reconstituted fine soil was consistent with the $\rho_{d\text{-}f}$ = 1.80 Mg/m^3 of in-situ fine soil measured by Lamas-Lopez (2016). Based on above features, the reconstituted fine soil was considered as representative of the in-situ fine soil. For the coarse grains fraction, the micro-ballast was adopted to replace the real ballast by following a parallel gradation method adopted by Wang et al. (2017) and Su et al. (2020a). The validity of this method was verified by Qi et al. (2020b), who performed comparisons between micro-ballast and ballast in terms of mechanical behavior under static and cyclic loadings. Note that the scaled fine/coarse soil mixture was used as representative of interlayer soil taken from Senissiat (near Lyon, France, Trinh 2011), which was far from the coastal. Thus, the salt content-related osmotic suction was ignored and only the matric suction was taken into account in this study.

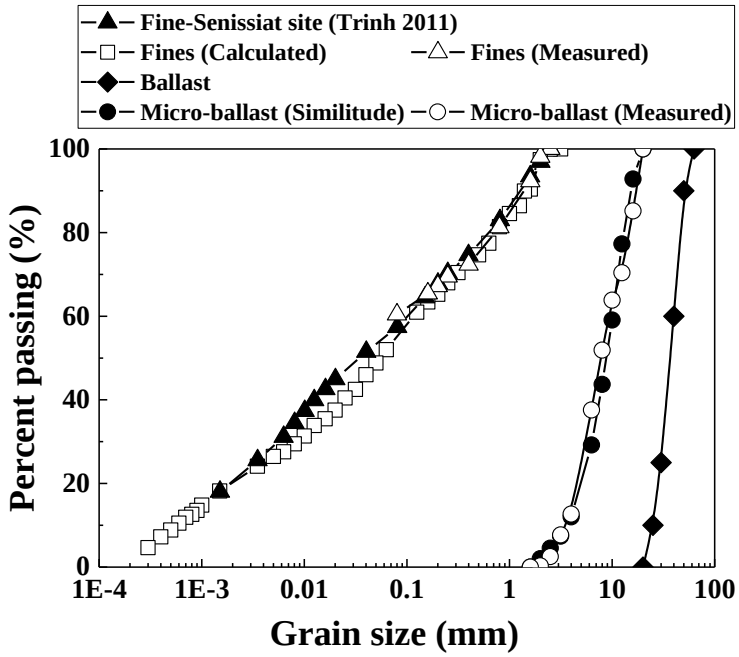

Fig. 1. Grain size distribution curves of fine soil and micro-ballast (after Wang et al. 2017)

Table 1. Constitution of fine soil

Soil classification	Commercial Soil	Mass proportion (%)	Range of grain size (mm)
Sand	C4	16.7	0.0009 – 0.50
	C10	20	0.0009 – 0.25
	HN34	3.3	0.063 - 0.50
	HN31	3.3	0.16 - 0.63
	HN0.4-0.8	6.7	0.25 - 1
	HN0.6-1.6	6.7	0.32 - 2
	HN1-2.5	13.3	0.32 – 3.20
Clay	Speswhite	23.3	0.0003 – 0.01
	Bentonite	6.7	0.001 – 0.01

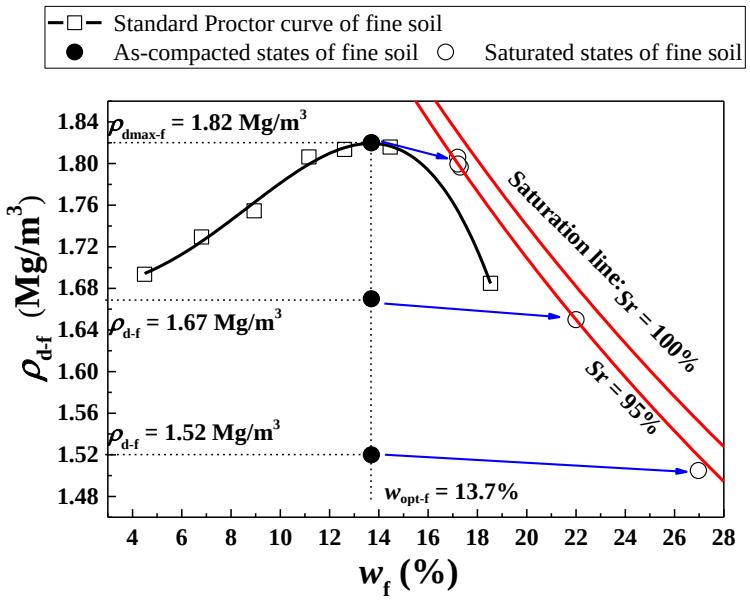

Fig. 2. As-compacted and saturated states of fine soil with respect to its standard Proctor compaction curve

Parameter f_v, widely adopted in previous studies (Seif El Dine et al. 2010; Wang et al. 2017, 2018; Su et al. 2020a, 2020b), was considered in this study. Based on the definition of f_v (Eq.(1)), which only quantified the amount of dry coarse grains in the mixture, all voids and water were assumed to be contained in the fine soil (Fig. 3), as in Wang et al. (2018) and Su et al. (2020a). Based on this assumption, the degree of saturation S_r of mixture can be related to the fine soil fraction. :

$$f_v = \frac{V_c}{V} = \frac{V_c}{V_c+V_f} = \frac{V_c}{V_c+V_{s-f}+V_{w-f}+V_{a-f}} \quad (1)$$

where V_f is the volume of fine soil; $V_{s\text{-}f}$, $V_{w\text{-}f}$ and $V_{a\text{-}f}$ are the volume of fine grains, water and air in the fine soil.

For the soil mixture at varying f_v, $\rho_{d\text{-}f}$ and water content w_f of fine soil, the mass of coarse grains $m_{s\text{-}c}$, fine grains $m_{s\text{-}f}$ and water content of fine soil $m_{w\text{-}f}$ could be determined as follows:

$$m_{s-c} = V_c \cdot G_{s-c} \cdot \rho_w = f_v \cdot V \cdot G_{s-c} \cdot \rho_w \quad (2)$$

$$m_{s-f} = \rho_{d-f} \cdot V_f = \rho_{d-f} \cdot V \cdot (1 - f_v) \quad (3)$$

$$m_{w-f} = w_f \cdot m_{s-f} \quad (4)$$

where $G_{s\text{-}c}$ is the specific gravity of coarse grains; ρ_w is the water unit mass.

For the soil mixture at a given $\rho_{d\text{-}f}$, the corresponding void ratio of fine soil e_f could be deduced using Eq. (5):

$$e_f = \frac{G_{s-f} \cdot \rho_w}{\rho_{d-f}} - 1 \tag{5}$$

where $G_{s\text{-}f}$ is the specific gravity of fine soil.

Then, the void ratio e_m of soil mixture can be determined:

$$e_m = \frac{V_{v-f}}{V_c + V_{s-f}} = \frac{V_{v-f}}{V - V_{v-f}} \tag{6}$$

$$V_{v-f} = e_f \cdot V_{s-f} \tag{7}$$

$$V_{s-f} = \frac{m_{s-f}}{G_{s-f} \cdot \rho_w} \tag{8}$$

where $V_{v\text{-}f}$ is the volume of voids in fine soil; $V_{s\text{-}f}$ is the volume of fine grains.

Combining Eqs. (1), (3) and (5)-(8), the void ratio e_m of soil mixture at varying f_v and $\rho_{d\text{-}f}$ was obtained:

$$e_m = -1 + \frac{1}{1 - \frac{(G_{s-f} \cdot \rho_w - \rho_{d-f}) \cdot (1 - f_v)}{G_{s-f} \cdot \rho_w}} \tag{9}$$

Fig. 4 shows the variations of e_f and e_m with f_v at a constant $\rho_{d\text{-}f}$ = 1.82 Mg/m^3. The e_f and e_m were obtained by substituting $\rho_{d\text{-}f}$ = 1.82 Mg/m^3 and $G_{s\text{-}f}$ = 2.68 (Duong et al. 2016) into Eqs. (5) and (9), respectively:

$$e_f = 0.47 \tag{10}$$

$$e_m = -1 + \frac{1}{1 - 0.32 \cdot (1 - f_v)} \tag{11}$$

As mentioned before, all voids and water were assumed to be contained in the fine soil. Thus, the S_r represented both degree of saturation of soil mixture and that of fine soil:

$$S_r = \frac{V_{w-f}}{V_{v-f}} \tag{12}$$

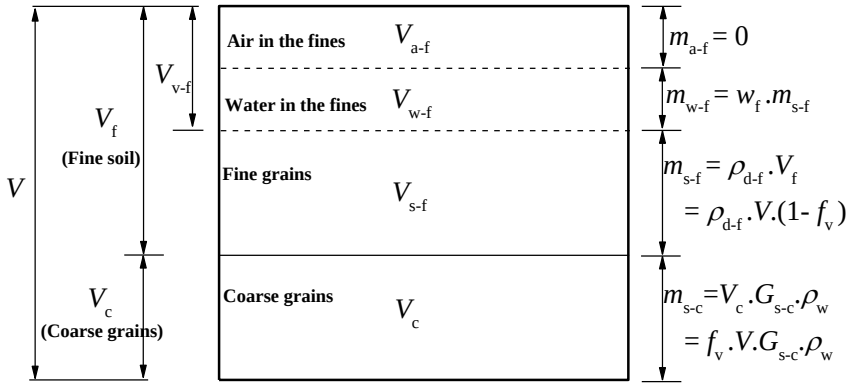

Fig. 3. Constitution of fine/coarse soil mixture

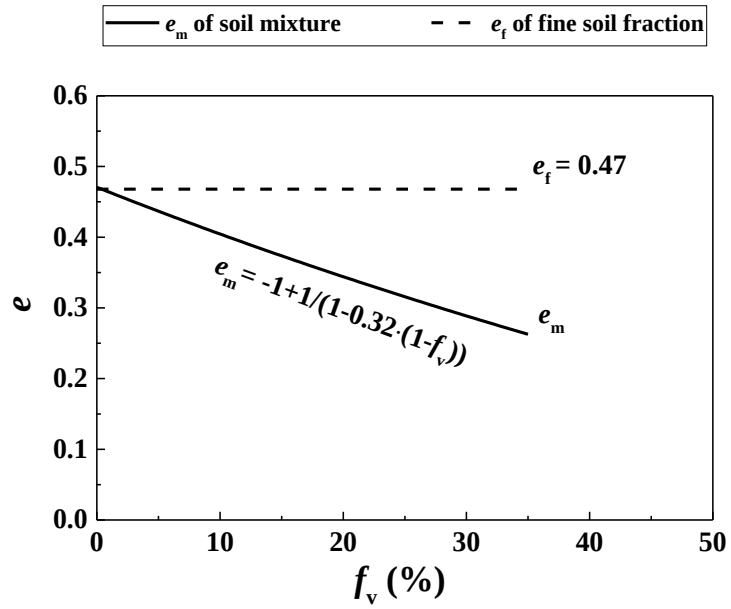

Fig. 4. Variations of void ratios with f_v at a constant ρ_{d-f} = 1.82 Mg/m^3

Filter paper method

The filter paper method (ASTM D5298-10, 2010) was used to measure the matric suction. Filter paper measurement was generally performed by putting a piece of filter paper between two soil disks to attain suction equilibrium between filter paper and soil disks (ASTM D5298-10 2010; Muñoz-Castelblanco et al. 2010; Kim et al. 2015; Jing 2017). Considering the maximum diameter d = 20 mm of coarse grains (Fig. 1), the soil disk was prepared at 100 mm diameter and 100 mm height. As for the preparation of soil disks, the fine soil (Fig. 5(a)) was prepared at a molding water content $w_{opt\text{-}f}$ = 13.7%, then stored in a container for at least 24 h, allowing water homogenization. After that, the fine soil was thoroughly mixed with the coarse grains (Fig. 5(a)) with their pre-determined masses at target f_v and $\rho_{d\text{-}f}$ values (Table 2). Note that a characteristic coarse grain content $f_{v\text{-}cha} \approx 27\%$ identified by Wang et al. (2018) separated the coarse grain skeleton fabric ($f_v > f_{v\text{-}cha}$) and the fine matrix macrostructure ($f_v < f_{v\text{-}cha}$) of mixture. Both fabrics were considered in this study with f_v ranging from 0% to 35%. The fine/coarse soil mixture were then compacted in four layers, with an equal amount of fine soil and coarse grains for each layer (Fig. 5(b)). Table 2 presents the variations of e_f, S_r and the dry density of soil mixture ρ_d with f_v and $\rho_{d\text{-}f}$ at a molding water content of fine $w_{opt\text{-}f}$ = 13.7%. After compaction, the soil disks at different f_v and $\rho_{d\text{-}f}$ values were wetted from the molding states to the saturated state. The approach proposed by Su et al. (2020c) was adopted during the wetting process: 10 g water was distributed uniformly on the surface of soil disk by a sprayer each time. The disk was then covered with plastic film for at least 7 h. Fig. 2 shows that the wetting process of soil disk from a molding state to a nearly saturated state induced a slight decrease of $\rho_{d\text{-}f}$ due to the swelling of fine soil, and consequently a slight increase of e_f and slight decrease of ρ_d (Table 2). The measured w_f and the corresponding S_r of soil disks at nearly saturated state were also presented in Table 2.

Fig. 5. (a) Preparation of fine soil and micro-ballast and (b) compaction of two soil disks

Table 2. As-compacted and saturated states of fine/coarse soil mixture

f_v (%)	As-compacted state					Saturated state				
	$\rho_{d\text{-}f}$ (Mg/m^3)	e_f	$w_{opt\text{-}f}$ (%)	S_r (%)	ρ_d (Mg/m^3)	$\rho_{d\text{-}f}$ (Mg/m^3)	e_f	Measured w_f(%)	Measured S_r(%)	ρ_d (Mg/m^3)
	1.82	0.47		78	1.82	1.81	0.48	17.2	95	1.81
0	1.67	0.60		61	1.67	1.65	0.62	22.0	95	1.65
	1.52	0.76	13.7	48	1.52	1.50	0.78	27.3	93	1.50
20	1.82	0.47		78	1.99	1.80	0.49	17.3	95	1.97
35	1.82	0.47		78	2.12	1.80	0.48	17.2	95	2.10

Note: f_v represents the volumetric ratio of coarse grains to the fine/coarse soil mixture. $\rho_{d\text{-}f}$, e_f, $w_{f,}$ and $w_{opt\text{-}f}$ represent the dry density, void ratio, water content and optimum water content of fine soil, respectively. S_r represents the degree of saturation of fine soil, which is also the degree of saturation of the mixture. ρ_d represents the dry density of soil mixture.

To obtain the drying soil-water retention curve of soil mixture at a given f_v and $\rho_{d\text{-}f}$, 10 suction measurements were conducted, corresponding to 10 target w_f values. When a soil disk reached a target w_f value, it was covered with plastic film for at least 24 h prior to measuring its matric suction. A set of three filter paper was prepared, with the middle filter paper (diameter d = 80mm) slightly smaller than the two outer filter paper (d = 90mm) to avoid contamination of

the middle one. The set of three filter papers was then placed between two soil disks. The whole set was covered with plastic film, and then sealed with wax. Note that an initial water content of 4.61% of the filter paper was measured, corresponding to a suction of 93 MPa. In this case, the filter paper followed a wetting process during the equilibration process between soil and filter paper. After equilibration, the water content of soil disks and the middle filter paper were measured, with a balance of 1/10000 g accuracy. The corresponding matric suction was then determined for varying f_v, $\rho_{d\text{-}f}$ and w_f values. It is worth noting that the volume of soil disks at different w_f values was also measured, by means of a caliper.

Mercury intrusion porosimetry test (MIP)

For the MIP tests, three soil disks were prepared at varying $\rho_{d\text{-}f}$ = 1.82, 1.67 and 1.52 Mg/m^3 with the same f_v = 0%. The freeze-drying method was adopted: fine soil was cut into small pieces of around 1.5 g each, and then immersed into nitrogen under vacuum; afterwards, the frozen soil was transferred to the chamber of a freeze dryer for lyophilizing. This method minimized the microstructure disturbance of fine soil, which was widely used in previous studies (Cui et al. 2002; Delage et al. 2006; Wang et al. 2014).

Results

To determine the equilibration time of samples with the filter paper method, three samples were prepared at the same f_v = 0%, $\rho_{d\text{-}f}$ = 1.82 Mg/m^3 and $w_{opt\text{-}f}$ = 13.7%, with 5, 7 and 9 days waited, respectively. Fig. 6 depicts the variations of matric suction and water content of filter paper with time. It appears that with the increase of time from 0 to 5, 7 and 9 days, the water content of filter paper increased from 4.61% to 30.59%, 32.02% and 32.11%, and the corresponding matric suction decreased from 93 MPa to 879, 679 and 670 kPa, respectively. This indicated that at least a time of 7 days was needed for the suction equilibration between soil and filter paper. Thereby, a duration of 7 days was adopted for all tests.

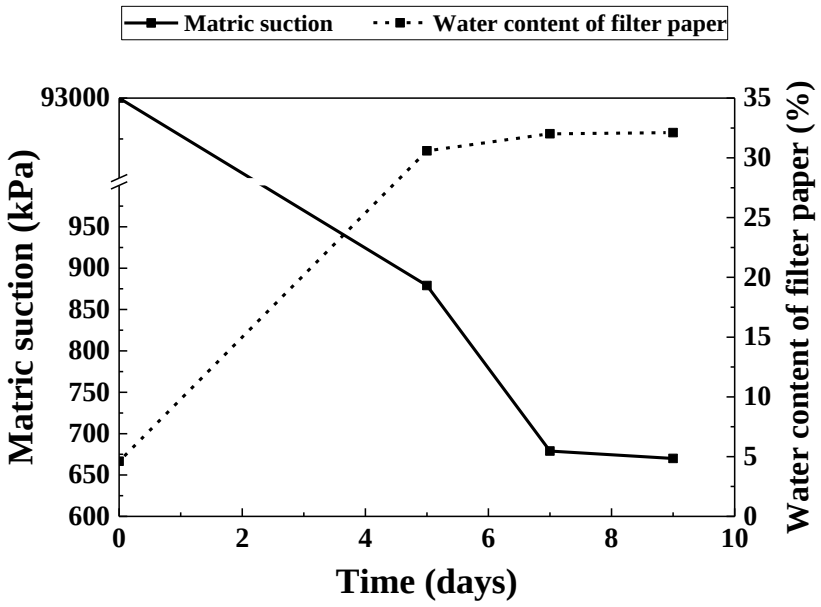

Fig. 6. Determination of equilibration time by filter paper method

Fig. 7 shows the drying SWRC expressed in terms of w_f and S_r with ψ and the variations of e_f with ψ for different f_v values (0%, 20% and 35%) and different initial $\rho_{d\text{-}f}$ values (1.82, 1.67 and 1.52 Mg/m^3). The retention curves were fitted with the van Genuchten model (1980). The legends were defined following the rule: 'f_v 0%- $\rho_{d\text{-}f}$1.82' refers to the f_v = 0% and the initial $\rho_{d\text{-}f}$ = 1.82 Mg/m^3. Fig. 7(a) depicts the variations of w_f with ψ for various f_v and $\rho_{d\text{-}f}$ values. It appears clearly that the water retention curves were only dependent on the dry density of fines $\rho_{d\text{-}f}$, and independent of the coarse grain content f_v. In addition, the gaps between the three curves for different $\rho_{d\text{-}f}$ values decreased with the increase of matric suction ψ. The curves converged to the same one beyond a threshold suction ψ = 715 kPa. Thus, the SWRC in low suction range (ψ < 715 kPa) was sensitive to the variation of $\rho_{d\text{-}f}$, while independent of $\rho_{d\text{-}f}$ in high suction range (ψ > 715 kPa).

Fig. 7(b) depicts the variations of void ratio of fine soil e_f with ψ for the fine/coarse soil mixture at varying f_v and $\rho_{d\text{-}f}$ values. It appears that such variations were also only dependent on $\rho_{d\text{-}f}$ and independent of f_v. In addition, the lower the $\rho_{d\text{-}f}$ value, the larger the decrease of e_f with increasing ψ, showing a larger volume change under the effect of suction for the case of lower $\rho_{d\text{-}f}$.

Fig.7(c) presents the variations of degree of saturation S_r with ψ for the fine/coarse soil mixture at varying f_v and $\rho_{d\text{-}f}$ values. The curves were found to be independent of f_v, which agreed with those in Fig.7 (a)-(b). In addition, the larger the $\rho_{d\text{-}f}$ value the higher the water retention capacity. With the decrease of $\rho_{d\text{-}f}$ from 1.82 to 1.67 and 1.52 Mg/m^3, the air entry value (AEV) decreased from 550 to 96 and 36 kPa respectively.

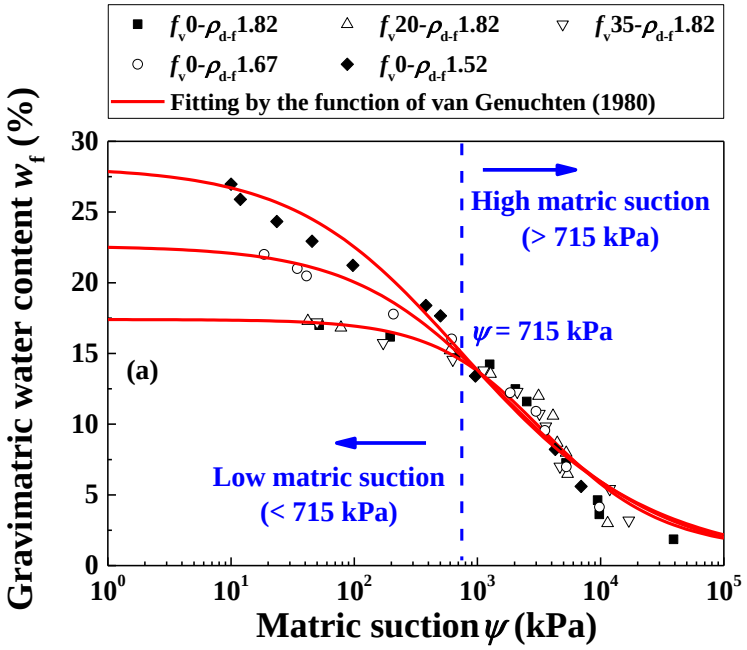

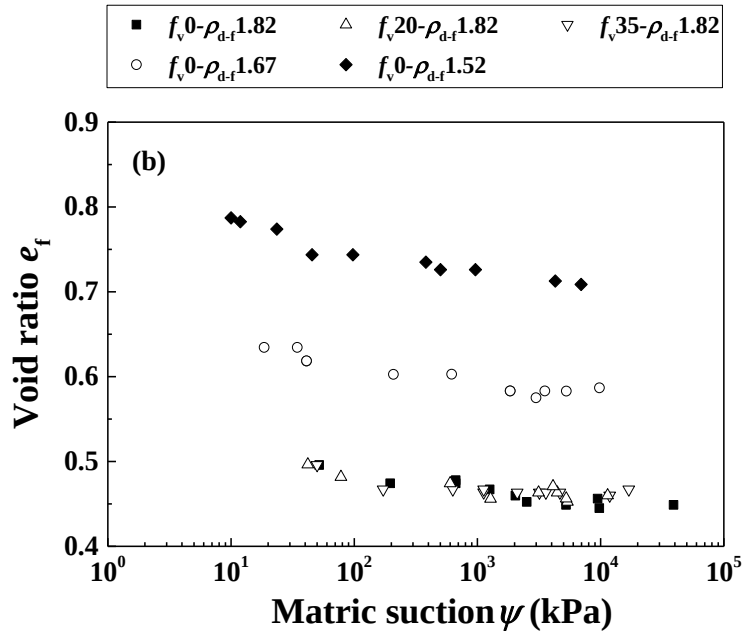

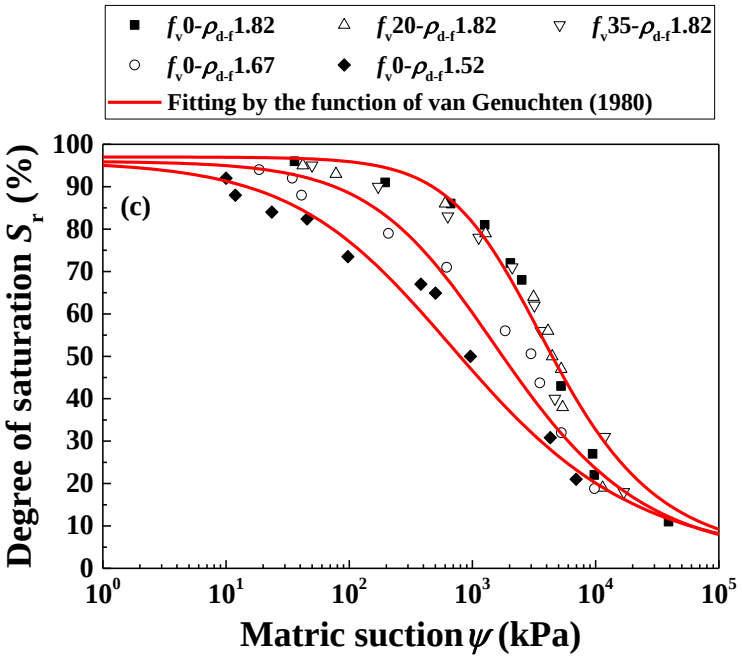

Fig. 7. Drying soil-water retention curves and variations of void ratios of fine soil with matric suction for varying f_v and $\rho_{d\text{-}f}$ values: (a) gravimetric water content of fine soil versus matric suction; (b) void ratio of fine soil versus matric suction; (c) degree of saturation versus matric suction

Fig. 8 shows the pore size distributions (PSD) of fine soil at $\rho_{d\text{-}f}$ = 1.82, 1.67 and 1.52 Mg/m^3. It can be observed from Fig. 8(a) that a decrease of $\rho_{d\text{-}f}$ resulted in an increase of intruded mercury void ratio e_M, which was a little smaller than the corresponding global e_f. Fig. 8(b) presents typical bi-modal porosity of fine soil, with a delimiting diameter d = 0.65 µm for micro- and macro-pores. For compacted soils, the micro-pores were generally within aggregates (intra-aggregate pores), while the macro-pores were between aggregates (inter-aggregate pores) (Delage et al. 1996). With the increase of $\rho_{d\text{-}f}$, the volume of inter-aggregate pores was observed to decrease, while that of intra-aggregate pores was almost constant, suggesting that the compaction process only affected the macro-pores, in agreement with Wang et al. (2014).

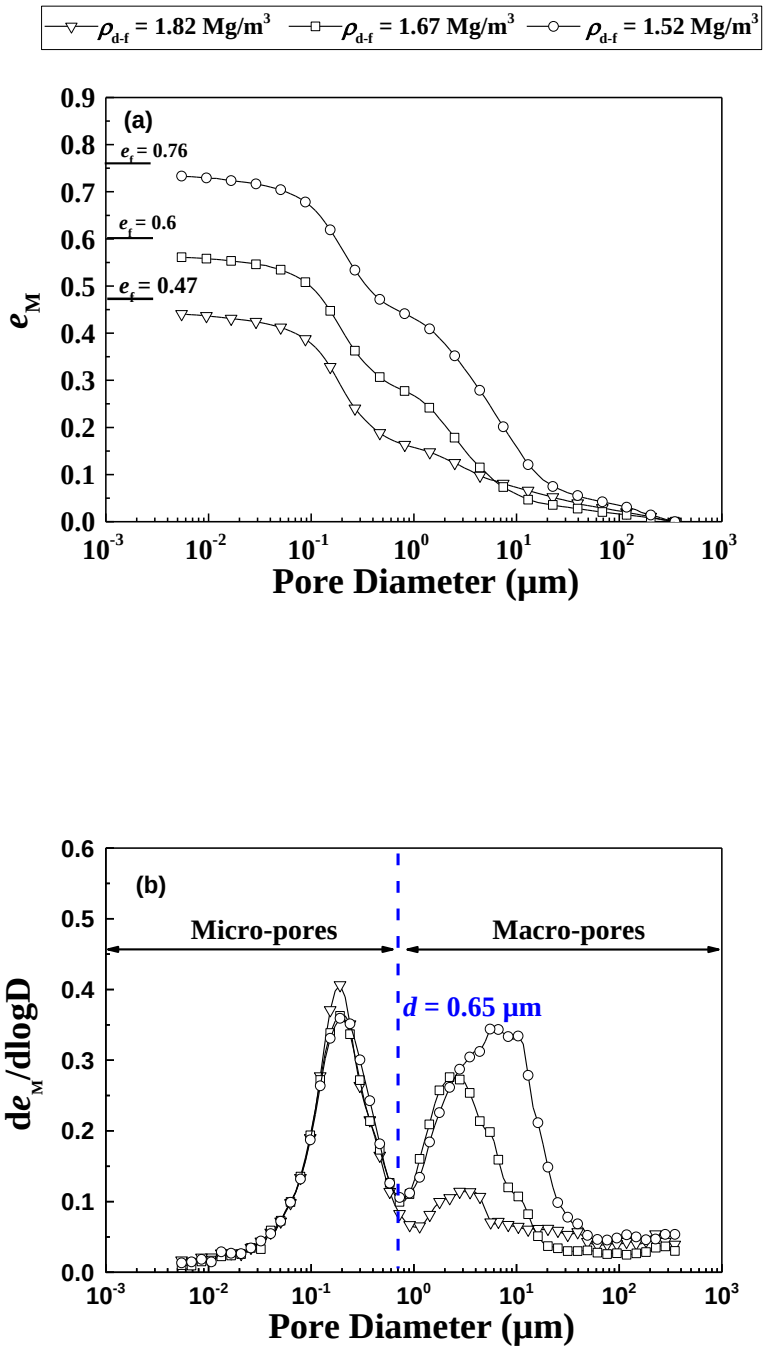

Fig. 8. Pore size distributions of fine soil at f_v = 0% and different $\rho_{d\text{-}f}$ values: (a) cumulative curves; (b) density function curves

Discussions

Effect of microstructure of fine soil on SWRC at varying $\rho_{d\text{-}f}$

Fig. 7(a) shows that $\rho_{d\text{-}f}$ affected the SWRC only for ψ < 715 kPa. Correspondingly, Fig. 8(b) indicates that a decrease of $\rho_{d\text{-}f}$ led to an increase of the volume of inter-aggregate pores (d > 0.65 μm) without modifying the volume of intra-aggregate pores (d < 0.65 μm). The delimiting d = 0.65 μm could be associated with an equivalent matric suction based on Laplace's law under the assumption of cylindrical pore shape:

$$\psi = \frac{4T_s \cdot \cos\theta}{d} \tag{13}$$

where T_s is the surface tension of water, equal to 0.073 N/m at temperature of 20 °C; θ is the contact angle between the liquid-air interface and the solid, taken equal to 0° in this study.

Substituting d = 0.65 μm into Eq. (13), the corresponding ψ was obtained:

$$\psi = 449 \text{ kPa} \tag{14}$$

It was found that this value was close to the AEV of 550 kPa for the mixture at $\rho_{d\text{-}f}$ = 1.82 Mg/m^3 (Fig. 7(c)), which was consistent with the findings of Zhang et al. (2018). This value was smaller than the threshold ψ = 715 kPa in Fig. 7(a). This difference could be explained as follows: the fine soil with varying $\rho_{d\text{-}f}$ values for MIP tests was compacted at a molding water content $w_{opt\text{-}f}$ = 13.7%, while the fine soil corresponding to the threshold point in Fig. 7(a) was subjected to a saturation process from the molding water content $w_{opt\text{-}f}$ = 13.7%, followed by a drying process. Li and Zhang (2009) studied the effect of wetting-drying history on bi-modal porosity of soil, and found that the drying process induced shrinkage of soil, leading to smaller intra-aggregate pores. Similarly, Sun and Cui (2020) investigated the soil-water retention curve of reconstituted silt, and reported that the drying process led to a shrinkage of soil and a smaller value of diameter of voids. It could be thus inferred that the larger threshold ψ = 715 kPa in Fig. 7(a) was the consequence of pore size decrease due to soil shrinkage shown in Fig. 8(b). It could be thus deduced that in low suction range (ψ < 715 kPa) the SWRC was governed by inter-aggregate pores, while in high suction range (ψ > 715 kPa) the SWRC was governed by intra-aggregate pores. The similar phenomenon was reported by Salager et al. (2013) while studying the water retention property of clayey soil. They identified a threshold suction ψ = 5000 kPa separating the inter-aggregate governing suction from intra-aggregate governing suction. With

the decrease of $\rho_{d\text{-}f}$, the volume of inter-aggregate pores increased (Fig. 8(b)), resulting in an increase of water volume in inter-aggregate pores; thereby, an increase of w_f was observed (Fig. 7(a)). However, such decrease of $\rho_{d\text{-}f}$ did not affect the volume of intra-aggregate pores (Fig. 8(b)); thus, a constant w_f was observed in high suction range (Fig. 7(a)). This also confirmed that the compaction effort greatly affected the inter-aggregate pores without touching the intra-aggregate pores (Delage et al. 1996).

Two categories of fine soil in the mixture at f_v = 35% were reported by Su et al. (2020c, 2021): a relatively dense fine soil in between coarse grains and a relatively loose fine soil in macro-pores among coarse grains. In other words, while compacted to $\rho_{d\text{-}f}$ =1.82 Mg/m^3, the dense fines had a higher $\rho_{d\text{-}f}$ and the loose fines had a lower $\rho_{d\text{-}f}$, with the global $\rho_{d\text{-}f}$ being 1.82 Mg/m^3. Thereby, a higher SWRC was expected for the dense fine soil in between coarse grains and a lower SWRC for the loose fine soil in macro-pores among coarse grains. However, as the SWRC at f_v = 35% was the same as that at f_v = 0% and 20% for $\rho_{d\text{-}f}$ = 1.82 Mg/m^3 (Fig. 7(c)), it could be inferred that in spite of the inhomogeneous distribution of fine soil in the mixture, the SWRC appeared to be controlled by the global dry density of fine soil $\rho_{d\text{-}f}$ only. Similarly, Zeng et al. (2020) studied the axial swelling property of compacted bentonite/claystone mixture, and found that this behavior was mainly dependent on the global ρ_d of mixture, irrespective of its heterogeneity.

Comparison of present study at constant $\rho_{d\text{-}f}$ with previous study at constant ρ_d

In present study, the different f_v = 0%, 20% and 35% corresponded to the same SWRC under the constant $\rho_{d\text{-}f}$ = 1.82 Mg/m^3 (Fig. 7(c)). On the contrary, Duong et al. (2014) investigated the hydraulic behavior of the upper part interlayer soil with two different f_v = 50.3% and 55.5% and a constant dry density of mixture ρ_d = 2.01 Mg/m^3 by infiltration column (Table 3). Fig. 9 shows that an increase of f_v from 50.3% to 55.5% led to a lower SWRC under the constant ρ_d = 2.01 Mg/m^3. This phenomenon could be attributed to the effect of $\rho_{d\text{-}f}$ on SWRC. Fig. 10 shows a constant e_m = 0.33 (corresponding to ρ_d = 2.01 Mg/m^3) for f_v = 50.3% and 55.5% in Duong et al. (2014), which was different from that in Fig. 4 of present study. While increasing f_v from 50.3% to 55.5%, the e_f was increased from 1.01 to 1.28; thereby, a decrease of $\rho_{d\text{-}f}$ from 1.33 to 1.17 Mg/m^3 (Table 3). As a result, the increase of f_v from 50.3% to 55.5% led to a lower SWRC (Fig. 9).

Table 3. Soil properties of Duong et al. (2014)

f_v (%)	ρ_d (Mg/m^3)	e_m	$\rho_{d\text{-}f}$ (Mg/m^3)	e_f
50.3	2.01	0.33	1.33	1.01
55.5			1.17	1.28

Note: e_m represents the void ratio of soil mixture.

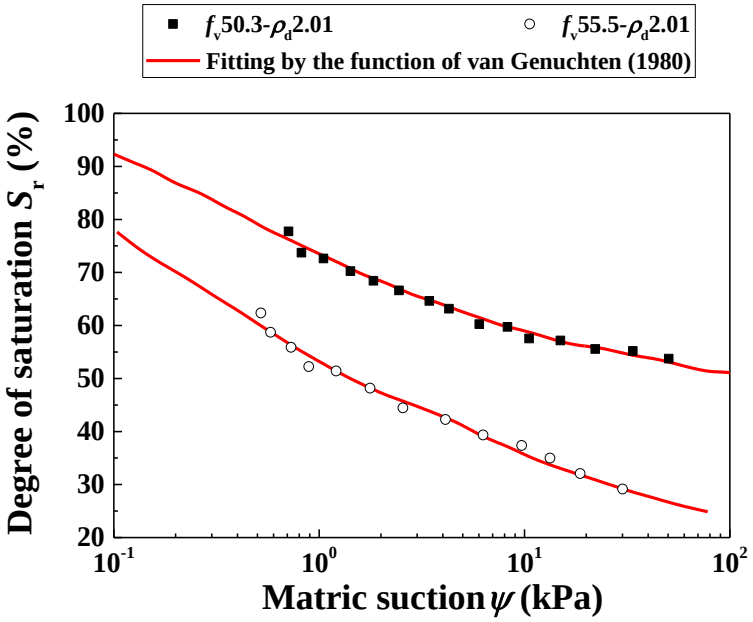

Fig. 9. Drying soil-water retention curves in the study of Duong et al. (2014)

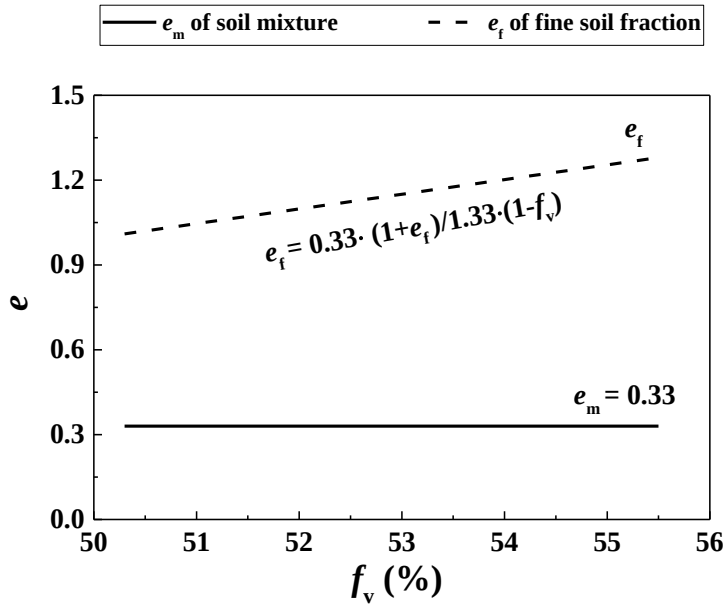

Fig. 10. Variations of void ratio with f_v at ρ_d = 2.01 Mg/m^3 in Duong et al. (2014)

The maximum degrees of saturation S_r of samples

It appears from Fig. 7(c) and Fig. 9 that the SWRCs all started at a degree of saturation S_r lower than 100%. Moreover, the values in Fig. 9 (S_r = 91% and 78% for f_v = 50.3% and 55.5% respectively) were smaller than the values around S_r = 95% for varying f_v = 0%, 20% and 35% at $\rho_{d\text{-}f}$ = 1.82 Mg/m^3 in Fig. 7(c), showing that the maximum S_r value reached during the saturation process decreased with the increase of f_v. Saba et al. (2014) worked on a compacted sand/bentonite mixture and found that the fine grains of larger sizes (e.g. the maximum d = 2 mm) was preferentially arranged with a large face side in the horizontal direction. In addition, due to the restriction of mould wall, more macro-pores were formed in the side part of sample, as evidenced by Zeng et al. (2020) on a compacted bentonite/claystone mixture. Such preferential presence of macro-pores in the side part was further confirmed on the mixture of fine soil and micro-ballast by Wang et al. (2018) and Qi et al. (2020a) through observation at X-ray μCT. As these macro-pores could not retain water under the effect of gravity, a maximum value of S_r = 95% was obtained. With the increase of f_v, the addition of coarse grains increased the mould wall restriction effect, generating thus more macro-pores. This led to a decrease of the initial S_r value of the SWRC with f_v. It is worth noting that Duong et al. (2014) adopted the ballast grains of maximum d = 60 mm to prepare the sample of d = 300 mm and h = 600 mm, while in this study the micro-ballast of maximum d = 20 mm (Fig. 1) was adopted to prepare

soil disk of d = 100 mm and h = 100 mm. Much larger mould wall restriction effect was thus expected in the case of Duong et al. (2014) due to the larger dimensions of the grains and the sample. Consequently, much lower maximum degrees of saturation (S_r = 91% and 78% for f_v = 50.3% and 55.5%) were obtained in their case.

Conclusions

To investigate the role of fine soil on the soil-water retention property of fine/coarse soil mixture, three f_v = 0%, 20% and 35% at the same $\rho_{d\text{-}f}$ = 1.82 Mg/m^3 and three $\rho_{d\text{-}f}$ = 1.82, 1.67 and 1.52 Mg/m^3 at the same f_v = 0% were considered. A filter paper method was applied to measure the matric suction of soil mixture at different water contents. Mercury intrusion porosimetry tests were performed for microstructure observation of fine soil at varying $\rho_{d\text{-}f}$. The results obtained allowed the following conclusions to be drawn.

The drying SWRC of mixture was found to be only dependent on $\rho_{d\text{-}f}$ and independent of f_v. A typical bi-modal microstructure of fine soil was identified for varying $\rho_{d\text{-}f}$ values, defining a micro-pore and a macro-pore populations. When expressed in terms of w_f with ψ, the SWRC was found to be significantly affected by $\rho_{d\text{-}f}$ for the matric suction ψ lower than 715 kPa. By contrast, when ψ was higher than 715 kPa, the SWRC kept the same, independent of $\rho_{d\text{-}f}$. Interestingly, a delimiting pore diameter d = 0.65 µm was identified, separating micro-pores (or intra-aggregate pores) from macro-pores (or inter-aggregate pores). This delimiting diameter corresponded to a matric suction of 449 kPa, which was smaller than the threshold ψ = 715 kPa due to the effect of volume change experienced in the course of soil wetting/drying from the remolded state ($w_{opt\text{-}f}$ = 13.7%). Thus, the SWRC in low suction range (ψ < 715 kPa) was governed by macro-pores, while in high suction range (ψ > 715 kPa) by micro-pores. In addition, the SWRC of mixture appeared to be controlled by the global fine soil dry density $\rho_{d\text{-}f}$ only. The effect of the possible heterogeneity of fine soil distribution inside the mixture seemed to be negligible.

When expressed in terms of S_r with ψ, the SWRC appeared to be significantly affected by $\rho_{d\text{-}f}$, while unaffected by f_v. This helped better understand the observation of Duong et al. (2014) – the water retention capacity was decreased by the increase of f_v: in the study of Duong et al. (2014), a constant ρ_d = 2.01 Mg/m^3 was adopted instead of a constant $\rho_{d\text{-}f}$. In this case, an increase of f_v resulted in a decrease of $\rho_{d\text{-}f}$, thereby a decrease of water retention capacity.

The initial S_r of the SWRC appeared to decrease with the increase of f_v. At f_v = 0%, due to the effect of mould wall restriction, macro-pores were formed in the side part of sample. As these macro-pores could not retain water under the effect of gravity, the maximum value of S_r = 95% smaller than 100% was obtained in the saturation process. With the increase of f_v, the addition of coarse grains increased the mould wall restriction effect, generating more macro-pores and thus lower maximum S_r. This phenomenon was expected to be more pronounced in the case of larger grains and larger sample dimensions.

From a practical point of view, these findings suggest that when investigating the water-retention property of interlayer soil, the scaled coarse grains at small size can be used as a substitute for real ballast grains at large size. With the increasing depth of interlayer soil, the decrease of f_v induced no changes on water-retention capacity of interlayer soil, provided that the $\rho_{d\text{-}f}$ of fine soil kept constant. When the water retention property is determined, it can be incorporated in the mechanical models to better describe the variation of permanent strain of unsaturated interlayer soil under the effect of cyclic loadings. In addition, it is worth noting that to some extent these findings can be helpful in evaluating the effects of $\rho_{d\text{-}f}$ and f_v on the water retention property of mixtures with varying types of coarse and fine soil.

Acknowledgements

This work was supported by the China Scholarship Council (CSC) and Ecole des Ponts ParisTech.

References

ASTM D5298-10. 2010. Standard test method for measurement of soil potential (suction) using filter paper. West Conshohocken, PA: ASTM International.

Baetens, J. M., Verbist, K., Cornelis, W. M., Gabriels, D., and Soto, G. 2009. On the influence of coarse fragments on soil water retention. Water resources research, 45(7).

Cui, Y.J., Loiseau, C. and Delage, P. 2002. Microstructure changes of a confined swelling soil due to suction. In *Unsaturated Soils: Proceedings of the Third International Conference on Unsaturated Soils, UNSAT 2002, 10-13 March 2002, Recife, Brazil* (Vol. 2, p. 593). CRC Press.

Cui, Y.J., Duong, T.V., Tang, A.M., Dupla, J.C., Calon, N. and Robinet, A. 2013. Investigation of the hydro-mechanical behaviour of fouled ballast. Journal of Zhejiang University Science A, 14(4), pp.244-255.

Cui, Y. J. 2018. Mechanical behaviour of coarse grains/fines mixture under monotonic and cyclic loadings. Transportation Geotechnics, 17, 91-97.

Delage, P., Audiguier, M., Cui, Y.J. and Howat, M.D. 1996. Microstructure of a compacted silt. *Canadian Geotechnical Journal*, *33*(1), pp.150-158.

Delage, P., Marcial, D., Cui, Y.J. and Ruiz, X. 2006. Ageing effects in a compacted bentonite: a microstructure approach. *Géotechnique*, *56*(5), pp.291-304.

Duong, T. V., Cui, Y. J., Tang, A. M., Dupla, J. C., and Calon, N. 2014. Effect of fine particles on the hydraulic behavior of interlayer soil in railway substructure. Canadian geotechnical journal, 51(7), 735-746.

Duong, T. V., Cui, Y. J., Tang, A. M., Dupla, J. C., Canou, J., Calon, N., and Robinet, A. 2016. Effects of water and fines contents on the resilient modulus of the interlayer soil of railway substructure. Acta Geotechnica, 11(1), 51-59.

Fiès, J. C., Louvigny, N. D. E., and Chanzy, A. 2002. The role of stones in soil water retention. European Journal of Soil Science, 53(1), 95-104.

Gao, Y., Sun, D. 2017. Soil-water retention behavior of compacted soil with different densities over a wide suction range and its prediction. Computers and Geotechnics, 91(nov.):17-26.

Jing, P. 2017. Experimental study and modelling of the elastoplastic behaviour of unbound granular materials under large number of cyclic loadings at various initial hydric states (Doctoral dissertation, Université de Strasbourg).

Kim, H., Ganju, E., Tang, D., Prezzi, M., and Salgado, R. 2015. Matric suction measurements of compacted subgrade soils. Road Materials and Pavement Design, 16(2), 358-378.

Li, X., and Zhang, L. M. 2009. Characterization of dual-structure pore-size distribution of soil. Canadian geotechnical journal, 46(2), 129-141.

Lamas-lopez, F. 2016. Field and laboratory investigation on the dynamic behavior of conventional railway track-bed materials in the context of traffic upgrade. PhD Thesis, Ecole Nationale des Ponts et Chaussées, Université Paris-Est.

Muñoz-Castelblanco, J. A., Pereira, J. M., Delage, P., and Cui, Y. J. 2010. Suction measurements on a natural unsaturated soil: A reappraisal of the filter paper method. In Unsaturated Soils-Proc. Fifth Int. Conf. on Unsaturated Soils (Vol. 1, pp. 707-712). CRC Press.

Qi, S., Cui, Y.J., Chen, R.P., Wang, H.L., Lamas-Lopez, F., Aimedieu, P., Dupla, J.C., Canou, J. and Saussine, G. 2020a. Influence of grain size distribution of inclusions on the mechanical behaviours of track-bed materials. Géotechnique, 70(3), pp.238-247.

Qi, S., Cui, Y.J., Dupla, J.C., Chen, R.P., Wang, H.L., Su, Y., Lamas-Lopez, F. and Canou, J. 2020b. Investigation of the parallel gradation method based on the response of track-bed materials under cyclic loadings. Transportation Geotechnics, p.100360.

Romero, E., Gens, A., and Lloret, A. 1999. Water permeability, water retention and microstructure of unsaturated compacted Boom clay. Engineering Geology, 54(1-2), 117-127.

Romero, E., DELLA VECCHIA, G. A. B. R. I. E. L. E., and Jommi, C. 2011. An insight into the water retention properties of compacted clayey soils. Géotechnique, 61(4), 313-328.

Simms, P. H., and Yanful, E. K. 2002. Predicting soil—Water characteristic curves of compacted plastic soils from measured pore-size distributions. Géotechnique, 52(4), 269-278.

Seif El Dine, B., Dupla, J. C., Frank, R., Canou, J., and Kazan, Y. 2010. Mechanical characterization of matrix coarse-grained soils with a large-sized triaxial device. Canadian Geotechnical Journal, 47(4), 425-438.

Salager, S., Nuth, M., Ferrari, A., and Laloui, L. 2013. Investigation into water retention behaviour of deformable soils. Canadian Geotechnical Journal, 50(2), 200-208.

Saba, S., Barnichon, J.D., Cui, Y.J., Tang, A.M., Delage, P. 2014. Microstructure and anisotropic swelling behaviour of compacted bentonite/sand mixture. Journal of Rock Mechanics and Geotechnical Engineering 6(2), 126-132.

Su, Y., Cui, Y. J., Dupla, J. C., and Canou, J. 2020a. Investigation of the effect of water content on the mechanical behavior of track-bed materials under various coarse grain contents. Construction and Building Materials, 263, 120206.

Su, Y., Cui, Y. J., Dupla, J. C., Canou, J., and Qi, S. 2020b. A fatigue model for track-bed materials with consideration of the effect of coarse grain content. Transportation Geotechnics, 100353.

Su, Y., Cui, Y.J., Dupla, J.C., Canou, J., Qi, S. 2020c. Developing a sample preparation approach to study the mechanical behavior of unsaturated fine/coarse soil mixture. Geotechnical Testing Journal. https://doi.org/10.1520/GTJ20190450

Su, Y., Cui, Y. J., Dupla, J. C., and Canou, J. 2021. Effect of water content on resilient modulus and damping ratio of fine/coarse soil mixture with varying coarse grain contents. Transportation Geotechnics, 100452.

Sun, W. J., and Cui, Y. J. 2020. Determining the soil-water retention curve using mercury intrusion porosimetry test in consideration of soil volume change. Journal of Rock Mechanics and Geotechnical Engineering, 12(5), 1070-1079.

Trinh, V. N. 2011. Comportement hydromécanique des matériaux constitutifs de plateformes ferroviaires anciennes. PhD Thesis, Ecole Nationale des Ponts et Chaussées, Université Paris-Est.

van Genuchten, M. T. 1980. A closed-form equation for predicting the hydraulic conductivity of unsaturated soils. Soil science society of America journal, 44(5), 892-898.

Wang, Q., Cui, Y. J., Tang, A. M., Xiang-Ling, L., and Wei-Min, Y. 2014. Time-and density-dependent microstructure features of compacted bentonite. Soils and Foundations, 54(4), 657-666.

Wang, H. L., Cui, Y. J., Lamas-Lopez, F., Dupla, J. C., Canou, J., Calon, N., ... and Chen, R. P. 2017. Effects of inclusion contents on resilient modulus and damping ratio of unsaturated track-bed materials. Canadian Geotechnical Journal, 54(12), 1672-1681.

Wang, H.L., Cui, Y.J., Lamas-Lopez, F., Calon, N., Saussine, G., Dupla, J.C., Canou, J., Aimedieu, P. and Chen, R.P. 2018. Investigation on the mechanical behavior of track-bed materials at various contents of coarse grains. *Construction and Building Materials*, *164*, pp.228-237.

Zhang, F., Cui, Y. J., and Ye, W. M. 2018. Distinguishing macro-and micro-pores for materials with different pore populations. Géotechnique Letters, 8(2), 102-110.

Zeng, Z., Cui, Y. J., Conil, N., and Talandier, J. 2020. Experimental study on the aeolotropic swelling behaviour of compacted bentonite/claystone mixture with axial/radial technological voids. Engineering Geology, 278, 105846.

CHAPTER III. MECHANICAL BEHAVIOR OF SOIL MIXTURE UNDER MONOTONIC LOADING

Field observation showed that with respect to rainfall and evaporation, water content varied in the interlayer soil. For fine soil fraction, different compaction water contents led to different microstructures of fine soil, and thus different mechanical behaviors. In addition, for a soil compacted at a given water content, the further variation of water content could lead to significant change of the mechanical behavior of mixture.

The effect of microstructure of fine soil on the mechanical behavior of mixture was studied. The microstructure of fine soil was investigated by mercury intrusion porosimetry tests, and its effect on the mechanical behavior of mixture was examined by monotonic triaxial tests. The results showed that for the fine matrix macrostructure of mixture, a strong microstructure effect of fine soil on the overall mechanical behavior of mixture was identified. On the contrary, for the coarse grain skeleton fabric, a very limited microstructure effect was observed. These results were presented in a paper published in Geotechnical Testing Journal.

The effect of water content on the mechanical behavior of mixture was investigated by monotonic triaxial tests. Varying water contents of fine soil w_f, coarse grain contents f_v and confining pressures were considered. The results showed that variations of maximum deviator stress, elastic modulus, friction angle and dilatancy angle with f_v followed a bi-linear mode, defining a characteristic coarse grain content $f_{v\text{-}cha}$ at a given water content: $f_{v\text{-}cha} \approx 25\%$, 29% and 33% for $w_f = 17.6\%$, 10.6% and 7.0%, respectively. The increase of $f_{v\text{-}cha}$ with the decrease of w_f was attributed to the shrinkage property of fine soil. This part corresponded to a paper published in Construction and Building Materials.

Su, Y., Cui, Y. J., Dupla, J. C., Canou, J., & Qi, S. 2021. Geotechnical Testing Journal, 44(4).

Developing a sample preparation approach to study the mechanical behaviour of unsaturated fine/coarse soil mixture

Yu Su[1], Yu-Jun Cui[1], Jean-Claude Dupla[1], Jean Canou[1], Shuai Qi[1,2]

Abstract: An interlayer soil was identified in the conventional French railway substructure, corresponding to a mixture of fine soils and coarse grains. As the overall mechanical behaviour of the interlayer soil can be conditioned by the microstructure of the fine soils, for the laboratory testing, it is important to develop an appropriate protocol for the sample preparation by compaction, which allows this microstructure effect to be minimised. In this study, two sample preparation approaches were considered for a fine/coarse mixture, with two distinct volumetric contents of coarse grains f_v (volumetric ratio of coarse grain to total sample). The microstructure of fine soils was investigated using mercury intrusion porosimetry, and its effect on the overall mechanical behaviour was examined through monotonic triaxial tests. Results showed that while compacted dry of optimum, the fine soils exhibited a bi-modal porosity microstructure. By contrast, while compacted wet of optimum, the fine soils exhibited a uni-modal porosity microstructure. When f_v = 10%, the sample was characterised by a fine matrix macrostructure with coarse grains floating in it. In that case, strong effect of the microstructure of fine soils on the overall mechanical behaviour was identified. On the contrary, when f_v = 35%, the sample was characterised by a coarse grain skeleton. In that case, very limited microstructure effect of fine soils on the overall mechanical behaviour was observed. Thus, while preparing samples of unsaturated fine/coarse soil mixture by compaction to study the overall mechanical behaviour, it is important to account for the f_v value. At low f_v, the compaction at different water contents is to be avoided because of the significant effect of microstructure of fines. On the contrary, at high f_v, the samples at different water contents can be prepared by compacting the mixture at the desired water contents.

Keywords: interlayer soils; volumetric contents of coarse grains; microstructure; compaction; shear strength

Introduction

Most French conventional railway tracks were constructed by putting ballast directly on the subgrade. Due to the penetration of ballast and subgrade under the effect of train circulation over years, an interlayer of ballast/subgrade soil was created. Considering its high dry density (2.4 Mg/m^3) and high bearing capacity (Trinh 2011), the French railway company (SNCF) decided to keep it as part of the substructure in the national track renewal program (Cui et al. 2014).

[1]Ecole des Ponts ParisTech, Laboratoire Navier/CERMES, 6 – 8 av. Blaise Pascal, Cité Descartes, Champs-sur-Marne, 77455 Marne – la – Vallée cedex 2, France
[2]Zhejiang University, Dept. of Civil Engineering, 38 Zheda Road, Hangzhou 310027, China

The coarse grains in the interlayer soil were not uniformly distributed, with a content decreasing over depth. For the upper part, the effects of fine content and water content were studied by monotonic and cyclic triaxial tests (Trinh et al. 2012; Cui et al. 2013, 2014; Duong et al. 2013, 2014, 2016; Lamas-Lopez et al. 2015, 2016). In order to extend the study to the whole interlayer, Wang et al. (2017, 2018a, 2018b) and Qi et al. (2020) worked on compacted fine/coarse soil mixture at different volumetric contents of coarse grains, f_v (volumetric ratio of coarse grain to total sample). Results revealed that there was a characteristic $f_{v\text{-}cha}$ value, below which the mixture was characterised by a fine matrix with coarse grains floating in it, while beyond which the mixture was characterised by a coarse grain skeleton.

It is worth noting that in the previous studies, the fine soil state was fixed at the optimum water content and maximum dry density in order to fix the soil suction for all samples. This is obviously not the case in field conditions where suction varies with variations of water content. Thus, it is important to extend the study to the effect of water content. A challenging question arises in that case for the preparation of samples: may the samples be prepared by directly compacting the mixture at different desired water contents?

Previous studies revealed significant difference in microstructure of fine-grained soils compacted at different remolding water contents and the strong effect of soil microstructure on the overall hydro-mechanical behaviour of fine-grained soils. Through scanning electron microscope (SEM) and mercury intrusion porosimetry (MIP), a bi-modal porosity microstructure with well-developed aggregates was observed on the dry side of optimum, while a uni-modal porosity microstructure characterised by a global fine matrix was identified on the wet side of optimum (Diamond et al. 1970; Delage et al. 1996). The plastic limit w_p (or PL) can be considered as the critical water content separating the aggregate microstructure from matrix microstructure (Ahmed et al. 1974). For the bi-modal porosity microstructure, changes in inter-aggregate voids were dominant during compression, while changes in intra-aggregate pores were dominant during saturation and drying (Li and Zhang 2009; Zhang and Li 2010; Zhang et al. 2018a). Through changes of small shear modulus and suction with remolding water content, Zhang et al. (2018b) found that when the water content was higher than the optimum one, the total suction controlled the soil stiffness. By contrast, when the water content was lower than the optimum one, it was the contact surface between aggregates that controlled the soil stiffness.

In this study, in order to address the question about the possible effect of the microstructure of fine soils on the overall mechanical behaviour of the fine/coarse soil mixture, two different

volumetric contents of coarse grains, f_v, were considered: 10% and 35%, representing a fine matrix macrostructure and a coarse grain skeleton microstructure, respectively, according to Wang et al. (2017, 2018a, 2018b). The target water contents w_f for the fine soil were w_1 = 11% (S_r = 62%) and w_2 = 16% (S_r = 91%), representing the dry and wet sides of optimum water content of fine soil ($w_{opt\text{-}f}$ = 13.7%), respectively. Two different approaches were adopted to prepare the samples at the target water contents w_f. The first approach was to compact at the optimum water content of fines $w_{opt\text{-}f}$ = 13.7%. Then, the sample was dried or wetted to reach the target water content w_f. The second approach was to directly compact the sample at the target water content w_f. Mercury intrusion porosimetry was applied to study the microstructure of fine soils and monotonic triaxial tests were performed to investigate the overall mechanical behaviour. The results obtained allowed the effect of sample preparation on the overall mechanical behaviour to be clarified for unsaturated fine/coarse soil mixtures.

Materials and methods

Sample preparation approaches

The materials used by Wang et al. (2018a) were adopted in this study: nine different commercial soils were mixed to constitute the fine soils (Fig. 1) and micro-ballast (Fig. 2) was prepared using three granular soils by following the similitude method (Wang et al. 2018a). The reconstituted fine soil and micro-ballast can be observed in Fig. 3. The values of specific gravity G_s of fine soil and micro-ballast were 2.68 and 2.67, respectively. The liquid limit and plasticity index of the fine soils are 32% and 20%, respectively (Fig. 4). The standard proctor compaction curve was determined following ASTM D698-12, *Standard test methods for laboratory compaction characteristics of soil using standard effort (12 400 ft-lbf/ft3 (600 kN-m/m^3))*, for the reconstituted fine soils (Fig. 5), defining an optimum water content $w_{opt\text{-}f}$ = 13.7% and a maximum dry density $\rho_{dmax\text{-}f}$ = 1.82 Mg/m^3.

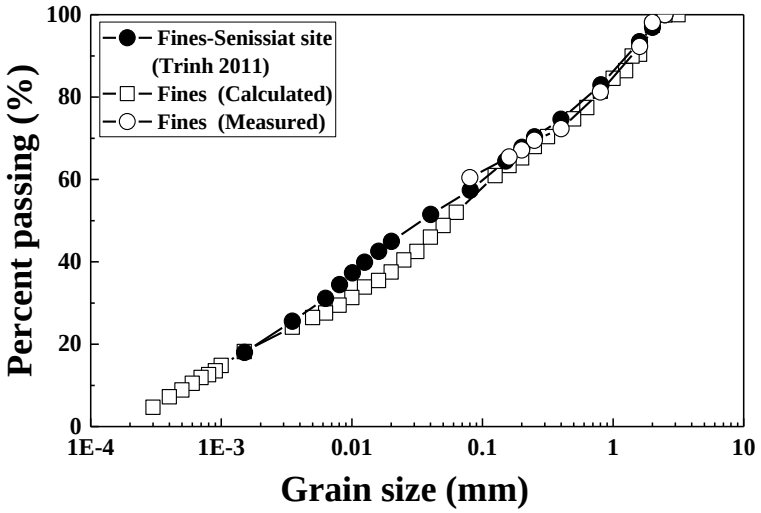

Fig. 1. Grain size distribution curves of fine soils (after Wang et al. 2018a)

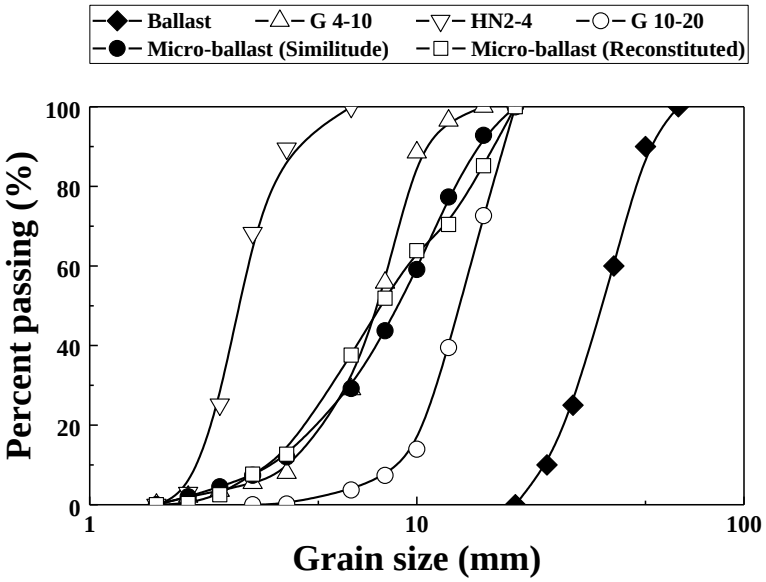

Fig. 2. Grain size distribution curves of micro-ballast and ballast (after Wang et al. 2018a)

Fig. 3. Photographs of reconstituted fine soil and micro-ballast

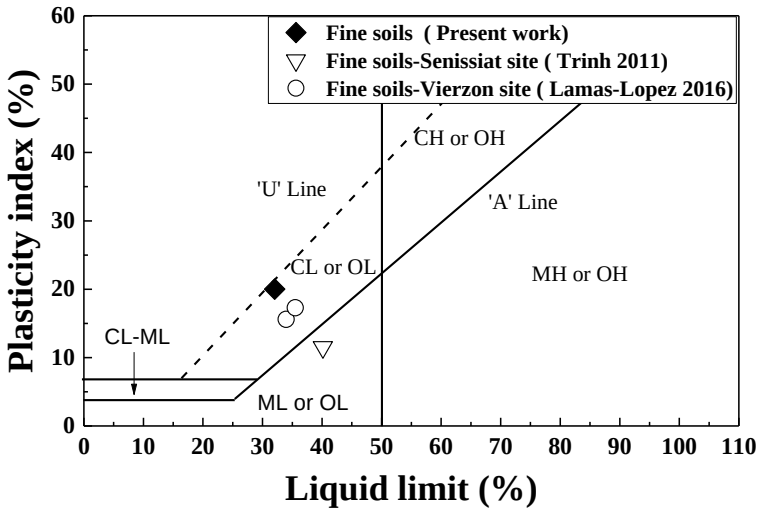

Fig. 4. Plasticity of fine soils (after Wang et al. 2018a)

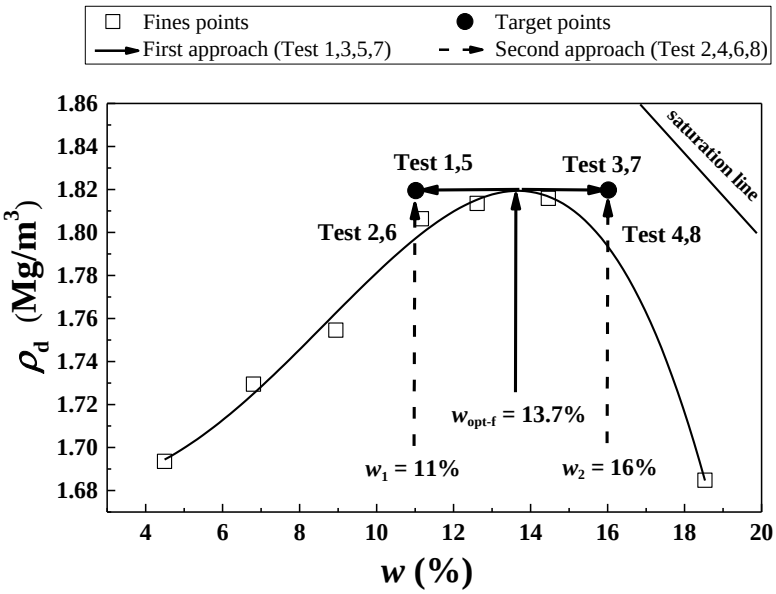

Fig. 5. Fine soil states defined in the two sample preparation approaches

For the preparation of fine/coarse soil mixture samples at target water contents w_f, two different approaches were considered (Fig. 5): in the first approach, the fine soil was prepared at optimum water content $w_{opt\text{-}f}$ = 13.7%, then stored in hermetic container for 24 h for moisture homogenization. The fine/coarse soil mixture was then prepared by mixing the fine soil and the micro-ballast to reach the desired f_v value, with the pre-determined mass of fine soil and coarse grains (see more details in Wang et al. 2018a). The soil mixture under different f_v values were compacted in three layers to reach the sample size of 100 mm diameter and 200 mm height, with the equal amounts of fine soil and coarse grains for each layer. The photographs of the compacted samples at different f_v values are presented in Fig. 6. The compacted sample was then covered by plastic film and conserved for 24 h prior to drying or wetting to reach the target fine water content (w_1 = 11% on the dry side or w_2 = 16% on the wet side). It is worth noting that while controlling the fine content, all water was considered as being contained in the fines. Because a too fast drying process would give rise to sample damage by fissuring, a milder drying method was adopted: the sample was exposed to air for 1 h each time, and then covered with plastic film for moisture equilibration. The time of equilibration needed was determined through the measurements of suctions and water contents in three positions: in the center, at ½ r and r, r being the radius of the sample. Note that the suction was determined using the chilled-mirror dew-point technique (Leong et al. 2003). Results showed that at least 7 h was needed to

reach reasonable equilibrium in terms of suction and water content (Table 1). In the case of wetting process, 10 g water was sprayed on the sample each time prior to covering it with plastic film for equilibration. The same equilibration time of at least 7 h was adopted. In the second approach, water was simply added into the fine soil to reach the target water content $w_1 = 11\%$ on the dry side or $w_2 = 16\%$ on the wet side. Micro-ballast was then added to reach the desired f_v values. The mixture samples were prepared by compaction to reach the size of 100 mm diameter and 200 mm height.

As shown in Table 2, the first approach was applied to Test 1, Test 3, Test 5, and Test 7, with all tests duplicated. The second approach was applied to Test 2, Test 4, Test 6, and Test 8, with only Test 2 duplicated.

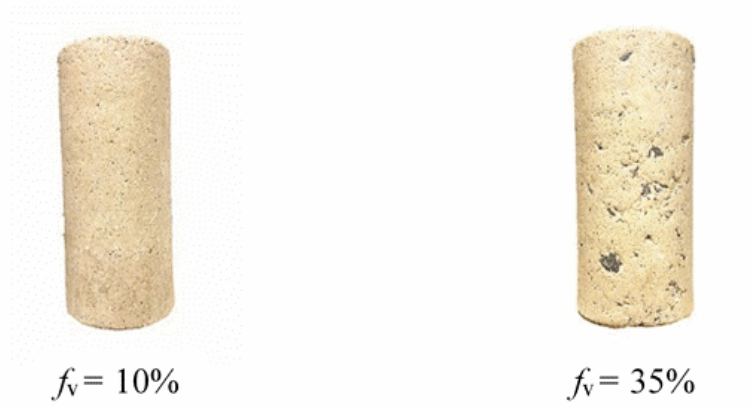

Fig. 6. Photographs of samples compacted at $w_{opt\text{-}f} = 13.7\%$ and under various coarse grain contents

Table 1. Suction and water content measured at different equilibration times for fine soils

Position	Suction (MPa)	Water content (%)	Suction (MPa)	Water content (%)
	After 6h		After 7h	
center	0.33	12.7	0.32	12.9
1/2 r	0.24	13.5	0.35	12.8
r	0.46	13.7	0.33	13.1

Table 2. Soil properties of samples tested

Test	Sample preparation approach	f_v (%)	Target w_f (%)	Target S_r (%)	Target $\rho_{dmax\text{-}f}$ (Mg/m^3)	Measured w_f (%)	Measured $\rho_{dmax\text{-}f}$ (Mg/m^3)	Sample ρ_d (Mg/m^3)
1	first	10	11	62	1.82	11.1	1.81	1.90
1'	first		11	62		11.0	1.82	1.90
2	second		11	62		11.3	1.82	1.91
2'	second		11	62		11.1	1.82	1.91
3	first		16	91		15.8	1.82	1.90
3'	first		16	91		15.7	1.82	1.90
4	second		16	91		15.7	1.82	1.91
5	first	35	11	62		10.8	1.80	2.10
5'	first		11	62		10.9	1.80	2.09
6	second		11	62		11.1	1.80	2.10
7	first		16	91		15.8	1.80	2.10
7'	first		16	91		15.9	1.80	2.10
8	second		16	91		15.8	1.80	2.10

Note: f_v represents the ratio of volumetric coarse grain content to the total volume of the sample (Wang 2018a). w_f and $\rho_{dmax\text{-}f}$ represent the water content and the maximum dry density of fine soils, respectively. ρ_d represents the dry density of fine/coarse soil mixture sample. S_r represents the degree of saturation of fine soil, which is also the degree of saturation of sample.

Monotonic triaxial tests

The mechanical behaviour of fine/coarse soil mixture was investigated by performing monotonic triaxial tests under drained conditions. After installation of the sample, no saturation procedure was applied. A confining pressure σ_3 = 30 kPa was applied in all tests, which corresponded to the average horizontal stress estimated in the field under the effect of train loading by considering the Poisson's ratio and the depth of interlayer soil (Duong et al. 2016). For the samples at w_1 = 11% (S_r = 62%), after application of a confining pressure σ_3 = 30 kPa, they were sheared directly because only air was expected to be expelled, which was normally quite fast. However, for the samples at w_2 = 16% (S_r = 91%), after application of the same confining pressure σ_3 = 30 kPa, one night was waited prior to shearing because in that case pore water pressure could be generated. In order to ensure the full dissipation of pore water pressure during shearing, a shearing rate as low as 0.1 mm/min was adopted based on the parameter t_{90} (time for 90% consolidation) obtained from a separate consolidation test on a saturated sample (ASTM D7181-11, *Standard Test Method for Consolidated Drained Triaxial Compression Test*

for Soils). Note that the same shearing rate was adopted by Trinh (2011) in the triaxial tests on the mixture of ballast grains/subgrade soil under unsaturated and saturated conditions. The tests ended either when the deviator stress reached the peak value or when the axial strain reached 15% in case of absence of peak deviator stress (ASTM D7181-11).

As shown in Table 2, two volumetric contents of coarse grains were considered: f_v = 10% and f_v = 35%, representing a fine matrix macrostructure and a coarse grain skeleton microstructure, respectively. Test 1 to Test 4 were conducted at f_v = 10%, while Test 5 to Test 8 were conducted at f_v = 35%. Note that Test 1', Test 2', Test 3', Test 5' and Test 7'were duplicated tests of Test 1, Test 2, Test 3, Test 5 and Test 7, respectively. As shown in Fig. 5, the first approach was applied to Test 1, Test 5 on samples dried to w_1 = 11%, and to Test 3, Test 7 on samples wetted to w_2 = 16%. The second approach was applied to Test 2 and Test 6 on samples at w_1 = 11%, to Test 4 and Test 8 on samples at w_2 = 16%.

Mercury intrusion porosimetry (MIP)

In order to study the microstructure patterns of fine soils contained in the samples with two f_v values (10% and 35%) and two w values (11% and 16%), after performing the monotonic triaxial tests, fine soils at the positions far from the shear band were taken and prepared by freeze-drying method for microstructure observation. In the freeze drying, fine soils were cut into small pieces of about 1g each and then immersed into liquid nitrogen under vacuum at the freezing point (-210 °C). After that, the frozen samples were transferred into the chamber of a freeze dryer for 24 h, enabling the ice to be eliminated by sublimation. This procedure allowed the sample microstructure disturbance to be minimized, guaranteeing the quality of MIP tests (Cui et al. 2002; Delage et al. 2006).

In this study, five MIP tests were performed on the specimens at f_v = 10%: three at w_1 = 11% (Test 1, Test 2 and duplicated Test 2') and two at w_2 = 16% (Test 3 and Test 4). In addition, five MIP tests were performed on specimens at f_v = 35%: three at w_1 = 11% (Test 5, Test 6 and Test 6') and two at w_2 = 16% (Test 7 and Test 8). Note that the MIP tests were labeled with the same numbers as the monotonic triaxial tests in further analysis.

Experimental results

Shear behaviour

The results from monotonic triaxial test at two different f_v values (10% and 35%) and two different water contents (w = 11% and 16%) were presented in Figs. 7-10, with the deviator stress q and the volumetric strain ε_v plotted against the axial strain ε_a. Comparison between the duplicated tests (Test1 against Test 1', Test 2 against Test 2', Test 3 against Test 3', Test 5 against Test 5' and Test 7 against Test 7') showed that the results were quite similar, showing a satisfactory repeatability.

Figs. 7(a)-10(a) showed the variation of deviator stress q with axial strain ε_a. It appeared from Fig. 7(a) that the deviator stress q of Test 1 (first approach) increased with the axial strain ε_a until reaching a peak deviator stress q_{max} = 397 kPa, then decreased and finally stabilized at q = 200 kPa, while for Test 2 (second approach), the peak deviator stress was less pronounced and much lower (q_{max} = 230 kPa). This suggested different stress-strain behaviours of samples at f_v = 10% and w_1 = 11% when prepared by two different approaches. It was observed from Fig. 8(a) that the higher water content (w_2 = 16%) led to the disappearance of peak deviator stress. Moreover, the whole stress-strain curves became almost the same with the quite close maximum deviator stresses: q_{max} = 132 kPa for Test 3 (first approach) and q_{max} = 115 kPa for Test 4 (second approach), respectively, showing a clear water content effect. When the value of f_v increased to 35%, both approaches (Tests 5 with the first approach and Test 6 with the second approach) gave rise to quite similar stress-strain curves with marked peaks at w_1 = 11% (Fig. 9(a)). The peak deviator stress of Test 5 was q_{max} = 459 kPa, quite close to the value of Test 6: q_{max} = 490 kPa. When the water content increased to w_2 = 16% (Fig. 10(a)), as in the case of f_v = 10%, no marked peak was observed. Moreover, the whole stress-strain curves became almost the same with quite close maximum deviator stresses: q_{max} = 242 kPa for Test 7 (first approach) and q_{max} = 225 kPa for Test 8 (second approach).

Summarizing, with two different sample preparation approaches, the stress-strain curves were different at a value of f_v as low as 10% and at a water content corresponding to the dry side of optimum (w_1 = 11%). On the contrary, no significant difference was observed between the two sample preparation approaches at a value of f_v as high as 35%, or at a water content corresponding to the wet side of optimum (w_2 = 16%).

Figs. 7(b) -10(b) showed the variation of volumetric strain ε_v with axial strain ε_a. In Fig. 7(b) for all samples, the volumetric strain ε_v started with a contractancy stage followed by a dilatancy stage. The dilatancy appeared more pronounced for Test 1, as compared to that of Test 2. At the higher water content (w_2 = 16%) in Fig. 8(b), the first (Test 3) and the second (Test 4) sample preparation approaches gave rise to quite similar pure contractancy curves, evidencing a significant water content effect. In the case of f_v = 35%, all curves were characterised by a contractancy stage followed by a dilatancy stage (Figs. 9(b) and 10(b)), with the dilantancy much larger than that at f_v = 10%, in particular in the case of dry side of optimum (Fig. 9(b)). Moreover, there was little difference between the curves of the first sample preparation approach and those of the second sample preparation approach: for both dry side (Fig. 9(b)) and wet side (Fig. 10(b)), the curves were almost the same.

Overall, as for the stress-strain curves, the volumetric strain-axial strain curves also showed different behaviours at f_v = 10% on the dry side of optimum (w_1 = 11%), but quite similar behaviours at f_v = 35% or on the wet side of optimum (w_2 = 16%).

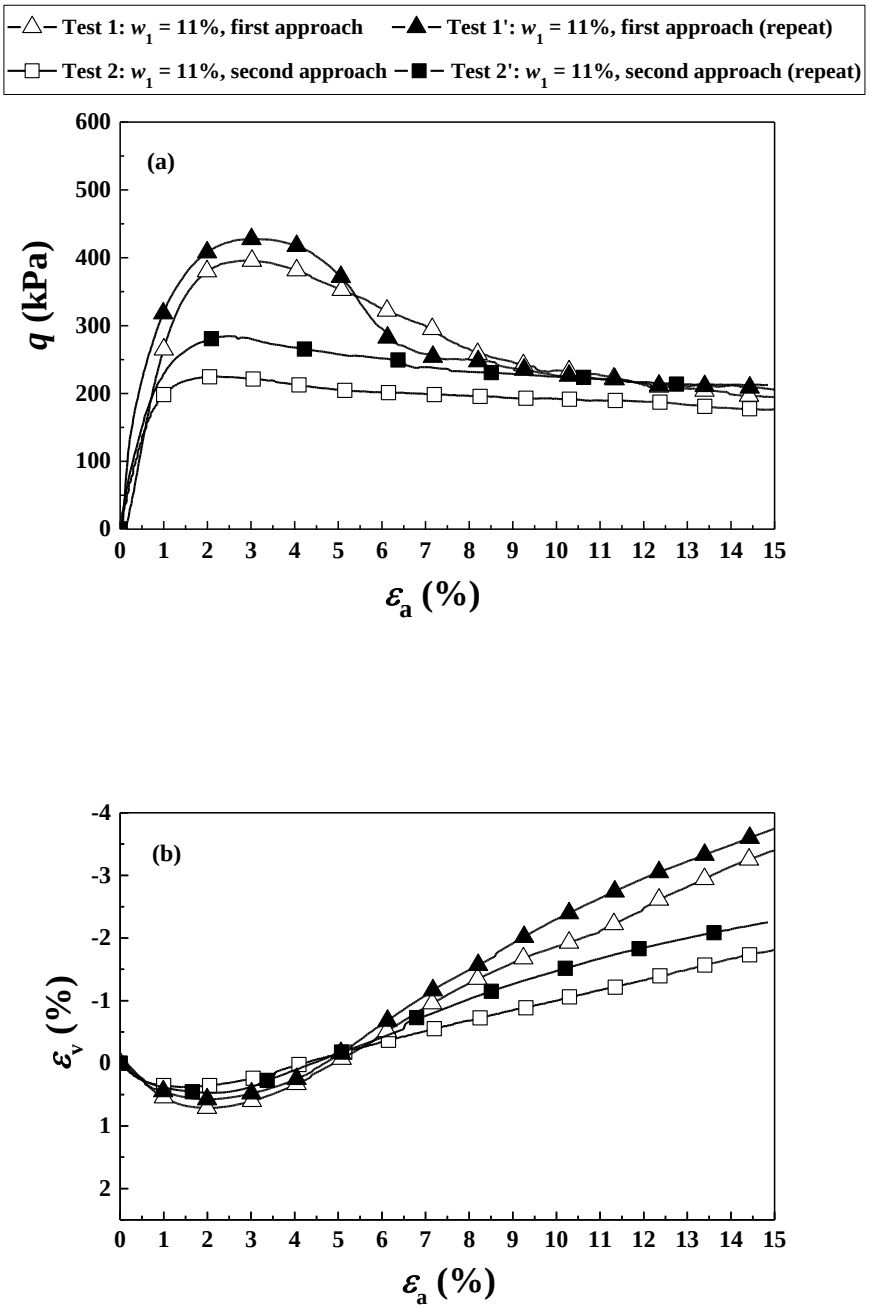

Fig. 7. Triaxial test results of samples at f_v = 10% on the dry side (w_1 = 11%):

(a) stress-strain curves; (b) volumetric strain- axial strain curves

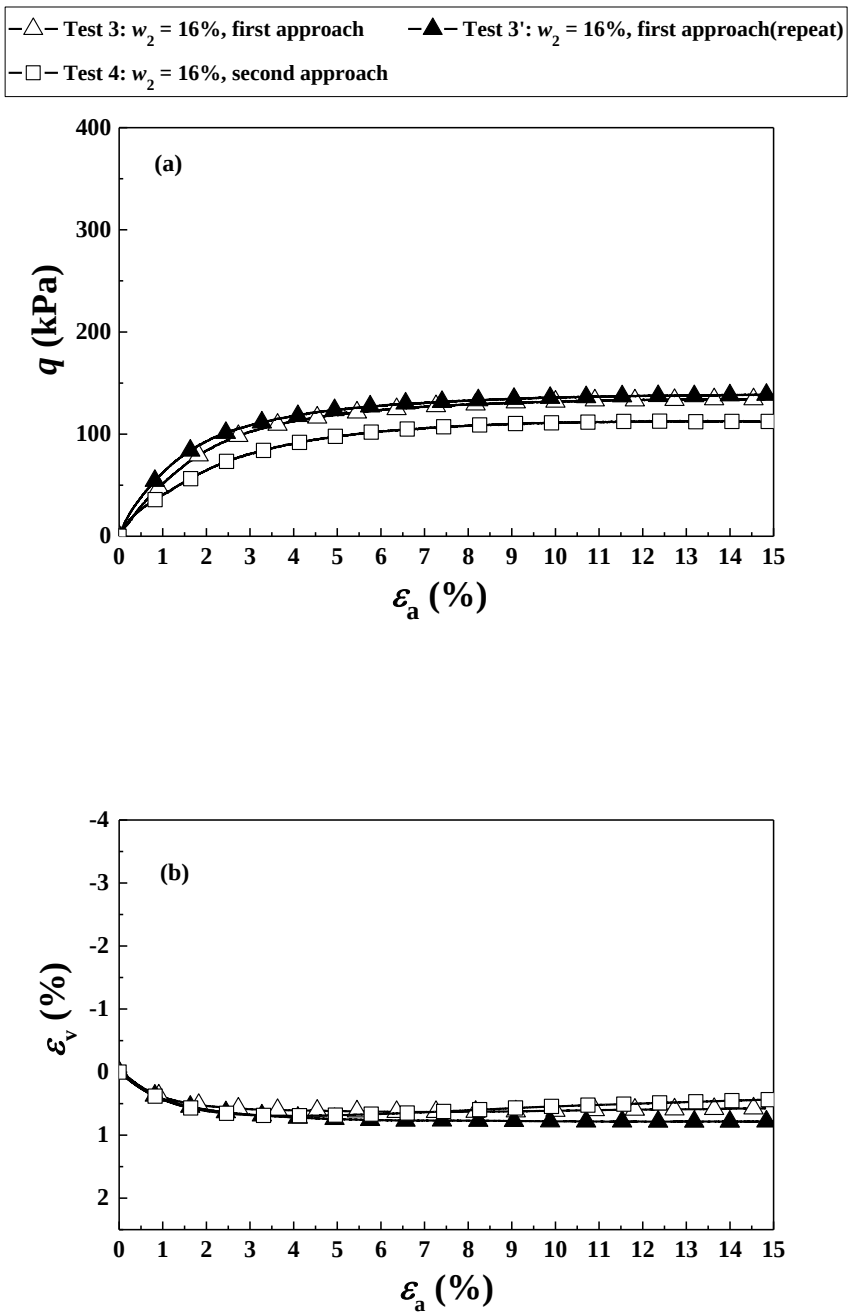

Fig. 8. Triaxial test results of samples at f_v = 10% on the wet side (w_2 = 16%):

(a) stress-strain curves; (b) volumetric strain- axial strain curves

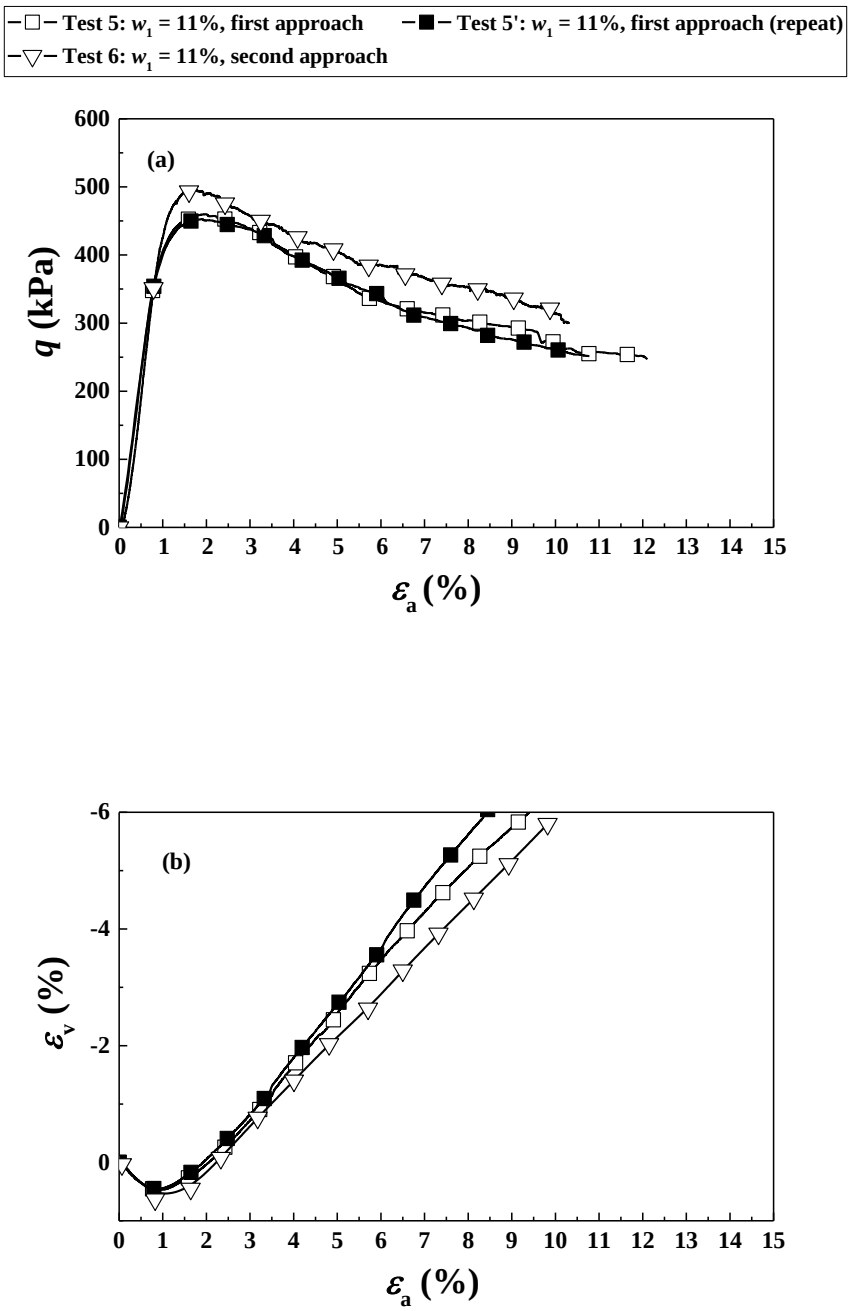

Fig. 9. Triaxial test results of samples at f_v = 35% on the dry side (w_1 = 11%):

(a) stress-strain curves; (b) volumetric strain- axial strain curves

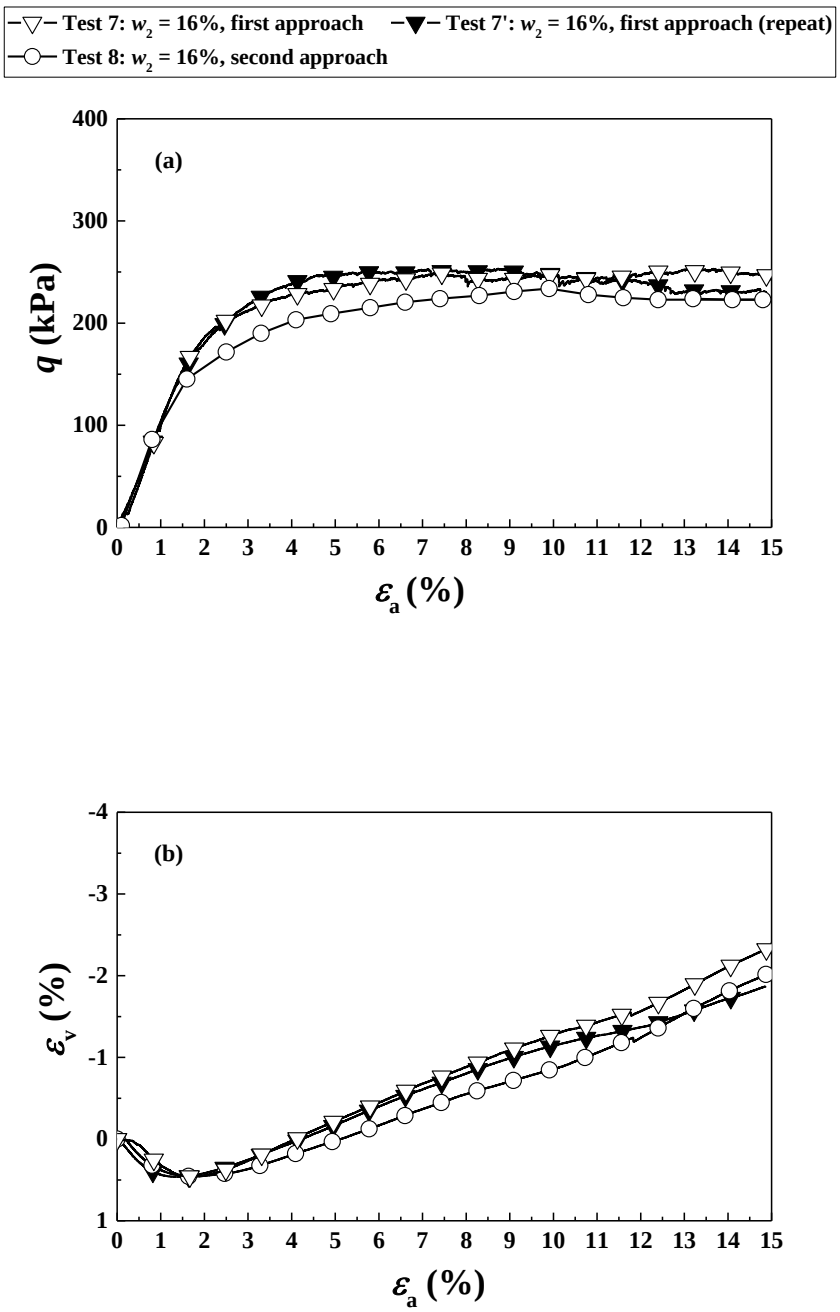

Fig. 10. Triaxial test results of samples at f_v = 35% on the wet side (w_2 = 16%):

(a) stress-strain curves; (b) volumetric strain- axial strain curves

Mechanical parameters

For further analysis, four mechanical parameters were adopted, including the maximum deviator stress q_{max} as mentioned previously, the initial Young's modulus E_0, the Poisson's ratio v and the dilatancy angle ψ. The initial Young's modulus E_0 was defined as the ratio of deviator stress to axial strain from 0% to 1% (Wang et al. 2018a; Qi et al. 2020). Based on the volumetric strain-axial strain curve in Fig. 11, taking Test 2 for example, the Poisson's ratio v and dilatancy angle ψ were determined using Eqs. (1) and (2) (Vermeer 1998), respectively:

$$v = (1- k_c)/2 \tag{1}$$

$$\sin \psi = k_d/(-2+ k_d) \tag{2}$$

where k_c and k_d were the slopes of volumetric strain-axial strain curves in the contractancy and dilatancy phases, respectively.

The values of four mechanical parameters for all tests were determined and then presented in Table 3. As for the shear behaviour, satisfactory repeatability of test results can be observed through comparison of duplicated tests (Test1 against Test 1', Test 2 against Test 2', Test 3 against Test 3', Test 5 against Test 5' and Test 7 against Test 7').

At f_v = 10% and w_1 = 11%, the maximum deviator stress q_{max} = 397 kPa and 230 kPa, the initial Young's modulus E_0 = 27.5 MPa and 20.1 MPa and the dilatancy angle ψ = 8.05 degree and 4.01 degree were observed for Test 1 (first approach) and Test 2 (second approach) respectively. Thus, significant difference existed between Test 1 (first approach) and Test 2 (second approach). Moreover, the values of Poisson's ratio v were 0.23 and 0.24 for Test 1 (first approach) and Test 2 (second approach) respectively, indicating little influence by the sample preparation approaches. The same observation of Poisson's ratio v can be made when comparing Test 3 (first approach) with Test 4 (second approach), Test 5 (first approach) with Test 6 (second approach), and Test 7 (first approach) with Test 8 (second approach). At f_v = 10% and w_2 = 16%, very close values of maximum deviator stress (q_{max} =132 kPa and 115 kPa) and initial Young's modulus (E_0 =5.1 MPa and 4.5 MPa) were observed for Test 3 (first approach) and Test 4 (second approach), respectively. When the value of f_v increased to 35%, two sample preparation approaches gave quite similar values of maximum deviator stress (q_{max} = 459 kPa and 490 kPa), initial Young's modulus (E_0 = 40.4 MPa and 41.9 MPa) and dilatancy angle (ψ = 17.46 degree and 16.26 degree) for Test 5 (first approach) and Test 6 (second approach),

respectively. The same observation can be made when comparing Test 7 (first approach) with Test 8 (second approach).

Overall, two different approaches only led to different values of mechanical parameters at low f_v value (f_v = 10%) and on the dry side of optimum (w_1 = 11%), which was consistent with the observation of stress-strain curves and volumetric strain-axial strain curves.

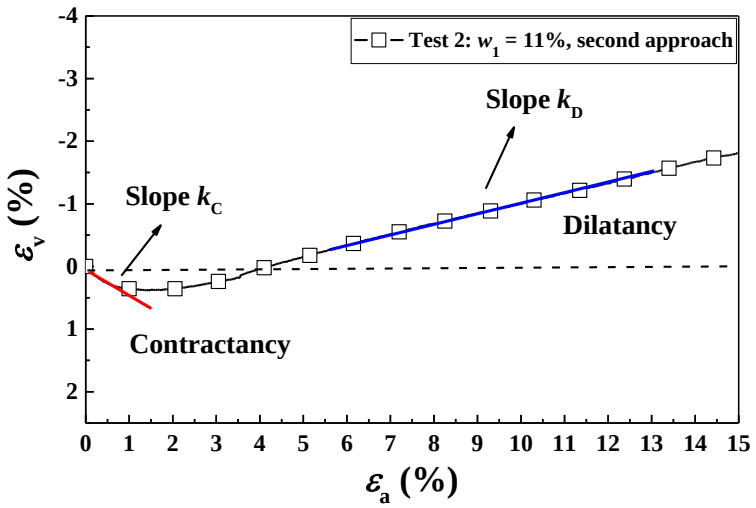

Fig. 11. Determination of Poisson's ratio and dilatancy angle

Table 3. Mechanical parameter from triaxial tests

Mechanical parameter	f_v = 10% (w_1=11%)				f_v = 10% (w_2=16%)			f_v = 35% (w_1=11%)			f_v = 35% (w_2=16%)		
	Test 1	Test 1'	Test 2	Test 2'	Test 3	Test 3'	Test 4	Test 5	Test 5'	Test 6	Test 7	Test 7'	Test 8
q_{max} (kPa)	397	427	230	284	132	135	115	459	451	490	242	230	225
E_0 (MPa)	27.5	31.4	20.1	22.5	5.1	5.7	4.5	40.4	40.4	41.9	9.9	9.9	9.8
v	0.23	0.23	0.24	0.24	0.34	0.33	0.33	0.23	0.23	0.22	0.34	0.32	0.32
ψ (degree)	8.05	8.63	4.01	5.74	/	/	/	17.46	18.06	16.26	5.34	5.22	4.76

Microstructure of fine soils

The pore size distribution (PSD) curves obtained from MIP tests were shown in Figs. 12-13, with the global fine soil void ratio (e = 0.47) plotted. Fig. 12 (a_1) showed that the final value of intruded mercury void ratio e_M was a little smaller than the global void ratio e. In addition, a typical bi-modal porosity was identified for Test 1(first approach), Test 2 (second approach) and Test 2' (second approach) in Fig. 12 (b_1), with two pore populations: micro-pores with the same size 0.2 µm, and macro-pores with a size 3 µm for Test 1 and 2 µm for Test 2 and Test 2'. Note that the PSD curves obtained from Test 2 (second approach) were close to that of Test 2' (second approach), showing a satisfactory repeatability of MIP tests. On the wet side (w_2 = 16% in Figs. 12 (a_2)-(b_2)), quite similar uni-modal microstructures were identified for Test 3 (first approach) and Test 4 (second approach), with the same family of micro-pores at a size 0.6 µm.

Figs. 13 (a_1)-(b_1) showed that a bi-modal porosity was observed for Test 5 (first approach), Test 6 (second approach) and Test 6' (second approach), with two pore populations: micro-pores at the same size of 0.3 µm, and macro-pores at different sizes of 3 µm, 2 µm and 9 µm for Test 5 (first approach), Test 6 (second approach) and Test 6' (second approach), respectively. In addition, the quantity of macro-pores of Test 5 (first approach) appeared quite limited, while that of Test 6 (second approach) and Test 6' (second approach) was much larger. Note that the fine soils with different quantity of macro-pores of Test 6 and Test 6' were taken from the same sample at f_v = 35%, indicating the non-uniform distribution of fine soils in the coarse grain skeleton. From Figs. 13(a_2)-(b_2), the same uni-modal microstructure with a population of micro-pores of 0.3 µm diameter was identified for Test 7 (first approach) and Test 8 (second approach). These observations of microstructure of fine soil compacted at different water content were in full agreement with previous findings of Delage et al. (1996).

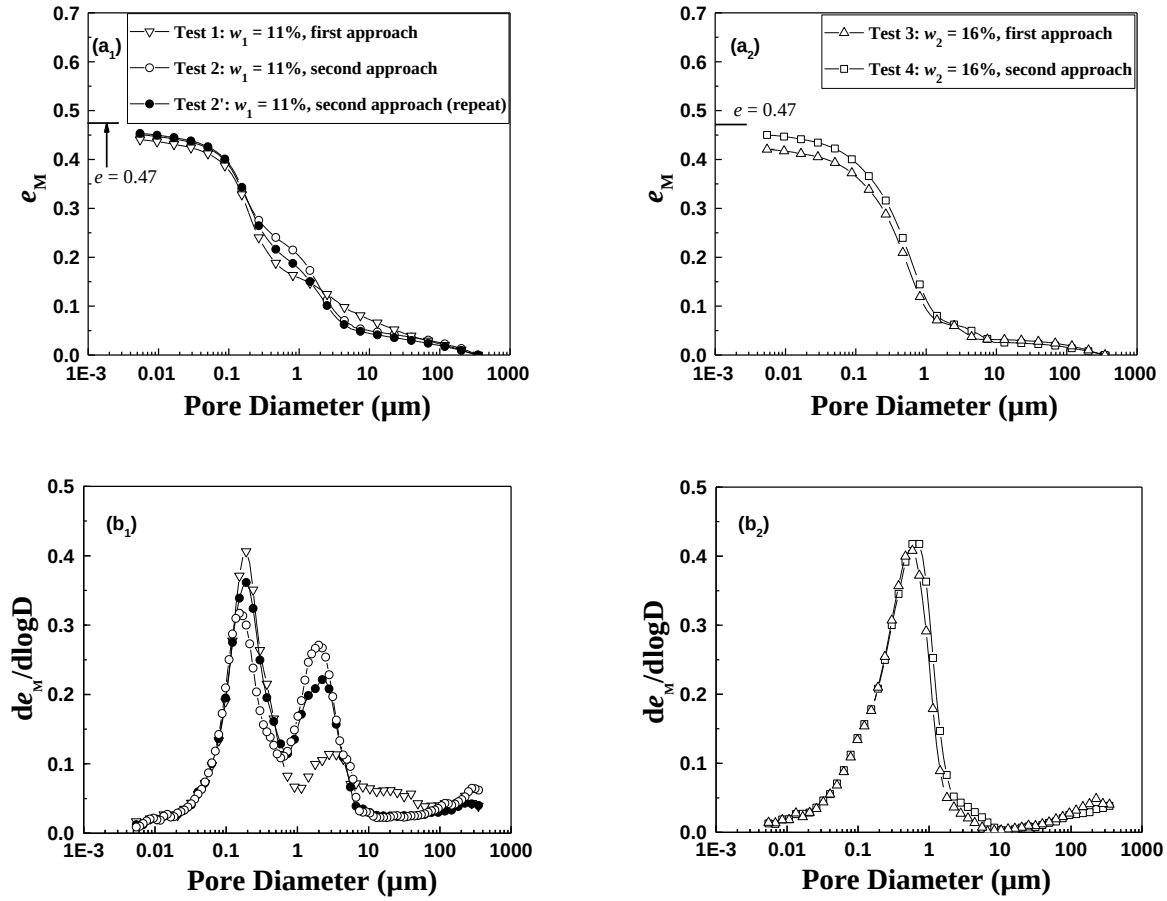

Fig. 12. Pore size distribution of fine soils for samples at f_v = 10%:

(a_1) - (b_1) on the dry side (w_1 = 11%); (a_2) - (b_2) on the wet side (w_2 = 16%)

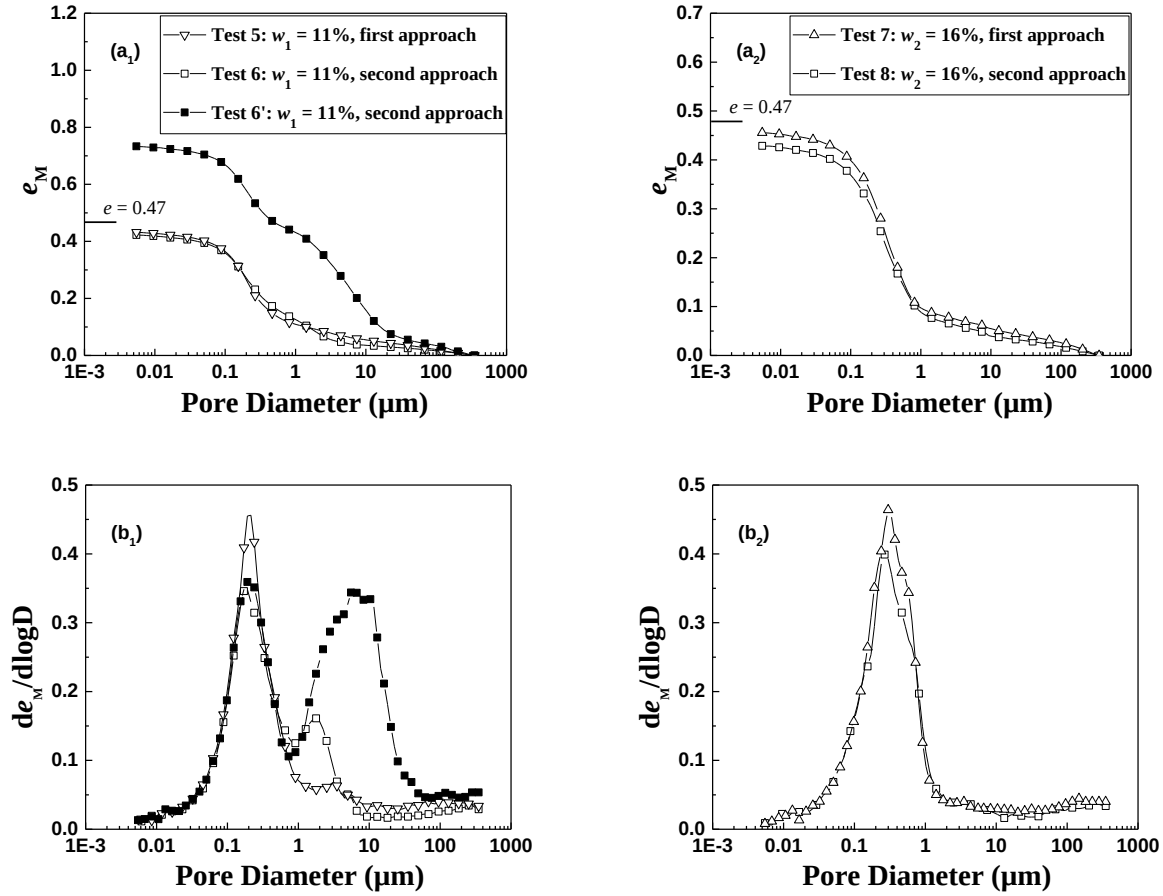

Fig. 13. Pore size distribution of fine soils for samples at f_v = 35%:

(a_1) - (b_1) on the dry side (w_1 = 11%); (a_2) - (b_2) on the wet side (w_2 = 16%)

Interpretation and discussion

The effect of matric suction on sample preparation

The results obtained from MIP tests showed a bi-modal porosity at w_1 = 11% on the dry side (Fig. 12(a_1) - (b_1) and Fig. 13(a_1) - (b_1)), and a uni-modal porosity at w_2 = 16% on the wet side (Fig. 12(a_2) - (b_2) and Fig. 13(a_2) - (b_2)). These results obtained can be explained by the effect of matric suction on sample preparation by compaction.

At a water content as low as w_1 = 11% on the dry side of optimum, fine aggregates with high matric suction inside were preserved. As a result, further compaction mainly made re-arrangement of the aggregates. This led to the existence of both small pores inside aggregates and large pores among aggregates. However, at a water content as high as w_2 = 16% on the wet side of optimum, the initial fine aggregates were expected to be destroyed by the water

hydration or the decrease of matric suction. As a result, a fine matrix structure was expected to be formed after compaction, leading to a uni-modal pore-size distribution.

At the optimum water content $w_{opt\text{-}f}$ = 13.7%, the matric suction inside the fine aggregates was normally lower than that at w_1 = 11%, but high enough to keep certain mechanical resistance of the aggregates. In other words, the aggregates at $w_{opt\text{-}f}$ = 13.7% were expected to be more deformable than those at w_1 = 11%. As a result, under the effect of further compaction, fewer large pores were produced in the case of $w_{opt\text{-}f}$ = 13.7%. When drying from $w_{opt\text{-}f}$ = 13.7% to w_1 = 11%, the matric suction was increased and some shrinkage was expected, enlarging the large pores a little. By contrast, when wetting from $w_{opt\text{-}f}$ = 13.7% to w_2 = 16%, the matric suction was decreased and some swelling was expected, decreasing the large pores a little. Even though some microstructure changes could occur during drying or wetting, it appeared that the effects of drying or wetting were much less significant than those of the remolded water content (see Figs. 12-13).

Shear strength of soil mixture and microstructure of fine soils

The results obtained from monotonic triaxial test indicated that the shear strength was different between Test 1 and Test 2 at f_v = 10% and w_1 = 11%, with two different sample preparation approaches. On the contrary, no marked difference of shear strength was observed between Test 3 and Test 4 at f_v = 10% and w_2 = 16%, even though the sample preparation approaches were also different. Moreover, quite similar shear strength was identified for Test 5 and Test 6 and for Test 7 and Test 8 at f_v = 35%, whatever the water content values (dry side or wet side).

Wang et al. (2018a) showed that at f_v = 10% (smaller than the characteristic value $f_{v\text{-}cha} \approx 27\%$), the fine/coarse soil mixture was characterized by a fine matrix macrostructure with coarse grains floating in it. By contrast, at f_v = 35% (larger than $f_{v\text{-}cha} \approx 27\%$), the mixture was characterized by a coarse grain skeleton microstructure. As a consequence, the shear strength of Test 1 to Test 4 at f_v = 10% was governed by the fine soils. In that case, the changes of microstructure of fine soils with compaction water content greatly affected the overall mechanical behaviours. On the dry side, bi-modal porosity existed in the samples (Test 1 and Test 2 in Fig. 12(b_1)), corresponding to the micro-pores within aggregates (intra-aggregate pores) and the macro-pores between aggregates (inter-aggregate pores). In that case, the inter-aggregate pores played an important role in the structure of fine soils and the assembly of aggregates governed the soil stiffness. Since the quantity of inter-aggregate pores for Test 2 was

much larger than that of Test 1 (Fig. 12 (b_1)), less pronounced peak deviator stress was identified for Test 2 (q_{max} = 230 kPa) as compared to Test 1 (q_{max} = 397 kPa) in Fig. 7. The similar observation was made by Zhang et al. (2018b) on the stiffness of fine soils with different remolding water contents: the inter-aggregate pores dominated the soil microstructure on the dry side of Proctor optimum. With the increase of water content, the increase of inter-aggregate contact surface gave rise to the increase of maximum shear modulus G_{max} or soil stiffness. Vanapalli et al. (1996a, 1996b) also found the effect of inter-aggregate contact surface on unsaturated shear strength of compacted glacier till. The results showed that for a given matrix suction, the specimens prepared at higher water content have larger shear strength. In addition, it has been reported by several investigators that the unsaturated shear strength and soil-water retention curves were dependent on soil microstructure which was in turn dependent on the remolding water content (Delage et al. 1996; Vanapalli et al. 1996a, 1996b; Birle et al. 2008).

By contrast, on the wet side (w_2 = 16%), all aggregates were destroyed and a uni-modal porosity was usually observed (Test 3 and Test 4 in Fig. 12(b_2)). Thus, quite similar global mechanical behaviours were expected (Fig. 8).

When the value of f_v became 35%, higher than $f_{v\text{-}cha} \approx 27\%$, the soil microstructure was rather characterised by a coarse grain skeleton. Thus, the mechanical responses in Test 5 to Test 8 at f_v = 35% were expected to be governed by the coarse grains skeleton (Figs. 9-10), whatever the microstructure of fines – bi-modal for Test 5 and Test 6 at w_1 = 11% (Figs. 13(a_1) - (b_1)) and uni-modal for Test 7 and Test 8 at w_2 = 16% (Figs. 13(a_2) - (b_2)). Indeed, the same shear behaviours were observed from Test 5 and Test 6 at w_1 = 11% shown in Fig. 9, and the same shear behaviours were observed from Test 7 and Test 8 at w_2 = 16% shown in Fig. 10.

Distribution of fine soils

Comparison of the PSD curves between Test 6 and Test 6' at f_v = 35% (Figs. 13(a_1) - (b_1)) showed that they were not the same, even though both were of bi-modal nature. For further analysis, the PSD curve of Test 2 at f_v = 10% was put together with those of Test 6 and Test 6' at f_v = 35% in Figs. 14(a) - (b). It appeared that the PSD curve of Test 6' was characterised by a larger value of intruded mercury void ratio (e_M = 0.72) and a larger quantity of macro-pores, as compared with that of Test 6. The quantity of macro-pores of Test 2 was between those of Test 6 and Test 6'. This suggested two categories of fine soils in the coarse grains skeleton structure (f_v = 35%), namely dense fine soils in-between coarse grains (Test 6) and loose fine

soils in macro-pores among grains (Test 6'). On the contrary, in the case of fine matrix macrostructure (f_v = 10%), fine soils were relatively uniformly distributed.

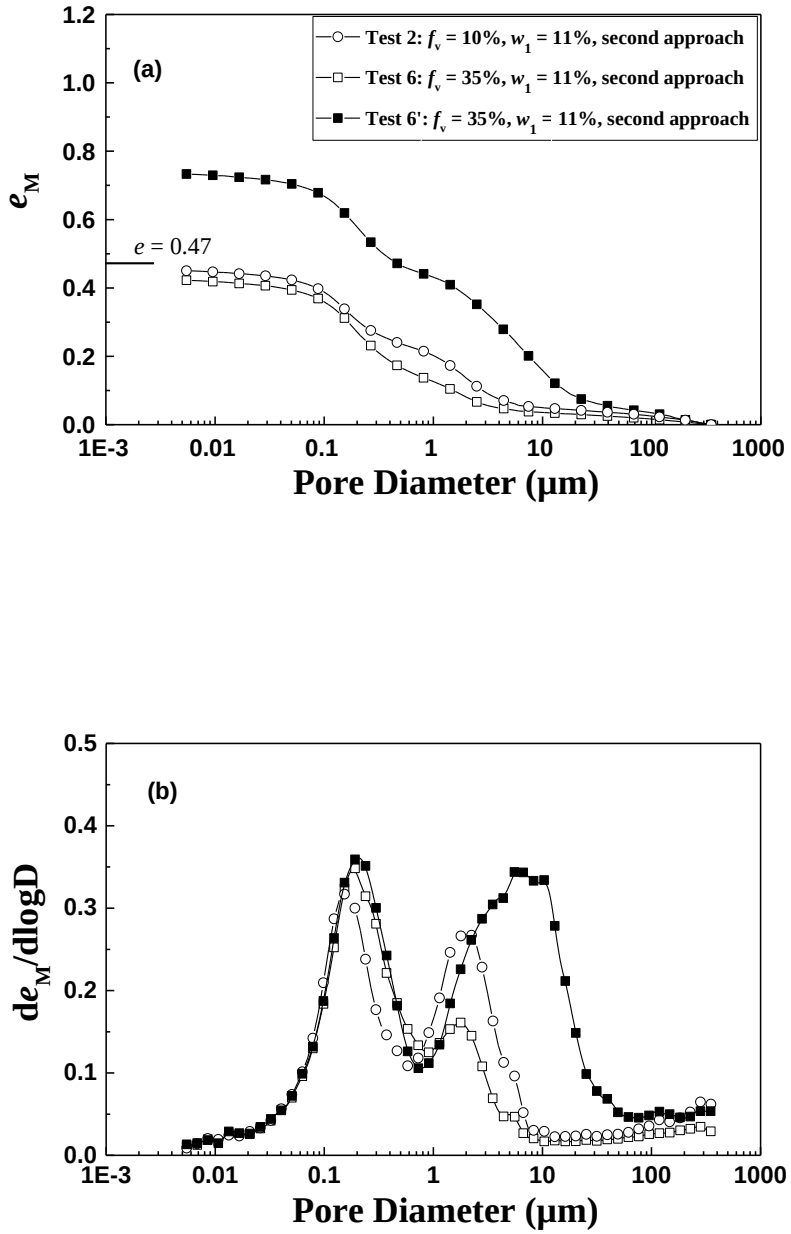

Fig. 14. Comparison of pore size distribution of fine soils for samples at f_v = 10% and f_v = 35%

At f_v = 10%, the inter-particle forces were expected to be transmitted in the fine matrix, leading to a relatively uniform void ratio of fines (Test 2, Fig. 14). The situation was different at f_v = 35%, with two categories of fine soils. The dense fine soils located in-between coarse grains were compressed when the inter-particle forces were transmitted along the coarse grains skeleton, leading to a smaller void ratio and a smaller macro-pores volume of fine soils (Test 6, Fig. 14). By contrast, the loose fine soils surrounded by coarse grains were less compressed, giving rise to a larger void ratio and a larger macro-pores volume of fine soils (Test 6', Fig. 14).

The results showed that the micro-pores of samples compacted dry of optimum were almost unaffected by the compaction efforts, while the macro-pores were strongly dependent on the compaction efforts. This was consistent with the observation by Miao et al. (2007) who studied the microstructure of expansive soil with varying dry densities by mercury intrusion tests: with the increase of dry density (compaction efforts), the volume of micro-pores remained constant, while that of macro-pores significantly decreased.

Despite the existence of two categories of fine soil at high f_v = 35%, the overall mechanical behaviour was governed by the coarse grain skeleton. In other words, the variability of void ratio of fine soils has no effect on the overall mechanical behaviour of fine/coarse soil mixture in that case.

Conclusions

For the fine/coarse soil mixture, two sample preparation approaches were adopted: the first approach was to compact the fine/coarse soil mixture at the optimum water content of fines $w_{opt\text{-}f}$, then dry or wet the sample to reach the target water content w_f (w_1 = 11% on the dry side or w_2 = 16% on the wet side). The second approach was to directly compact the fine/coarse soil mixture at the target water content w_f. Through monotonic triaxial tests and mercury intrusion porosimetry observation, the effect of microstructure of fine soils on the overall mechanical behaviours of the soil mixture was evidenced.

As expected, a bi-modal microstructure of fine soils was identified on the dry side and a uni-modal microstructure on the wet side, in agreement with the findings of Delage et al. (1996). According to the studies by Wang et al. (2017, 2018a, 2018b), at f_v = 10%, the soil mixture was characterized by a fine matrix macrostructure with coarse grains floating in it, while at f_v = 35%, a coarse grains skeleton was formed. It was observed that in the former there was a strong effect

of microstructure of fine soils on the overall mechanical behaviour of the fine/coarse soil mixture, while in the latter case the effect of microstructure of fine soils became quite limited. Moreover, it was found that at f_v = 35%, the microstructures of fine soil were not uniform, with dense fines in-between coarse grains and loose fines surrounded by coarse grains.

Therefore, to minimize the effect of microstructure of fine soils on the overall mechanical behaviour of soil mixture during sample preparation, at low f_v with the macrostructure defined by fine matrix, only the first sample preparation approach can be adopted for the dry side but the two approaches can be adopted for the wet side. On the contrary, at high f_v with the microstructure defined by coarse grains skeleton, the two sample preparation approaches can be adopted, whatever the remolded water content. However, this conclusion is valid only when the mechanical behaviour is addressed. It is anticipated that the hydraulic behaviour must be significantly different between dry and wet samples, whatever the f_v values, because of the different microstructures created while compacting at different water contents.

It is worth noting that to some extent the obtained results can be helpful in evaluating the effect of the formation process on the global mechanical behavior for the interlayer soil or the fouled ballast.

Acknowledgements

This work was supported by the China Scholarship Council (CSC) and Ecole des Ponts ParisTech.

References

Ahmed, S., C. W. Lovell, & S. Diamond. 1974. Pore sizes and strength of compacted clay. Journal of the Geotechnical Engineering Division, ASCE, 100 (GT4): 407-425

ASTM International. 2011. Standard Test Method for Consolidated Drained Triaxial Compression Test for Soils. ASTM D7181-11. West Conshohocken, PA: ASTM International approved July 1, 2011. https://doi.org/10.1520/D7181-11

ASTM International. 2012. Standard Test Methods for Laboratory Compaction Characteristics of Soil Using Standard Effort (12400 ft-lbf/ft3 (600 kN-m/m3)). ASTM D698-12. West Conshohocken, PA: ASTM International approved June 10, 2000. https://doi.org/10.1520/D0698-12

Birle, E., D. Heyer and N. Vogt. 2008. Influence of the initial water content and dry density on the soil–water retention curve and the shrinkage behavior of a compacted clay. *Acta Geotechnica*, *3*(3), p.191. https://doi.org/10.1007/s11440-008-0059-y.

Cui, Y. J., C. Loiseau, and P. Delage. 2002. Microstructure Changes of a Confined Swelling Soil Due to Suction Controlled Hydration. In Unsaturated Soils: Proceedings of the Third International Conference on Unsaturated Soils, UNSAT 2002, 10–13 March 2002, Recife, Brazil, Vol. 2, edited by J. F. T. Jucá, T. M. P. de Campos, and F. A. M. Marinho, 593–598. Lisse, the Netherlands: A. A. Balkema.

Cui, Y.J., T.V. Duong, A.M. Tang, , J.C. Dupla, N. Calon, and A. Robinet. 2013. Investigation of the hydro-mechanical behaviour of fouled ballast. Journal of Zhejiang University Science A, 14(4), pp.244-255. https://doi.org/10.1631/jzus.A1200337.

Cui, Y.J., F. Lamas-Lopez, V.N. Trinh, N. Calon, S.C. D'aguiar, J.C. Dupla, A.M. Tang, J. Canou, and A. Robinet. 2014. Investigation of interlayer soil behaviour by field monitoring. *Transportation Geotechnics*, *1*(3), pp.91-105. https://doi.org/10.1016/j.trgeo.2014.04.002.

Diamond, S., 1970. Pore size distributions in clays. *Clays and clay minerals*, *18*(1), pp.7-23. https://doi.org/10.1346/CCMN.1970.0180103.

Delage, P., M. Audiguier, Y.J. Cui, and M.D. Howat. 1996. Microstructure of a compacted silt. *Canadian Geotechnical Journal*, *33*(1), pp.150-158. https://doi.org/10.1139/t96-030.

Delage, P., D. Marcial, Y.J. Cui, and X. Ruiz. 2006. Ageing effects in a compacted bentonite: a microstructure approach. *Géotechnique*, *56*(5), pp.291-304. https://doi.org/10.1680/geot.2006.56.5.291.

Duong, T.V., A.M. Tang, Y.J. Cui, V.N. Trinh, J.C. Dupla, , N. Calon, J. Canou, and A. Robinet. 2013. Effects of fines and water contents on the mechanical behavior of interlayer soil in ancient railway sub-structure. *Soils and foundations*, *53*(6), pp.868-878. https://doi.org/10.1016/j.sandf.2013.10.006.

Duong, T.V., Y.J. Cui, A.M. Tang, J.C. Dupla, J. Canou, N. Calon, and A. Robinet. 2014. Investigating the mud pumping and interlayer creation phenomena in railway sub-structure. *Engineering geology*, *171*, pp.45-58. https://doi.org/10.1016/j.enggeo.2013.12.016.

Duong, T.V., Y.J. Cui, A.M. Tang, J.C. Dupla, J. Canou, N. Calon, and A. Robinet. 2016. Effects of water and fines contents on the resilient modulus of the interlayer soil of railway substructure. *Acta Geotechnica*, *11*(1), pp.51-59. https://doi.org/10.1007/s11440-014-0341-0.

Lamas-Lopez, F., d'Aguiar, S. C., Robinet, A., Cui, Y. J., Calon, N., Canou, J., ... & Tang, A. M. 2015. In-situ investigation of the behaviour of a French conventional railway platform. Proc., Transportation Research Board TRB 2015.

Lamas-Lopez, F. 2016. Field and laboratory investigation on the dynamic behaviour of conventional railway track-bed materials in the context of traffic upgrade (Doctoral dissertation, Paris Est).

Leong, E.C., S. Tripathy, and H. Rahardjo. 2003. Total suction measurement of unsaturated soils with a device using the chilled-mirror dew-point technique. *Geotechnique*, *53*(2), pp.173-182. https://doi.org/10.1680/geot.2003.53.2.173.

Li, X. and L.M. Zhang. 2009. Characterization of dual-structure pore-size distribution of soil. *Canadian geotechnical journal*, *46*(2), pp.129-141. https://doi.org/10.1139/T08-110.

Miao, L., S.L. Houston, Y. Cui, and J. Yuan. 2007. Relationship between soil structure and mechanical behavior for an expansive unsaturated clay. *Canadian Geotechnical Journal*, *44*(2), pp.126-137. https://doi.org/10.1139/t06-108.

Qi, S., Y.J. Cui, R.P. Chen, H.L. Wang, , F. Lamas-Lopez, , P. Aimedieu, J.C. Dupla, J. Canou, and G. Saussine. 2020. Influence of grain size distribution of inclusions on the mechanical behaviours of track-bed materials. *Géotechnique*, pp.1-10. https://doi.org/10.1680/jgeot.18.P.047.

Trinh, V. N. 2011. Comportement hydromécanique des matériaux constitutifs de plateformes ferroviaires anciennes. PhD Thesis, Ecole Nationale des Ponts et Chaussées, Université Paris-Est.

Trinh, V.N., A.M. Tang, Y.J. Cui, , J.C. Dupla, J. Canou, N. Calon, L. Lambert, , A. Robinet, and O. Schoen. 2012. Mechanical characterisation of the fouled ballast in ancient railway track substructure by large-scale triaxial tests. *Soils and foundations*, *52*(3), pp.511-523. https://doi.org/10.1016/j.sandf.2012.05.009.

Vanapalli, S.K., D.G. Fredlund, D.E. Pufahl, and A.W. Clifton, 1996a. Model for the prediction of shear strength with respect to soil suction. *Canadian Geotechnical Journal*, *33*(3), pp.379-392. https://doi.org/10.1139/t96-060.

Vanapalli, S.K., D.G. Fredlund, D.E. Pufahl. 1996b. The relationship between the soil-water characteristic curve and the unsaturated shear strength of a compacted glacial till. *Geotechnical Testing Journal*, *19*(3), pp.259-268. https://doi.org/10.1520/GTJ10351J.

Vermeer, P. A. 1998. Non-associated Plasticity for Soils, Concrete and Rock. In Physics of Dry Granular Media, edited by H. J.Herrmann, J. P. Hovi, and S. Luding, 163–196. Dordrecht, the Netherlands: Springer. https://doi.org/10.1007/978-94-017-2653-5_10

Wang, H.L., Y.J. Cui, F. Lamas-Lopez, J.C. Dupla, J. Canou, N. Calon, G. Saussine, P. Aimedieu, and R.P. Chen. 2017. Effects of inclusion contents on resilient modulus and damping ratio of unsaturated track-bed materials. *Canadian Geotechnical Journal*, *54*(12), pp.1672-1681. https://doi.org/10.1139/cgj-2016-0673.

Wang, H.L., Y.J. Cui, F. Lamas-Lopez, N. Calon, G. Saussine, J.C. Dupla, J. Canou, P. Aimedieu, and R.P. Chen. 2018a. Investigation on the mechanical behavior of track-bed materials at various contents of coarse grains. *Construction and Building Materials*, *164*, pp.228-237. https://doi.org/10.1016/j.conbuildmat.2017.12.209.

Wang, H.L., Y.J. Cui, F. Lamas-Lopez, J.C. Dupla, J. Canou, N. Calon, G. Saussine, , P. Aimedieu, and R.P. Chen. 2018b. Permanent deformation of track-bed materials at various inclusion contents under large number of loading cycles. *Journal of Geotechnical and Geoenvironmental Engineering*, *144*(8), p.04018044. https://doi.org/10.1061/(ASCE)GT.1943-5606.0001911.

Zhang, L.M. and X. Li. 2010. Microporosity structure of coarse granular soils. *Journal of Geotechnical and Geoenvironmental Engineering*, *136*(10), pp.1425-1436. https://doi.org/10.1061/(ASCE)GT.1943-5606.0000348.

Zhang, F., Y.J. Cui, and W.M. Ye. 2018a. Distinguishing macro-and micro-pores for materials with different pore populations. *Géotechnique Letters*, *8*(2), pp.102-110. https://doi.org/10.1680/jgele.17.00144.

Zhang, T.W., Y.J. Cui, F. Lamas-Lopez, N. Calon, and S. Costa D'Aguiar. 2018b. Compacted soil behaviour through changes of density, suction, and stiffness of soils with remoulding water content. *Canadian Geotechnical Journal*, *55*(2), pp.182-190. https://doi.org/10.1139/cgj-2016-0628.

Su, Y., Cui, Y. J., Dupla, J. C., & Canou, J. 2020. Construction and Building Materials, 263, 120206.

Investigation of the effect of water content on the mechanical behavior of track-bed materials under various coarse grain contents

Yu Su, Yu-Jun Cui, Jean-Claude Dupla, Jean Canou

Abstract: In the French conventional railway track, an interlayer was created naturally through the interpenetration of ballast and subgrade under the effect of long-term train loading. Field investigation showed that the proportion of ballast grains decreased over depth in the interlayer. Moreover, the water content of interlayer soils varied depending on the weather conditions, which can strongly affect the mechanical behavior of interlayer soil. In this study, the effect of water content on the mechanical behavior of interlayer soils under various coarse grain contents was investigated by monotonic triaxial tests. Three water contents of fine soil (w_f = 17.6%, 10.6%, and 7.0%), five volumetric coarse grain contents (f_v = 0%, 10%, 20%, 35%, and 45%) and three confining pressures (σ_3 = 30, 60 and 120 kPa) were considered. Results showed that a decrease of w_f led to an increase of shear strength and soil stiffness due to the effect of suction, and to an increase of dilatancy due to the aggregation of fine soils. Moreover, the variations of maximum deviator stress q_{max}, Young's modulus E_0, dilatancy angle ψ and friction angle φ with f_v followed a bi-linear pattern for the three σ_3 values, defining a characteristic volumetric coarse grain content $f_{v\text{-}cha}$ value for a given w value: $f_{v\text{-}cha} \approx$ 25%, 29% and 33% for w_f = 17.6%, 10.6% and 7.0%, respectively. The $f_{v\text{-}cha}$ corresponded to the transition from a structure dominated by fine soils to a structure dominated by coarse grains. The increase of $f_{v\text{-}cha}$ with the decrease of w_f could be attributed to the swelling and shrinkage of fines. While drying from optimum water content of fines $w_{opt\text{-}f}$ =13.7% to a lower w_f value, more coarse grains were needed to constitute the global skeleton due to the increase of the global volume of macro-pores resulted from the shrinkage of fine soils. By contrast, while wetting from $w_{opt\text{-}f}$ =13.7% to a higher w_f value, since the global volume of macro-pores decreased due to the swelling of fine soils, less coarse grains were required to constitute the global skeleton.

Keywords: fabric/structure of soils; partial saturation; laboratory tests; compaction; shear strength

Introduction

Most French conventional railway track was constructed by putting the ballast layer on the subgrade soil directly. Due to the long-term train circulation, a layer namely interlayer was naturally formed in the substructure, mainly by the interpenetration of ballast and subgrade. Considering its high dry density (2.4 Mg /m^3) and high bearing capacity (Trinh 2011), the

Ecole des Ponts ParisTech, Laboratoire Navier/CERMES, 6 – 8 av. Blaise Pascal, Cité Descartes, Champs-sur-Marne, 77455 Marne – la – Vallée cedex 2, France

French railway company (SNCF) has decided to keep it as part of the substructure in the execution of the track renewal program (Cui et al. 2013).

Based on the field investigation, the content of ballast grains was found to decrease over depth (Trinh 2011). Globally, the interlayer can be separated into two parts: the upper part dominated by ballast grains and the lower part dominated by fine soils. For the upper part, the effects of fine soil content and water content on the mechanical behavior were studied by Trinh et al. (2012), Cui et al. (2013), Duong et al. (2013, 2014, 2016) and Lamas-Lopez et al. (2015, 2016) by performing monotonic and cyclic triaxial tests. In order to extend the study to the whole interlayer, Wang et al. (2017, 2018a, 2018b) and Qi et al. (2020) investigated the effect of coarse grain content f_v (volumetric ratio of coarse grains to total sample) on the mechanical behavior. Results revealed existence of a characteristic volumetric coarse grain content $f_{v\text{-}cha}$, below which the soil was characterised by a fine matrix with coarse grains floating in it, while beyond which the soil was characterised by a coarse grain skeleton. It is worth noting that in the previous studies, the effect of f_v on the mechanical behavior was investigated under constant water content conditions. This is obviously not the field condition where the water content varies depending on the weather conditions, resulting in changes in mechanical behavior. Therefore, from a practical point of view, it appears essential to investigate the effect of water content on the mechanical behavior of interlayer soil.

There are several studies addressing the effect of coarse grain content on the mechanical behavior of soil. Seif El Dine et al. (2010) worked on sandy matrix with f_v of gravels, showing an increase of shear strength with the increase of f_v. However, Vallejo (2001) showed an opposite trend when the mass proportion of coarse particles was beyond 65% for a mixture of rock and sand. It is worth noting that the fines involved in their studies were cohesionless soils like sand and glass beads, which did not represent the natural fine soils in the interlayer. Wang et al. (2017, 2018a, 2018b) studied the effect of f_v on the static and dynamic responses of interlayer soil, and identified a characteristic value $f_{v\text{-}cha}$ that could be used to differentiate two distinct soil fabrics. Qi et al. (2020) investigated the effect of the coefficient of uniformity C_u of coarse grains on the mechanical behavior of interlayer soils, and found that the decrease of C_u led to an increase of $f_{v\text{-}cha}$. A few studies were undertaken to investigate the water content effect on the mechanical behavior of substructure soils in terms of shear strength, resilient modulus, etc. Trinh et al. (2012) investigated the effect of water content on the mechanical behavior of fouled ballast at different water contents and found that the lower the water content,

the higher the shear strength. Duong et al. (2016) studied the effect of water content on the resilient modulus of the upper part interlayer soil by large-scale cyclic triaxial tests, and reported that the increase of water content gave rise to a decrease of resilient modulus. To the author's knowledge, there has been no work addressing the effect of water content on $f_{v\text{-}cha}$.

In this study, the effect of water content on the mechanical behavior of the interlayer soil at various f_v values was investigated by performing monotonic triaxial tests under different confining pressures. Three water contents of fine soil (17.6%, 10.6%, and 7.0%), five coarse grain contents (0%, 10%, 20%, 35%, and 45%) and three confining pressures (30, 60 and 120 kPa) were considered. The mechanical properties including Young's modulus E_0, Poisson's ratio v, dilatancy angle ψ, friction angle φ and cohesion c were analyzed. The results obtained allowed the effect of water content on the characteristic volumetric coarse grain content $f_{v\text{-}cha}$ to be clarified.

Materials and methods

Materials and sample preparation

Since it was difficult to obtain intact interlayer soil, the studied soil was reconstituted in the laboratory. For the fines, in order to simulate the grain size distribution of fine soils from 'Senissiat site' (Fig. 1), nine different commercial soils including sand and clay were mixed, with the pre-determined proportions shown in Table 1. The liquid limit and plasticity index of the reconstituted fine soil were 32% and 20%, respectively defining the fine soil as CL according to the universal soil classification system (Fig. 2). A good agreement between real fine soil and reconstituted fine soil was observed in terms of grain size distribution (Fig. 1), liquid limit and plasticity index (Fig. 2). Standard Proctor compaction was performed following ASTM D698-12 for the reconstituted fine soil (Fig. 3), allowing an optimum water content $w_{opt\text{-}f}$ = 13.7% and a maximum dry density $\rho_{dmax\text{-}f}$ = 1.82 Mg/m^3 to be identified.

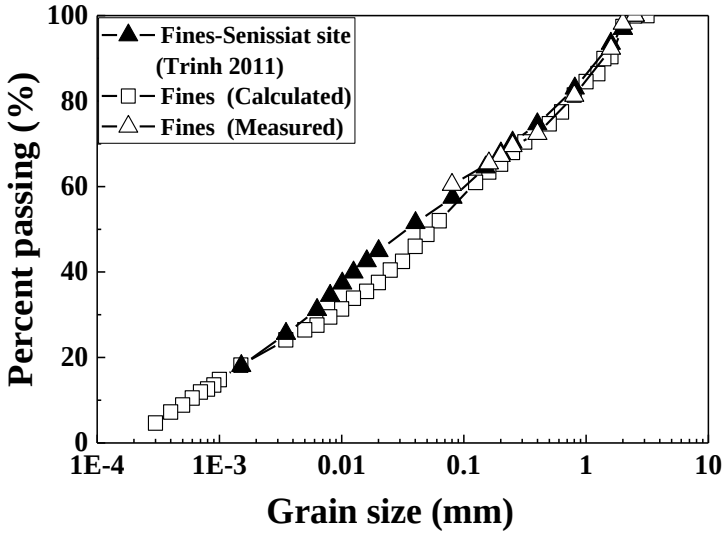

Fig. 1. Grain size distribution curves of fine soils (after Wang et al. 2018a)

Table 1. The constitution of fine soil

Soil	Mass proportion (%)	Grain size range (mm)
HN34	3.3	0.063 - 0.50
HN31	3.3	0.16 - 0.63
HN0.4-0.8	6.7	0.25 - 1
HN0.6-1.6	6.7	0.32 - 2
HN1-2.5	13.3	0.32 – 3.20
C4	16.7	0.0009 – 0.50
C10	20	0.0009 – 0.25
Speswhite	23.3	0.0003 – 0.01
Bentonite	6.7	0.001 – 0.01

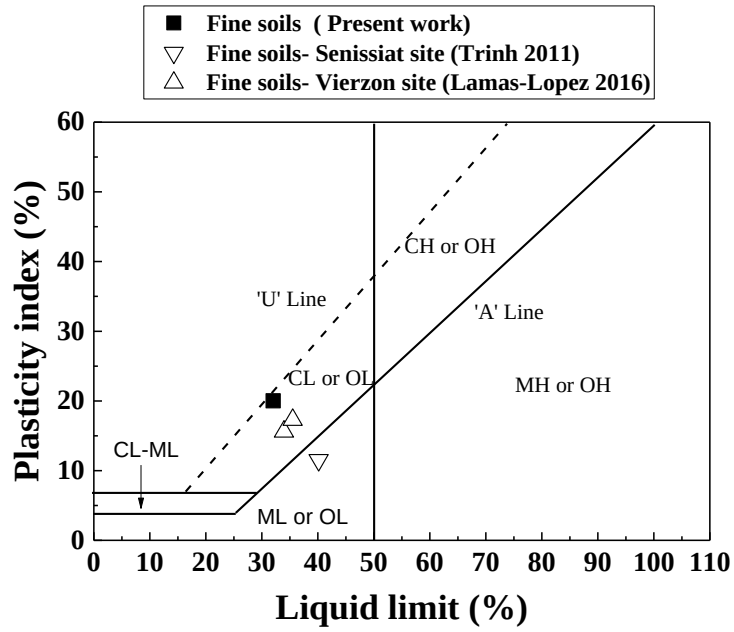

Fig. 2. Plasticity of fine soils (after Wang et al. 2018a)

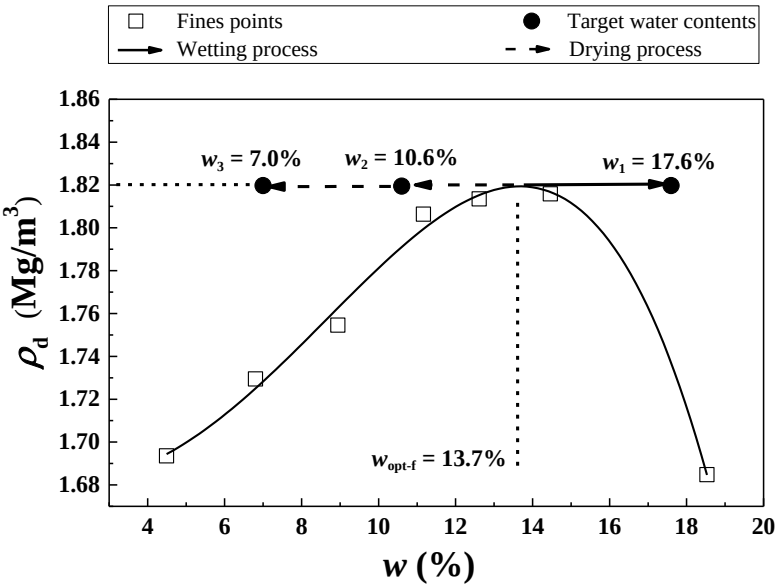

Fig. 3. Samples states with respect to the compaction curve

For the coarse grains, following the parallel similitude method adopted by Wang et al. (2018a) and Qi et al. (2020), micro-ballast was prepared to represent the real ballast by using three granular materials G 4-10, HN 2-4 and G 10-20, as shown in Fig. 4. In order to quantify the amount of micro-ballast in a sample, a parameter namely volumetric coarse grain content f_v (Seif El Dine et al. 2010; Wang et al. 2017; Wang et al. 2018a, 2018b; Qi et al. 2020) was adopted:

$$f_v = V_{in} / V_{total} \tag{1}$$

where V_{in} and V_{total} represent the coarse grain volume and the total sample volume, respectively. Note that the total sample volume V_{total} was composed of the coarse grain volume V_{in} and the fine soil volume V_{fines}. The dry density of fine soil in all samples was controlled at $\rho_{dmax\text{-}f}$ = 1.82 Mg/m^3 (Table 2). At a given f_v value, the dry mass of coarse grain, the dry mass of fine soil and the water content contained in the fine soil can be calculated. Details about the calculation could be found in Wang et al. (2018a).

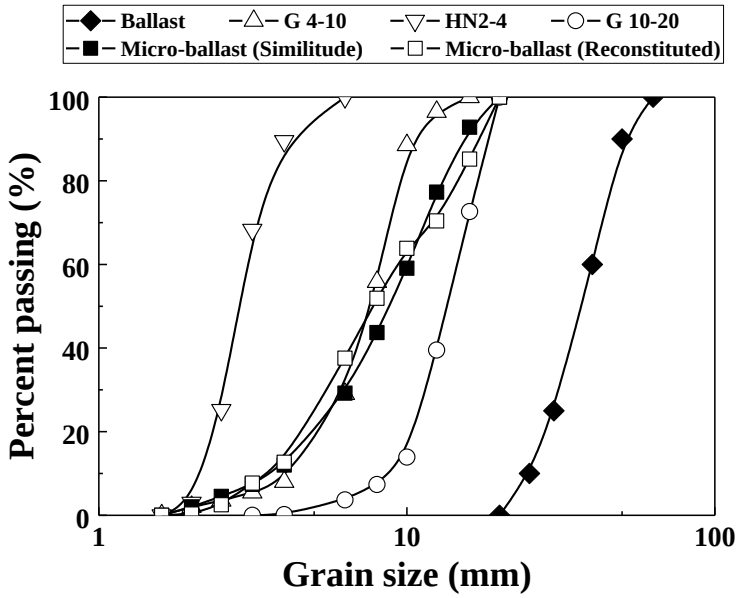

Fig. 4. Grain size distribution curves of micro-ballast and ballast (after Wang et al. 2018a)

Table 2. Experimental program

f_v (%)	Initial water content $w_{opt\text{-}f}$ (%)	Target w_f (%)	Target S_r (%)	Target $\rho_{dmax\text{-}f}$ (Mg/m^3)	Target ρ_d (Mg/m^3)	Measured ρ_d (Mg/m^3)	Confining pressure σ_3 (kPa)		
		17.6	100			1.80	30	60	120
0		10.6	60		1.82	1.85	30	60	120
		7.0	40			1.86	30	60	120
		17.6	100			1.88	30	60	120
10		10.6	60		1.91	1.93	30	60	120
		7.0	40			1.94	30	60	120
		17.6	100			1.97	30	60	120
20	13.7	10.6	60	1.82	1.99	2.01	30	60	120
		7.0	40			2.03	30	60	120
		17.6	100			2.11	30	60	120
35		10.6	60		2.12	2.13	30	60	120
		7.0	40			2.13	30	60	120
		17.6	100			2.20	30	60	120
45		10.6	60		2.21	2.22	30	60	120
		7.0	40			2.23	30	60	120

Note: f_v represents the ratio of volumetric inclusion content to the total volume of the sample (Wang et al. 2018a). $w_{opt\text{-}f}$, w_f, S_r and $\rho_{dmax\text{-}f}$ represent the optimum water content, the water content, the degree of saturation and the maximum dry density of fine soils, respectively. ρ_d represents the dry density of soil mixture sample. Measured ρ_d represents the dry density of soil mixture sample after wetting or drying from compaction water content $w_{opt\text{-}f}$ to target w_f.

For the preparation of samples at target f_v and w_f, the fine soil was prepared at optimum water content $w_{opt\text{-}f}$ = 13.7%, then stored in a container for 24 h for moisture homogenization. The fine soil was then mixed with micro-ballast grains thoroughly to reach the target f_v value. In order to attain a satisfactory homogeneity of the soil mixture, it was dynamically compacted in three layers, with the equivalent amount of fine soil and micro-ballast for each layer, to reach a total size of 100 mm diameter and 200 mm height. Fig.5 shows the samples with various f_v values, compacted at $w_{opt\text{-}f}$ = 13.7%. Note that at a given compaction effort, the dry density of fine soil changes with the variation of coarse grain content f_v. Since the dry density of fine soil in all samples was controlled at $\rho_{dmax\text{-}f}$ = 1.82 Mg/m^3, the compaction efforts was higher for the

samples at higher f_v values. As a result, higher ρ_d values were obtained for the samples with higher f_v values, as shown in Table 2.

f_v = 0% f_v = 10% f_v = 20% f_v = 35% f_v = 45%

Fig. 5. Photographs of the samples with various coarse grain contents and compacted at $w_{opt\text{-}f}$ = 13.7%

After reaching the target f_v value, either a wetting or a drying process was adopted to obtain the target w_f: w_1 = 17.6% on the wet side of optimum; w_2 = 10.6% and w_3 = 7.0% on the dry side of optimum. In the case of drying process, considering that a too fast drying would lead to sample damage by fissuring, a milder drying method was performed: the sample was exposed to the air in the laboratory for 1 h each time, and then wrapped with plastic film for equilibration. The time of equilibration needed was determined by measurement of suction and water content in three positions: in the center, ½ r and r, with r being radius of the sample. The results obtained showed that 7 h was required for reaching reasonable equilibration in terms of suction and water content (Table 3). In the case of wetting process, 10 g water was sprayed on the sample each time prior to covering it with plastic film for equilibration. The same equilibration time of at least 7 h was adopted.

Table 3. Suction and water content measured at different equilibration times for fine soils

Position	Suction (MPa)	Water content (%)	Suction (MPa)	Water content (%)
	After 6h		After 7h	
center	0.33	12.7	0.32	12.9
1/2 r	0.24	13.5	0.35	12.8
r	0.46	13.7	0.33	13.1

When wetting or drying to a target w_f, the volume of sample was measured by means of a caliper. The volume changes from initial water content $w_{opt\text{-}f}$ = 13.7% to different target w_f values are presented in Fig. 6. It appears that at a given f_v value, an increase of water content from $w_{opt\text{-}f}$ = 13.7% to w_1= 17.6% led to sample swelling, while a decrease of water content from $w_{opt\text{-}f}$ = 13.7% to w_2= 10.6% or w_3= 7.0% led to sample shrinkage. Moreover, under a given water content, the sample exhibited lower swelling-shrinkage with higher f_v values, illustrating the sensitivity of fine soil to water content changes. The measured dry densities of samples after wetting or drying are shown in Table 2.

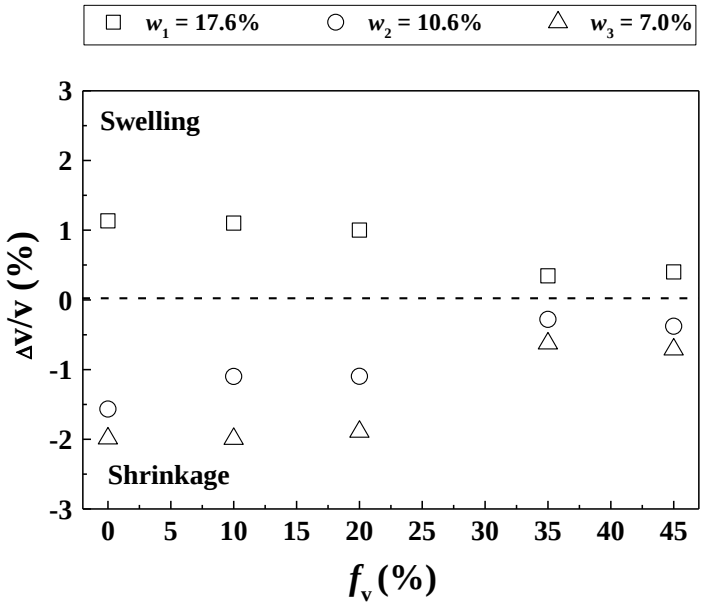

Fig. 6. Volume change of samples at different f_v values for the three target water contents

Monotonic triaxial tests

The monotonic triaxial apparatus shown in Fig. 7 was adopted in this study. The mechanical behavior of soil at five different f_v values (0%, 10%, 20%, 35%, and 45%) and three different w_f contents (17.6%, 10.6%, and 7.0%) was investigated by monotonic triaxial tests, under three different σ_3 values (30, 60 and 120 kPa). These confining pressures σ_3 were determined by the consideration of wheel load of train, the depth of interlayer soil from 250 mm to 600 mm and the Poisson ratio of 0.3-0.4 proposed by Selig and Waters (1994). Considering the wheel load of 16-22 tons per axle in France and 30 tons per axle of heavier train in other countries (Alias 1984), the corresponding range of vertical stress was estimated at 40 - 90 kPa and 120 – 140 kPa

(Duong et al. 2013), respectively; the average horizontal stress was estimated at 30 kPa and 60 kPa, respectively. In this study, the maximum horizontal stress 120 kPa was adopted, which was the same to that adopted by Wang et al. (2018a). Note that all samples were prepared to reach the target water contents (w_1 = 17.6% on the wet side, or w_2 = 10.6% and w_3 = 7.0% on the dry side) prior to starting the test. For the samples at w_1 = 17.6% (S_r = 100%), an overnight consolidation under the corresponding confining pressure was adopted prior to shearing, to ensure the dissipation of pore water pressure. On the contrary, for the samples at w_2 = 10.6% (S_r = 60%) or w_3 = 7.0% (S_r = 40%), after an application of σ_3, the sample was directly sheared, because only air was expected to be expelled. A shear rate as low as 0.1mm/min was adopted for all tests. The tests ended when a peak deviator stress appeared or the axial strain ε_1 reached 15% in case without occurrence of peak deviator stress.

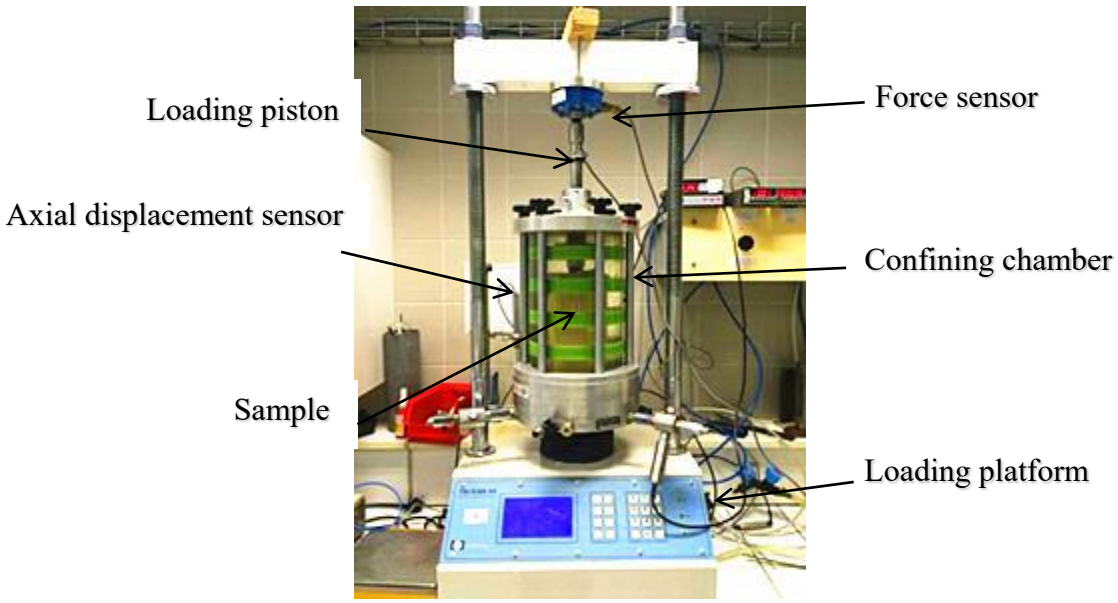

Fig. 7. Photograph of the monotonic triaxial testing system

Experimental results

Variation of shear behavior with f_v

The variations of deviator stress q and volumetric strain ε_v with axial strain ε_1 for samples at w_1 = 17.6% and five different f_v values are depicted in Fig. 8. It can be observed from Figs. 8a$_1$-8a$_3$ that under a given confining pressure σ_3 value, the maximum deviator stress q_{max} increased slowly with the increase of f_v for $f_v \leq 20\%$, while the increase of q_{max} was more pronounced for $f_v \geq 35\%$. The similar phenomena can be observed for the case of w_2 = 10.6% and w_3 = 7.0%.

In Fig. 8b$_1$, pure contractancy behaviour was observed for samples at $f_v \leq 20\%$, while for samples at $f_v \geq 35\%$, a behavior of contractancy followed by dilatancy was identified. Moreover, the larger the f_v value, the more pronounced the dilatancy behaviour. This dilatancy was however reduced by the increase of confining pressure: when σ_3 was increased from 60 kPa (Fig. 8b$_2$) to 120 kPa (Fig. 8b$_3$), the contractancy increased and the dilatancy decreased.

Variation of maximum deviator stress q_{max} with w_f

Fig. 9 depicts the variations of q_{max} against f_v at different σ_3 values for three different water contents. In the case of $w_1 = 17.6\%$ (Fig. 9a), it appears that under a given σ_3 value, the variation of q_{max} followed a bi-linear pattern with two different slopes, which defined a characteristic volumetric coarse grain content $f_{v\text{-}cha}$. Moreover, similar $f_{v\text{-}cha}$ values (around 25%) could be identified for the three different σ_3 values. Physically, the $f_{v\text{-}cha}$ value distinguished two different soil fabrics: when $f_v \leq f_{v\text{-}cha}$, the soil fabric was governed by fine soil dominated structure, while when $f_v \geq f_{v\text{-}cha}$ it was governed by coarse grain dominated structure, in agreement with the observations by Wang et al. (2018a) and Qi et al. (2020).

The same phenomena were observed for the two other water contents: $w_2 = 10.6\%$ (Fig. 9b) and $w_3 = 7.0\%$ (Fig. 9c). For each water content, q_{max} varies in a bi-linear fashion with with f_v, defining a $f_{v\text{-}cha}$ value which is independent of the σ_3 value. The values of $f_{v\text{-}cha}$ were 29% and 33% for $w_2 = 10.6\%$ and $w_3 = 7.0\%$, respectively. Comparison of the $f_{v\text{-}cha}$ values at different water contents showed that $f_{v\text{-}cha}$ increased with the decrease of water content.

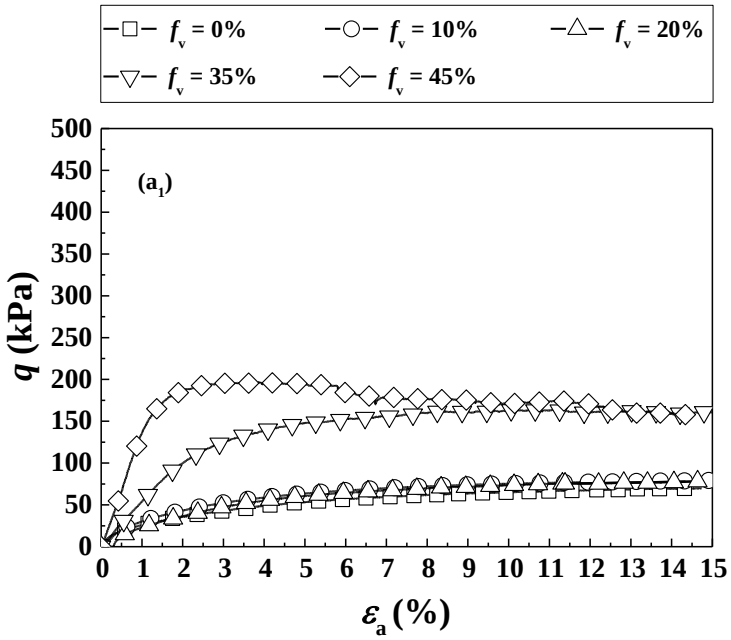
f_v = 0%
f_v = 10%
f_v = 20%
f_v = 35%
f_v = 45%
(a1)
q (kPa)
ε_a (%)

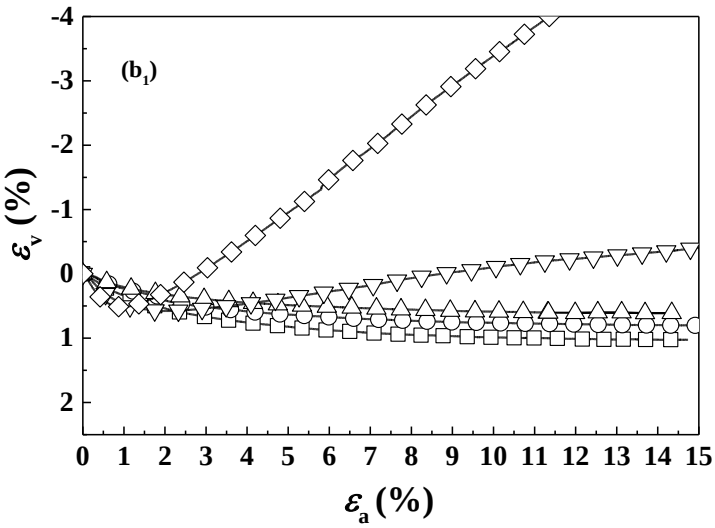
(b1)
ε_v (%)
ε_a (%)

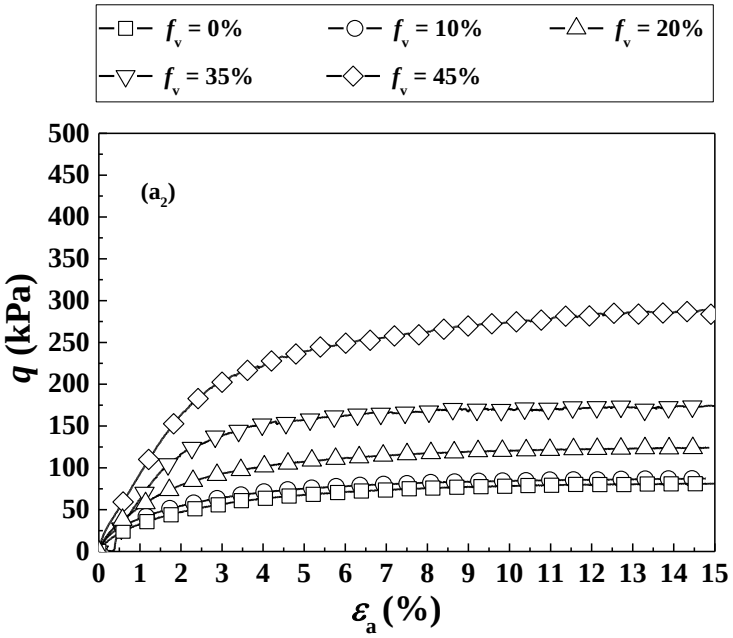
f_v = 0%
f_v = 10%
f_v = 20%
f_v = 35%
f_v = 45%
(a$_2$)
q (kPa)
ε_a (%)

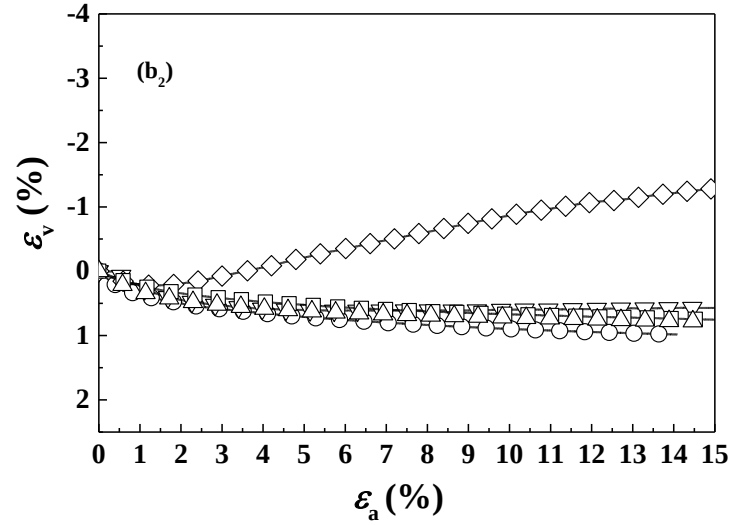
(b$_2$)
ε_v (%)
ε_a (%)

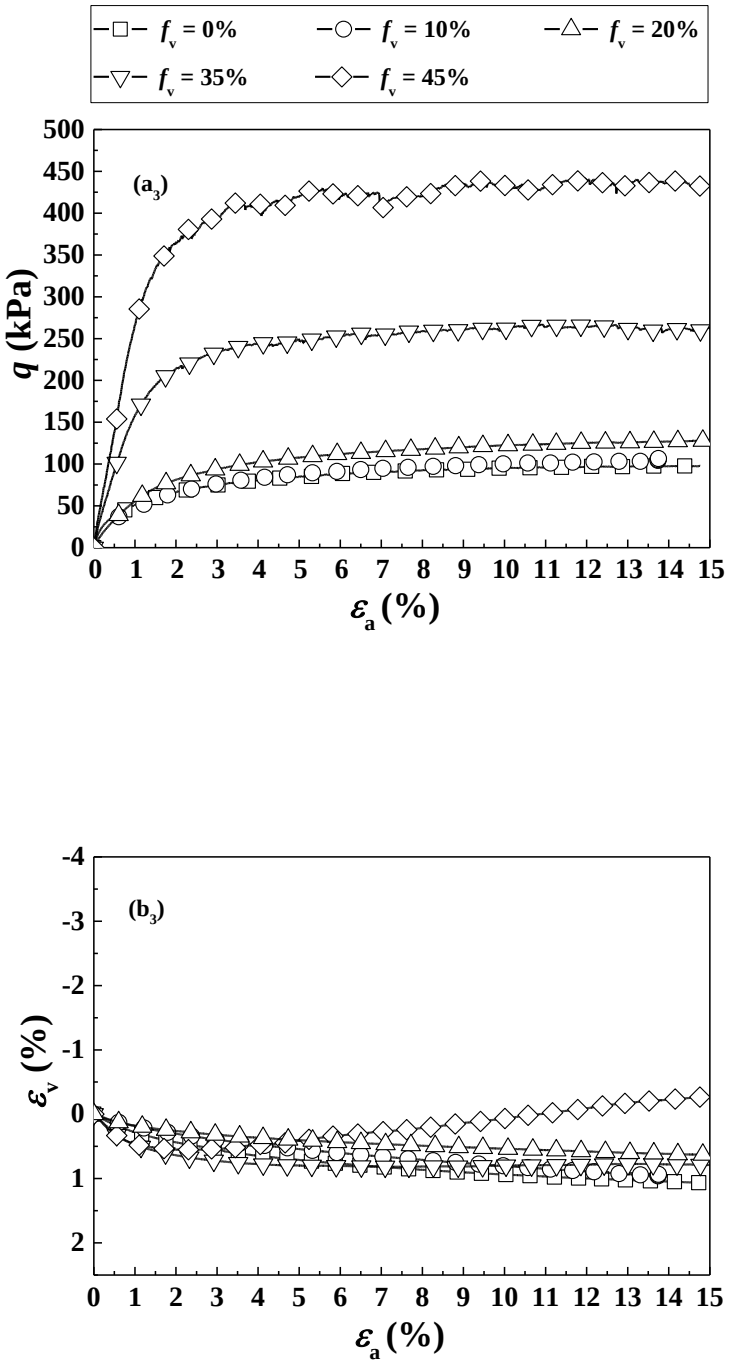

Fig. 8. Results from the tests at w_1=17.6% and different f_v values under:

(a_1) - (b_1) σ_3= 30 kPa; (a_2) - (b_2) σ_3= 60 kPa; (a_3) - (b_3) σ_3= 120 kPa

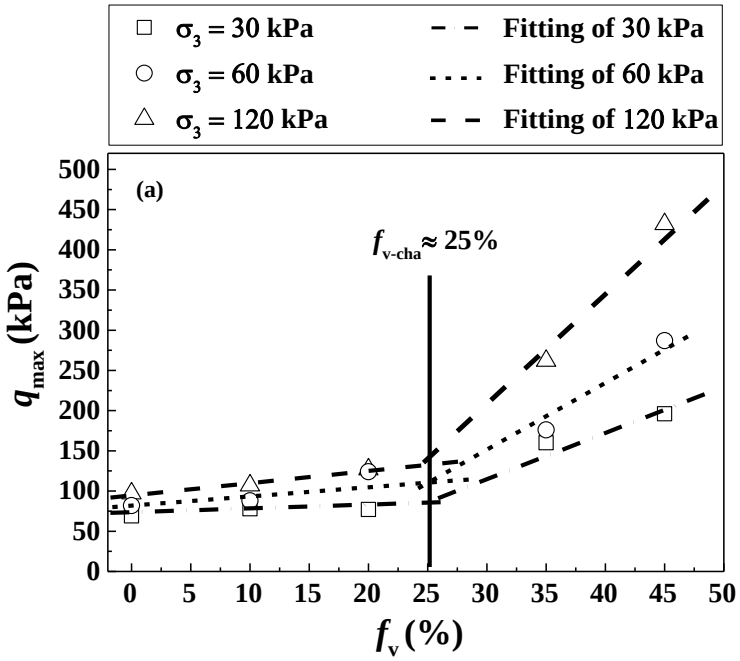
□ σ3 = 30 kPa
○ σ3 = 60 kPa
△ σ3 = 120 kPa
Fitting of 30 kPa
Fitting of 60 kPa
Fitting of 120 kPa
(a)
fv-cha≈ 25%
qmax (kPa)
fv (%)

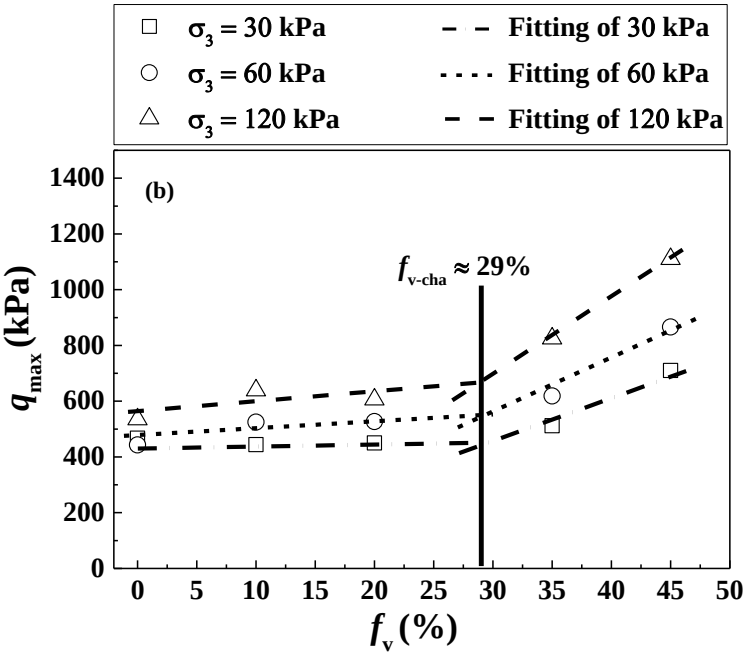
□ σ3 = 30 kPa
○ σ3 = 60 kPa
△ σ3 = 120 kPa
Fitting of 30 kPa
Fitting of 60 kPa
Fitting of 120 kPa
(b)
fv-cha ≈ 29%
qmax (kPa)
fv (%)

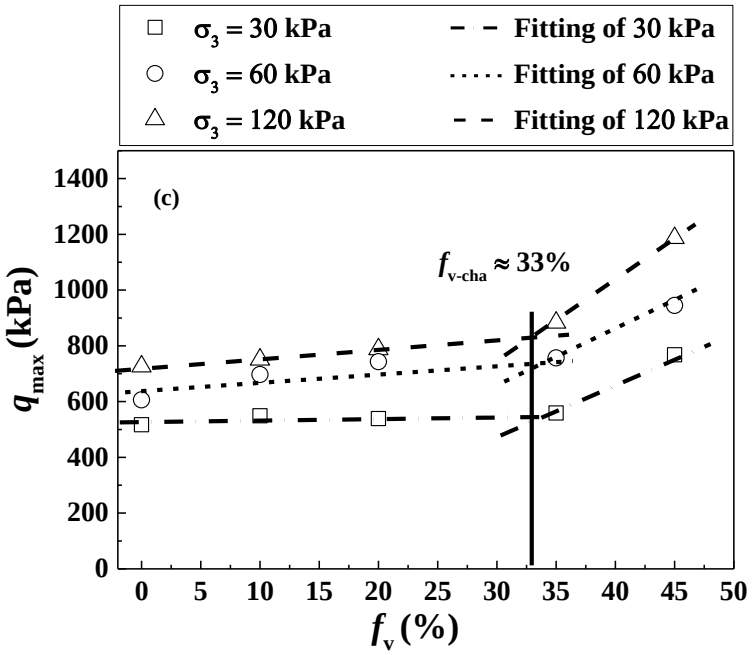

Fig. 9. Variations of peak deviator stress with f_v under different σ_3 values for:

(a) w_1 = 17.6%; (b) w_2 = 10.6%; (c) w_3 = 7.0%

Variation of Young's modulus E_0 with w_f

In this study, the Young's modulus E_0, was defined as the ratio of deviator stress to axial strain from 0% to 1%. Fig. 10 shows the variations of E_0 with f_v under different σ_3 values for the three water contents. The effect of w on Young's modulus E_0 can be clearly observed: at a given f_v and σ_3, E_0 increased with the decrease of water content. This was attributed to the increase of suction with the decrease of water content. At a given water content, a bi-linear fitting could be also applied to represent changes of E_0 with f_v for all σ_3 values. This also defined a characteristic volumetric coarse grain content $f_{v\text{-}cha}$, which was independent of σ_3. As far as the variation of $f_{v\text{-}cha}$ with w_f was concerned, it appeared from Fig. 10 that $f_{v\text{-}cha}$ increased with the decrease of w_f: $f_{v\text{-}cha}$ was around 25% for w_1 = 17.6% (Fig. 10a), 29% for w_2 = 10.6% (Fig. 10b) and 33% for w_3 = 7% (Fig. 10c), which agreed well with the previous observation while studying the effect of water content on q_{max} in Fig. 9.

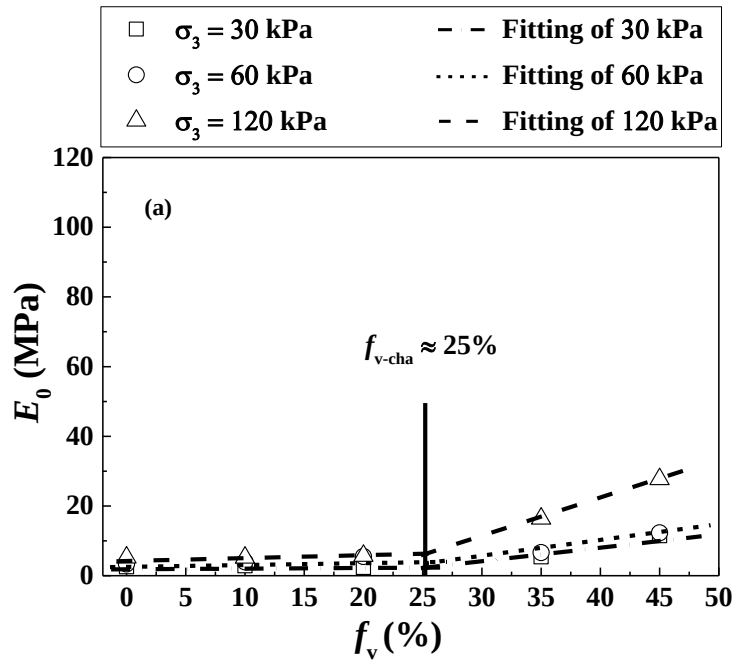
□ σ3 = 30 kPa
○ σ3 = 60 kPa
△ σ3 = 120 kPa
Fitting of 30 kPa
Fitting of 60 kPa
Fitting of 120 kPa
(a)
fv-cha ≈ 25%
E0 (MPa)
fv (%)
0
20
40
60
80
100
120
0
5
10
15
20
25
30
35
40
45
50

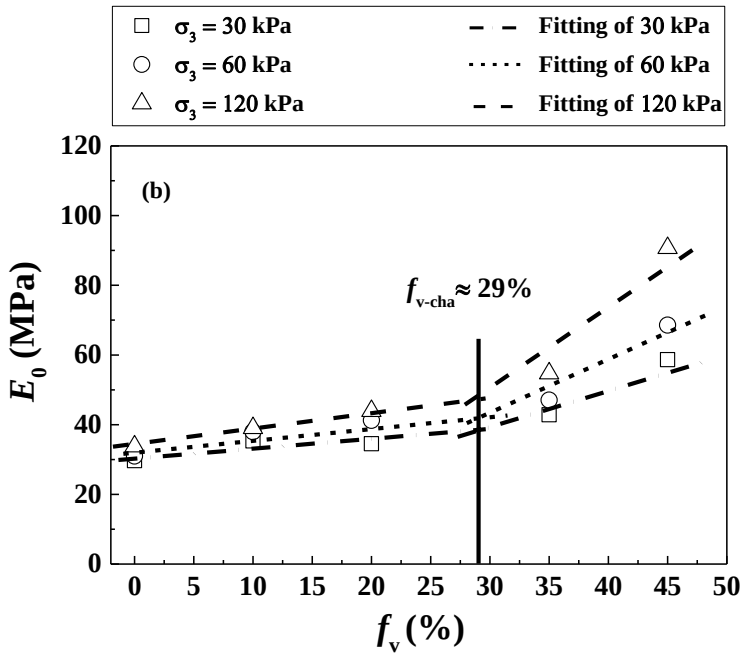
□ σ3 = 30 kPa
○ σ3 = 60 kPa
△ σ3 = 120 kPa
Fitting of 30 kPa
Fitting of 60 kPa
Fitting of 120 kPa
(b)
fv-cha ≈ 29%
E0 (MPa)
fv (%)
0
20
40
60
80
100
120
0
5
10
15
20
25
30
35
40
45
50

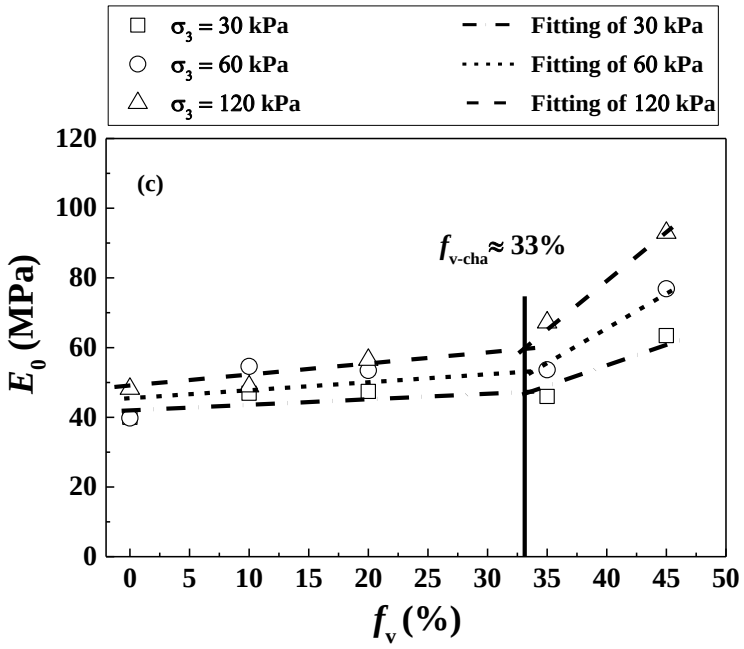

Fig. 10. Variations of initial Young's modulus with f_v under different σ_3 values for:

(a) w_1 = 17.6%; (b) w_2 = 10.6%; (c) w_3 = 7.0%

Variations of Poisson's ratio v and dilatancy angle ψ with w_f

Based on the volumetric strain-axial strain curves, the Poisson's ratio v and the dilatancy angle ψ were determined using respectively Eqs. (1) and (2) (Vermeer 1998):

$$v = (1- k_c)/2 \quad (1)$$

$$\sin \psi = k_D /(-2+ k_D) \quad (2)$$

where k_c and k_D are the slopes of volumetric strain-axial strain curves in the contractancy phase and dilatancy phase, respectively.

Fig. 11 depicts the variations of Poisson's ratio v versus f_v at different σ_3 values for three water contents. At w_1 = 17.6% (Fig. 11a), v was not significantly influenced by σ_3 and f_v, with the values fluctuating around v = 0.36. The values of v at $f_v \leq 20\%$ were slightly larger than those at $f_v \geq 35\%$. This was due to the transition of soil fabric from fine soils dominated structure to

coarse grains dominated structure, which resulted in the increase of soil stiffness and the decrease of horizontal strain. Moreover, the difference of v between $f_v \leq 20\%$ and $f_v \geq 35\%$ decreased with the decrease of water content. The average value of v was 0.21 at $w_2 = 10.6\%$ (Fig. 11b) and 0.19 at $w_3 = 7.0\%$ (Fig. 11c). At $w_3 = 7.0\%$, the v remained almost unchanged with the increase of f_v. Overall, it appeares that the average value of v decreased with the decreasing water content, suggesting that the lateral strain was reduced by the increase of suction or decrease of water content.

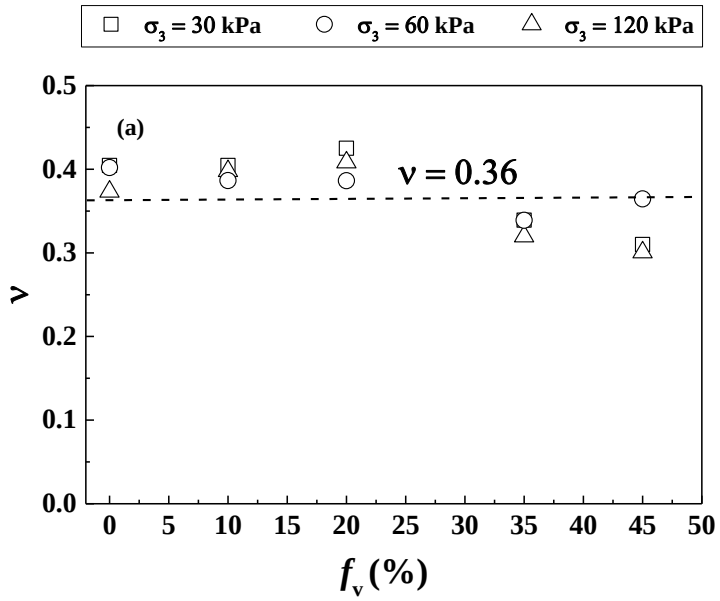

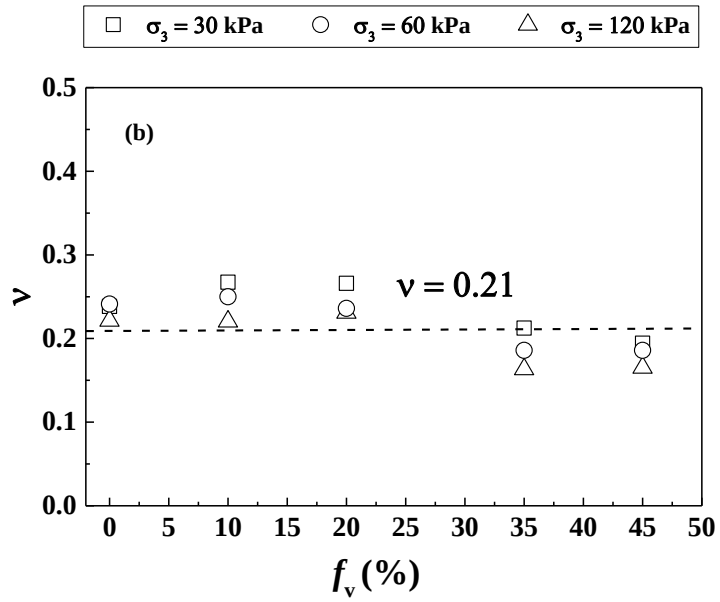

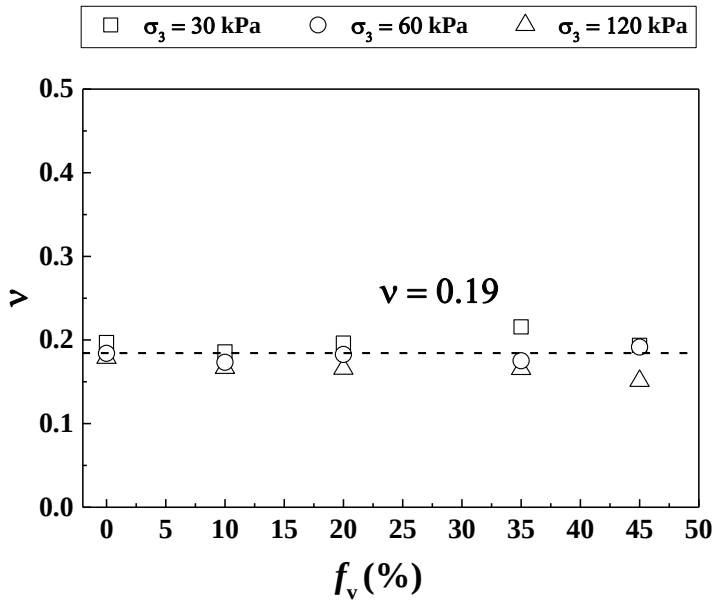

Fig. 11. Variations of Poisson's ratio with f_v under different σ_3 values for:

(a) w_1 = 17.6%; (b) w_2 = 10.6%; (c) w_3 = 7.0%

The effect of w_f on the dilatancy angle ψ can be clearly observed in Fig. 12: under given f_v and σ_3 values, the ψ increased with the decrease of w_f. This could be attributed to the aggregation of fine soil induced by the increase of suction. Indeed, a lower water content would generate a higher suction. In that case, the fine soils behaved more like granular materials, exhibiting more dilatancy behavior, as shown by Cui and Delage (1996) and Ng et al. (2017).

As shown in Fig. 12a (w_1 = 17.6%), no dilatancy behavior was observed for f_v varying from 0% to 20% at all σ_3 values, whereas an obvious dilatancy behaviour was observed for f_v = 35% at σ_3 = 30 kPa and for f_v = 45% at all σ_3 values. In addition, in Fig. 12b and Fig. 12c, a distinct change of ψ was observed from $f_v \leq 20\%$ to $f_v \geq 35\%$, defining a value of characteristic volumetric coarse grain content $f_{v\text{-}cha} \approx 29\%$ at w_2 = 10.6% and $f_{v\text{-}cha} \approx 33\%$ at w_3 = 7.0%. This increase of $f_{v\text{-}cha}$ with the decrease of water content was consistent with the observation of water effect on q_{max} and E_0.

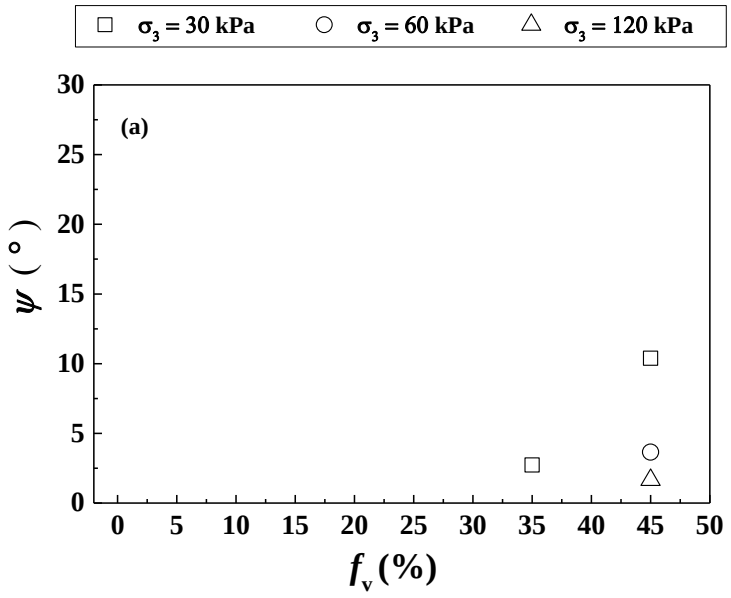
□ σ3 = 30 kPa
○ σ3 = 60 kPa
△ σ3 = 120 kPa
(a)
ψ (°)
fv (%)

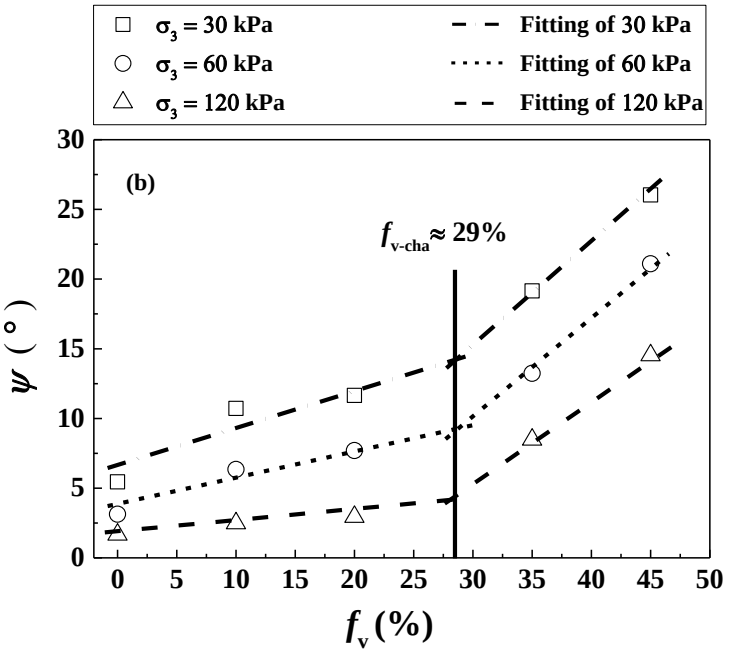
□ σ3 = 30 kPa
○ σ3 = 60 kPa
△ σ3 = 120 kPa
Fitting of 30 kPa
Fitting of 60 kPa
Fitting of 120 kPa
(b)
fv-cha≈ 29%
ψ (°)
fv (%)

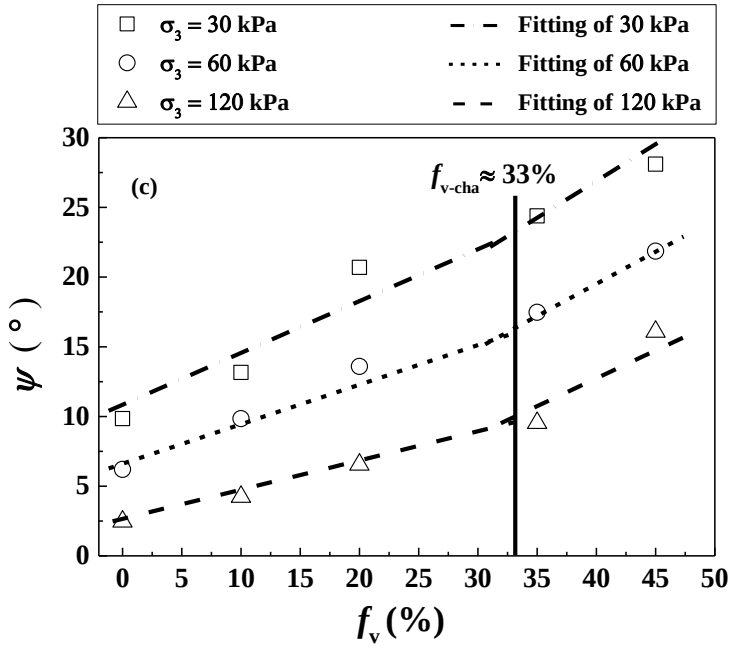

Fig. 12. Variations of dilatancy angle with f_v under different σ_3 values for:

(a) w_1 = 17.6%; (b) w_2 = 10.6%; (c) w_3 = 7.0%

Variations of cohesion c and friction angle φ with w_f

The values of cohesion *c* and friction angle φ were determined based on the peak deviator stress values. Fig.13 depicts the variation of cohesion *c* with w_f. It can be observed that at a given f_v, the cohesion *c* increased with the decrease of water content. This could be attributed to the effect of suction on the fine soil.

For the friction angle φ, Fig.14 shows that φ increased with the decrease of w_f. This confirmed the aggregation phenomenon with the decrease of w_f for the fine soils. The similar observation was made by Zhao et al. (2013) while studying the shear strength of a mixture of sand, silt and gravel. Moreover, under a given w_f, a bi-linear pattern of increasing trend with f_v was observed for φ. A value of $f_{v\text{-}cha}$ could be thus identified for each water content: $f_{v\text{-}cha} \approx$ 25%, 29%, 33% for w_f = 17.6%, 10.6%, 7.0%, respectively, in agreement with the effects of water content on q_{max}, E_0 and ψ.

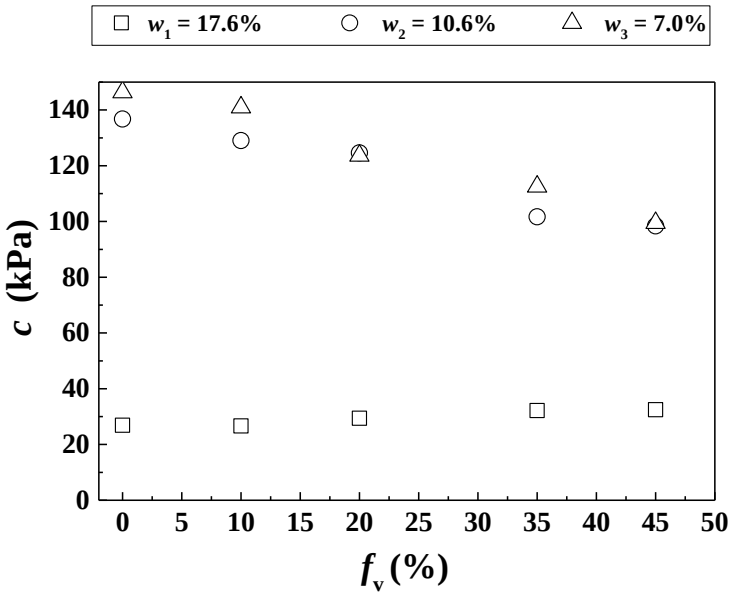

Fig. 13. Variations of cohesion with f_v under different water contents

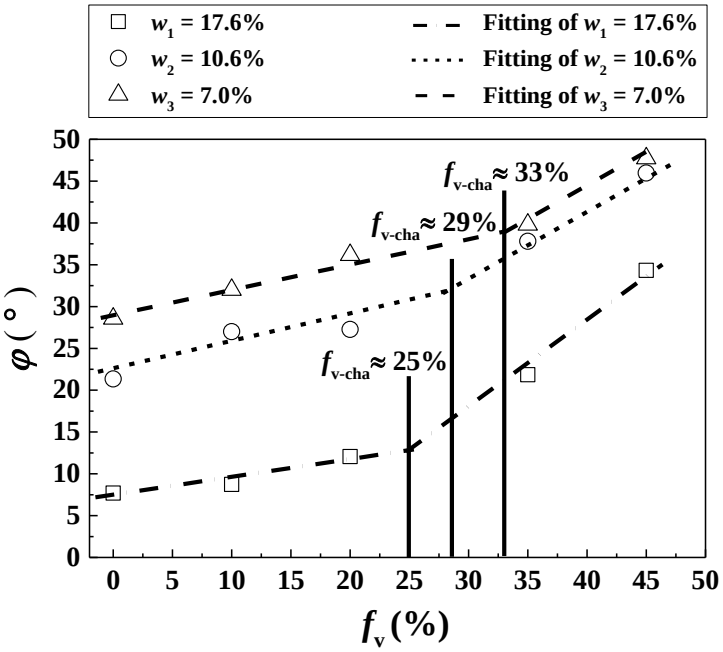

Fig. 14. Variations of friction angle with f_v under different water contents

Discussions

The test results showed that the value of $f_{v\text{-}cha}$ increased with the decrease of water content, as shown in Table 4. Wang et al. (2018a) obtained a value of $f_{v\text{-}cha}$ equal to 27% at the optimum water content $w_{opt\text{-}f}$ = 13.7%, which came to confirm the observation made in this study.

As mentioned before, the $f_{v\text{-}cha}$ corresponded to the transition of soil fabric: when $f_v \leq f_{v\text{-}cha,}$ the soil fabric was the fine soil dominated structure, while when $f_v \geq f_{v\text{-}cha,}$ the soil fabric changed to the coarse grains dominated structure. In other words, the $f_{v\text{-}cha}$ represented the minimum f_v value needed for forming a coarse grains dominated structure. When $f_v \geq f_{v\text{-}cha}$, two categories of fine soil were expected, namely a first category of dense fine soil situated between coarse grains and a second category of loose fine soil situated in the macro-pores surrounded by coarse grains. The former contributed to the loading-bearing skeleton of coarse grains, whereas the latter contributed little, as concluded by de Frias Lopez (2016) through discrete element analysis.

The variation of $f_{v\text{-}cha}$ with w_f could be attributed to the swelling upon wetting and shrinkage upon drying of these two categories of fines. With the decrease of water content, the two categories of fine soil would shrink. The shrinkage of the first category of fines would lead to a decrease of macro-pores between coarse grains, while the shrinkage of the second category would lead to an increase of macro-pores surrounded by coarse grains. As the density was expected to be higher and the quantity was expected to be smaller for the first category of fines, the decrease of macro-pores volume due to the shrinkage of the first category of fines was expected to be much smaller than the increase of macro-pores volume due to the shrinkage of the second category of fines. This was supported by the observation from Zhang and Li (2010) using mercury intrusion porosimetry, who studied the fine/coarse soil mixture and reported that the structure supported by coarse grains was stable, and thus the shrinkage of clayey soils gave rise to an increase of the volume of macro-pores surrounded by coarse particles. The effect of shrinkage of fine soil was also observed by Fies et al. (2002) for the ternary mixtures of sand, silt and clay soils. They reported that when the fine fraction contained larger than 25% clay content, the shrinkage of fine fraction gave rise to the formation of macro-pores among the coarse fraction. It is worth noting that in this study, 30% of clay content of Speswhite and Bentonite were shown in Table 1 for the fine fraction, which contributed to the formation of macro-pores in the coarse grain skeleton. Thus, with the increase of volume of macro-pores, more coarse grains were needed to constitute a global skeleton. This is characterized by the increase of $f_{v\text{-}cha}$ value.

Conclusions

The effect of w_f on the mechanical behavior of interlayer soil at various f_v was investigated by monotonic triaxial tests. Three water contents (w_f = 17.6%, 10.6%, and 7.0%), five volumetric coarse grain contents (f_v = 0%, 10%, 20%, 35% and 45%) and three confining pressures (σ_3 = 30, 60 and 120 kPa) were considered. The obtained results allowed the following conclusions to be drawn.

The decrease of water content led to an increase of the peak deviator stress q_{max} and the Young's modulus E_0. This could be explained by the effect of suction with the decrease of water content. The Poisson's ratio v was found to decrease with the decrease of water content, because the horizontal deformation was reduced by the increase of suction. The dilatancy angle ψ and the friction angle φ were found to increase with the decrease of water content. This was attributed to the aggregation of fine soil induced by the increase of suction, enhancing the dilatancy behavior and the friction of soil. A larger cohesion c was observed at lower w_f, also due to the effect of suction in fine soil.

The variation of q_{max}, E_0, ψ, and φ with f_v followed a bi-linear pattern, defining a same characteristic $f_{v\text{-}cha}$ value for a given w_f value: $f_{v\text{-}cha} \approx 25\%$, 29% and 33% for w_f = 17.6%, 10.6% and 7.0%, respectively. The value of $f_{v\text{-}cha} \approx 27\%$ at w_{opt} = 13.7% reported by Wang et al. (2018a) came to support this observation. This was attributed to the swelling upon wetting and shrinkage upon drying of two categories of fine soil: a first category of dense fine soil situated between coarse grains and a second category of loose fine soil situated in the macro-pores surrounded by coarse grains. With the decrease of water content, the two categories of fine soils would shrink. Moreover, the shrinkage of the first category of fines would lead to a decrease of macro-pores between coarse grains, while the shrinkage of the second category would lead to an increase of macro-pores surrounded by coarse grains. As the decrease of macro-pores volume due to the shrinkage of the first category of fines was expected to be much smaller than the increase of macro-pores volume due to the shrinkage of the second category of fines, the global macro-pores volume was increasing with the decrease of water content. In that case, more coarse grains were needed to constitute a global skeleton, leading to an increase of $f_{v\text{-}cha}$.

Acknowledgements

This work was supported by the China Scholarship Council (CSC) and Ecole des Ponts ParisTech.

References

Alias La voie ferr´ee. 1984. Techniques de construction et d'entretien. 2nd Ed., Eyrolles.

ASTM D698-12. 2012. Standard test methods for laboratory compaction characteristics of soil using standard effort. ASTM International, West Conshohocken, Pa.

Cui, Y. J., & Delage, P. 1996. Yeilding and plastic behaviour of an unsaturated compacted silt. Géotechnique, 46(2), 291-311.

Cui, Y.J., Duong, T.V., Tang, A.M., Dupla, J.C., Calon, N. and Robinet, A., 2013. Investigation of the hydro-mechanical behaviour of fouled ballast. Journal of Zhejiang University Science A, 14(4), pp.244-255.

Duong, T.V., Tang, A.M., Cui, Y.J., Trinh, V.N., Dupla, J.C., Calon, N., Canou, J. and Robinet, A., 2013. Effects of fines and water contents on the mechanical behavior of interlayer soil in ancient railway sub-structure. *Soils and foundations*, *53*(6), pp.868-878.

Duong, T.V., Cui, Y.J., Tang, A.M., Dupla, J.C., Canou, J., Calon, N. and Robinet, A., 2014. Investigating the mud pumping and interlayer creation phenomena in railway sub-structure. *Engineering geology*, *171*, pp.45-58.

Duong, T.V., Cui, Y.J., Tang, A.M., Dupla, J.C., Canou, J., Calon, N. and Robinet, A., 2016. Effects of water and fines contents on the resilient modulus of the interlayer soil of railway substructure. *Acta Geotechnica*, *11*(1), pp.51-59.

de Frias Lopez, R., Silfwerbrand, J., Jelagin, D., & Birgisson, B. 2016. Force transmission and soil fabric of binary granular mixtures. Géotechnique, 66(7), 578-583.

Fiès, J. C., Louvigny, N. D. E., & Chanzy, A. 2002. The role of stones in soil water retention. European Journal of Soil Science, 53(1), 95-104.

Lamas-Lopez, F., d'Aguiar, S.C., Robinet, A., Cui, Y.J., Calon, N., Canou, J., Dupla, J.C. and Tang, A.M., 2015. In-situ investigation of the behaviour of a French conventional railway platform. In *Proceedings of the transportation research board 94th annual meeting. Washington, DC* (pp. 15-1076).

Lamas-lopez, F. 2016. Field and laboratory investigation on the dynamic behavior of conventional railway track-bed materials in the context of traffic upgrade. PhD Thesis, Ecole Nationale des Ponts et Chaussées, Université Paris-Est.

Ng, C. W. W., Baghbanrezvan, S., Sadeghi, H., Zhou, C., & Jafarzadeh, F. 2017. Effect of specimen preparation techniques on dynamic properties of unsaturated fine-grained soil at high suctions. Canadian Geotechnical Journal, 54(9), 1310-1319.

Qi, S., Cui, Y. J., Chen, R. P., Wang, H. L., Lamas-Lopez, F., Aimedieu, P., ... & Saussine, G. 2020. Influence of grain size distribution of inclusions on the mechanical behaviours of track-bed materials. Géotechnique, 70(3), 238-247.

Selig, E. T., & Waters, J. M. 1994. Track geotechnology and substructure management. Thomas Telford.

Seif El Dine, B., Dupla, J. C., Frank, R., Canou, J., & Kazan, Y. 2010. Mechanical characterization of matrix coarse-grained soils with a large-sized triaxial device. Canadian Geotechnical Journal, 47(4), 425-438.

Trinh, V. N. 2011. Comportement hydromécanique des matériaux constitutifs de plateformes ferroviaires anciennes. PhD Thesis, Ecole Nationale des Ponts et Chaussées, Université Paris-Est.

Trinh, V.N., Tang, A.M., Cui, Y.J., Dupla, J.C., Canou, J., Calon, N., Lambert, L., Robinet, A. and Schoen, O., 2012. Mechanical characterisation of the fouled ballast in ancient railway track substructure by large-scale triaxial tests. *Soils and foundations*, *52*(3), pp.511-523.

Vermeer, P. A. 1998. Non-associated Plasticity for Soils, Concrete and Rock. In Physics of Dry Granular Media, edited by H. J.Herrmann, J. P. Hovi, and S. Luding, 163–196. Dordrecht, the Netherlands: Springer. https://doi.org/10.1007/978-94-017-2653-5_10

Vallejo, L. E. 2001. Interpretation of the limits in shear strength in binary granular mixtures. Canadian Geotechnical Journal, 38(5), 1097-1104.

Wang, H.L., Cui, Y.J., Lamas-Lopez, F., Dupla, J.C., Canou, J., Calon, N., Saussine, G., Aimedieu, P. and Chen, R.P., 2017. Effects of inclusion contents on resilient modulus and damping ratio of unsaturated track-bed materials. *Canadian Geotechnical Journal*, *54*(12), pp.1672-1681.

Wang, H.L., Cui, Y.J., Lamas-Lopez, F., Calon, N., Saussine, G., Dupla, J.C., Canou, J., Aimedieu, P. and Chen, R.P., 2018a. Investigation on the mechanical behavior of track-bed materials at various contents of coarse grains. *Construction and Building Materials*, *164*, pp.228-237.

Wang, H.L., Cui, Y.J., Lamas-Lopez, F., Dupla, J.C., Canou, J., Calon, N., Saussine, G., Aimedieu, P. and Chen, R.P., 2018b. Permanent deformation of track-bed materials at various inclusion contents under large number of loading cycles. *Journal of Geotechnical and Geoenvironmental Engineering*, *144*(8), p.04018044.

Zhang, L.M. and Li, X., 2010. Microporosity structure of coarse granular soils. *Journal of Geotechnical and Geoenvironmental Engineering*, *136*(10), pp.1425-1436.

Zhao, H. F., Zhang, L. M., & Fredlund, D. G. 2013. Bimodal shear-strength behavior of unsaturated coarse-grained soils. Journal of geotechnical and geoenvironmental engineering, 139(12), 2070-2081.

CHAPTER IV. MECHANICAL BEHAVIOR OF SOIL MIXTURE UNDER CYCLIC LOADING

In-situ investigation showed that the interlayer soil was subjected to varying traffic loadings. With respect to rainfall and evaporation, the variation of water content induced changes of dynamic properties of interlayer soil, which can significantly affect the stability of rail tracks.

The effect of water content on the permanent strain of mixture with varying coarse grain contents f_v was studied. A multi-stage loading procedure was adopted, with various deviator stresses of 10, 15, 20, 25, 30 kPa applied. A large number of loading cycles N = 90000 was adopted for each stage. Comparison with previous studies showed that when the dry density of fine soil $\rho_{d\text{-}f}$ kept constant, an increase of f_v led to a decrease of permanent strain, due to the reinforcement effect of coarse grains. On the contrary, when the dry density of mixture ρ_d kept constant, the $\rho_{d\text{-}f}$ decreased with increasing f_v, and the suction decreased accordingly. When the negative effect of decreasing suction prevailed on the positive effect of increasing f_v, the permanent strain increased with increasing f_v. This part corresponded to a paper submitted to Acta Geotechnica.

The effect of water content on resilient modulus and damping ratio of mixture with varying coarse grain contents f_v were also investigated. A multi-stage loading procedure was adopted, with various deviator stresses of 10, 30, 50, 100, 200 kPa applied. A small number of loading cycles N = 100 was adopted for each stage. Results showed that an increase of water content led to a decrease of resilient modulus owing to the decrease of suction while an increase of damping ratio owing to the increase of soil viscosity. Through the variations of resilient modulus and damping ratio with coarse grain content, a characteristic coarse grain content $f_{v\text{-}cha}$ was identified at a given water content: $f_{v\text{-}cha} \approx 25.5\%$ and 32.0% at a water content of 17.6% and 10.6%, respectively. The increase of $f_{v\text{-}cha}$ with decreasing water content was explained by the shrinkage property of fine soil. Comparison of the $f_{v\text{-}cha}$ values under cyclic loading and monotonic loading showed that cyclic loading led to a slightly larger value than monotonic loading, evidencing the effect of cyclic loading on soil fabric. These results were presented in a paper published in Transportation Geotechnics.

Su, Y., Cui, Y. J., Dupla, J. C., & Canou, J. 2021. Submitted to Acta Geotechnica.

Effect of water content on permanent deformation of fine/coarse soil mixtures with varying coarse grain contents and subjected to multi-stage cyclic loading

Yu Su, Yu-Jun Cui, Jean-Claude Dupla, Jean Canou

Abstract: An interlayer soil in ancient rail tracks was identified as a mixture of ballast grains and subgrade fines. As the permanent strain ε_1^p of such mixture was affected by water content, cyclic triaxial tests were performed, under varying water contents of fines w_f and coarse grain contents f_v. Comparison between present and previous studies showed the significant effect of sample preparation method on ε_1^p. In present study, a constant fine dry density $\rho_{d\text{-}f}$ was maintained, leading to an unchanged suction of mixture whatever the f_v value. In this case, only the reinforcement effect of f_v on ε_1^p was identified. By contrast, in previous studies, the global dry density of mixture ρ_d was kept constant, resulting in a decrease of $\rho_{d\text{-}f}$ with increasing f_v and consequently a decrease of suction. In this case, when the negative effect of decreasing suction prevailed on the positive reinforcement effect of increasing f_v, the ε_1^p increased.

Keywords: interlayer soil; cyclic triaxial test; permanent deformation; water content; coarse grain content; fabric/ structure of soils

Introduction

An interlayer was created in most conventional French rail tracks, mainly due to the interpenetration of ballast grains and subgrade fine soils. This interlayer was maintained in the railway substructure in the French program of rail track renewal considering its high dry density (2.4 Mg/m^3, Trinh 2011), Cui et al. (2013) and, hence, bearing capacity. As an important component of rail track, the interlayer soil diffused static and dynamic stresses into the substructure, avoiding excessive deformation. In this case, the deformation behavior of interlayer soil appeared to be significant, especially for the long-term stability of rail track. Field observation showed that the ballast grain content decreased over depth in the interlayer soil (Trinh 2011). However, the interlayer could be approximately divided into two parts: the upper part dominated by ballast grains and the lower part dominated by subgrade fine soil. With the unstable groundwater and climate change (rainfall and evaporation), the water content of interlayer soil can change over time, significantly affecting its permanent deformation behavior.

Ecole des Ponts ParisTech, Laboratoire Navier/CERMES, 6 – 8 av. Blaise Pascal, Cité Descartes, Champs-sur-Marne, 77455 Marne – la – Vallée cedex 2, France

Thus, in order to ensure the good serviceability of the tracks, it is essential to understand the effect of water content on the permanent deformation of interlayer soil.

The effect of coarse grain content on permanent deformation of soil have been investigated by several investigators. Song and Ooi (2010) studied the deformation behaviour of aggregates with varying fine soil contents, and found that increasing fine content gave rise to an increase of permanent deformation of soil mixtures. Wang et al. (2018a) investigated the effect of coarse grain content f_v (ratio of coarse grain volume to total volume) on permanent strain of interlayer soil by cyclic triaxial tests. They identified a characteristic coarse grain content $f_{v\text{-}cha}$ in a narrow range from 25.8% to 27.8%: a large decrease of permanent strain with f_v was observed at $f_v \leq f_{v\text{-}cha}$, but a slight decrease of that at $f_v \geq f_{v\text{-}cha}$. It is worth noting that these tests were performed under a constant water content of fine soils fraction $w_{opt\text{-}f}$ = 13.7%, and the effect of water content was not specifically addressed . Some studies evidenced the effect of water content on permanent deformation of substructures: at saturation, an excess pore water pressure accumulated under traffic loadings led to a decrease of effective stress and an increase of permanent deformation. When the water content decreased, the permanent deformation appeared to decrease, which was attributed to the contribution of suction (Gidel et al. 2001; Werkmeister et al. 2001; Nie et al. 2020; Trinh et al. 2012; Jing 2017; Wan et al. 2020). Gu et al. (2020) studied the permanent deformation of unbound granular materials by suction-controlled cyclic triaxial tests, and reported that an increase of suction led to a decrease of accumulated permanent strain exponentially under varying deviator stress amplitudes. Duong et al. (2013) investigated the effect of water content on permanent deformation of the upper interlayer soil with varying fine soil contents, and found that the effects of water content and fine content on permanent deformation were strongly related. At saturated state, an increase of fine content gave rise to an increase of permanent deformation, while at unsaturated state, an opposite trend was observed, due to the contribution of suction developed in the fines. Jing (2017) studied the deformation behaviour of granular material with varying water contents and fine contents, and also reported that increasing fine content led to an increase of permanent deformation under saturated condition and a decrease of that under unsaturated condition. Note that in most studies, the dry density of fine/coarse soil mixtures remained constant during the sample preparation; thereby a variation of dry density of fine soil fraction was induced with varying fine contents (or coarse grain contents). In that case, both suction and coarse grain content varied, rendering the test results difficult to be analysed.

This study aims at investigating the effect of water content on the permanent deformation of fine/coarse soil mixtures under various coarse grain contents. A series of cyclic triaxial tests were performed for this purpose. Emphasis was put on keeping the fine dry density $\rho_{d\text{-}f}$ constant in all samples, allowing a constant suction of soil mixtures whatever the f_v value. A multi-step loading procedure at various deviator stress amplitudes of 10, 15, 20, 25 and 30 kPa was applied, with a number of loading cycles at 90000 for each stress amplitude. Two target water contents of fine soil (17.6% and 10.6%) and five coarse grain contents (0%, 10%, 20%, 35% and 45%) were considered.

Materials and sample preparation

Considering the difficulty of obtaining intact interlayer soil from the field, the reconstituted soils consisting of fine soil and coarse grains were fabricated in the laboratory. For re-constituting the fine soil, nine different commercial soils (Table 1) are mixed with the pre-determined proportions, to obtain a similar grain size distribution curve of fines from 'Senissiat site' (Fig. 1). Note that in this study fines refer to the soil finer than ballast in the field, which correspond to a mixture encompassing grains of clay to sand sizes. The liquid limit and plasticity index of reconstituted fine soil were 32% and 20%, respectively, classifying the soil as CL based on the universal soil classification system. Fig. 2 presents the standard proctor compaction curve of fine soil, defining an optimum water content $w_{opt\text{-}f}$ = 13.7% and a maximum dry density $\rho_{dmax\text{-}f}$ = 1.82 Mg/m^3.

For the coarse grains, based on a parallel gradation method applied by Wang et al. (2018b) , Qi et al. (2020a) and Su et al. (2020a, 2020b, 2021a), which was verified later by Qi et al. (2020b), micro-ballast was adopted to replace the real ballast in Fig.1. A parameter of coarse grain content f_v (Wang et al. 2018b), defined as the ratio of the volume of coarse grains V_c to the total volume of fine/coarse mixture V (Eq. (1)), was adopted in this study. All voids and water were assumed to be contained in the fine soil (Fig. 3). Thus, under a given f_v, the dry density of fine soil $\rho_{d\text{-}f}$ and the water content of fine soil w_f, the masses of coarse grain $m_{s\text{-}c}$, fine grain $m_{s\text{-}c}$ and the water content of fine soil $m_{w\text{-}f}$ were calculated by Eqs. (2) – (4), respectively.

$$f_v = \frac{V_c}{V} = \frac{V_c}{V_c + V_f} = \frac{V_c}{V_c + V_{s-f} + V_{w-f} + V_{a-f}} \quad (1)$$

where V_f is the volume of fine soil; $V_{s\text{-}f}$, $V_{w\text{-}f}$ and $V_{a\text{-}f}$ are the volume of fine grains, water and air in the fine soil, respectively.

$$m_{s-c} = V_c \cdot G_{s-c} \cdot \rho_w = f_v \cdot V \cdot G_{s-c} \cdot \rho_w \quad (2)$$

$$m_{s-f} = \rho_{d-f} \cdot V_f = \rho_{d-f} \cdot V \cdot (1 - f_v) \quad (3)$$

$$m_{w-f} = w_f \cdot m_{s-f} \quad (4)$$

where $G_{s\text{-}c}$ is the specific gravity of coarse grains (= 2.68 Mg/m^3); ρ_w is the water unit mass.

Table 1. Nine different commercial soils

Soil classification	Commercial Soil	Mass proportion (%)	The range of grain size (mm)
Sand	HN34	3.3	0.063 - 0.50
	HN31	3.3	0.16 - 0.63
	HN0.4-0.8	6.7	0.25 - 1
	HN0.6-1.6	6.7	0.32 - 2
	HN1-2.5	13.3	0.32 – 3.20
	C4	16.7	0.0009 – 0.50
	C10	20	0.0009 – 0.25
Clay	Speswhite	23.3	0.0003 – 0.01
	Bentonite	6.7	0.001 – 0.01

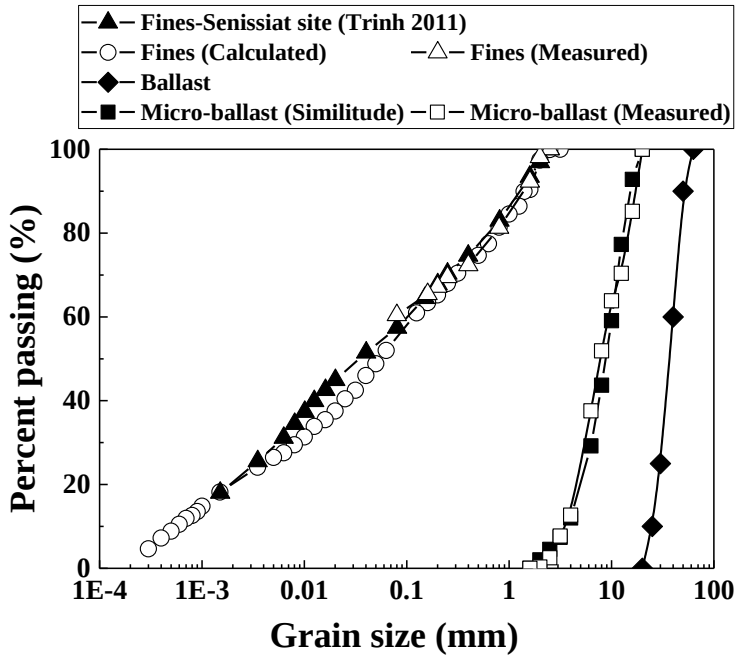

Fig. 1. Grain size distribution curves of fine soil and micro-ballast (after Wang et al. 2018a)

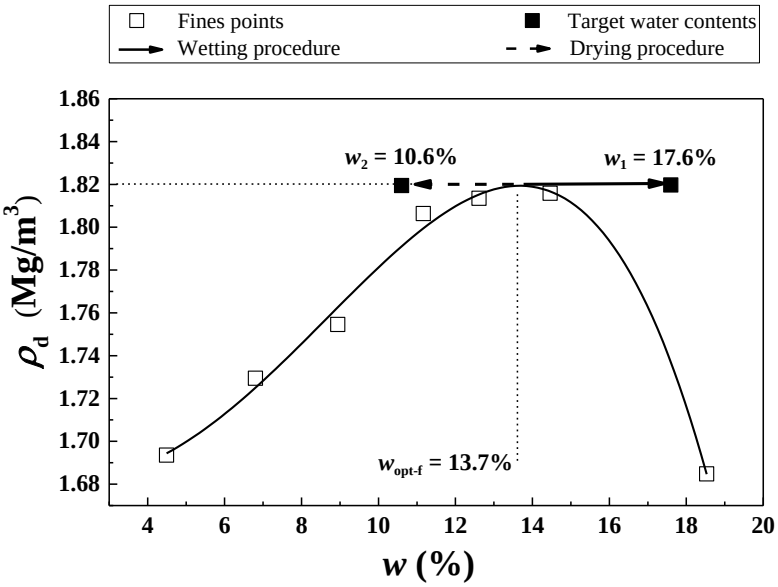

Fig. 2. Preparation of samples at two target water contents with respect to compaction curve of the fine soil

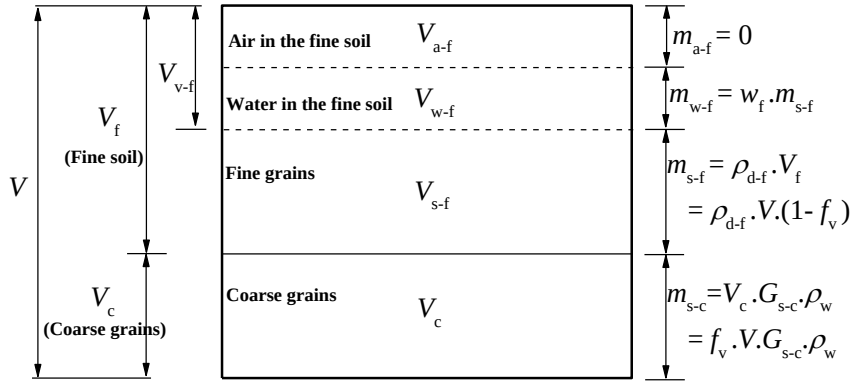

Fig. 3. Constitution of fine/coarse soil mixture

In order to prepare a sample at a target f_v value and a target water content w_f, the fine soil was prepared at $w_{opt\text{-}f}$ = 13.7%, then stored in a container for 24h for the purpose of moisture homogenization. After that, the fine soil was mixed with coarse grains at the pre-determined mass to reach the target f_v value. The soil mixture was then dynamically compacted in three layers, with the equivalent amounts of fine soil and coarse grains for each layer, to attain a size of 100 mm diameter and 200 mm height. Note that the fine soil was kept at the maximum dry density $\rho_{dmax\text{-}f}$ = 1.82 Mg/m^3 for all samples with varying f_v values. With a higher f_v value, more compaction energy was needed for the soil mixtures; thereby, a higher dry density ρ_d of sample is obtained (Table 2). It is worth noting that when $f_v > f_{v\text{-}cha}$, the coarse grains constitute the skeleton of soil mixture (Wang et al. 2018a). For this fabric, two categories of fine soil were identified by Su et al. (2020c) – dense fine soil between coarse grains and loose fine soil surrounded by coarse grains. Accordingly, a relative high $\rho_{d\text{-}f}$ and low $\rho_{d\text{-}f}$ was obtained for dense fines and loose fines, respectively, even though the global $\rho_{d\text{-}f}$ of fine soil remained constant (1.82 Mg/m^3).

After compacting a sample at a target f_v value, either a wetting or a drying process was adopted for the sample to reach the target water contents w_f (Fig. 2): w_1 = 17.6% (S_r = 100%) on the wet side and w_2 = 10.6% (S_r = 60%) on the dry side. The approach of wetting or drying from $w_{opt\text{-}f}$ = 13.7% to the target w_f value proposed by Su et al. (2020c) was applied: in the case of drying, the sample was each time exposed to the air for 1 h in the laboratory, and then covered with plastic film for at least 7 h equilibration. In the case of wetting, 10 g water was sprayed on the sample each time, and then wrapped it with plastic film and conserved for the same equilibration time of at least 7 h.

During the wetting and drying processes, the volume change of samples under different f_v values was recorded (Fig. 4). It can be observed that at a given f_v value, the swelling of sample upon wetting from $w_{opt\text{-}f}$ = 13.7% to w_1 = 17.6% or shrinkage of that upon drying from $w_{opt\text{-}f}$ = 13.7% to w_2 = 10.6% occurred. Moreover, the magnitude of swelling-shrinkage of sample decreased with the increase of f_v, which was attributed to (*i*) a reduction of fine soil, which was sensitive to water content change and (*ii*) part of total stress supported by the coarse grain skeleton at $f_v > f_{v\text{-}cha}$ (Wang et al. 2018a). This response of fine/coarse soil mixture appeared to be dominated by the fine matrix for f_v < 20% but the coarse grain skeleton for f_v > 35% (Fig. 4). The measured dry density ρ_d of sample after wetting or drying is shown in Table 2.

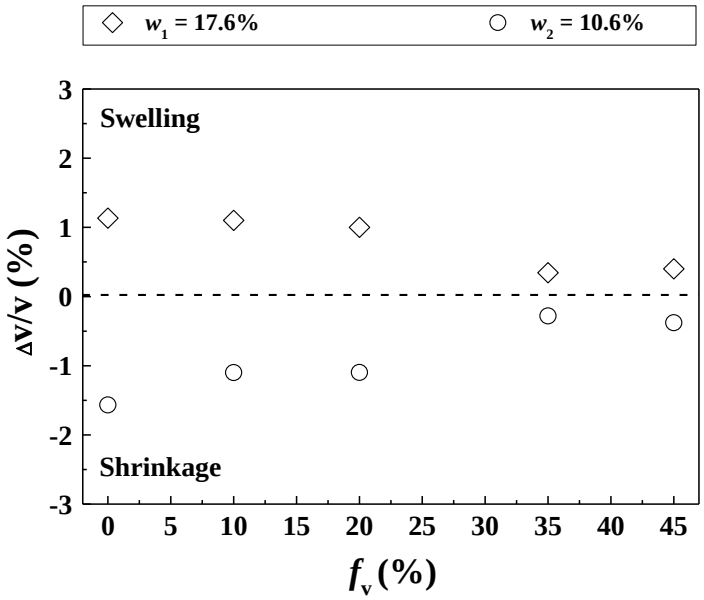

Fig. 4. Variations of sample volume with f_v at two target water contents

Table 2. Experimental program of cyclic triaxial tests

f_v (%)	Initial water content $w_{opt\text{-}f}$ (%)	Target w_f (%)	Target S_r (%)	Target $\rho_{dmax\text{-}f}$ (Mg/m^3)	Target ρ_d (Mg/m^3)	Measured ρ_d (Mg/m^3)
0	13.7	17.6	100	1.82	1.82	1.80
		10.6	60			1.85
10		17.6	100		1.91	1.88
		10.6	60			1.93
20		17.6	100		1.99	1.97
		10.6	60			2.01
35		17.6	100		2.12	2.11
		10.6	60			2.13
45		17.6	100		2.21	2.20
		10.6	60			2.22

Note: f_v represents the volumetric ratio of coarse grains to fine/coarse soil mixtures. $w_{opt\text{-}f}$, w_f, S_r and $\rho_{dmax\text{-}f}$ represent the optimum water content, water content, degree of saturation and maximum dry density of fine soil, respectively. ρ_d represents the dry density of soil mixtures sample. Measured ρ_d represents the dry density of soil mixtures sample after wetting or drying from compaction water content $w_{opt\text{-}f}$ to target $w_{f..}$

Cyclic triaxial tests

The cyclic triaxial apparatus used by Wang et al. (2017) was adopted in this study, hosting a sample with 100 mm diameter and 200 mm height. Using a 50 kN hydraulic actuator enabled a force or displacement controlled mode to be applied in both monotonic and cyclic triaxial tests. As for the cyclic loading, different signal shapes, amplitudes, frequencies and large number of cycles (up to several millions) can be applied. A linear variable displacement transducer (LVDT) was adopted to monitor the axial displacement, with a minimum capacity of ± 0.1mm. Considering the height (= 200mm) of the sample, the corresponding minimum measurement capacity of axial strain was ± 0.05%. A force sensor installed at the bottom was adopted to monitor the axial force.

A series of cyclic triaxial tests were performed on the samples at two target w_f values (w_1 = 17.6% and w_2 = 10.6%) and five f_v values (0%, 10%, 20%, 35% and 45%) with drainage valves open to air. A constant confining pressure σ_3 = 30 kPa was applied, corresponding to the estimated average horizontal stress in the field by the consideration of train loadings, the depth of interlayer soil and the Poisson's ratio (Duong et al. 2016). In the case of w_1 = 17.6% (S_r = 100%),

after applying the confining pressure σ_3 = 30 kPa, an overnight consolidation of the sample was adopted, with both the top and bottom porous disks exposed to the air. This allowed for the fully dissipation of generated pore water pressure. On the contrary, in the case of w_2 = 10.6% (S_r = 60%), after application of the confining pressure σ_3 = 30 kPa, the cyclic loading was directly applied, because only air was expected to be expelled.

Fig. 5 shows a sine-shaped signal applied at a frequency of 1.78 Hz, corresponding to that excited by two bogies at a train speed of 50 km/h. A multi-step loading procedure proposed by Gidel et al. (2001), applied later by Wang et al. (2018a) was adopted, which can not only reduce the number of tests but also avoid experimental dispersion due to the variability of sample. Fig. 6 depicts a multi-step loading procedure with various deviator stress amplitudes Δq of 10, 15, 20, 25 and 30 kPa, and a number of loading cycles N = 90000 for each Δq value. The deviator stress amplitude Δq was defined as the difference of maximum deviator stress q_{max} and minimum deviator stress q_{min}. These Δq values corresponded to the vertical stresses at varying depths of interlayer soil in the field, as reported by Lamas-Lopez (2016). The number of loading cycles N = 90000 was considered large enough for the stabilization of permanent strain under a given Δq value, according to the number applied in previous studies (Gidel et al. 2001; Trinh et al. 2012; Duong et al. 2013; Lamas-Lopez et al. 2016). Note that a constant cyclic stress ratio $\Delta q/\Delta p$ = 3 was adopted, which represented the typical stress path in the interlayer (Trinh et al. 2012). During the tests, the deviator stress and axial strain were recorded.

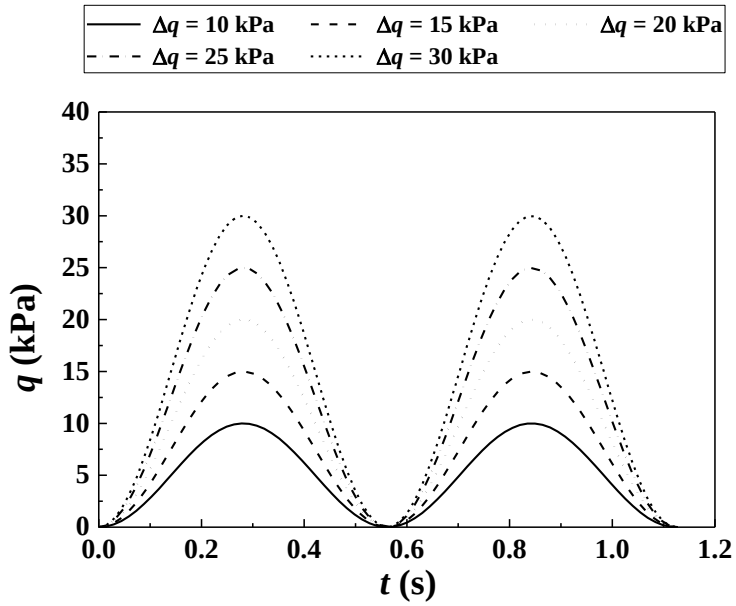

Fig. 5. Typical sine-shaped signals applied in cyclic triaxial tests

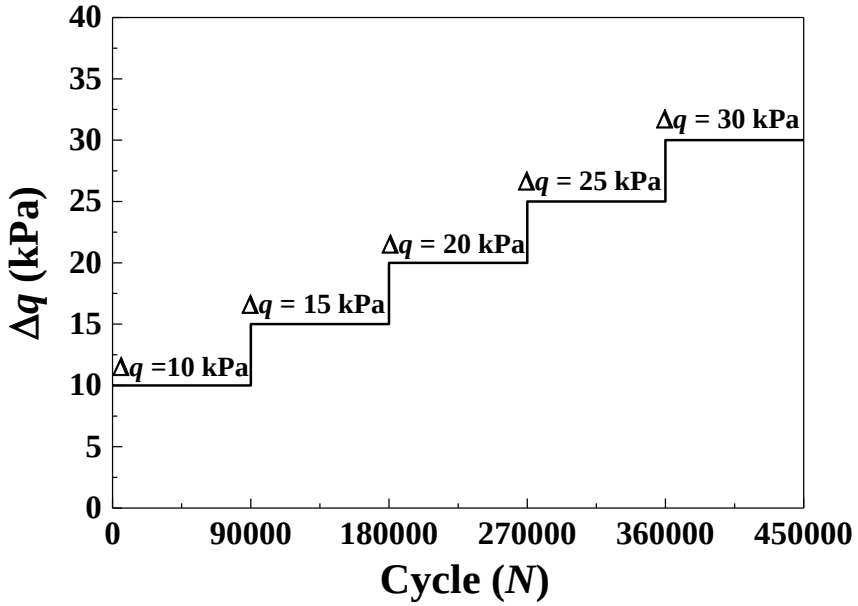

Fig. 6. Multi-step loading procedure with various stress amplitudes Δq

Results and discussions

Effect of water content on the evolution of permanent strain with loading cycles

Fig.7 depicts the evolution of axial strain ε_1 with loading cycles N at f_v = 0% and w_1= 17.6% under various Δq values ranging from 10 kPa to 30 kPa. It can be observed that under a given Δq value, the axial strain ε_1 increased significantly at the beginning of loading cycles, and then gradually stabilized. With the increase of Δq, the axial strain ε_1 increased significantly. In addition, the axial strain ε_1 could be separated into two parts: a plastic strain ε_1^p and a resilient strain ε_1^r. For the plastic strain ε_1^p, it increased with N and the increasing rate decreased with N under a constant Δq value. On the contrary, the resilient strain ε_1^r remained almost unchanged at a given Δq value and increased with increasing Δq.

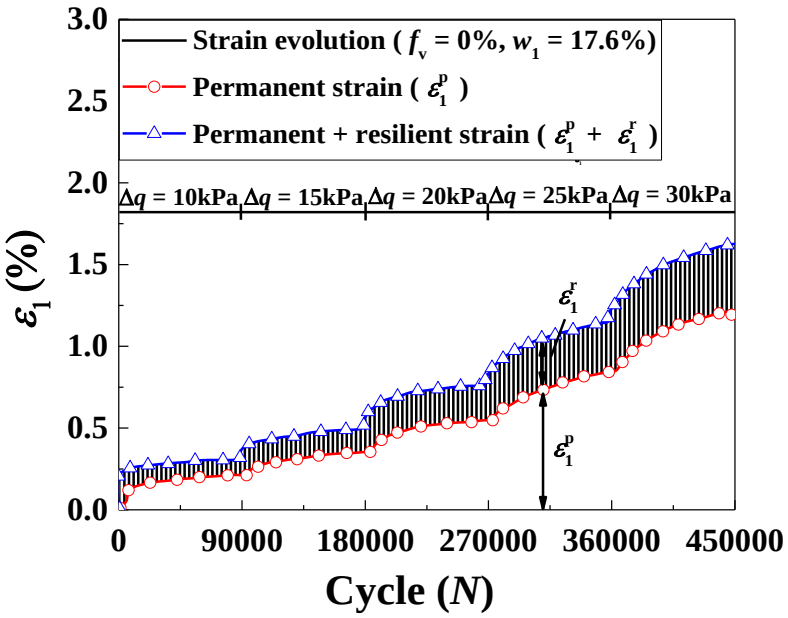

Fig. 7. Determination of permanent strain and resilient strain

Fig. 8 presents the evolutions of ε_1^p with N under various Δq values for f_v = 0% and three water contents. At w_1 = 17.6%, the permanent strain ε_1^p increased with N sharply at the initial loading cycles N, and then gradually reached stabilization under a specific Δq value. With the increase of Δq, the permanent strain ε_1^p growed significantly. The similar observation can be made in the case of $w_{opt\text{-}f}$ = 13.7% (obtained by Wang et al. 2018a) and w_2 = 10.6%. In addition, it can be observed that the decrease of water content from w_1 = 17.6% to $w_{opt\text{-}f}$ = 13.7% or w_2 = 10.6%

led to a pronounced decrease of ε_1^p. This could be explained by the contribution of suction, as reported by Duong et al. (2013, 2014) and Jing (2017).

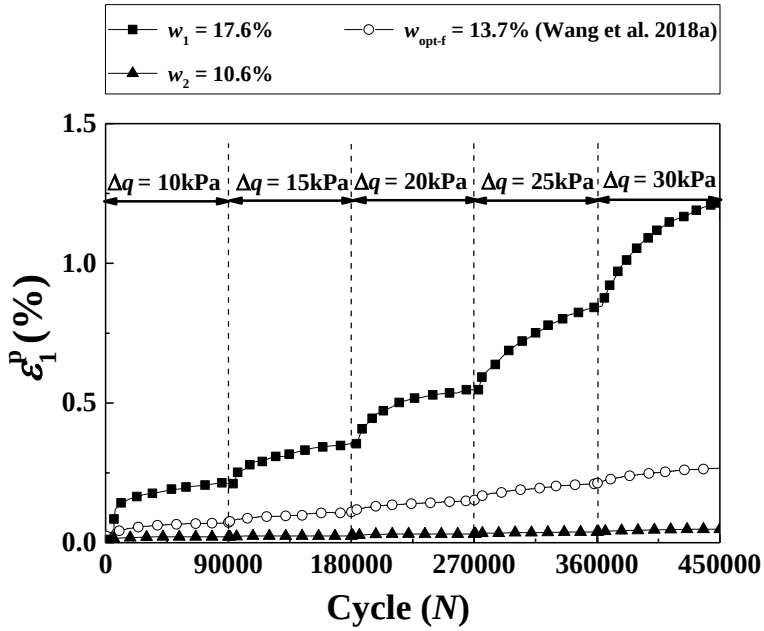

Fig. 8. Evolutions of permanent strain with number of cycles at f_v = 0% and different Δq values for three different water contents

Fig. 9 shows the effect of water content on the evolutions of ε_1^p with N under various f_v values. In the case of w_1 = 17.6% (Fig. 9 (a)), under a given f_v value, the increasing trend of ε_1^p versus N decreased with the increase of N at a constant Δq value. However, ε_1^p increased significantly with the increase of Δq. In addition, it can be found that with the increase of f_v, the permanent strain ε_1^p decreased. This was attributed to the reinforcement effect of coarse grains in the soil mixtures. Moreover, different decreasing trends of ε_1^p with f_v was evidenced at $f_v \leq 20\%$ and $f_v \geq 35\%$: a pronounced decrease of ε_1^p with f_v at $f_v \leq 20\%$ and a slight decrease of that at $f_v \geq 35\%$. This could be explained by the transition of two soil fabrics: a fine soil dominated fabric at $f_v \leq 20\%$ and a coarse grain dominated fabric at $f_v \geq 35\%$. Note that for the coarse grain skeleton fabric (f_v >35), two categories of fine soil were identified by Su et al. (2020c) – dense fines (with $\rho_{d\text{-}f}$ higher than 1.82 Mg/m^3) and loose fines (with $\rho_{d\text{-}f}$ lower than 1.82 Mg/m^3). In spite of this inhomogeneous distribution of fine soil in the mixture, the suction of mixture was found to be mainly controlled by the global dry density of fines $\rho_{d\text{-}f}$ = 1.82 Mg/m^3 (Su et al. 2021b). The similar observation was made at $w_{opt\text{-}f}$ = 13.7% (Fig. 9 (b)), which was obtained by Wang

et al. (2018a). At w_2 = 10.6% (Fig. 9 (c)), the ε_1^p at f_v = 0% was very small, with a maximum value around 0.05% identified. The ε_1^p at f_v = 10%, 20%, 35% and 45% was expected to be smaller than that at f_v = 0%. Considering the minimum measurement capacity (0.05%) of axial strain by the adopted LVDT, inaccuracy measurements of ε_1^p at f_v = 10%, 20%, 35% and 45% were generated. Therefore, these results are not presented in Fig. 9 (c).

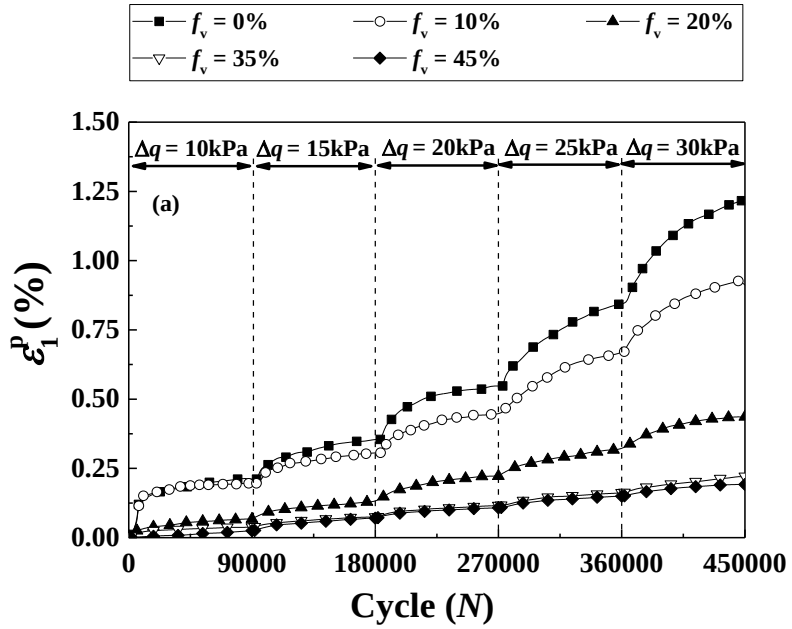

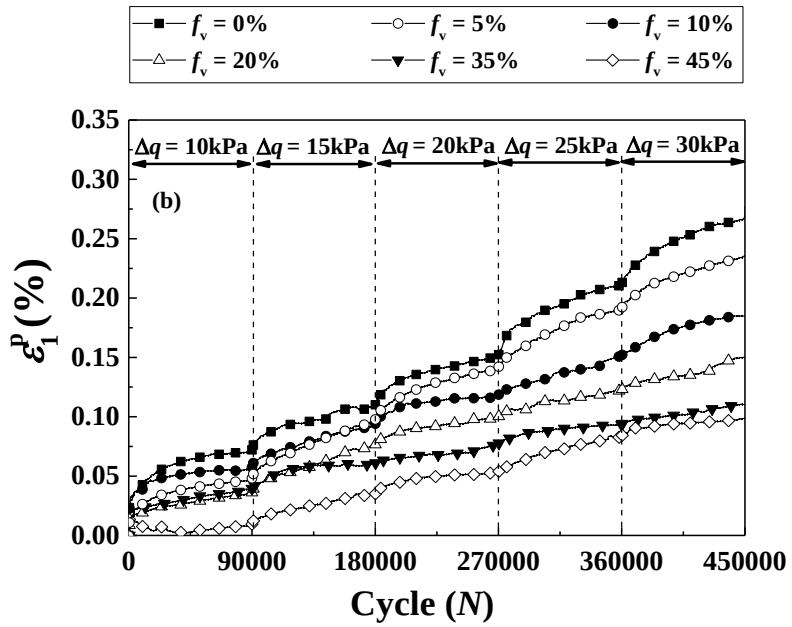

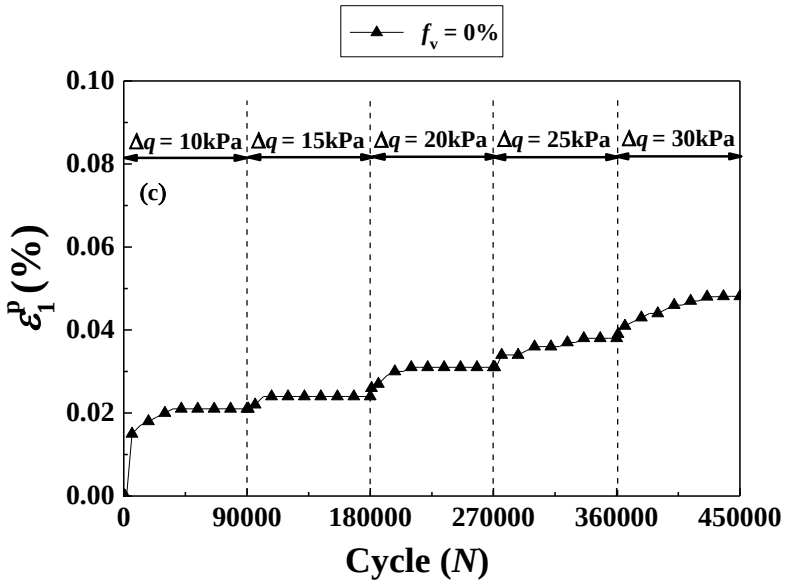

Fig. 9. Evolutions of permanent strain with number of cycles at different f_v and Δq values for various water contents: (a) w_1 = 17.6%; (b) $w_{opt\text{-}f}$ = 13.7% (after Wang et al. 2018a); (c) w_2 = 10.6%

Estimation of permanent strain

Considering a multi-step loading procedure applied in this study, the loading history would significantly affect the evolution of permanent strain ε_1^p with N under various water contents and coarse grain contents. Thereby, the estimation approach proposed by Gidel et al. (2001) was adopted to eliminate such effect of loading history on permanent strain. As shown in Fig. 10, the permanent strain ε_1^p evolved with N at two successive loading levels: loading level M and loading level M+1. To eliminate the effect of loading level M on permanent strain at loading level M+1, the increment of permanent strain $\delta\varepsilon_1^{p\,(M+1)}$ at loading level M+1 was transferred to start at $\varepsilon_1^p = 0$ and N = 0, which was the starting point of permanent strain at loading level M. As shown in Eq. (1), the estimated permanent strain $\varepsilon_1^{p\,(M+1)}$ at loading level M+1 without the influence of loading history can be determined:

$$\varepsilon_1^{p\,(M+1)} = \varepsilon_1^{p\,(M)} + \delta\varepsilon_1^{p\,(M+1)} \tag{5}$$

where $\varepsilon_1^{p\,(M+1)}$ represents the estimated permanent strain at loading level M+1, $\varepsilon_1^{p\,(M)}$ represents measured permanent strain at loading level M, $\delta\varepsilon_1^{p\,(M+1)}$ represents the increment of

permanent strain at loading level M+1. Note that the estimated $\varepsilon_1^{p\,(M+1)}$ at N = 90000 coincides with the measured $\varepsilon_1^{p\,(M+1)}$ at N = 180000. In addition, the slope θ of estimated $\varepsilon_1^{p\,(M+1)}$ with N after N = 90000 was kept the same as that in the last cycle of measured $\varepsilon_1^{p\,(M+1)}$, which enabled a linear increase of estimated $\varepsilon_1^{p\,(M+1)}$ with N after N = 90000 in Fig. 10.

Fig. 11 presents the evolution of the estimated ε_1^p with N at f_v = 0% and w_1 = 17.6% under various Δq values. With the increase of Δq, the estimated ε_1^p appears to grow. In addition, it can be found that the estimated ε_1^p was larger than the measure ε_1^p under the same Δq and N values (except Δq = 10 kPa). For instance, at Δq = 30 kPa and N = 450000, the estimated ε_1^p = 1.75% was much larger than the measured ε_1^p = 1.20%. This could be attributed to the effect of loading history. Different from the estimated ε_1^p under a constant Δq = 30 kPa, the measured ε_1^p experienced a series of lower stress amplitudes Δq = 10, 15, 20 and 25 kPa prior to Δq = 30 kPa, which resulted in a smaller value. Considering that a relative good accuracy for the estimated ε_1^p could be obtained at the first loading stage (e.g. N = 0 ~ 90000 in this study), as reported by Gidel et al. (2001) and confirmed later by Lamas-Lopez (2016) and Wang et al. (2018a), the estimated end-stage permanent strains ε_1^p (at N = 90000) under various Δq values were selected for further analysis.

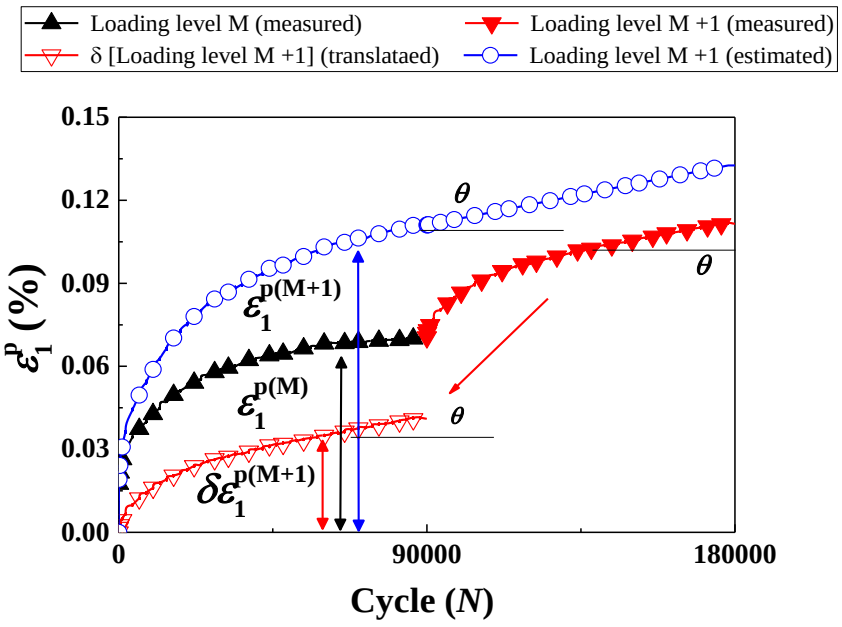

Fig. 10. Estimation method of ε_1^p proposed by Gidel et al. (2001)

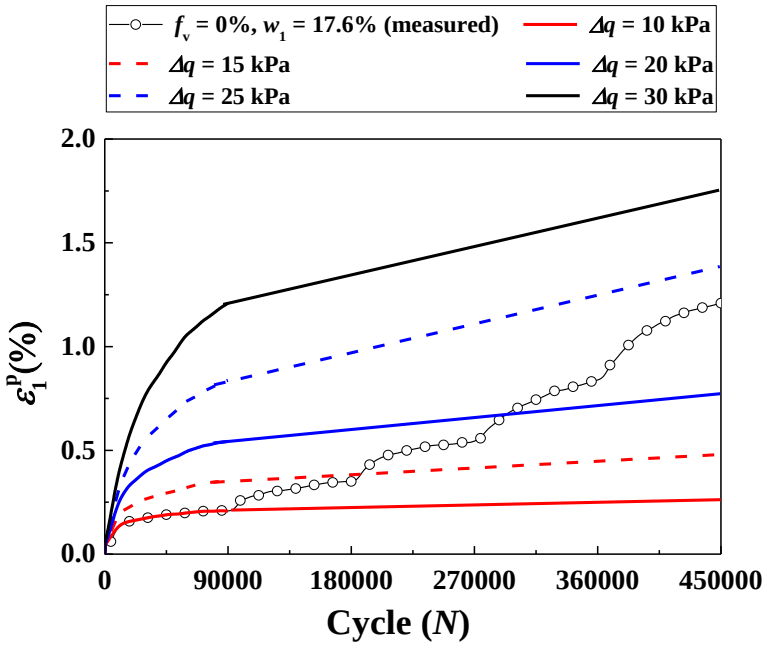

Fig. 11. Evolutions of estimated permanent strain with number of cycles at various Δq values for f_v = 0% and w_1 = 17.6%

Effect of water content on the variations of estimated end-stage ε_1^p with Δq

Fig. 12 shows the variations of estimated end-stage ε_1^p with Δq under different f_v values for two water contents. In the case of w_1 = 17.6% (S_r = 100%, Fig. 12 (a)), the estimated end-stage ε_1^p increased with increasing Δq for various f_v values. Under a given Δq, the ε_1^p decreased with the increase of f_v, evidencing the reinforcement effect of coarse grains. The similar observation was obtained at $w_{opt\text{-}f}$ = 13.7% (S_r = 78%) (Fig. 12 (b)). In addition, the decrease of water content from w_1 = 17.6% to $w_{opt\text{-}f}$ = 13.7% led to a decline of the estimated end-stage ε_1^p, owing to the contribution of suction.

The study of Dong et al. (2013) was carried out at a constant dry density of mixture ρ_d for varying f_v values (50.3%, 55.5% and 61.4%), and therefore the fines fraction density $\rho_{d\text{-}f}$ decreased as f_v increased (Table 3). Fig. 13 shows that the estimated end-stage ε_1^p increased with Δq for the three f_v values and three w values. Under saturated conditions (w = 12%, Fig. 13 (a)), an increase of f_v led to a decrease of ε_1^p under a constant Δq, which was consistent with that observed in Fig. 12 (a). On the contrary, under unsaturated conditions (w = 6% and w = 4%,

Figs. 12 (b) - (c)), an increase of f_v resulted in an increase of the estimated end-stage ε_1^p under a constant Δq, which was contradictory with the observation in Fig. 12 (b). This could be explained by the fact that the permanent strain behavior of soil mixtures was affected by both the reinforcement effect of coarse grains and the effect of suction in fines. Under saturated conditions, without the effect of suction, the reinforcement effect of f_v played a dominant role in the permanent strain behavior of mixtures. In this case, an increase of f_v induced a decrease of ε_1^p (Fig. 12 (a) and Fig. 13 (a)). By contrast, under unsaturated conditions, both the reinforcement effect of coarse grains and the effect of suction in fines affected the permanent strain behavior. Note that the suction of fines fraction was strongly related to its $\rho_{d\text{-}f}$ under a constant water content, as evidenced by Romero et al. (1999) and Gao and Sun (2017). In the present study, the fine soil was controlled at $\rho_{dmax\text{-}f}$ = 1.82 Mg/m^3 (Table 2), leading to an unchanged suction (= 739 kPa in Wang et al. 2018a) at $w_{opt\text{-}f}$ = 13.7% under varying f_v values. This was supported by the findings of Su et al. (2021b) on the same fine/coarse soil mixture, who reported that the soil-water retention curve was only affected by the dry density of fine soil $\rho_{d\text{-}f}$, while independent of coarse grain content f_v. In this case, the reinforcement effect of f_v on the permanent strain behavior was clearly identified: an increase of f_v led to a smaller ε_1^p (Fig. 12 (b)). Conversely, in the study of Duong et al. (2013), the $\rho_{d\text{-}f}$ of fine soil declines from 1.33 Mg/m^3 to 1.17 and 0.94 Mg/m^3 with the increasing f_v values from 50.3% to 55.5% and 61.4% (Table 3), which would result in a decrease of suction within the fine fraction. In this case, the negative effect of decreasing suction prevailed on the positive reinforcement effect of increasing f_v. As a result, the ε_1^p increased with increasing f_v. (Fig. 13 (b) – (c)).

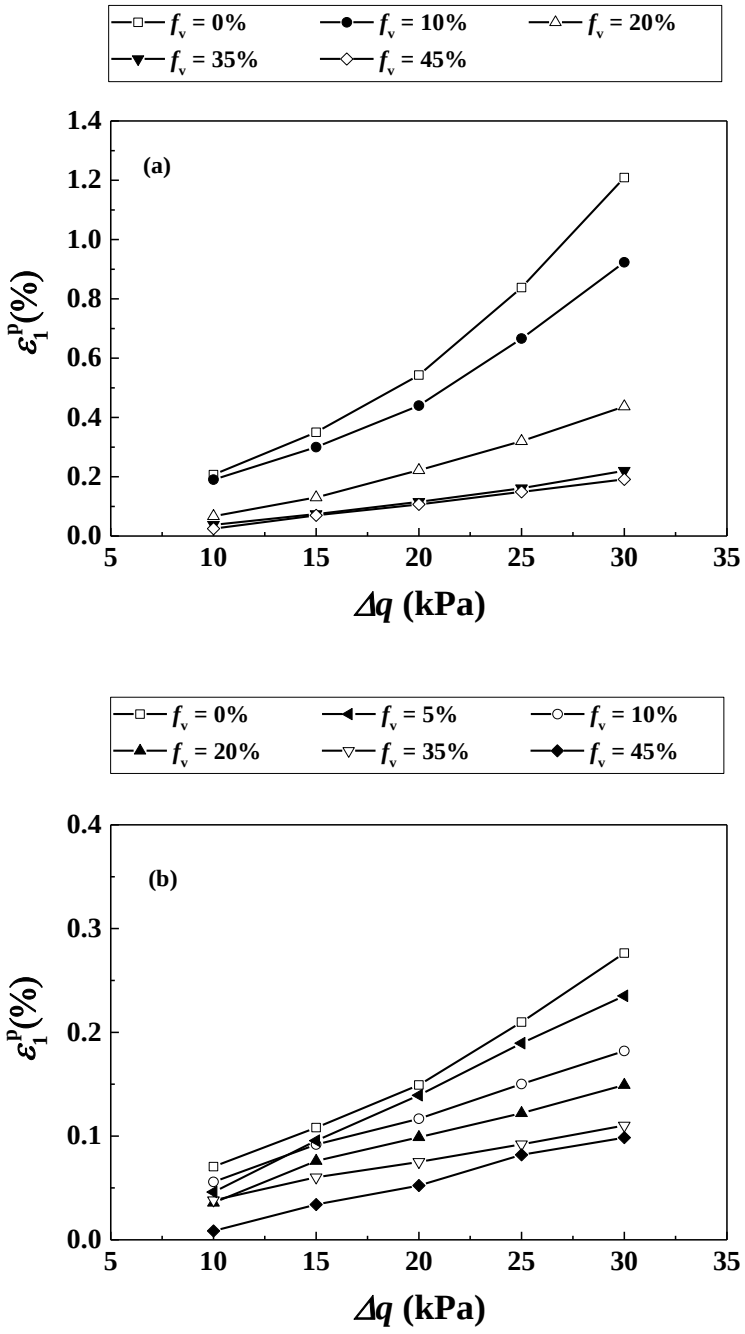

Fig. 12. Variations of estimated end-stage permanent strain with Δq at different f_v values for various water contents: (a) w_1= 17.6%; (b) $w_{opt\text{-}f}$ = 13.7%

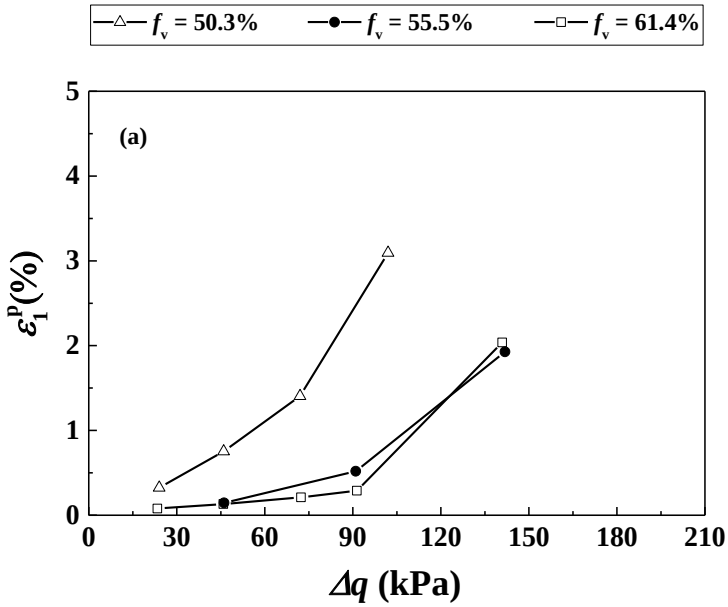
f_v = 50.3%
f_v = 55.5%
f_v = 61.4%
(a)
ε_1^p(%)
Δq (kPa)
0
1
2
3
4
5
0
30
60
90
120
150
180
210

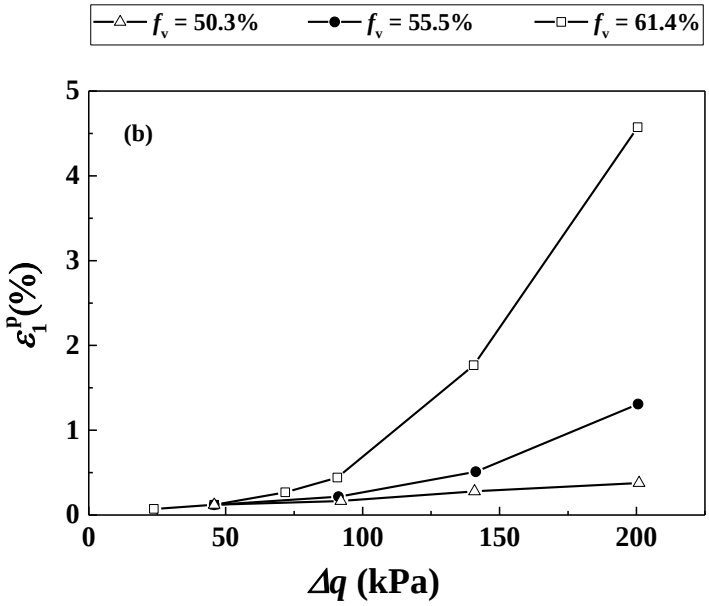
f_v = 50.3%
f_v = 55.5%
f_v = 61.4%
(b)
ε_1^p(%)
Δq (kPa)
0
1
2
3
4
5
0
50
100
150
200

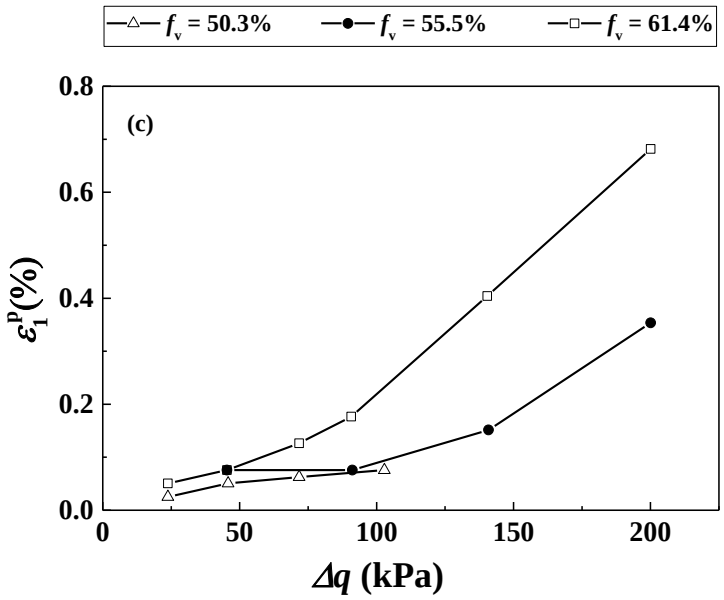

Fig. 13. Variations of estimated end-stage permanent strain with Δq at different f_v values for various water contents: (a) w = 12%; (b) w = 6%; (3) w = 4% (after Duong et al. 2013)

Table 3. Soil properties of Duong et al. (2013)

f_v (%)	w (%)				S_r (%)		ρ_d (Mg/m^3)	$\rho_{d\text{-}f}$ (Mg/m^3)
50.3	4	6	12	32	49	100	2.01	1.33
55.5	4	6	12	32	49	100		1.17
61.4	4	6	12	32	49	100		0.94

Note: w represents the water content of soil mixtures.

Conclusions

To investigate the effect of water content on permanent strain ε_1^p of fine/coarse soil mixtures under varying coarse grain contents, a series of cyclic triaxial tests were performed. For the cyclic triaxial test, a multi-step loading procedure under various stress amplitudes Δq of 10, 15, 20, 25 and 30 kPa was applied, with a number of loading cycles N = 90000 for each Δq value.

Two target fines water contents w_f (w_1 = 17.6% and w_2 = 10.6%) and five coarse grain contents f_v (0%, 10%, 20%, 35% and 45%) were considered. The estimation approach of ε_1^p proposed by Gidel et al. (2001) was adopted to eliminate the effect of loading history on ε_1^p. Through the comparison of the present study and the study of Duong et al. (2013), the effects of water content and coarse grain content on the permanent strain behavior of fine/coarse soil mixtures were clarified. The following conclusions to be drawn:

A decrease of water content led to a decrease of permanent strain ε_1^p, due to the contribution of suction. An increase of f_v gave rise to a decrease of ε_1^p, owing to the reinforcement effect of f_v. The comparison of present study and the study of Duong et al. (2013) indicated a significant effect of sample preparation approach on the permanent strain behavior of soil mixtures. In the present study, a constant $\rho_{d\text{-}f}$ of fine soil fraction was maintained, leading to an unchanged suction of soil mixtures with varying f_v values. In this case, the reinforcement effect of f_v on the permanent strain behavior was clearly identified: an increase of f_v led to a decrease of ε_1^p. Conversely, in the study of Duong et al. (2013), with a global dry density kept constant, an increase of f_v led to a decrease of the dry density of fines $\rho_{d\text{-}f}$ and consequently a decrease of suction. In that case, when the negative effect of decreasing suction prevailed on the positive reinforcement effect of increasing f_v, the ε_1^p increased with the increase of f_v.

Acknowledgements

This work was supported by the China Scholarship Council (CSC) and Ecole des Ponts ParisTech.

References

Cui, Y.J., Duong, T.V., Tang, A.M., Dupla, J.C., Calon, N. and Robinet, A., 2013. Investigation of the hydro-mechanical behaviour of fouled ballast. Journal of Zhejiang University Science A, 14(4), pp.244-255.

Duong, T.V., Tang, A.M., Cui, Y.J., Trinh, V.N., Dupla, J.C., Calon, N., Canou, J. and Robinet, A., 2013. Effects of fines and water contents on the mechanical behavior of interlayer soil in ancient railway sub-structure. *Soils and foundations*, *53*(6), pp.868-878.

Duong, T. V., Cui, Y. J., Tang, A. M., Dupla, J. C., & Calon, N. 2014. Effect of fine particles on the hydraulic behavior of interlayer soil in railway substructure. Canadian geotechnical journal, 51(7), 735-746.

Duong, T.V., Cui, Y.J., Tang, A.M., Dupla, J.C., Canou, J., Calon, N. and Robinet, A., 2016. Effects of water and fines contents on the resilient modulus of the interlayer soil of railway substructure. *Acta Geotechnica*, *11*(1), pp.51-59.

Gidel, G., Hornych, P., Breysse, D., & Denis, A. 2001. A new approach for investigating the permanent deformation behaviour of unbound granular material using the repeated loading triaxial apparatus. Bulletin des laboratoires des Ponts et Chaussées, (233).

Gao, Y., Sun, DA. 2017. Soil-water retention behavior of compacted soil with different densities over a wide suction range and its prediction. Computers and Geotechnics, 91, 17-26.

Gu, C., Zhan, Y., Wang, J., Cai, Y., Cao, Z., & Zhang, Q. (2020). Resilient and permanent deformation of unsaturated unbound granular materials under cyclic loading by the large-scale triaxial tests. *Acta Geotechnica*, *15*(12), 3343-3356.

Jing, P. 2017. Experimental study and modelling of the elastoplastic behaviour of unbound granular materials under large number of cyclic loadings at various initial hydric states (Doctoral dissertation).

Jing, P., Nowamooz, H., & Chazallon, C. 2018. Permanent deformation behaviour of a granular material used in low-traffic pavements. Road Materials and Pavement Design, 19(2), 289-314.

Lamas-lopez, F. 2016. Field and laboratory investigation on the dynamic behavior of conventional railway track-bed materials in the context of traffic upgrade. PhD Thesis, Ecole Nationale des Ponts et Chaussées, Université Paris-Est.

Nie, R., Li, Y., Leng, W., Mei, H., Dong, J., & Chen, X. (2020). Deformation characteristics of fine-grained soil under cyclic loading with intermittence. *Acta Geotechnica*, 1-14.

Qi, S., Cui, Y.J., Chen, R.P., Wang, H.L., Lamas-Lopez, F., Aimedieu, P., Dupla, J.C., Canou, J. and Saussine, G., 2020a. Influence of grain size distribution of inclusions on the mechanical behaviours of track-bed materials. Géotechnique, 70(3), pp.238-247.

Qi, S., Cui, Y.J., Dupla, J.C., Chen, R.P., Wang, H.L., Su, Y., Lamas-Lopez, F. and Canou, J., 2020b. Investigation of the parallel gradation method based on the response of track-bed materials under cyclic loadings. Transportation Geotechnics, p.100360.

Romero, E., Gens, A., & Lloret, A. 1999. Water permeability, water retention and microstructure of unsaturated compacted Boom clay. Engineering Geology, 54(1-2), 117-127.

Song, Y., & Ooi, P. S. 2010. Interpretation of shakedown limit from multistage permanent deformation tests. Transportation research record, 2167(1), 72-82.

Su, Y., Cui, Y. J., Dupla, J. C., & Canou, J. 2020a. Investigation of the effect of water content on the mechanical behavior of track-bed materials under various coarse grain contents. Construction and Building Materials, 263, 120206.

Su, Y., Cui, Y. J., Dupla, J. C., Canou, J., & Qi, S. 2020b. A fatigue model for track-bed materials with consideration of the effect of coarse grain content. Transportation Geotechnics, 23, 100353.

Su, Y., Cui, Y. J., Dupla, J. C., Canou, J., & Qi, S. 2020c. Developing a Sample Preparation Approach to Study the Mechanical Behavior of Unsaturated Fine/Coarse Soil Mixture. Geotechnical Testing Journal, 44(4).

Su, Y., Cui, Y. J., Dupla, J. C., & Canou, J. 2021a. Effect of water content on resilient modulus and damping ratio of fine/coarse soil mixtures with varying coarse grain contents. Transportation Geotechnics, 26, 100452.

Su, Y., Cui, Y. J., Dupla, J. C., & Canou, J. 2021b. Soil-water retention behaviour of fine/coarse soil mixture with varying coarse grain contents and fine soil dry densities. Canadian Geotechnical Journal, (ja).

Trinh, V. N. 2011. Comportement hydromécanique des matériaux constitutifs de plateformes ferroviaires anciennes. PhD Thesis, Ecole Nationale des Ponts et Chaussées, Université Paris-Est.

Trinh, V.N., Tang, A.M., Cui, Y.J., Dupla, J.C., Canou, J., Calon, N., Lambert, L., Robinet, A. and Schoen, O., 2012. Mechanical characterisation of the fouled ballast in ancient railway track substructure by large-scale triaxial tests. *Soils and foundations*, *52*(3), pp.511-523.

Werkmeister, S., Dawson, A. R., & Wellner, F. 2001. Permanent deformation behavior of granular materials and the shakedown concept. Transportation Research Record, 1757(1), 75-81.

Wan, Z., Bian, X., Li, S., Chen, Y., & Cui, Y. 2020. Remediation of mud pumping in ballastless high-speed railway using polyurethane chemical injection. Construction and Building Materials, 259, 120401.

Wang, H. L., Cui, Y. J., Lamas-Lopez, F., Dupla, J. C., Canou, J., Calon, N., ... & Chen, R. P. 2017. Effects of inclusion contents on resilient modulus and damping ratio of unsaturated track-bed materials. Canadian Geotechnical Journal, 54(12), 1672-1681.

Wang, H.L., Cui, Y.J., Lamas-Lopez, F., Dupla, J.C., Canou, J., Calon, N., Saussine, G., Aimedieu, P. and Chen, R.P., 2018a. Permanent deformation of track-bed materials at various inclusion contents under large number of loading cycles. *Journal of Geotechnical and Geoenvironmental Engineering*, *144*(8), p.04018044.

Wang, H.L., Cui, Y.J., Lamas-Lopez, F., Calon, N., Saussine, G., Dupla, J.C., Canou, J., Aimedieu, P. and Chen, R.P., 2018b. Investigation on the mechanical behavior of track-bed materials at various contents of coarse grains. *Construction and Building Materials*, *164*, pp.228-237.

Su, Y., Cui, Y. J., Dupla, J. C., & Canou, J. 2021. Transportation Geotechnics, 26, 100452.

Effect of water content on resilient modulus and damping ratio of fine/coarse soil mixtures with varying coarse grain contents

Yu Su, Yu-Jun Cui, Jean-Claude Dupla, Jean Canou

Abstract: For the French ancient rail track, owing to the effect of traffic loadings, an interlayer was naturally created due to the interpenetration of ballast grains and subgrade fine soil. Under the effect of rainfall/evaporation, the water content of interlayer soil can vary, affecting its dynamic properties such as resilient modulus and damping ratio. In order to investigate the effect of water content on the resilient modulus and the damping ratio of interlayer soil, a series of cyclic triaxial tests were carried out, following a multi-step loading procedure with various deviator stress amplitudes of 10, 30, 50, 100 and 200 kPa. Two target fines water contents (17.6% and 10.6%) and five coarse grain contents (0%, 10%, 20%, 35% and 45%) were considered. Results showed that under a given coarse grain content, an increase of water content led to a decrease of resilient modulus owing to the decrease of suction while an increase of damping ratio owing to the increase of soil viscosity. Through the variations of resilient modulus and damping ratio with coarse grain content, a characteristic coarse grain content was identified, defining two distinct soil fabrics: a fine soil dominated fabric when the coarse grain content was smaller than the characteristic value, and a coarse grain dominated fabric when the coarse grain content was larger than the characteristic value. Moreover, a constant characteristic coarse grain content was obtained at a given water content: 25.5% at 17.6% water content and 32.0% at 10.6% water content. The increase of characteristic coarse grain content with the decrease of water content could be explained by the swelling-shrinkage of fine soil: with a decrease of water content, the shrinkage of fine soil led to an increase of the volume of macro-pores. More coarse grains were thus needed to constitute the global skeleton, giving rise to an increase of the characteristic coarse grain content. In addition, comparison of the values of characteristic coarse grain content obtained from cyclic tests with those from monotonic tests showed that at a given water content, cyclic loading led to a slightly larger value than monotonic loading, evidencing the more significant effect of cyclic loading on soil fabric.

Keywords: interlayer soil; cyclic triaxial test; water content; coarse grain content; resilient modulus; damping ratio

Introduction

In France, new rail tracks were constructed with a sub-ballast layer which separated the ballast layer from subgrade soil, while ancient tracks were constructed by putting ballast directly on subgrade soil without separation layer. Owing to the effect of train circulation, an interlayer was created in the ancient rail tracks by the interpenetration of ballast grains and subgrade fine soil. Since the interlayer was kept in railway substructure during the national renewal program

Ecole des Ponts ParisTech, Laboratoire Navier/CERMES, 6 – 8 av. Blaise Pascal, Cité Descartes, Champs-sur-Marne, 77455 Marne – la – Vallée cedex 2, France

thanks to its expected favorable mechanical behaviour (Cui et al. 2013), it appears necessary to evaluate its hydro-mechanical behavior, in particular its dynamic properties under traffic loadings.

In-situ investigation showed a decrease of ballast grain content over depth (Trinh 2011). Wang et al. (2017, 2018a, 2018b) conducted a series of tests to clarify the effect of coarse grain content f_v (ratio of coarse grains volume to total volume) on the static and dynamic behaviors of interlayer soil under constant water content condition. They identified a characteristic coarse grain content $f_{v\text{-}cha}$, which separated two soil fabrics: one characterized by a fine matrix with dispersed coarse grains and another by a coarse grain skeleton with fines contained in large pores among coarse grains or at the grain/grain contacts. Under rainfall and evaporation, the water content of interlayer soil varies in the field. As a result, the dynamic properties of interlayer soil can change, greatly affecting the mechanical behavior of track bed. Thus, in order to ensure the serviceability of the rail track, the effect of water content on the dynamic properties of interlayer soil should be investigated in depth.

The dynamic properties of soils are generally characterized by the resilient modulus and the damping ratio. They are often determined based on the hysteresis loops obtained from cyclic triaxial tests (Stewart 1982; Selig and Waters 1994; Menq 2003). Lin et al. (2000) investigated the dynamic behavior of a gravelly cobble deposit mixed with fine soil by cyclic triaxial tests. Their results showed that the gravel content greatly affected the nonlinear shear modulus-shear strain and damping ratio-shear strain relations. Tennakoon and Indraratna (2014) studied the dynamic characteristics of fouled ballast by performing a series of large-scale cyclic triaxial tests, and concluded that increasing the fouling magnitude resulted in a decrease of resilient modulus. Wang et al. (2017) and Cui (2018) studied the effect of coarse grain content f_v on the dynamic response of interlayer soil. The results indicated that an increase of coarse grain content f_v gave rise to an increase of resilient modulus and a decrease of damping ratio. Moreover, a characteristic coarse grain content $f_{v\text{-}cha}$ was identified, dividing the soil fabrics into two zones - a fine matrix zone and a coarse grain skeleton zone. Mousa et al. (2020) investigated the effect of proportion of reclaimed asphalt pavement on the resilient modulus behavior of unbound granular materials, and indicated that the addition of reclaimed asphalt pavement tended to increase the resilient modulus of mixtures. The effect of water content was also addressed in some studies. Lamas-Lopez (2016) investigated the effect of water content on the resilient modulus and the damping ratio of the upper part interlayer soil, and reported that an increase of

water content resulted in a decrease of resilient modulus and an increase of damping ratio. Zhalehjoo et al. (2018) studied the resilient deformation of unbound granular materials by repeated load triaxial tests, and reported that an increase of water content induced a decrease of resilient modulus. Khasawneh and Al-jamal (2019) analysed a large quantity of data on the resilient modulus of fine-grained soils, and found that the change of water content affected the resilient modulus more significantly than the change of fine soil content. Jibon et al. (2020) investigated the resilient modulus of subgrade soil by cyclic triaxial tests, and found that the variation of water content significantly affected the resilient modulus of plastic soils, but slightly affected the resilient modulus of non-plastic soil. Duong et al. (2016) investigated the effects of water content and fine soil content on the resilient modulus of the upper part interlayer soil (corresponding to the case of coarse grain skeleton) by large-scale triaxial tests, and found that an increase of water content led to a decrease of resilient modulus. The effect of fine content was found to be strongly related to the water content/degree of saturation. At saturated sate, the higher the fine content the smaller the resilient modulus, while at unsaturated state, the higher the fine content the larger the resilient modulus due to the contribution of suction developed in fine soil.

It is worth noting that a constant dry density ρ_d of soil mixtures was controlled in the study of Duong et al. (2016). Thereby, the suction in soil mixtures changed with changes of coarse grain content f_v, because the dry density of fines changed with f_v. In that case, the dynamic properties identified were the results under the combined effect of suction and f_v. In other words, the effects of suction (or water content) and f_v could not be appreciated separately. In addition, previous studies did not pay attention to the effect of water content on the characteristic coarse grain content $f_{v\text{-}cha}$ under cyclic loadings.

This study aims at investigating the effect of water content on the dynamic properties of the whole interlayer soil with varying coarse grain contents f_v (with thus both the fine matrix fabric and coarse grain skeleton fabric). Note that the fine dry density $\rho_{d\text{-}f}$ remained constant for all samples, allowing a constant suction of soil mixtures with varying f_v values. Cyclic triaxial tests were performed for this purpose. A multi-step loading procedure with various loading amplitudes (10, 30, 50, 100 and 200 kPa) was adopted. Two water contents (17.6% and 10.6%) and five coarse grain contents (0%, 10%, 20%, 35%, and 45%) were considered. The obtained results allowed the resilient modulus and the damping ratio to be determined, and their variations with coarse grain content and water content to be further analysed.

Materials and methods

Fine soil and coarse grains

Considering the extreme difficulty of extracting intact interlayer soil from the field for large quantity and limited variability, reconstituted soil was fabricated instead in the laboratory using both fine-grained and coarse-grained soils. The fine soil part was fabricated using nine different commercial soils (Table 1), keeping the grain size distribution similar to that from 'Senissiat site' (Trinh 2011), as shown in Fig. 1. The liquid limit and the plasticity index of the reconstituted fine soil were 32% and 20%, respectively. Following ASTM D698-12, the standard proctor compaction curve of reconstituted fine soil was determined (Fig. 2), defining an optimum water content $w_{opt\text{-}f}$ = 13.7% and a maximum dry density $\rho_{dmax\text{-}f}$ = 1.82 Mg/m^3.

For the coarse grains part, following the similitude method applied by Wang et al. (2018a) and Qi et al. (2020a) and verified later by Qi et al. (2020b), micro-ballast was adopted to replace the real ballast (Fig.1). Parameter f_v was adopted to represent the amount of micro-ballast in the fine/coarse soil mixtures. Under a given f_v value, the dry mass of coarse grains and dry mass of fine soil could be determined (see details in Wang et al. 2018a).

Table 1. Nine different commercial soils used for fine soil preparation

Soil classification	Commercial Soil	Mass proportion (%)	The range of grain size (mm)
Sand	HN34	3.3	0.063 - 0.50
	HN31	3.3	0.16 - 0.63
	HN0.4-0.8	6.7	0.25 - 1
	HN0.6-1.6	6.7	0.32 - 2
	HN1-2.5	13.3	0.32 – 3.20
	C4	16.7	0.0009 – 0.50
	C10	20	0.0009 – 0.25
Clay	Speswhite	23.3	0.0003 – 0.01
	Bentonite	6.7	0.001 – 0.01

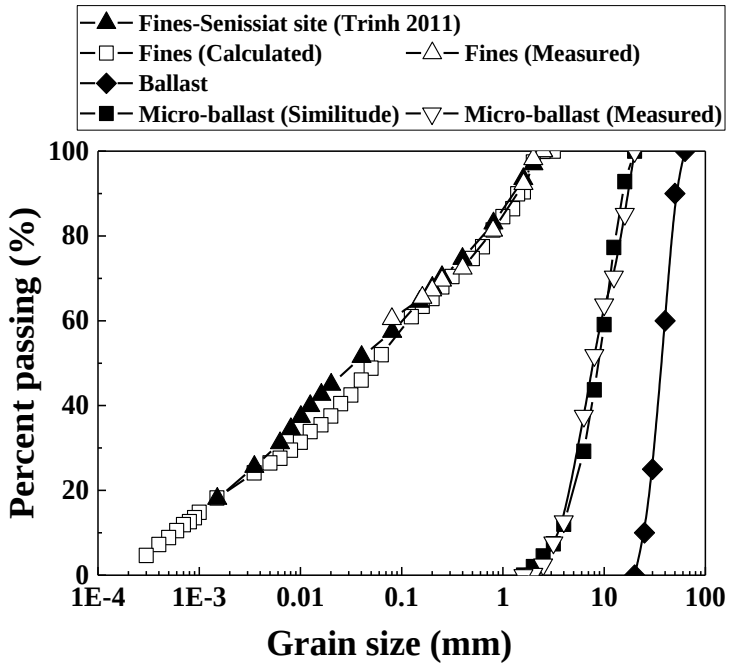

Fig. 1. Grain size distribution curves of fines and micro-ballast (after Wang et al. 2018a)

In order to prepare a sample at a target coarse grain content f_v and a target water content of fine soil w_f, the fine soil was prepared at the optimum water content $w_{opt\text{-}f}$ = 13.7%, then preserved in a container for 24 h allowing moisture homogenization. The fine soil was then mixed thoroughly with micro-ballast at the pre-determined mass to reach the target f_v value. After that, the soil mixture was dynamically compacted in three layers, with the equivalent amounts of fine soil and coarse grains for each layer, to finally attain a diameter of 100 mm and a height of 200 mm. It is worth noting that the fine soil in all samples was fixed at a dry unit mass $\rho_{dmax\text{-}f}$ = 1.82 Mg/m^3 (Table 2). Thus, more compaction energy was required for the sample at higher f_v value, resulting in a higher dry unit mass ρ_d as shown in Table 2.

After obtaining the target f_v value, either a wetting or a drying process was applied to attain a target w_f value: w_1 = 17.6% (S_r = 100%) on the wet side of optimum or w_2 = 10.6% (S_r = 60%) on the dry side of optimum (Fig.2). For this purpose, a method proposed by Su et al. (2020a) was adopted: in the case of drying, the sample was each time exposed to the air in the laboratory for 1 h and then covered with plastic film for at least 7 h equilibration. In the case of wetting, 10 g water was each time sprayed on the sample before wrapping it with plastic film for at least 7 h equilibration. Fig. 3 indicates that either swelling or shrinkage of samples at different f_v values occurred, upon wetting from $w_{opt\text{-}f}$ = 13.7% to w_1 = 17.6% or drying from $w_{opt\text{-}f}$ = 13.7% to w_2 = 10.6%. It appears that the swelling-shrinkage of sample decreased with the increase of

f_v value, indicating the sensitivity of fine soil to water content change. The measured ρ_d of samples after wetting or drying to the target w_f value are presented in Table 2.

Table 2. Experimental program

f_v (%)	Initial water content $w_{opt\text{-}f}$ (%)	Target w_f (%)	Target S_r (%)	Target $\rho_{dmax\text{-}f}$ (Mg/m^3)	Target ρ_d (Mg/m^3)	Measured ρ_d (Mg/m^3)
0	13.7	17.6	100	1.82	1.82	1.80
		10.6	60			1.85
10		17.6	100		1.91	1.88
		10.6	60			1.93
20		17.6	100		1.99	1.97
		10.6	60			2.01
35		17.6	100		2.12	2.11
		10.6	60			2.13
45		17.6	100		2.21	2.20
		10.6	60			2.22

Note: f_v represents the volumetric ratio of dry coarse grains to the total sample. $w_{opt\text{-}f}$, w_f, S_r and $\rho_{dmax\text{-}f}$ represent the optimum water content, the water content, the degree of saturation and the maximum dry density of fine soils, respectively. ρ_d represents the dry density of soil mixtures sample. Measured ρ_d represents the dry density of soil mixtures sample after wetting or drying from compaction water content $w_{opt\text{-}f}$ to target w_f.

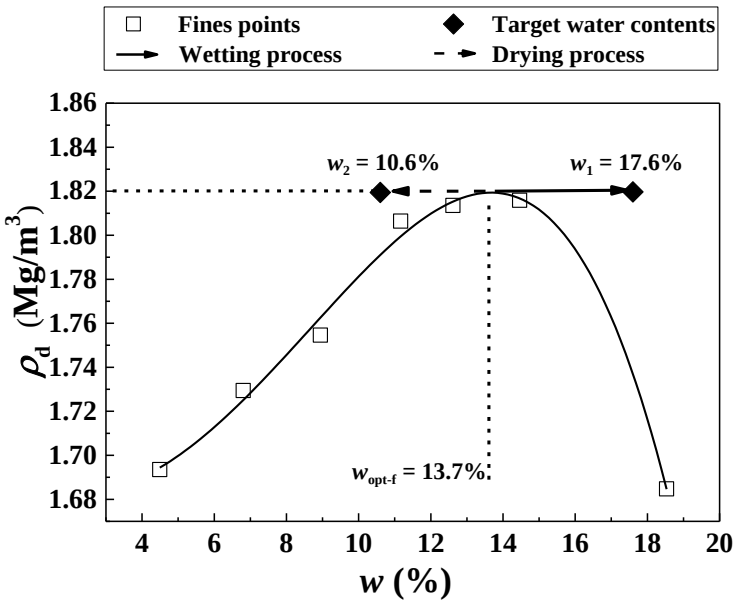

Fig. 2. Samples states at two target water contents with respect to the compaction curve

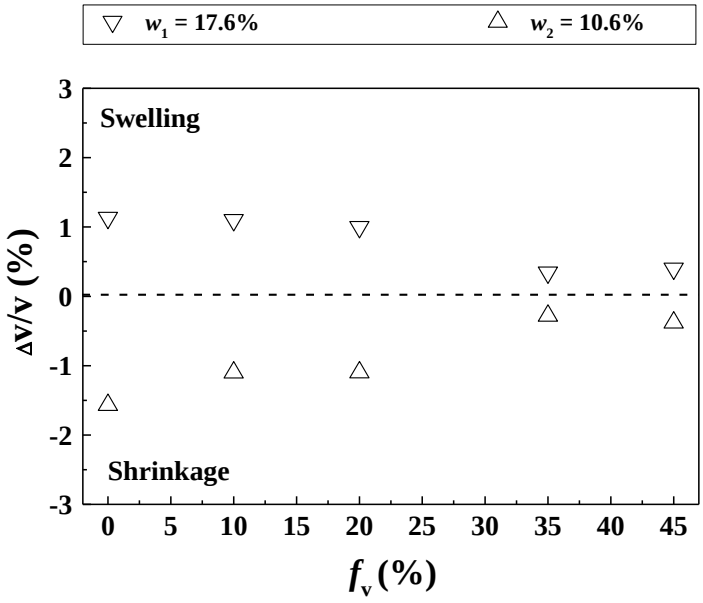

Fig. 3. Volume change of samples with f_v at two target water contents

Cyclic triaxial tests

The cyclic triaxial apparatus used by Wang et al. (2017) was adopted in this study, hosting a sample of 100 mm diameter and 200 mm height. A 50 kN hydraulic actuator was adopted, enabling either a displacement or force controlled mode in monotonic and cyclic triaxial tests. For the cyclic loading, different signal shapes, amplitudes, frequencies and large number of cycles (up to several millions) could be applied. A linear variable displacement transducer (LVDT) was used for the measurement of axial displacement, and a force sensor installed at the bottom allowed the monitoring of axial force.

Cyclic triaxial tests were performed on the samples at two water contents (w_1 = 17.6% and w_2 = 10.6%) and five different f_v values (0%, 10%, 20%, 35% and 45%) with the drainage valve open. A confining pressure σ_3 = 30 kPa was applied in all tests, which corresponded to the average horizontal stress estimated in the field condition by considering the train loading, the depth of interlayer and the Poisson's ratio (Duong et al. 2016). For the samples at w_1 = 17.6% (S_r = 100%), an overnight consolidation under σ_3 = 30 kPa was adopted prior to the cyclic loading, because in that case pore water pressure could be generated. By contrast, for samples at w_2 = 10.6% (S_r = 60%), after application of σ_3 = 30 kPa, the cyclic loading was performed directly, for only air was expected to be expelled. Fig. 4 depicts the various sine-shaped signals

applied at a frequency of 1.78 Hz corresponding to that excited between two bogies at a train speed of 50 km/h.

A series of cyclic loadings with various loading amplitudes Δq = 10, 15, 20, 25 and 30 kPa were applied, with a number of loading cycles N = 90000 for each Δq value. Note that Δq was defined as the difference between the maximum deviator stress q_{max} and the minimum deviator stress q_{min}. After that, the multi-step loading procedure proposed by Gidel et al. (2001) and applied later by Duong et al. (2016) and Wang et al. (2017) was adopted, as shown in Fig. 5 with Δq plotted against N. The values of Δq at 10, 30, 50, 100 and 200 kPa were applied and each with N = 100 cycles, as in Lamas-Lopez (2016) and Wang et al. (2017). These Δq values were selected by accounting for the train wheel load and the depth of interlayer soil from 250 mm to 600 mm. Considering the wheel load of 16-22 tons per axle in France and 30 tons per axle of heavier train in other countries (Alias 1984), the corresponding range of vertical stress was estimated at 40 - 90 kPa and 120 - 140 kPa (Duong et al. 2013), respectively. A maximum value of Δq = 200 kPa was adopted to consider the maximum vertical stress distributed on the top of railway substructure. Note that the application of Δq equal to 10 and 30 kPa was to ensure the continuity of a multi-step loading stresses Δq. During the tests, the axial force and axial displacement were monitored.

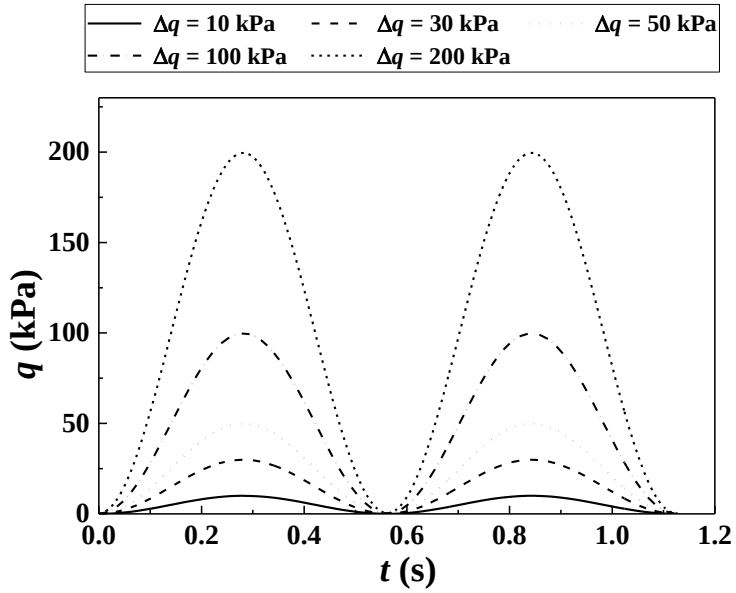

Fig. 4. Typical sine-shaped signals with various stress amplitudes Δq

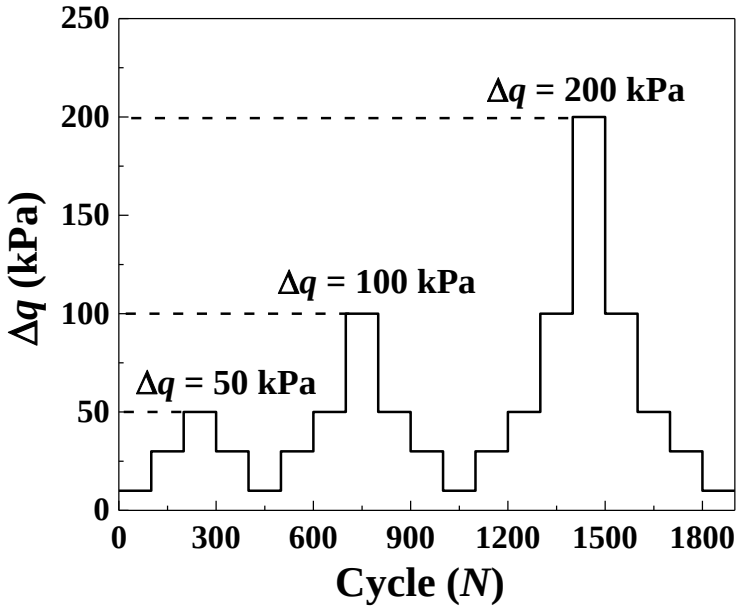

Fig. 5. Multi-step loading procedure applied in cyclic triaxial tests

Experimental results

Fig. 6 depicts typical hysteresis loops for various deviator stress amplitudes Δq at f_v = 0% and two target water contents. It can be observed that at a given water content, the size of hysteresis loop increased with the increase of Δq. When $\Delta q \leq 30$ kPa, the hysteresis loops were small because of the large number of loading cycles applied under this stress level to approach an in-situ soil state, prior to starting the multi-step loading procedure shown in Fig. 5. By contrast, when Δq increased to a larger value, especially at 100 kPa for w_1 =17.6% and 200 kPa for w_2 = 10.6%, a larger unclosed hysteresis loop occurred, with the axial strain consisting of two parts: permanent strain ε_1^p and elastic strain ε_1^r. Note that at w_1 =17.6%, the used LVDT reached its measurement capacity around 70 mm by the end of loading under Δq = 100 kPa. Thus, the tests at w_1 =17.6% ended at N = 1400 (Fig. 5). In addition, a decrease of water content from w_1 =17.6% to w_2 = 10.6% led to a decrease of the size of hysteresis loops, indicating that both permanent strain ε_1^p and elastic strain ε_1^r decreased with the decrease of water content.

To further clarify the effect of water content, the variations of ε_1^p and ε_1^r with loading cycles N at f_v = 0% are plotted in Fig. 7 for the two target water contents. At a given water content, the permanent strain ε_1^p and elastic strain ε_1^r increased slowly with Δq until Δq = 100 -200 kPa. Then, a sharp increase was observed for both strains. As shown in Fig. 7, the decrease of water

content from w_1 =17.6% (Fig. 7 (a_1) - (b_1)) to w_2 = 10.6% (Fig. 7 (a_2) - (b_2)) resulted in a large decrease of both strains.

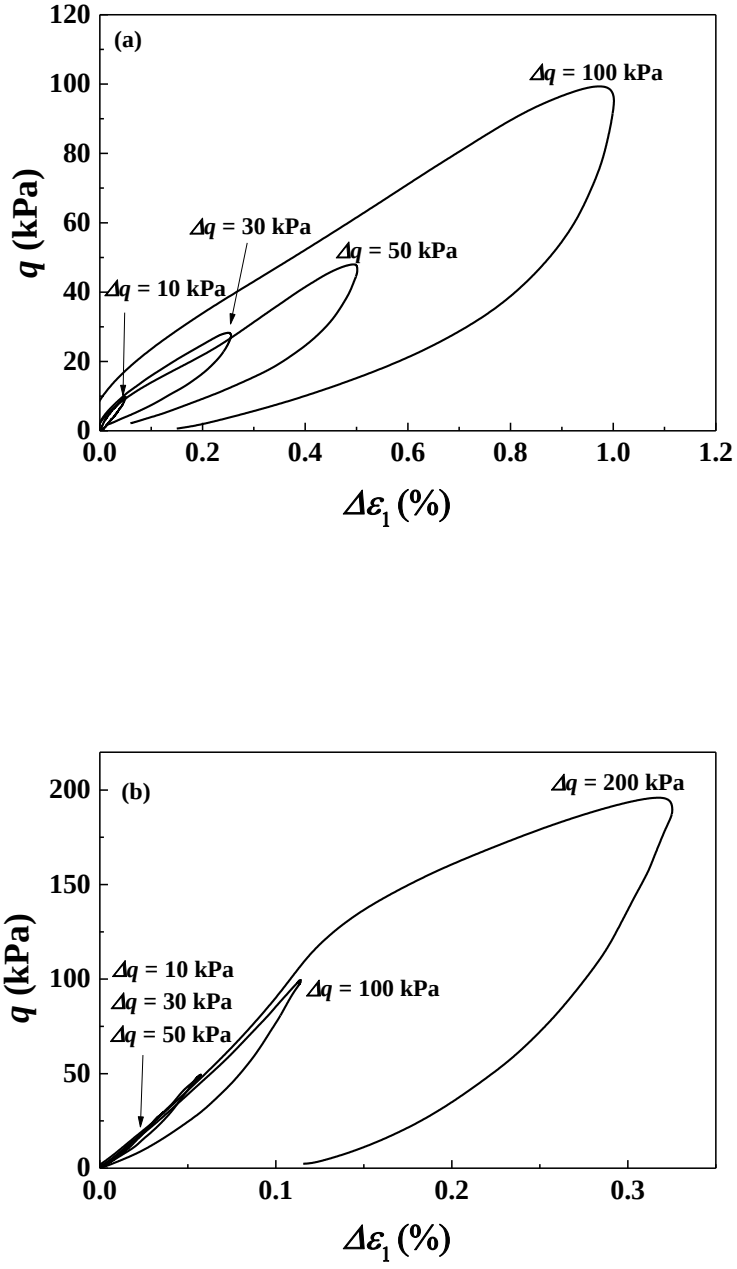

Fig. 6. Typical hysteresis loops for various deviator stress amplitudes Δq at f_v = 0% and two target water contents: (a) w_1 = 17.6%; (b) w_2 = 10.6%

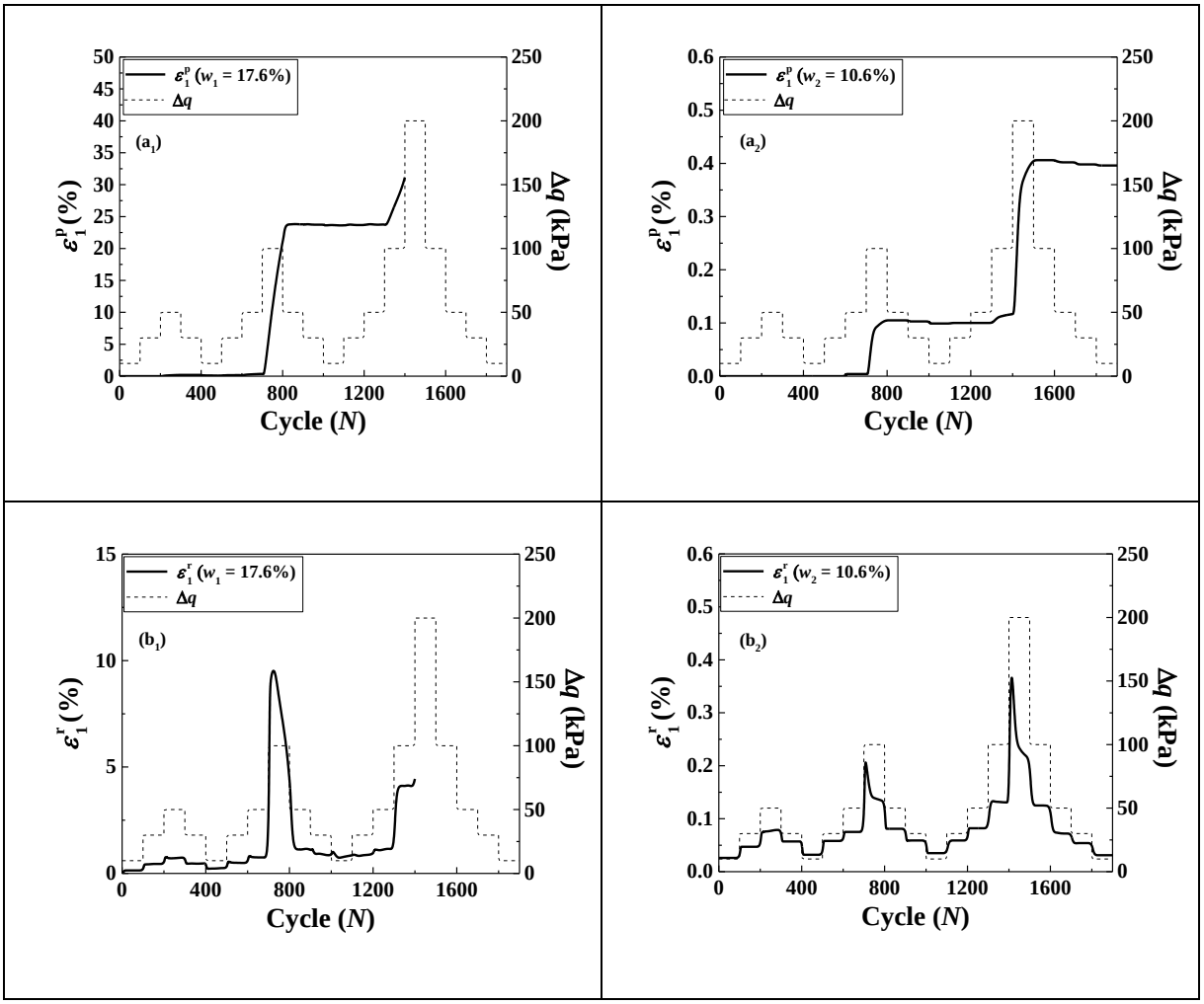

Fig. 7. Variations of permanent strain and resilient strain with loading cycles at f_v = 0% and two target water contents: (a1) - (b1) w_1 = 17.6%; (a2) - (b2) w_2 = 10.6%

Fig. 8 illustrates the variation of hysteresis loops with N for the first 100 cycles of Δq = 100 kPa at f_v = 0% and two target water contents. At w_1 = 17.6%, the size of hysteresis loop became smaller and more stable with the increase of N, which could be explained by the decrease of permanent strain ε_1^p and eventually a purely resilient behavior. The same observation could be made for w_2 = 10.6%. Furthermore, when the water content decreased from w_1 = 17.6% to w_2 = 10.6%, the size of hysteresis loop decreased largely, suggesting that a decrease of water content promoted the resilient behavior.

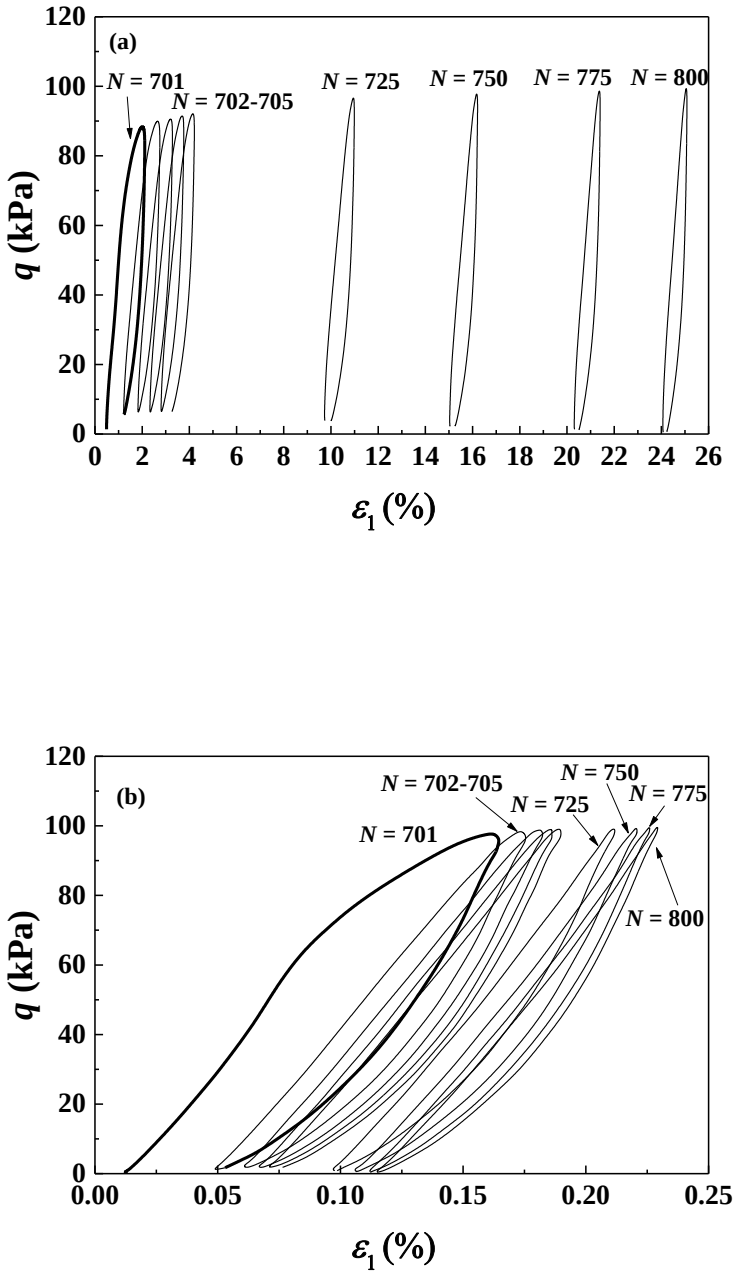

Fig. 8. Hysteresis loops at the first 100 loading cycles (N = 701- 800) of Δq = 100 kPa for the samples at f_v = 0% and two target water contents: (a) w_1 = 17.6%; (b) w_2 = 10.6%

Fig. 9 (a) defines the resilient modulus M_r as the secant slope of hysteresis loop (Seed et al. 1986; Rollins et al.1998; Tennakoon and Indraratna 2014):

$$M_r = \frac{\Delta q}{\varepsilon_1^r} \quad (1)$$

where Δq is the deviator stress amplitude, ε_1^r is the resilient strain.

Fig. 9 (b) defines the damping ratio D_r as the ratio of dissipated energy to the total energy during a given cycle (Seed et al. 1986; Rollins et al.1998; Tennakoon and Indraratna 2014):

$$D_r = \frac{E_{loop}}{4\pi E_d} \quad (2)$$

where E_{loop} is the area of hysteresis loop, E_d is the area of triangle, which is determined by the maximum deviator stress and the maximum axial strain in one cycle.

Fig. 10 depicts the variations of M_r with N under the two target water contents. It appears clearly that a higher water content gave rise to a lower M_r. Moreover, at a lower content w_2 = 10.6%, M_r appeared to increase with the increase of Δq; in particular, a sudden increase at the first cycle and a stabilization at the end were identified. The variations of M_r with Δq at a higher water content w_1 = 17.6% were not as clear as that at w_2 = 10.6%: the first increases of Δq up to 50 kPa seemed to decrease M_r; the second increases of Δq up to 100 kPa did not affect M_r and the third increases of Δq also seemed to decrease M_r. Thus, opposite variation trends of M_r with Δq could occur when increasing the water content from 10.6% to 17.6%. The similar phenomenon was reported by Yang et al. (2008) on subgrade soil through suction-controlled cyclic triaxial tests. They found that M_r decreased with the increasing Δq at low matrix suctions ranging from 50 to 150 kPa, while increased with the increasing Δq at a high matrix suction of 450 kPa. Ng et al. (2013) studied the effects of Δq and suction on M_r of subgrade soil by suction-controlled cyclic triaxial tests, and reported that M_r decreased with the increase of Δq at low matrix suctions ranging from 0 to 250 kPa. Moreover, they developed a model describing the variations of M_r with Δq considering the opposite variation trends of M_r with Δq in low and high suctions ranges. Han and Vanapalli (2015) also proposed a model describing the variation of M_r of subgrade soil with suction using the soil-water retention curve. But their model did not take the effect of Δq into account.

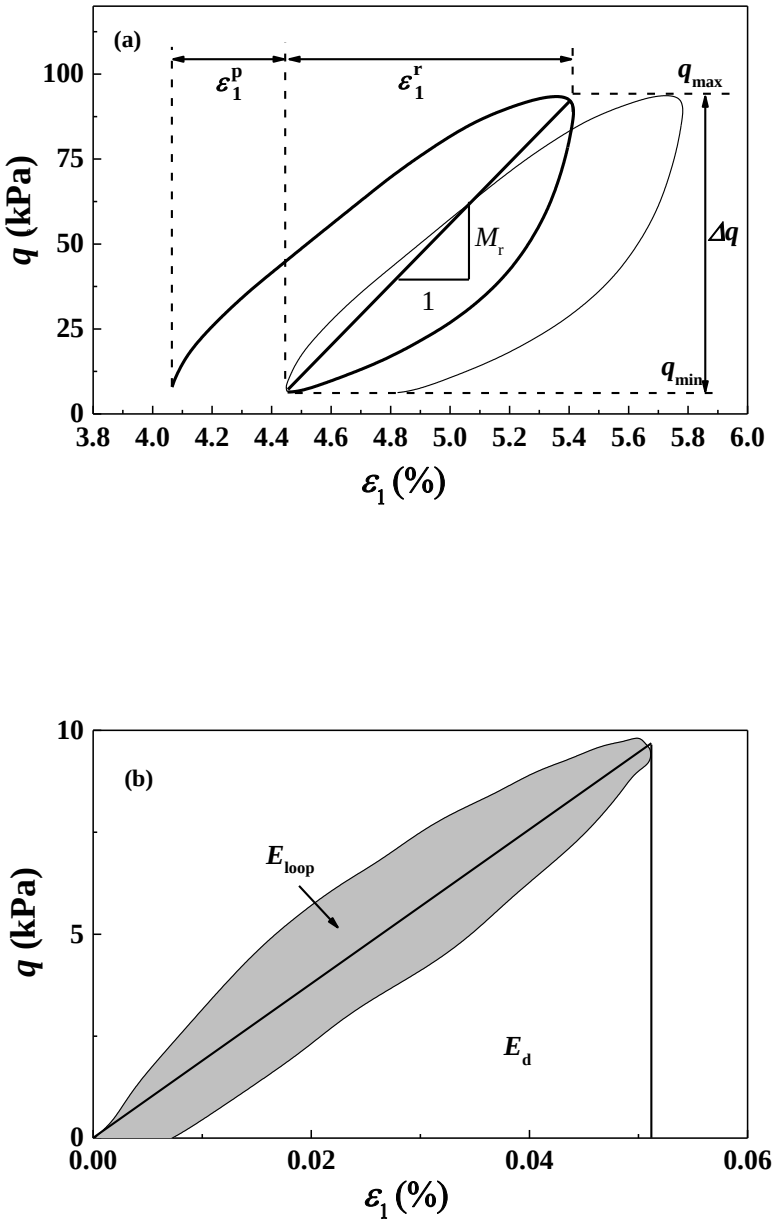

Fig. 9. Determination of (a) resilient modulus M_r and (b) damping ratio D_r

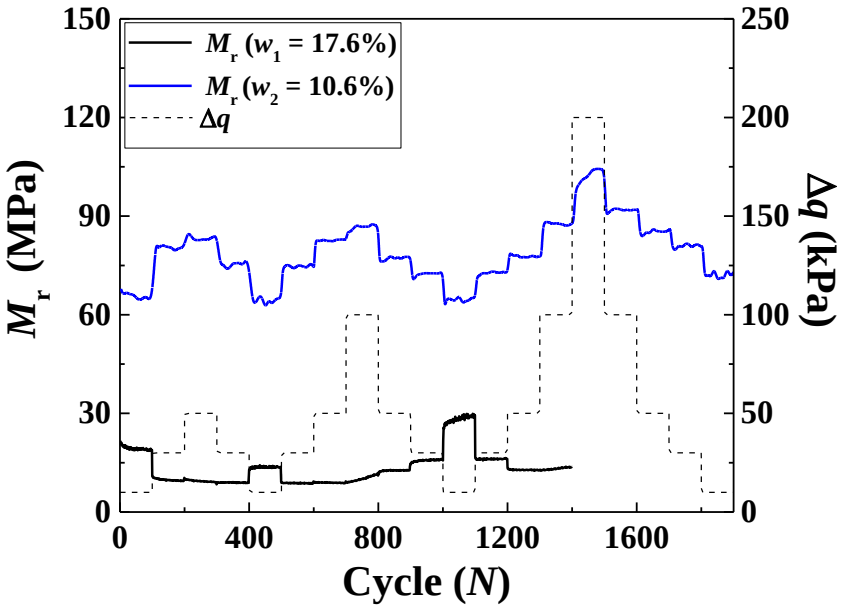

Fig. 10. Variations of M_r with number of loading cycles N at f_v = 0% and two target water contents

To further analyze the effect of water content on resilient modulus M_r, the values of M_r at the first cycles (start-stages) and last cycles (end-stages) of Δq = 50, 100 and 200 kPa are chosen for comparison in Fig. 11 for the five different f_v values and two different w_f values. Note that the legend "N201-50kPa" referred to the number of loading cycles N = 201 and the deviator stress amplitude Δq = 50 kPa. Figs. 11 (a_1) - (b_1) show that in the case of w_1 = 17.6%, at the start-stages of Δq = 50 and 100 kPa, M_r increased slowly with f_v at $f_v \leq 20\%$, while a large increase of M_r with f_v occurred at $f_v \geq 35\%$. A bilinear fitting was attempted for such M_r variation. It could be found that at the start-stages of Δq = 50 and 100 kPa, a quite similar characteristic coarse grain content $f_{v\text{-}cha} \approx 25.5\%$ was identified at the intersection points of two fitting lines, indicating that the $f_{v\text{-}cha}$ was independent of stress amplitude Δq. It could be deduced that when $f_v \leq f_{v\text{-}cha}$, the fine soil dominated the fabric of soil mixtures and the increase of coarse grain content f_v led to a slight increase of M_r. By contrast, when $f_v \geq f_{v\text{-}cha}$, the coarse grains dominated the soil fabric and the increase of f_v led to a significant increase of M_r.

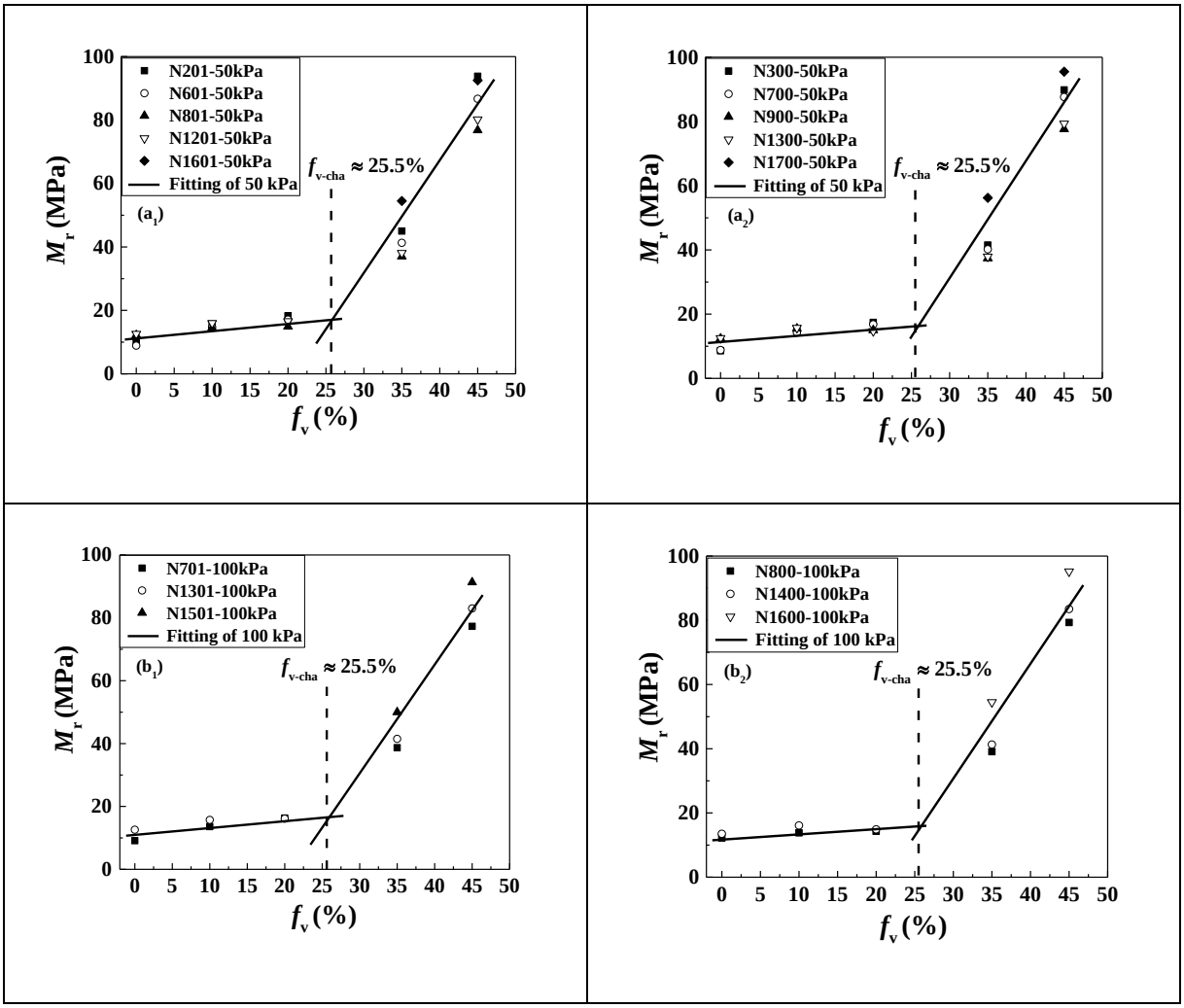

Fig. 11. Variations of M_r with f_v at w_1 = 17.6% and (a_1) start-stage of Δq = 50 kPa, (b_1) start-stage of Δq = 100 kPa, (a_2) end-stage of Δq = 50 kPa and (b_2) end-stage of Δq = 100 kPa

When it comes to the end-stages of Δq = 50 and 100 kPa (Figs. 11 (a_2) - (b_2)), the same observation was made in terms of variations of M_r with f_v. Interestingly, while fitting the distinct increasing rates of M_r with f_v at $f_v \leq 20\%$ and $f_v \geq 35\%$, the value of $f_{v\text{-}cha}$ appeared to approach 25.5%, in agreement with the value identified based on the data corresponding to the start-stages of Δq = 50 and 100 kPa.

Figs. 12 (a_1) - (b_1) show the different variations of M_r with f_v at $f_v \leq 20\%$ and $f_v \geq 35\%$ at the start-stages of Δq = 50, 100 and 200 kPa for the case of w_2 = 10.6%. A characteristic coarse grain content $f_{v\text{-}cha}$ was identified around 32.0% for various stress amplitudes Δq. The similar phenomenon could be observed for the end-stages of Δq = 50, 100 and 200 kPa (Figs. 12 (a_2) - (b_2)). Using two lines to fit the increasing trend of M_r with f_v, the value of $f_{v\text{-}cha}$ was found to be 32.0%, in agreement with the value identified using data corresponding to the start-stages of Δq = 50, 100 and 200 kPa.

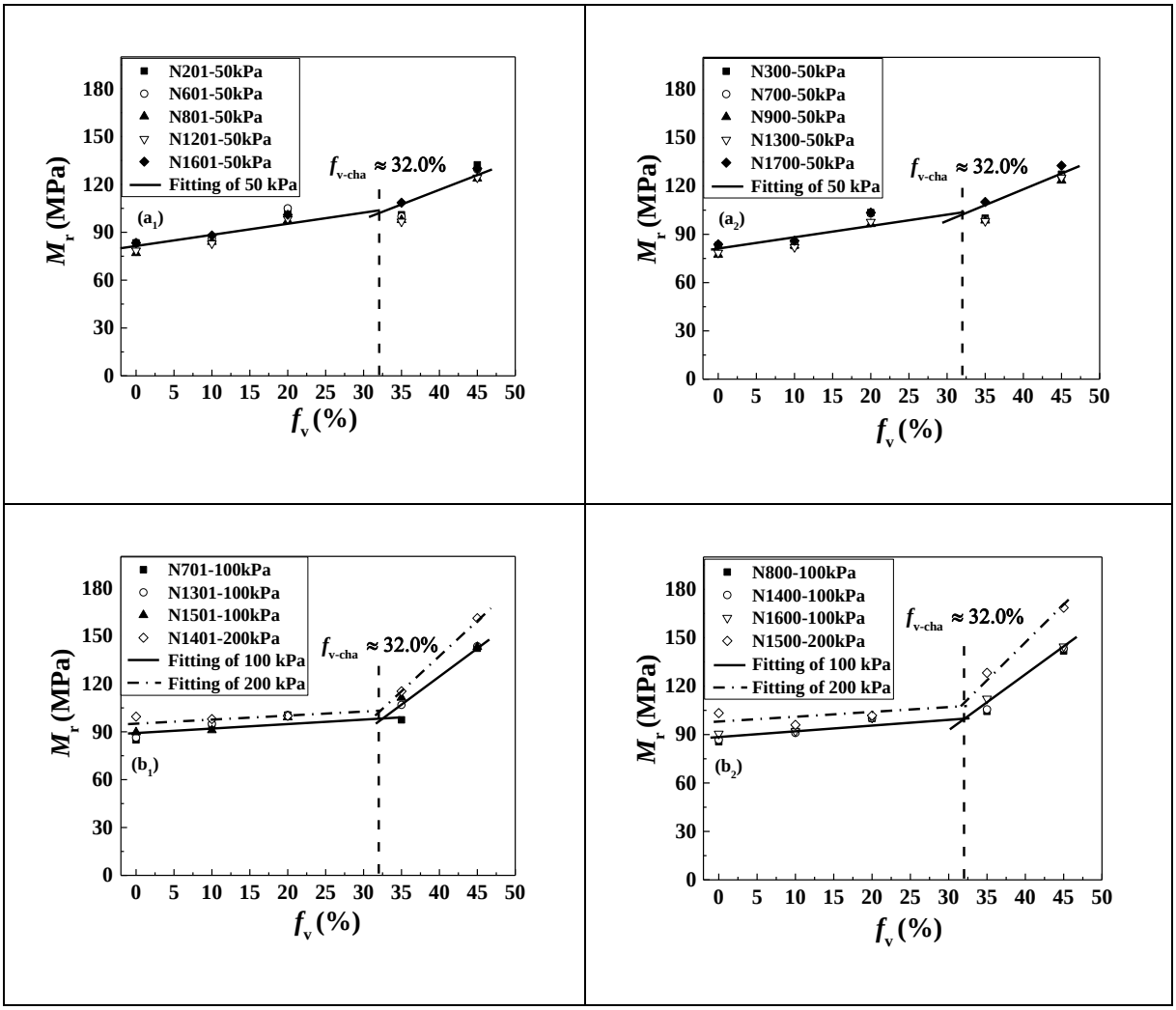

Fig. 12. Variations of M_r with f_v at w_2 = 10.6% and (a_1) start-stage of Δq = 50 kPa, (b_1) start-stage of Δq = 100 and 200 kPa, (a_2) end-stage of Δq = 50 kPa and (b_2) end-stage of Δq = 100 and 200 kPa

Fig. 13 depicts the effect of water content on D_r at f_v = 0%. Under a constant water content, D_r increased sharply with Δq at the first loading cycle, and then decreased gradually until a stable state. This can be explained by the evolution of hysteresis loops with N at a given Δq value, as observed in Fig. 8: at a constant w_f value and Δq = 100 kPa, the size of hysteresis loops decreased with N, suggesting less energy loss and giving rise to a smaller D_r value. When the water content decreased from w_1 = 17.6% to w_2 = 10.6%, a significant decrease of D_r was observed, which was also in agreement with the variation of the size of hysteresis loops shown in Figs. 8 (a) - (b).

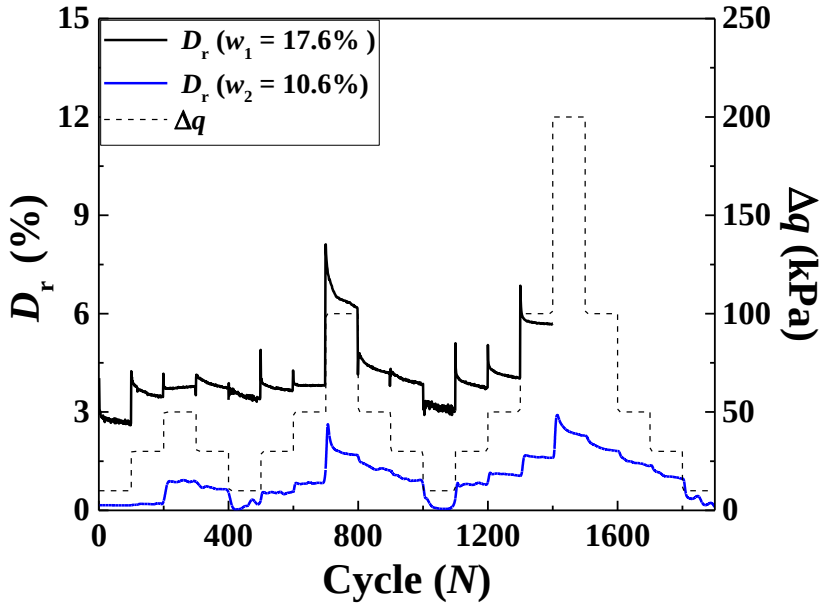

Fig. 13. Variations of D_r with loading cycles N at f_v = 0% and two target water contents

To further clarify the effect of water content on D_r, the values of D_r at the first cycles (start-stages) and the last cycles (end-stages) of Δq = 50, 100 and 200 kPa were selected for comparison. Figs. 14 (a_1) - (b_1) show two distinct decreasing slopes of D_r with f_v at $f_v \leq 20\%$ and $f_v \geq 35\%$ respectively for the start-stages of Δq = 50 and 100 kPa in the case of w_1 = 17.6%. A characteristic coarse grain content $f_{v\text{-}cha}$ could be also identified, around 25.5% under different Δq values. The same phenomenon was observed in Figs. 14 (a_2) - (b_2) for the end-stages of Δq = 50 and 100 kPa: applying two lines to fit the variation of D_r with f_v at $f_v \leq 20\%$ and $f_v \geq 35\%$ respectively, a value of $f_{v\text{-}cha}$ was identified, also around 25.5%. Interestingly, this $f_{v\text{-}cha}$ value was in good concordance with the value identified based on M_r data (Fig.11).

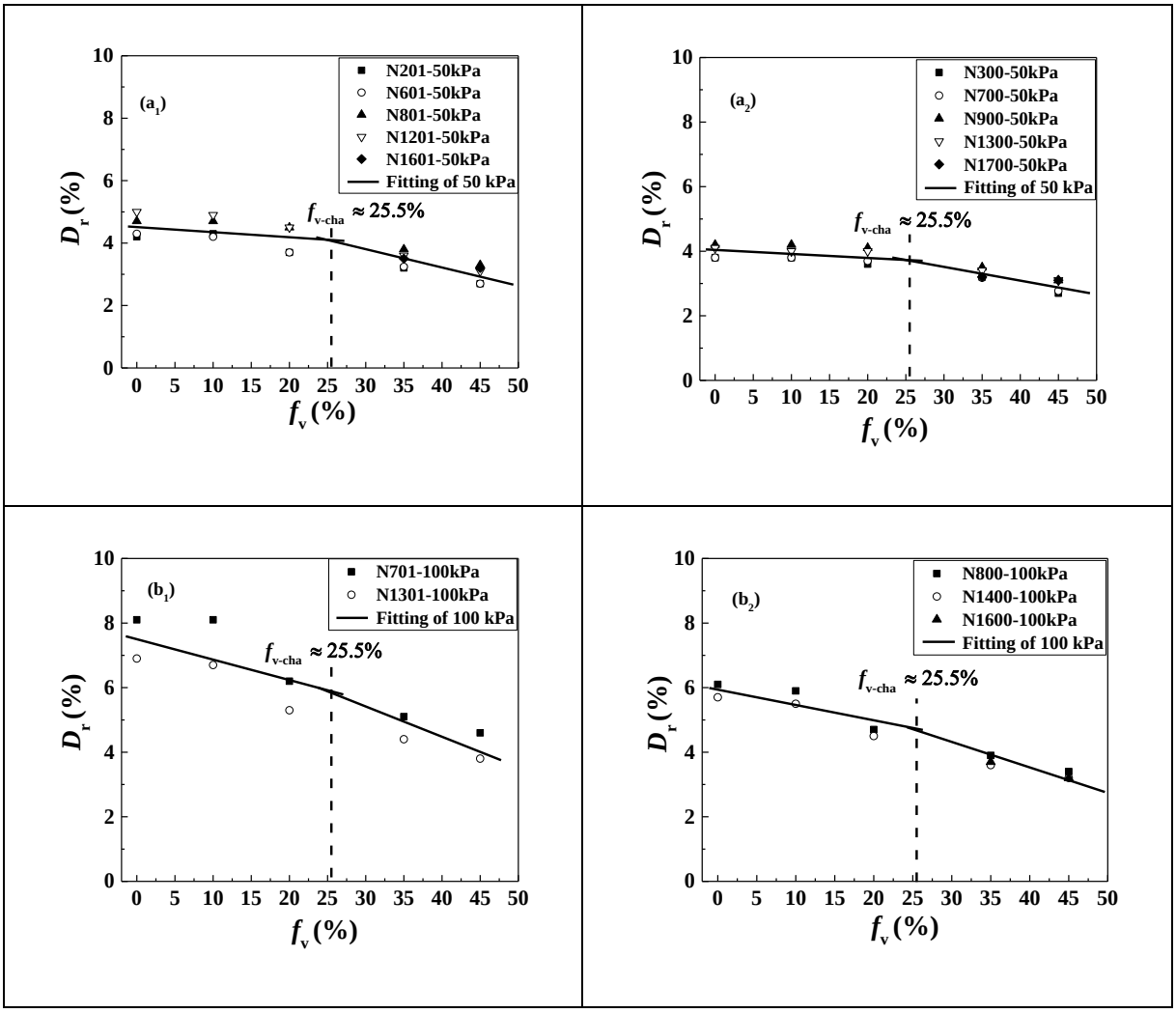

Fig. 14. Variations of D_r with f_v at w_1 = 17.6% and (a_1) start-stage of Δq = 50 kPa, (b_1) start-stage of Δq = 100 kPa, (a_2) end-stage of Δq = 50 kPa and (b_2) end-stage of Δq = 100 kPa

Fig. 15 shows the variation of D_r with f_v under various Δq values in the case of w_2 = 10.6%. No matter at the start-stages or end-stages of Δq = 50, 100 and 200 kPa, two different decreasing trends at $f_v \leq 20\%$ and $f_v \geq 35\%$ could be identified, defining a value of $f_{v\text{-}cha}$ close to 32.0%. This value was also in good concordance with that identified with M_r data (Fig. 12).

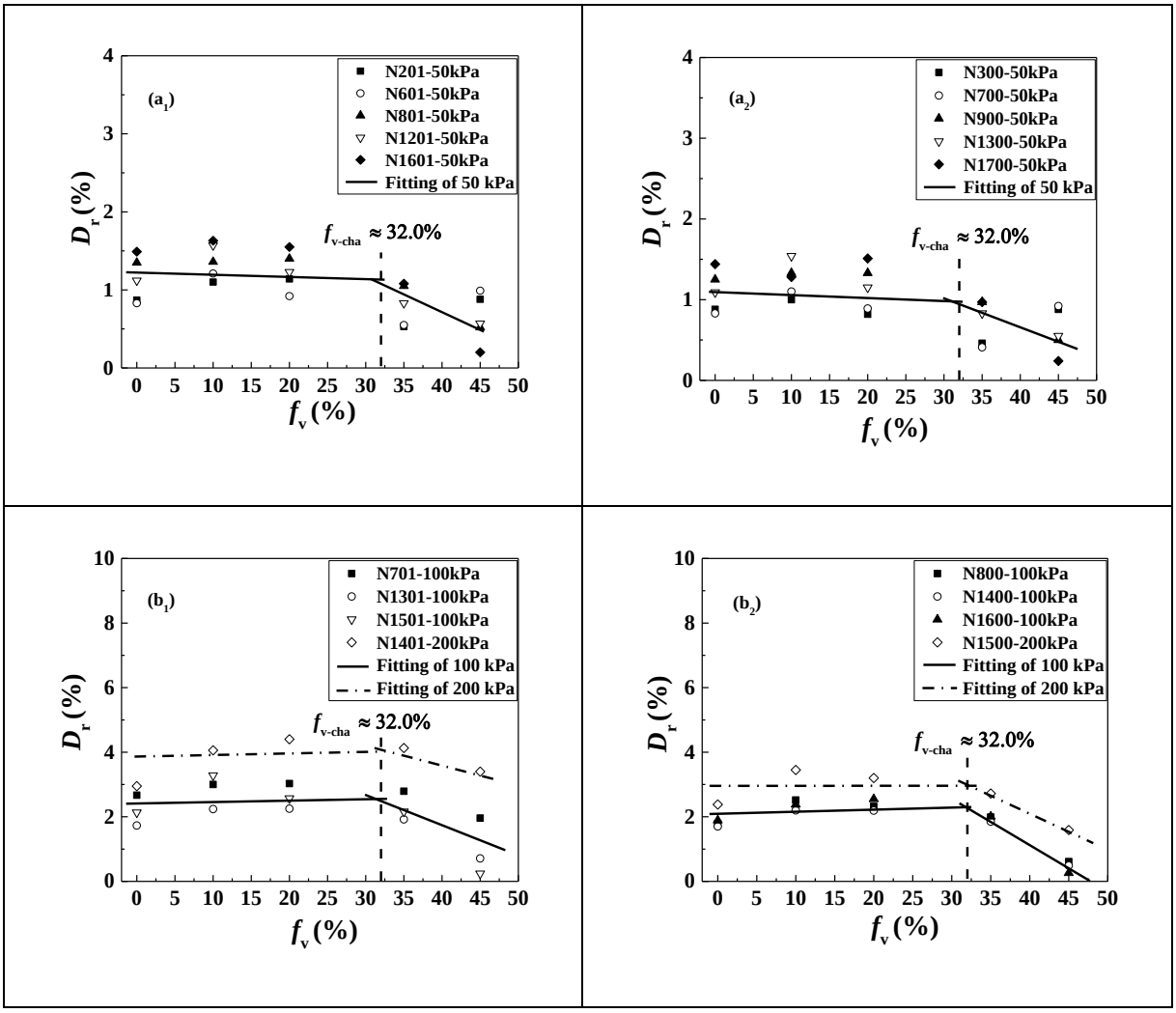

Fig. 15. Variations of D_r with f_v at w_2 = 10.6% and (a_1) start-stage of Δq = 50 kPa, (b_1) start-stage of Δq = 100 and 200 kPa, (a_2) end-stage of Δq = 50 kPa and (b_2) end-stage of Δq = 100 and 200 kPa

Interpretation and discussion

Based on the variations of M_r and D_r with f_v, a constant $f_{v\text{-}cha}$ value was obtained at a given water content: $f_{v\text{-}cha} \approx 25.5\%$ at $w_1 = 17.6\%$ and $f_{v\text{-}cha} \approx 32.0\%$ at $w_2 = 10.6\%$. Note that at $w_{opt\text{-}f} = 13.7\%$ a narrow range of $f_{v\text{-}cha}$ from 27.8% to 28.9% was found by Wang et al. (2017), defining an average value of 28.4%. This average value was considered in further analysis. It appears clearly from Table 3 that $f_{v\text{-}cha}$ increased with the decrease of water content.

Table 3. Variation of $f_{v\text{-}cha}$ with water content

w (%)	17.6	13.7	10.6
$f_{v\text{-}cha}$ (%)	25.5	28.4	32.0

Note: $f_{v\text{-}cha} \approx 28.4\%$ at $w_{opt\text{-}f} = 13.7\%$ was obtained by Wang et al. (2017)

As reported by Wang et al. (2017) and Qi et al. (2020a), the effect of coarse grain content f_v separated the soil fabrics of mixtures into two zones: a zone corresponding to a fine soil supported fabric at $f_v \leq f_{v\text{-}cha}$ and a zone corresponding to a coarse grain supported fabric at $f_v \geq f_{v\text{-}cha}$. According to Su et al. (2020a), two categories of fines existed in the coarse grain skeleton: the first category of dense fines in-between coarse grains and the second category of looser fines situated in the macro-pores surrounded by coarse grains. The former was expected to contribute to the force transmission between coarse grains, as shown by de Frias Lopez et al. (2016) on fine-coarse granular mixtures through discrete element analysis and Qi et al. (2020b) through the dynamic response of track-bed materials in cyclic triaxial tests.

The variation of $f_{v\text{-}cha}$ with water content could be explained by the swelling or shrinkage of fine soil, which contained 30% of clay soils (Speswhite and Bentonite) as shown in Table 1. When the water content decreased, shrinkage of both categories of fines occurred. The shrinkage of dense fines led to a decrease of the volume of macro-pores, whereas the shrinkage of loose fines resulted in an increase of the volume of macro-pores. The variation of the global volume of macro-pores was the result of the competition between the dense and loose fines. Owing to the expected higher density and smaller amount of dense fines, the variation of global volume of macro-pores was expected to be governed mainly by the volume change of loose fines. Thereby, an increase of global volume of macro-pores was expected during the drying process. The similar observation was made by Zhang and Li (2010) on fine/coarse soil mixtures using mercury intrusion porosimetry technique. They found that in the case of coarse grain supported structure, the shrinkage of fines upon drying led to a slight volume change of soil mixtures, but gave rise to a significant increase of volume of macro-pores. With a larger volume of macro-pores, more coarse grains were needed to constitute a global skeleton, giving rise to an increase of $f_{v\text{-}cha}$ value.

Su et al. (2020b) also identified the $f_{v\text{-}cha}$ values at different water contents by performing monotonic triaxial tests: $f_{v\text{-}cha} \approx 25\%$ at $w_1 = 17.6\%$, $f_{v\text{-}cha} \approx 27\%$ at $w_{opt\text{-}f} = 13.7\%$ and $f_{v\text{-}cha} \approx 29\%$ at $w_2 = 10.6\%$. Comparison between these $f_{v\text{-}cha}$ values and those obtained in this study by cyclic

triaxial tests showed that for a given water content, a slightly larger $f_{v\text{-}cha}$ value was obtained under cyclic loading. This could be explained by the more efficient effect of cyclic loading on the rearrangement of coarse grains. The similar phenomenon was observed by Duong et al. (2016) on upper part of interlayer soil, who reported that the cyclic loading resulted in a progressive stabilization of particles arrangement. Werkmeister et al. (2004) investigated the volume change behavior of unbound granular materials by cyclic triaxial tests, and found that the cyclic loading induced a denser soil structure and an increase of coarse grain contacts. It could be thus inferred that a relatively larger reduction of macro-pore volume is expected under cyclic loading, increasing the fraction of coarse grains required for constituting a grain skeleton fabric and leading to a larger $f_{v\text{-}cha}$ value.

Conclusions

To investigate the effect of water content on the dynamic properties of interlayer soil, a series of cyclic triaxial tests were performed, following a multi-step loading procedure with various Δq values. Two target fine water contents w_f (w_1 = 17.6% and w_2 = 10.6%) and five coarse grain contents f_v (0%, 10%, 20%, 35% and 45%) were considered, aiming at investigating the variations of the resilient modulus M_r and the damping ratio D_r with w_f and f_v. In particular, the values of M_r and D_r at the start-stages and end-stages of Δq = 50, 100 and 200 kPa were selected for comparison. The following conclusions were drawn:

Under a given f_v value, the increase of water content led to a decrease of M_r due to the contribution of suction while an increase of D_r owing to the increase of soil viscosity. Through the variations of M_r and D_r with f_v, a characteristic coarse grain content $f_{v\text{-}cha}$ was identified, defining two distinct soil fabrics: a fine matrix fabric at $f_v \leq f_{v\text{-}cha}$ and a coarse grain skeleton fabric at $f_v \geq f_{v\text{-}cha}$. Moreover, a constant $f_{v\text{-}cha}$ value was obtained at a given water content: $f_{v\text{-}cha} \approx 25.5\%$ at w_1 = 17.6% and $f_{v\text{-}cha} \approx 32.0\%$ at w_2 = 10.6%. Wang et al. (2017) identified a value $f_{v\text{-}cha} \approx 28.4\%$ at $w_{opt\text{-}f}$ = 13.7% under equivalent conditions. The increase of $f_{v\text{-}cha}$ with the decrease of water content could be explained by the swelling-shrinkage of fine soil. With the decrease of water content, the shrinkage of fine soil led to an increase of global volume of macro-pores. In that case, more coarse grains were required to constitute the global skeleton, giving rise to an increase of $f_{v\text{-}cha}$.

Comparison of $f_{v\text{-}cha}$ values obtained from monotonic and cyclic triaxial tests suggested that under a given water content, the value of $f_{v\text{-}cha}$ obtained under cyclic loading was slightly larger

than that under monotonic loading, evidencing the more efficient effect of cyclic loading on the rearrangement of coarse grains.

Ackknowledgements

This work was supported by the China Scholarship Council (CSC) and Ecole des Ponts ParisTech.

References

Alias La voie ferr´ee. 1984. Techniques de construction et d'entretien. 2nd Ed., Eyrolles.

ASTM D698-12. 2012. Standard test methods for laboratory compaction characteristics of soil using standard effort. ASTM International, West Conshohocken, Pa.

Cui, Y.J., Duong, T.V., Tang, A.M., Dupla, J.C., Calon, N. and Robinet, A., 2013. Investigation of the hydro-mechanical behaviour of fouled ballast. Journal of Zhejiang University Science A, 14(4), pp.244-255.

Cui, Y. J. 2018. Mechanical behaviour of coarse grains/fines mixture under monotonic and cyclic loadings. Transportation Geotechnics, 17, 91-97.

Duong, T.V., Cui, Y.J., Tang, A.M., Dupla, J.C., Canou, J., Calon, N. and Robinet, A., 2016. Effects of water and fines contents on the resilient modulus of the interlayer soil of railway substructure. *Acta Geotechnica*, *11*(1), pp.51-59.

de Frias Lopez, R., Silfwerbrand, J., Jelagin, D., & Birgisson, B. 2016. Force transmission and soil fabric of binary granular mixtures. Géotechnique, 66(7), 578-583.

Gidel, G., Hornych, P., Breysse, D., & Denis, A. 2001. A new approach for investigating the permanent deformation behaviour of unbound granular material using the repeated loading triaxial apparatus. Bulletin des laboratoires des Ponts et Chaussées, (233).

Han, Z., & Vanapalli, S. K. 2015. Model for predicting resilient modulus of unsaturated subgrade soil using soil-water characteristic curve. Canadian Geotechnical Journal, 52(10), 1605-1619.

Jibon, M., Mishra, D., & Kassem, E. 2020. Laboratory characterization of fine-grained soils for Pavement ME Design implementation in Idaho. Transportation Geotechnics, 25, 100395.

Khasawneh, M. A., & Al-jamal, N. F. 2019. Modeling resilient modulus of fine-grained materials using different statistical techniques. Transportation Geotechnics, 21, 100263.

Lin, S. Y., Lin, P. S., Luo, H. S., & Juang, C. H. 2000. Shear modulus and damping ratio characteristics of gravelly deposits. Canadian Geotechnical Journal, 37(3), 638-651.

Lamas-lopez, F. 2016. Field and laboratory investigation on the dynamic behavior of conventional railway track-bed materials in the context of traffic upgrade. PhD Thesis, Ecole Nationale des Ponts et Chaussées, Université Paris-Est.

Menq, F. Y. 2003. Dynamic properties of sandy and gravelly soils. Ph.D. thesis, The University of Texas at Austin.

Mousa, E., El-Badawy, S., & Azam, A. 2020. Evaluation of Reclaimed Asphalt Pavement as Base/Subbase Material in Egypt. Transportation Geotechnics, 100414.

Ng, C. W. W., Zhou, C., Yuan, Q., & Xu, J. 2013. Resilient modulus of unsaturated subgrade soil: experimental and theoretical investigations. Canadian Geotechnical Journal, 50(2), 223-232.

Qi, S., Cui, Y.J., Chen, R.P., Wang, H.L., Lamas-Lopez, F., Aimedieu, P., Dupla, J.C., Canou, J. and Saussine, G., 2020a. Influence of grain size distribution of inclusions on the mechanical behaviours of track-bed materials. *Géotechnique*, pp.1-10.

Qi, S., Cui, Y. J., Dupla, J. C., Chen, R. P., Wang, H. L., Su, Y., ... & Canou, J. 2020b. Investigation of the parallel gradation method based on the response of track-bed materials under cyclic loadings. Transportation Geotechnics, 100360.

Rollins, K. M., Evans, M. D., Diehl, N. B., & III, W. D. D. 1998. Shear modulus and damping relationships for gravels. Journal of Geotechnical and Geoenvironmental Engineering, 124(5), 396-405.

Stewart, H. E. 1982. The prediction of track performance under dynamic traffic loading. Ph.D. thesis, University of Massachusetts.

Seed, H. B., Wong, R. T., Idriss, I. M., & Tokimatsu, K. 1986. Moduli and damping factors for dynamic analyses of cohesionless soils. Journal of geotechnical engineering, 112(11), 1016-1032.

Selig, E. T., & Waters, J. M. 1994. Track geotechnology and substructure management. Thomas Telford, London, U.K.

Seif El Dine, B., Dupla, J. C., Frank, R., Canou, J., & Kazan, Y. 2010. Mechanical characterization of matrix coarse-grained soils with a large-sized triaxial device. Canadian Geotechnical Journal, 47(4), 425-438.

Su, Y., Cui, Y.J., Dupla, J.C., Canou, J., Qi, S., 2020a. Developing a sample preparation approach to study the mechanical behavior of unsaturated fine/coarse soil mixture. *Geotechnical Testing Journal*. (In press)

Su, Y., Cui, Y. J., Dupla, J. C., & Canou, J. 2020b. Investigation of the effect of water content on the mechanical behavior of track-bed materials under various coarse grain contents. Construction and Building Materials, 263, 120206.

Tennakoon, N., & Indraratna, B. 2014. Behaviour of clay-fouled ballast under cyclic loading. Géotechnique, 64(6), 502-506.

Trinh, V. N. 2011. Comportement hydromécanique des matériaux constitutifs de plateformes ferroviaires anciennes. PhD Thesis, Ecole Nationale des Ponts et Chaussées, Université Paris-Est.

Werkmeister, S., Dawson, A.R. and Wellner, F., 2004. Pavement design model for unbound granular materials. Journal of Transportation Engineering, 130(5), pp.665-674.

Wang, H.L., Cui, Y.J., Lamas-Lopez, F., Dupla, J.C., Canou, J., Calon, N., Saussine, G., Aimedieu, P. and Chen, R.P., 2017. Effects of inclusion contents on resilient modulus and damping ratio of unsaturated track-bed materials. *Canadian Geotechnical Journal*, *54*(12), pp.1672-1681.

Wang, H.L., Cui, Y.J., Lamas-Lopez, F., Calon, N., Saussine, G., Dupla, J.C., Canou, J., Aimedieu, P. and Chen, R.P., 2018a. Investigation on the mechanical behavior of track-bed materials at various contents of coarse grains. *Construction and Building Materials*, *164*, pp.228-237.

Wang, H.L., Cui, Y.J., Lamas-Lopez, F., Dupla, J.C., Canou, J., Calon, N., Saussine, G., Aimedieu, P. and Chen, R.P., 2018b. Permanent deformation of track-bed materials at various inclusion contents under large number of loading cycles. *Journal of Geotechnical and Geoenvironmental Engineering*, *144*(8), p.04018044.

Yang, S. R., Lin, H. D., Kung, J. H., & Huang, W. H. 2008. Suction-controlled laboratory test on resilient modulus of unsaturated compacted subgrade soils. Journal of Geotechnical and Geoenvironmental Engineering, 134(9), 1375-1384.

Zhang, L.M. and Li, X., 2010. Microporosity structure of coarse granular soils. *Journal of Geotechnical and Geoenvironmental Engineering*, *136*(10), pp.1425-1436.

Zhalehjoo, N., Tolooiyan, A., Mackay, R., & Bodin, D. 2018. The effect of instrumentation on the determination of the resilient modulus of unbound granular materials using advanced repeated load triaxial testing. Transportation Geotechnics, 14, 190-201.

CHAPTER V. MODELING OF THE MECHANICAL BEHAVIOR OF SOIL MIXTURE WITH CONSIDERATION OF SOIL-WATER RETENTION CURVE

In the three previous chapters, the water retention behavior and mechanical behavior under monotonic and cyclic loadings were investigated. Factors such as water content (or matric suction), coarse grain content, stress state and loading cycles were considered. The constitutive models were developed for the mechanical behavior of mixture with consideration of soil-water retention curve, allowing the aforementioned factors to be accounted for.

Modelling of the permanent strain of mixture was performed, with consideration of the effects of coarse grain content, deviator stress and loading cycles. Experimental data from previous studies were adopted to verify the proposed model. The results showed that the proposed fatigue model can well describe the variation of permanent strain with changes in coarse grain content, deviator stress and loading cycles, in the case of plastic shakedown. This part corresponded to a paper published in Transportation Geotechnics.

The aforementioned model was extended to the effect of matric suction by incorporating the soil-water retention curve. Different studies from literature were adopted to verify the proposed model. The model parameters were determined by fitting the variation of permanent strain with matric suction, coarse grain content, deviator stress and loading cycles under saturated conditions, and then adopted to predict the results under unsaturated condition. The results indicated a good agreement between the predictions and the measurements, showing the performance of the proposed model in describing the variation of permanent strain with these factors. Comparisons with representative existing models showed that the proposed model can provide better predictions. These results were presented in a paper submitted to Canadian Geotechnical Journal.

A constitutive model incorporating the soil-water retention curve was proposed for the resilient modulus of mixture, allowing the effects of matric suction, deviator stress and coarse grain content to be accounted for. The model was validated using experimental results from literature. Comparisons with the representative existing models showed that the proposed model is capable

of describing the suction-dependent effect of deviator stress on resilient modulus in the full suction range, while existing models can only give satisfactory simulations in the low suction range. These results were presented in a paper submitted to Acta Geotechnica.

Su, Y., Cui, Y. J., Dupla, J. C., Canou, J., & Qi, S. 2020. Transportation Geotechnics, 23, 100353.

A fatigue model for track-bed materials with consideration of the effect of coarse grain content

Yu Su[1], Yu-Jun Cui[1], Jean-Claude Dupla[1], Jean Canou[1], Shuai Qi[1,2]

Abstract: Previous studies showed that the permanent strain of interlayer soil in the French conventional railway substructure is highly dependent on the volumetric coarse grain content f_v (volumetric ratio of coarse grain to total sample). This study developed a fatigue model allowing the effects of coarse grain content f_v, stress state and number of loading cycles N on permanent strain to be accounted for. Data from the multi-stage loading cyclic tests of interlayer soil conducted at six different f_v values (0%, 5%, 10%, 20%, 35% and 45%) and five different maximum deviator stress Δq_{max} values (10 kPa, 15 kPa, 20 kPa, 25 kPa and 30 kPa) were reviewed and used for this purpose. The model parameters were determined by fitting the results from the tests at f_v = 0%, 5% and 35%. In order to validate the proposed fatigue model, the determined model parameters were then used to simulate the tests at f_v = 10%, 20% and 45%. The results obtained showed that the proposed model can well describe the permanent strain after a certain number of loading cycles, in the case of plastic shakedown.

Keywords: coarse grain content; permanent strain; fatigue model; cyclic triaxial tests; soil fabric

Introduction

Under the effect of long-term train circulation in the French conventional railway track, a new layer named interlayer was created, mainly by interpenetration of ballast and subgrade. Considering the high bearing capacity of the interlayer material corresponding to a mixture of ballast grains and fine soils, which was characterized by its high dry density of 2.4 Mg/m^3 (Trinh 2011), the French railway company (SNCF) decided to keep it as part of substructure in the national track renewal program. Field investigation showed that the proportion of ballast grains decreased over depth. Roughly, the interlayer could be divided into upper part which is dominated by ballast grains and lower part which is dominated by fine soils (Trinh et al. 2012). For the upper part, the effects of fine content and water content on permanent strain were studied by Trinh et al. (2012), Cui et al. (2013), Duong et al. (2013, 2014, 2016) and Lamas-Lopez et al. (2014, 2016) by performing monotonic and cyclic triaxial tests. The results showed that the higher the water content, the larger the permanent strain. At saturated state, the higher the fine

[1]Ecole des Ponts ParisTech, Laboratoire Navier/CERMES, 6 – 8 av. Blaise Pascal, Cité Descartes, Champs-sur-Marne, 77455 Marne – la – Vallée cedex 2, France
[2]Zhejiang University, Dept. of Civil Engineering, 38 Zheda Road, Hangzhou 310027, China

content, the larger the permanent strain. On the contrary, at unsaturated state, the higher the fine content, the lower the permanent strain due to the contribution of suction generated inside the fines. Wang et al. (2018a, 2018b, 2018c) further investigated the effect of volumetric coarse grain content f_v (volumetric ratio of coarse grain to total sample) on permanent strain using micro-ballast. A characteristic volumetric coarse grain content $f_{v\text{-}cha}$ was identified, below which the permanent strain decreased rapidly, and beyond which the permanent strain decreased relatively slowly. X-ray micro-tomography observation showed that the former case corresponded to a fine-matrix dominated structure, while the latter case corresponded to a coarse grain skeleton structure. Thus, it can be deduced that the permanent deformation of interlayer soil increases over depth due to the decreasing coarse grain content f_v. From a practical point of view, it is important to develop a model, allowing the effect of f_v on permanent strain to be accounted for.

A few attempts have been made to describe the permanent strain with different factors such as number of loading cycles *N*, stress state, soil physical state (water content and dry density), etc. Based on experimental results, Barksdale (1972), Sweere (1990) and Hornych (1993) developed various empirical approaches to describe the effect of *N* on permanent strain, among which the model proposed by Hornych (1993) was validated by a large number of tests and was adopted in French standard (AFNOR 1995). In general, these models were developed based on cyclic tests subjected to a single-stage loading, which required a large number of tests for the determination of parameters. To reduce the number of tests and also the experimental dispersion related to samples variability, multi-stage loading was generally recommended. Gidel et al. (2001) applied multi-stage loading on unbound granular material, and found that the permanent strain increased significantly when the deviator stress exceeded the past maximum value. Based on the results obtained, Gidel et al. (2001) developed a model of permanent strain, accounting for both *N* and stress state. To investigate the effect of water content on permanent strain of fouled ballast, Trinh et al. (2012) performed multi-stage loading cyclic tests at various water contents. Based on the results obtained, a fatigue model considering the effects of water content, *N* and stress state was developed. More recently, Jing et al. (2018) proposed an approach to describe the permanent strain of granular materials in low-traffic pavements, taking the effects of fine content, water content, *N* and stress state into account. To the authors' knowledge, for the interlayer soil of railway substructure, the effect of coarse grain content f_v on permanent strain has not been taken into account.

This study aims at developing a model of permanent strain for interlayer soil, accounting for the effects of number of loading cycles N, stress state and coarse grains content f_v. Firstly, based on the multi-stage loading cyclic test results obtained by Wang et al. (2018c), a general form of the model accounting for N, Δq_{max} and f_v was proposed. The model parameters were determined based on a part of cyclic tests from Wang et al. (2018c). In order to evaluate the performance of the proposed model, other tests were simulated using the parameters determined previously. The advantage and limitation of the model were also discussed.

Modelling of permanent strain

Review of multi-stage loading cyclic tests

Multi-stage loading cyclic tests were conducted on interlayer soil by Wang et al. (2018c). A material simulating the interlayer soil was reconstituted by mixing fines with micro-ballast at six different f_v values (0%, 5%, 10%, 20%, 35% and 45%). The samples were prepared by dynamic compaction by keeping the fine soils inside the mixture at optimum water content $w_{opt\text{-}f}$ = 13.7% and maximum dry density $\rho_{dmax\text{-}f}$ = 1.82 Mg/m^3, so that the suction developed inside the fines was expected to be similar for all samples. The effect of coarse grain content f_v on permanent strain was investigated through cyclic triaxial tests and the results are shown in Fig. 1, with five different maximum deviator stress Δq_{max} values (10 kPa, 15 kPa, 20 kPa, 25 kPa and 30 kPa) and 90000 loading cycles for each Δq_{max}. It appears that the permanent strain increased with the increasing loading cycles N and tended to stabilize at the end of each loading stage for a given f_v value.

To visualize the soil fabric with different f_v values, X-ray µCT scans were performed on as-compacted samples at six different f_v values (Fig. 2). It is observed that with the increase of f_v from 0% to 10%, the soil fabric was dominated by the fine soils, with coarse grains floating in it. At f_v = 20%, the contacts between aggregates started to develop, forming local coarse grain skeletons by location. On the contrary, at f_v = 35% and 45%, the coarse grains were in contact with each other, forming a global fabric of grain skeleton with fine soils situated among grains. Thus, with the increase of f_v from 0% to 45%, the soil fabric varies from a fine soils dominated structure to a coarse grain dominated structure.

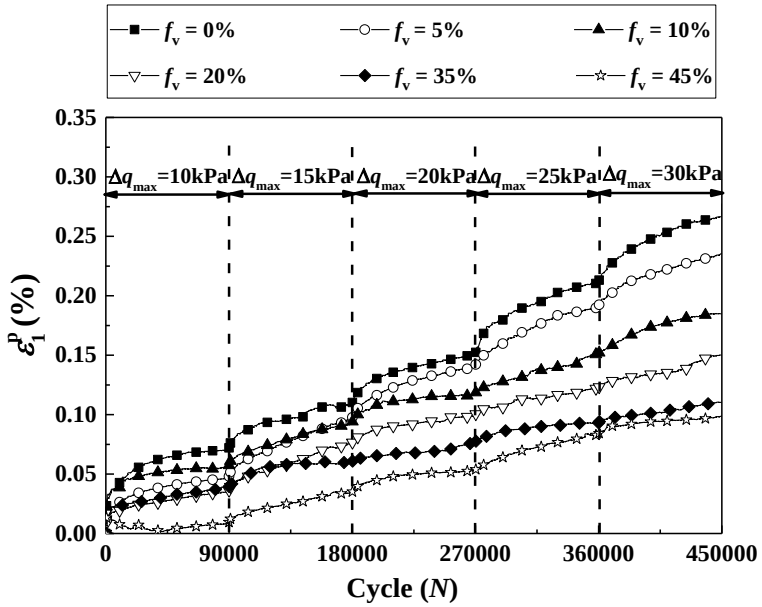

Fig. 1. Variations of permanent strain with the number of loading cycles N at different f_v and Δq_{max} values (after Wang et al. 2018c)

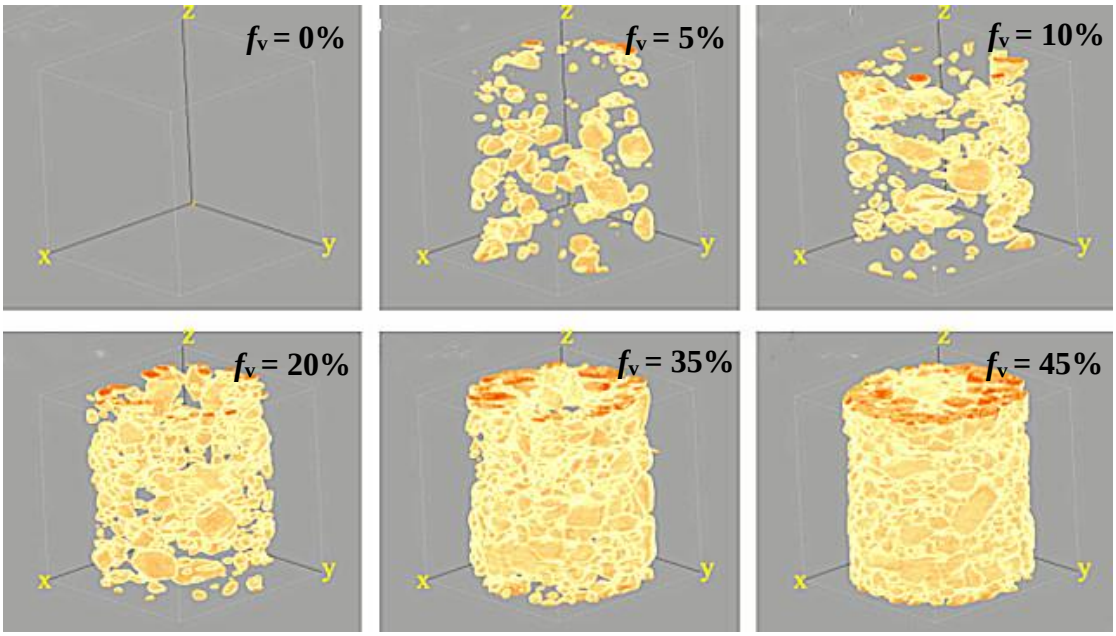

Fig. 2. 3D views of the coarse grain distributions in compacted samples (after Wang et al. 2018c)

Table 1. Fatigue models accounting for the effect of different factors on permanent strain reported in literatures

Reference	Variable	Fatigue model
Hornych (1993)	1) N	$\varepsilon_1^p = f(N) = A \cdot [1 - (\frac{N}{100})^{-B}])$
Gidel et al. (2001)	1) N 2) $\Delta q_{\max}$	$\varepsilon_1^p = g(\Delta p_{max}, \Delta q_{max}) \cdot h(N)$ $= g(\Delta p_{max}, \Delta q_{max}) \cdot a \cdot \left[1 - \left(\frac{N}{100}\right)^{-B}\right]$ $g(\Delta p_{max}, \Delta q_{max}) = \varepsilon_1^{p_0} (\frac{l_{max}}{p_a})^n \frac{1}{(m + \frac{s}{\Delta p_{max}} - \frac{\Delta q_{max}}{\Delta p_{max}})}$
Trinh et al. (2012)	1) N 2) $\Delta q_{\max}$ 3) w	$\varepsilon_1^p = t(w, \Delta q_{max}) \cdot h(N)$ $= t(w, \Delta q_{max}) \cdot a \cdot [1 - (\frac{N}{100})^{-B}]$ $t(w, \Delta q_{max}) = \varepsilon_1^{p_0} \cdot (w + a_1) \cdot (\frac{\Delta q_{max}}{p_a})^{\alpha}$

Development of a fatigue model

Table 1 shows three widely applied fatigue models, with N by Hornych (1993), with N and Δq_{max} by Gidel et al. (2001), with N and Δq_{max} and w by Trinh et al. (2012), allowing the assessment of permanent strain produced under the effect of different variables. As this study focuses on the modelling of the effect of f_v on permanent strain based on the cyclic test results obtained by Wang et al. (2018c) under constant water content condition, the effect of water content was not taken into account. Data from cyclic tests with different f_v values and w values are needed to generalize the study to water content effect. Most likely, the coupled effects of f_v w should be considered in that case. Table 1 shows that the effects of N and other variables are separated to different terms (Gidel et al. 2001; Trinh et al. 2012). Similarly, in this study, the proposed function k (f_v, Δq_{max}) is a term related to the effects of f_v and $\Delta q_{\max}$, while h (N) is a term related to N. The general form of this model is established as follows:

$$\varepsilon_1^p(f_v, \Delta q_{max}, N) = k(f_v, \Delta q_{max}) \cdot h(N) \quad (1)$$

where ε_1^p is the permanent strain, $\Delta q_{\max}$ is the deviator stress level.

To develop the model, the first step is to determine the form of $h(N)$. Adopting the fatigue model *f* (*N*) proposed by Hornych (1993) for this purpose (Eq. (2)):

$$f(N) = \varepsilon_1^{p*}(N) = \varepsilon_1^{p}(N) - \varepsilon_1^{p}(100) = A \cdot [1 - (\frac{N}{100})^{-B}] \quad \text{(for } N > 100 \text{ cycles)} \quad (2)$$

where ε_1^{p*} is the permanent strain after 100 cycles, parameter *A* represents the final stabilized maximum permanent strain, parameter *B* controls the evolution of permanent strain with increasing loading cycles *N*.

In order to consider the effect of $\Delta q_{\max}$, Eq. (2) is modified to Eq. (3). This modification is motivated by the change of physical meaning of parameter *A* while accounting for $\Delta q_{\max}$. As shown in Table 1, in the model of Hornych (1993), parameter *A* represents the stabilized maximum permanent strain. However, in the model considering *N* and $\Delta q_{\max}$ (Gidel et al. (2001), Trinh et al. (2012)), parameter a is used. The value of this parameter is close to '1' (a = 1.32 in Gidel et al. (2001); a = 0.76 in Trinh et al. (2012)) and it definitely does not represent the maximum permanent strain.

$$h(N) = a \cdot [1 - (\frac{N}{100})^{-B}] \quad \text{(for } N > 100 \text{ cycles)} \quad (3)$$

where *B* is a parameter.

After substituting Eq. (3) into Eq. (1), the fatigue model $\varepsilon_1^p(f_v, \Delta q_{max}, N)$ reads:

$$\varepsilon_1^p(f_v, \Delta q_{max}, N) = k(f_v, \Delta q_{max}) \cdot a \cdot [1 - (\frac{N}{100})^{-B}] \text{ (for } N > 100 \text{ cycles)} \quad (4)$$

Comparison between Eq. (4) and Eq. (2) shows that parameter '*A*' in Eq. (2) corresponds to '$k(f_v, \Delta q_{max}) \cdot a$' in Eq. (4). Since parameter 'a' is close to unity, the physical meaning is the same for '$k(f_v, \Delta q_{max})$' and parameter '*A*'. Different from '*A*' representing the maximum permanent strain (end-stage permanent strain), '$k(f_v, \Delta q_{max})$' represents the end-stage permanent strains at various loading levels Δq_{max} for each f_v..

Prior to determining the form of $k(f_v, \Delta q_{max})$in Eq. (4), the effects of coarse grain content f_v and deviator stress $\Delta q_{\max}$ on permanent strain need to be clarified. Fig. 3 shows the variations of end-stage permanent strain ε_1^p as a function of coarse grain content f_v for different $\Delta q_{\max}$ values. Note that the end-stage permanent strain ε_1^p was determined by a method proposed by Gidel et al. (2001), which was later applied by Lamas-Lopez (2016) and Wang et al. (2018c).

The details of determination of that could be found in Wang et al. (2018c). It is worth noting that, based on the results obtained by this method, the value of end-stage permanent strain ε_1^p corresponds to that of maximum permanent strain at a given f_v and Δq_{max} values (Figure 3). It appears that a polynomial expression can be used to well describe their relationship. Fig.4 depicts the variations of the end-stage permanent strain ε_1^p with Δq_{max}. Interestingly, a linear relationship is identified for all f_v values. Thus, the expression of $k(f_v, \Delta q_{max})$ can be formulated as follows:

$$k(f_v, \Delta q_{max}) = \varepsilon_1^{p_0} \cdot [f_v^2 + b f_v + c] \cdot (\frac{\Delta q_{max}}{P_a} + d) \tag{5}$$

where $\varepsilon_1^{p_0}$, b, c, d are parameters, and P_a is atmospheric pressure, taken equal to 100 kPa.

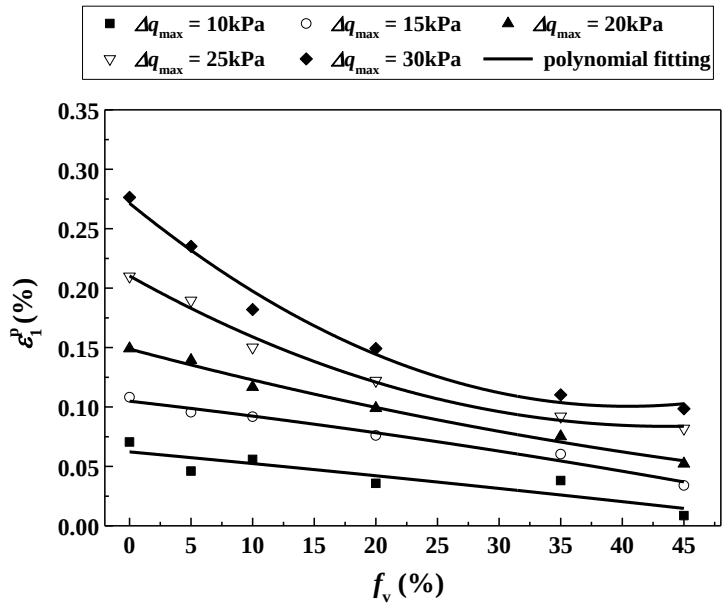

Fig. 3. Polynomial fitting of end-stage permanent strain ε_1^p with f_v at different Δq_{max} values (after Wang et al. 2018c)

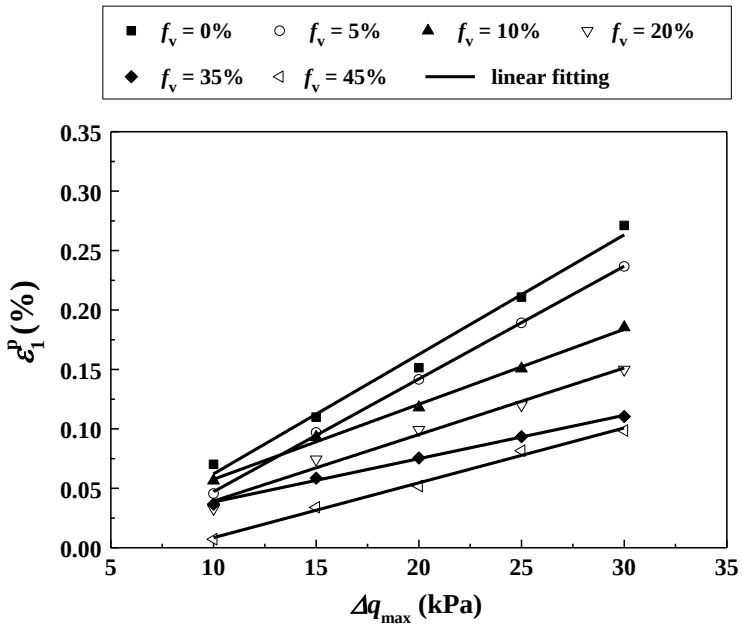

Fig. 4. Linear fitting of end-stage permanent strain ε_1^p with Δq_{max} at different f_v values

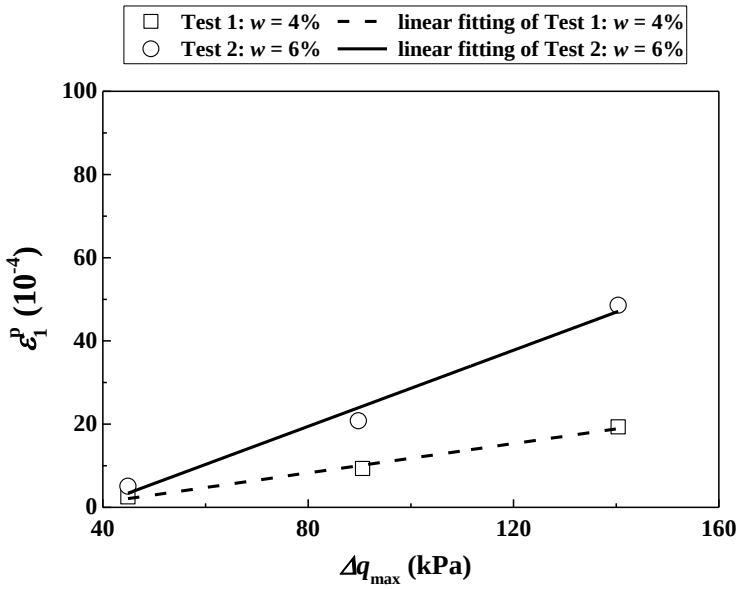

Fig. 5. Linear fitting of end-stage permanent strain ε_1^p with Δq_{max} at unsaturated water contents (after Trinh et al. 2012)

In the model proposed by Trinh et al. (2012) (Table 1), a power relation was adopted to relate the end-stage permanent strain to Δq_{max} at various water contents as follows:

$$t(w, \Delta q_{max}) = \varepsilon_1^{p_0} \cdot (w + a_1) \cdot \left(\frac{\Delta q_{max}}{P_a}\right)^{\alpha} \quad (6)$$

where $\varepsilon_1^{p_0}$, a_1 and α are parameters, and $P_a = 100$ kPa.

A power relationship was obtained by Trinh et al. (2012) between the end-stage permanent strain ε_1^p and Δq_{max} for three different water contents w = 4%, 6% and 12% (corresponding to S_r = 32%, 48% and 100%, respectively). In the case of constant water content considered in this study ($w_{opt\text{-}f}$ = 13.7%), a linear relationship is obtained with α = 1. Further examination reveals that the linear relationship is also valid when the soil is unsaturated (w = 4% and 6%) in the case of Trinh et al. (2012), as shown in Fig. 5.

After substituting Eq. (5) into Eq. (4), the fatigue model $\varepsilon_1^p(f_v, \Delta q_{max}, N)$ accounting for the effect of coarse grain content f_v, maximum deviator stress Δq_{max} and the number of loading cycles N is obtained:

$$\varepsilon_1^p(f_v, \Delta q_{max}, N) = \varepsilon_1^{p_0} \cdot [f_v^2 + b f_v + c] \cdot \left(\frac{\Delta q_{max}}{P_a} + d\right) \cdot a \cdot \left[1 - \left(\frac{N}{100}\right)^{-B}\right] \quad \text{(for } N > 100 \text{ cycles)} \quad (7)$$

where $\varepsilon_1^{p_0}$, b, c, d, a and B are parameters, and P_a=100 kPa.

Determination of model parameters

Wang et al. (2018c) investigated the effect of coarse grain content f_v on permanent strain with six different f_v values (0%, 5%, 10%, 20%, 35% and 45%). The measured data from the tests at f_v = 0%, 5%, 35% are used to determine the model parameters, with the following two steps:

The first step is to determine four parameters $\varepsilon_1^{p_0}$, b, c and d by fitting Eq. (5) to the end-stage permanent strains ε_1^p at f_v = 0%, 5%, 35%, as shown in Fig. 6. The values obtained are $\varepsilon_1^{p_0}$= 2.40, b = -1.03, c = 0.45, d = -0.05.

The second step is to determine parameters a and B by fitting Eq. (7) to the measured data at f_v = 0%, 5%, 35%. The parameters obtained are a = 1.20, B = 0.22.

Fig. 7 presents a comparison between the fitting curves and the measured data at f_v = 0%, 5%, 35%. It appears that the proposed fatigue model can well fit the experimental data. Moreover, better fitting can be obtained when the permanent strain stabilizes at the ends of loading stages.

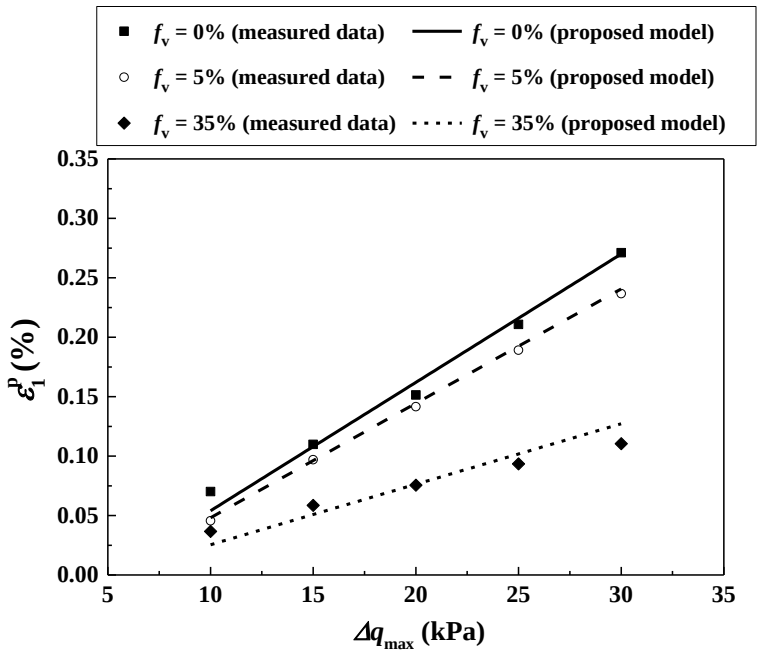

Fig. 6. Linear fitting of end-stage permanent strain ε_1^p with Δq_{max} using expression $t(f_v, \Delta q_{max})$ at f_v = 0%, 5% and 35%

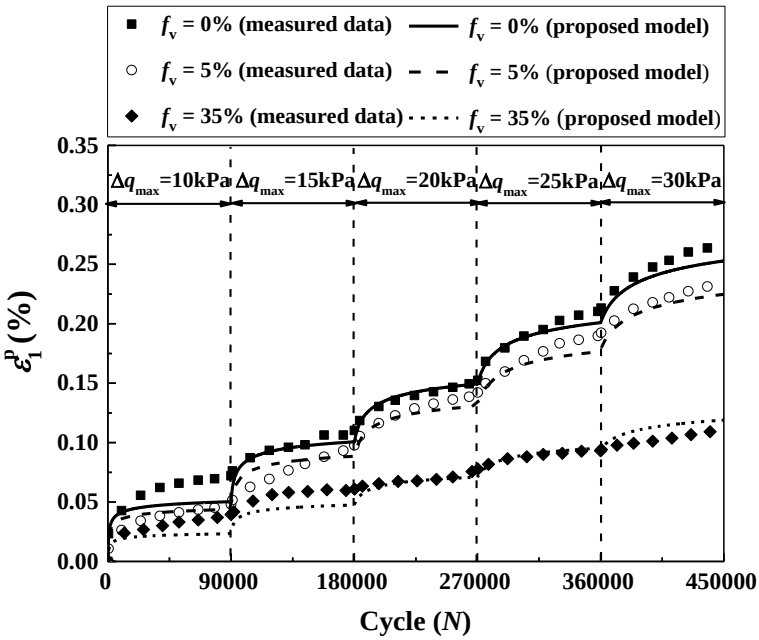

Fig. 7. Determination of parameters by fitting cyclic test results at f_v = 0%, 5% and 35%

After determining the model parameters, a sensitivity analysis of all parameters is performed based on the results from the multi-stage loading cyclic test at f_v = 5% (Wang et al. 2018c), and the results are shown in Fig. 8 and Fig. 9.

Since $k(f_v, \Delta q_{max})$ controls the end-stage permanent strain, the effects of parameters $\varepsilon_1^{p_0}$, *b*, *c* and *d* on permanent strain curve are explained separately in Fig. 8. Fig. 8a shows that the increase of $\varepsilon_1^{p_0}$ leads to larger increase of end-stage permanent strain, suggesting that parameter $\varepsilon_1^{p_0}$ controls the amplitude of permanent strain curve. The effect of f_v on permanent strain is reflected through parameters *b* and *c*. It can be observed that with the increase of parameter *b*, the amplitude of permanent strain curve changes slightly (Fig. 8b). In addition, Fig. 8c shows that the increase of parameter *c* gives rise to an increase of permanent strain, suggesting that parameter *c* controls the effect of f_v through the amplitude of permanent strain curve. Fig. 8d shows that the increase of parameter *d* results in parallel movement of permanent strain curve, indicating that parameter *d* mainly controls the interception of permanent strain curve.

Parameters a and *B* in *h* (*N*) expression affect the evolution of permanent strain with loading cycles *N*. It can be observed in Fig. 9a that the larger the value of parameter *B*, the larger the increase of permanent strain rate and the smaller the loading cycles *N* needed for permanent strain stabilization. Therefore, parameter *B* governs the evolution of permanent strain with increasing loading cycles *N*, which is consistent with previous studies (Hornych 1993; Gidel et al. 2001; Trinh et al. 2012; Jing et al. 2018). In addition, parameter a affects the amplitude of permanent strain (Fig. 9b), with its value being around unity (i.e., a = 1.32 in Gidel et al. (2001); a = 0.76 in Trinh et al. (2012); a = 1.20 in the present study).

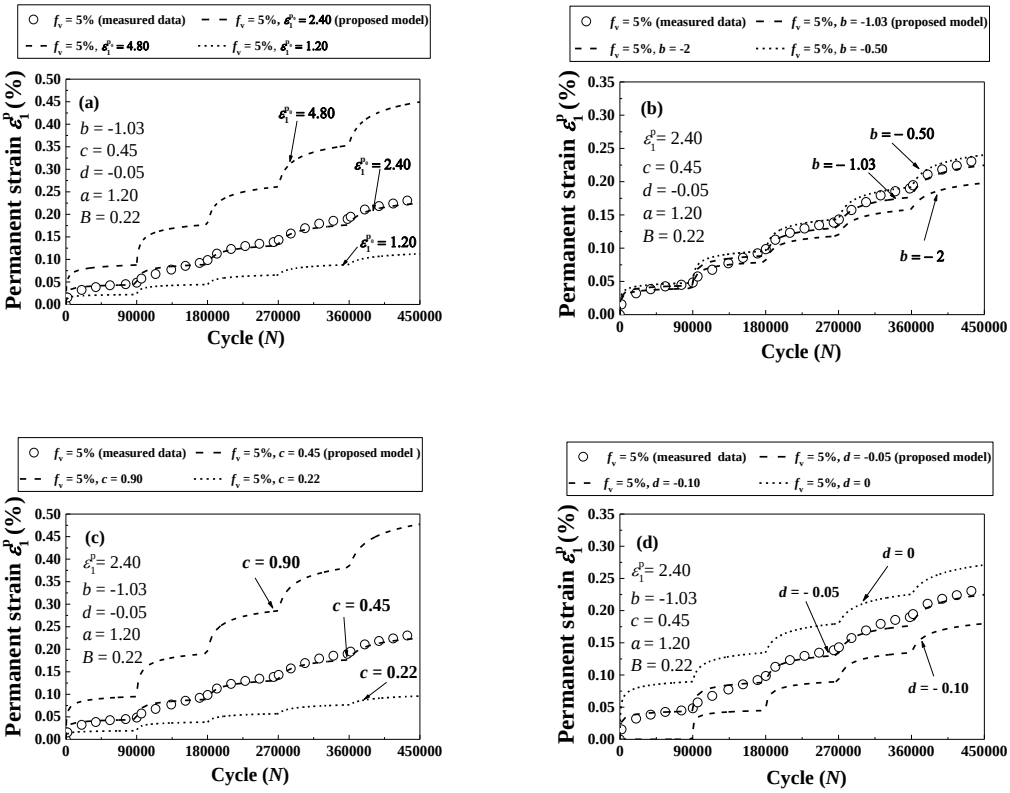

Fig. 8. Effects of parameters $\varepsilon_1^{p_0}$, b, c and d in $t(f_v, \Delta q_{max})$ on permanent strain curve: (a) parameter $\varepsilon_1^{p_0}$; (b) parameter b; (c) parameter c; (d) parameter d

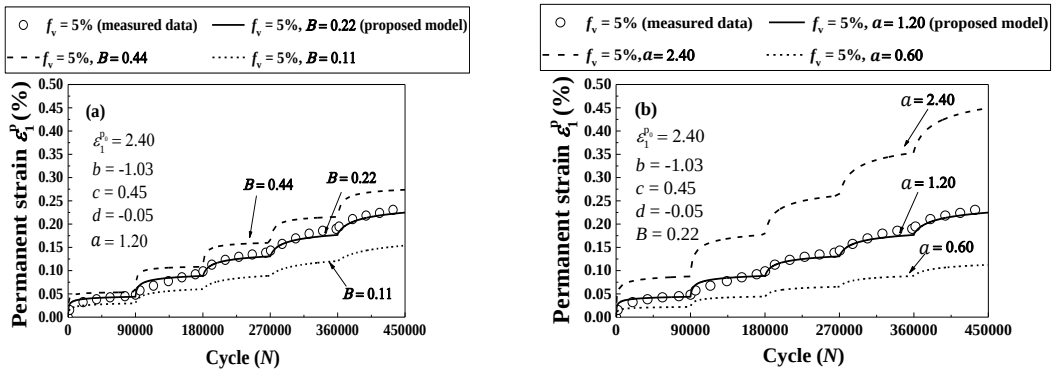

Fig. 9. Effects of parameters a and B in h (N) on the evolution of permanent strain with loading cycles N: (a) parameter B; (b) parameter a

Model validation

In order to evaluate the performance of the proposed fatigue model, the data from the multi-stage loading cyclic tests at f_v = 10%, 20% and 45% are simulated. The model parameters determined previously based on the results at f_v = 0%, 5%, 35% are used for this purpose. Fig. 10 presents a comparison between the measured data and the corresponding simulated ones. It appears clearly that the parameters determined with f_v = 0%, 5% and 35% enable satisfactory simulations of the tests at f_v = 10%, 20% and 45%, with the coefficients of determination R^2 above 0.94 at various f_v values, as shown in Table 2.

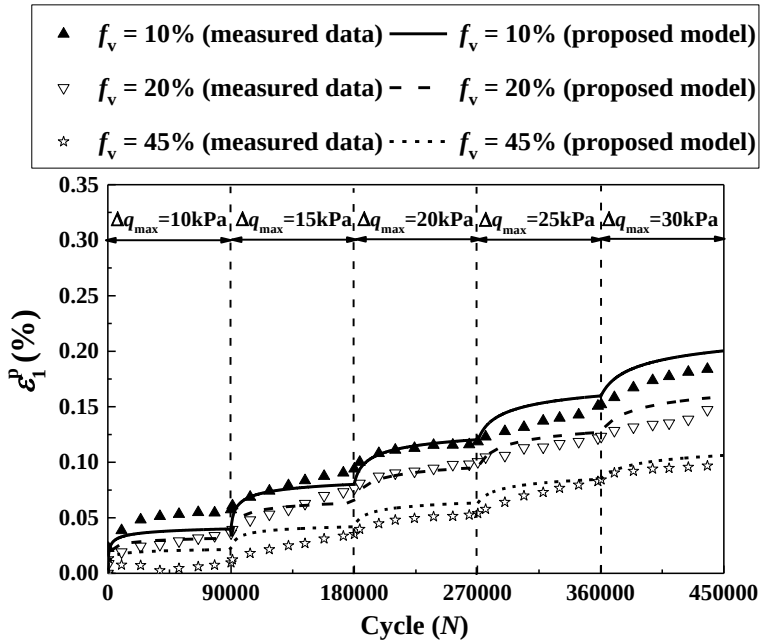

Fig. 10. Simulations of the cyclic test results by the proposed model for f_v = 10%, 20% and 45%

Table 2. Coefficients of determination R^2 of cyclic test results at various f_v values

f_v	0%	5%	10%	20%	35%	45%
R^2	0.95	0.97	0.94	0.97	0.94	0.94

Discussion of the proposed fatigue model

The relation of f_v with parameters b and c

As shown in Eq. (5), the effect of f_v on the end-stage permanent strain is reflected through parameters b and c. Based on the determined parameters $\varepsilon_1^{p_0}$ and d, it can be observed from Fig. 11 that the end-stage permanent strain $\bar{\varepsilon}_1^p$ decreases with the increasing f_v at different Δq_{max} values. In order to investigate the relation of f_v with parameters b and c, the effect of Δq_{max} on the end-stage permanent strain ε_1^p is eliminated as follows:

$$\bar{\varepsilon}_1^p = \frac{k(f_v,\Delta q_{max})}{\varepsilon_1^{p_0}\cdot(\frac{\Delta q_{max}}{P_a}+d)} = f_v^2 + bf_v + c \tag{8}$$

The variation of $\bar{\varepsilon}_1^p$ with f_v follows a polynomial relationship. When $f_v = 0$,

$$c = \bar{\varepsilon}_1^p \tag{9}$$

Thus, parameter c represents the end-stage permanent strain $\bar{\varepsilon}_1^p$ at $f_v = 0$.

The changing trend of $\bar{\varepsilon}_1^p$ with f_v can be determined from Eq. (8):

$$\frac{\partial \bar{\varepsilon}_1^p}{\partial f_v} = 2f_v + b \tag{10}$$

Eq. (10) indicates that when the change of permanent strain $\bar{\varepsilon}_1^p$ with f_v becomes zero; i.e. $\frac{\partial \bar{\varepsilon}_1^p}{\partial f_v} = 0$,

$$b = -2f_v \tag{11}$$

Considering that f_v can vary from 0 to 100%, parameter b ranges from 0 to -2.

Based on the aforementioned determined parameters b and c, Eq. (12) can be obtained by substituting these values into Eq. (8):

$$\bar{\varepsilon}_1^p = f_v^2 - 1.03f_v + 0.45 \tag{12}$$

It can be observed from Fig. 11 that the determined parameters allow a reasonable description of the variation of end-stage permanent strain $\bar{\varepsilon}_1^p$ with f_v at different Δq_{max} values. The main

discrepancy appears at Δq_{max} = 10 kPa, which is consistent with the observation shown in Fig. 7 and Fig. 10.

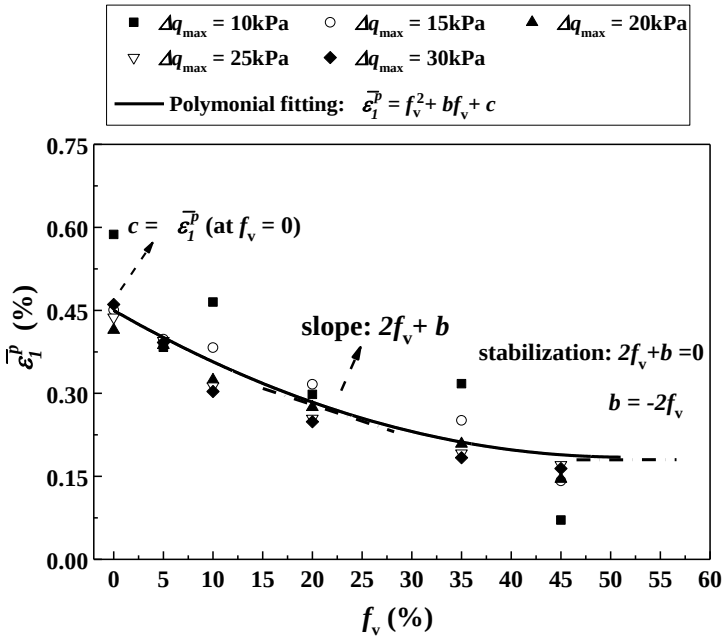

Fig. 11. Variations of end-stage permanent strain $\bar{\varepsilon}_1^p$ with coarse grain content f_v

Interpretation of permanent strain behaviors by shakedown theory

In terms of permanent strain behaviors, three categories are defined in shakedown theory (Werkmeister et al. 2001, 2004; Song et al. 2010): category A (plastic shakedown) characterized by stabilized permanent strain with loading cycles *N*, category B (plastic creep) characterized by failure at a large *N*, and category C (incremental collapse) characterized by failure at a small *N*. The criterion to classify the three categories is dependent on the accumulated permanent strain. Following the French standard AFNOR (2004), the limit of category A is reached when $\varepsilon_{1\,5000}^p - \varepsilon_{1\,3000}^p > 0.45 \times 10^{-4}$, where $\varepsilon_{1\,5000}^p$ and $\varepsilon_{1\,3000}^p$ are accumulated permanent strains at *N* = 5000 and 3000, respectively. In all the tests conducted by Wang et al. (2018c), the maximum difference between $\varepsilon_{1\,5000}^p$ and $\varepsilon_{1\,3000}^p$ occurs at f_v = 0% and Δq_{max} = 30 kPa, equal to 0.3×10^{-4}, smaller than the plastic shakedown limit. Thus, the response of all tests considered is within category A. Fig. 10 shows that the proposed fatigue model is relevant to describe the permanent strain behavior for category A. This confirms the assumption made by Hornych (1993) in their model that the permanent strain reaches a finite limit as loading cycles *N* tends toward infinite.

Conclusions

In order to model the effect of f_v on permanent strain of interlayer soil, a fatigue model $\varepsilon_1^p(f_v, \Delta q_{max}, N)$ was developed based on the results from multi-stage loading cyclic tests conducted by Wang et al. (2018c), at six different f_v values (0%, 5%, 10%, 20%, 35% and 45%) and five different Δq_{max} values (10 kPa, 15 kPa, 20 kPa, 25 kPa and 30 kPa), with 90000 loading cycles for each Δq_{max}. The proposed fatigue model accounts for the effects of coarse grain content f_v, maximum deviator stress Δq_{max} and loading cycles N on permanent strain. The model parameters were determined by fitting the cyclic tests at f_v = 0%, 5% and 35%, and then used to simulate the tests at f_v = 10%, 20% and 45%. A good agreement was obtained between the measurements and simulations, showing the performance of the proposed fatigue model for predicting permanent strain.

It is worth noting that the proposed model is valid when the permanent strain stabilizes at a certain number of cycles N. In other words, it can only describe the permanent strain of category A (plastic shakedown). Moreover, the fatigue model $\varepsilon_1^p(f_v, \Delta q_{max}, N)$ has not taken the effect of water content into account. Further experimental data are needed to take this effect into consideration.

Acknowledgements

This work was supported by the China Scholarship Council (CSC) and Ecole des Ponts ParisTech.

References

AFNOR, 1995. NF P98-235-1—Test relating to pavements. Unbound granular materials. Part 1: Repeated Loading Triaxial Test.

AFNOR, 2004, NF EN 13286-7—Unbound and Hydraulically Bound Mixtures. Part 7: Cyclic Load Triaxial Test for Unbound Mixtures.

Barksdale, R. D. 1972. Laboratory evaluation of rutting in base course materials. In Presented at the Third International Conference on the Structural Design of Asphalt Pavements, Grosvenor House, Park Lane, London, England, Sept. 11-15, 1972. (Vol. 1, No. Proceeding).

Cui, Y. J., Duong, T. V., Tang, A. M., Dupla, J. C., Calon, N., & Robinet, A. 2013. Investigation of the hydro-mechanical behaviour of fouled ballast. Journal of Zhejiang University Science A, 14(4), 244-255.

Duong, T. V., Tang, A. M., Cui, Y. J., Trinh, V. N., Dupla, J. C., Calon, N., ... & Robinet, A. 2013. Effects of fines and water contents on the mechanical behavior of interlayer soil in ancient railway sub-structure. Soils and foundations, 53(6), 868-878.

Duong, T. V., Cui, Y. J., Tang, A. M., Dupla, J. C., Canou, J., Calon, N., & Robinet, A. 2014. Investigating the mud pumping and interlayer creation phenomena in railway sub-structure. Engineering Geology, 171, 45-58.

Duong, T. V., Cui, Y. J., Tang, A. M., Dupla, J. C., Canou, J., Calon, N., & Robinet, A. 2016. Effects of water and fines contents on the resilient modulus of the interlayer soil of railway substructure. Acta Geotechnica, 11(1), 51-59.

Gidel, G., Hornych, P., Breysse, D., & Denis, A. 2001. A new approach for investigating the permanent deformation behaviour of unbound granular material using the repeated loading triaxial apparatus. Bulletin des laboratoires des Ponts et Chaussées, (233).

Hornych, P. 1993. Étude des déformations permanentes sous chargements répétés de trois graves non traitées. Bulletin de liaison des Laboratoires des Ponts et Chaussées, (184).

Jing, P., Nowamooz, H., & Chazallon, C. 2018. Permanent deformation behaviour of a granular material used in low-traffic pavements. Road Materials and Pavement Design, 19(2), 289-314.

Lamas-Lopez, F., d'Aguiar, S. C., Robinet, A., Cui, Y. J., Calon, N., Canou, J., ... & Tang, A. M. 2015. In-situ investigation of the behaviour of a French conventional railway platform. Proc., Transportation Research Board TRB 2015.

Lamas-Lopez, F. 2016. Field and laboratory investigation on the dynamic behaviour of conventional railway track-bed materials in the context of traffic upgrade (Doctoral dissertation, Paris Est).

Sweere, G.T.H., 1990. Unbound Granular Bases for Roads. PhD Thesis. Delft, Netherlands.

Song, Y., & Ooi, P. S. 2010. Interpretation of shakedown limit from multistage permanent deformation tests. Transportation research record, 2167(1), 72-82.

Trinh, V. N. 2011. Comportement hydromécanique des matériaux constitutifs de plateformes ferroviaires anciennes. PhD Thesis, Ecole Nationale des Ponts et Chaussées, Université Paris-Est.

Trinh, V. N., Tang, A. M., Cui, Y. J., Dupla, J. C., Canou, J., Calon, N., ... & Schoen, O. 2012. Mechanical characterisation of the fouled ballast in ancient railway track substructure by large-scale triaxial tests. Soils and foundations, 52(3), 511-523.

Werkmeister, S., Dawson, A. R., & Wellner, F. 2001. Permanent deformation behavior of granular materials and the shakedown concept. Transportation Research Record, 1757(1), 75-81.

Werkmeister, S., Dawson, A. R., & Wellner, F. 2004. Pavement design model for unbound granular materials. Journal of Transportation Engineering, 130(5), 665-674.

Wang, H. L., Chen, R. P., Qi, S., Cheng, W., & Cui, Y. J. 2018. Long-term performance of pile-supported ballastless track-bed at various water levels. Journal of Geotechnical and Geoenvironmental Engineering, 144(6), 04018035.

Wang, H. L., Cui, Y. J., Lamas-Lopez, F., Calon, N., Saussine, G., Dupla, J. C., ... & Chen, R. P. 2018. Investigation on the mechanical behavior of track-bed materials at various contents of coarse grains. Construction and Building Materials, 164, 228-237.

Wang, H. L., Cui, Y. J., Lamas-Lopez, F., Dupla, J. C., Canou, J., Calon, N., ... & Chen, R. P. 2018. Permanent deformation of track-bed materials at various inclusion contents under large number of loading cycles. Journal of Geotechnical and Geoenvironmental Engineering, 144(8), 04018044.

Su, Y., Cui, Y. J., Dupla, J. C., Canou, J., & Duan, S. Q. 2021. Submitted to Canadian Geotechnical Journal.

A fatigue model for fine/coarse soil mixture accounting for the effects of coarse grain content and suction by incorporating soil-water retention curve

Yu Su[1], Yu-Jun Cui[1], Jean-Claude Dupla[1], Jean Canou[1], Shu-Qian Duan[1,2]

Abstract: Experimental observations showed that the permanent strain ε_1^p of fine/coarse soil mixture was significantly affected by the number of loading cycles *N*, deviator stress σ_d, coarse grain content f_v and matric suction ψ. In this study, a fatigue model incorporating soil-water retention curve was developed, allowing the combined effects of *N*, σ_d, f_v and ψ on ε_1^p to be accounted for. Several studies were selected from literature to verify the proposed model. The model parameters were determined by fitting the variations of ε_1^p with *N*, σ_d, f_v and ψ under saturated condition, and then adopted to predict the results under unsaturated condition. A good agreement was obtained between the model predictions and the experimental results, showing the performance of the proposed model in describing the variations of ε_1^p with *N*, σ_d, f_v and ψ in the case of plastic shakedown. Comparisons with three representative existing models showed that the proposed model incorporating ψ provides better predictions of ε_1^p than the existing models considering the water content, for both the case of constant dry density of fine soil fraction $\rho_{d\text{-}f}$ and the case of constant dry density of mixture ρ_d. This was explained as follows: for the latter case, keeping the ρ_d constant, an increasing f_v induced a decreasing $\rho_{d\text{-}f}$ and hence a decrease of ψ. For both cases, the effect of $\rho_{d\text{-}f}$ on ε_1^p was rather reflected by ψ than by water content.

Keywords: fine/coarse soil mixture; fatigue model; permanent strain; coarse grain content; matric suction; soil-water retention curve

Introduction

An interlayer soil was identified in the French conventional rail tracks, corresponding to a mixture of fine soil and coarse grains. Wang et al. (2018) studied the effect of coarse grain content f_v (the ratio of the volume of coarse grain to that of mixture) on permanent strain of such mixture by cyclic tests under a constant optimum moisture content of fine soil fraction $w_{opt\text{-}f}$, and found that an increase of f_v led to a decrease of permanent strain. Su et al. (2021a) also reported that an increasing f_v induced a decrease of permanent strain under both unsaturated and saturated conditions. On the contrary, Duong et al. (2013) found that an increase of f_v induced a decrease of permanent strain under saturated condition, while an opposite trend was

[1]Ecole des Ponts ParisTech, Laboratoire Navier/CERMES, 6 – 8 av. Blaise Pascal, Cité Descartes, Champs-sur-Marne, 77455 Marne – la – Vallée cedex 2, France
[2]Zhengzhou University, School of Civil Engineering, Zhengzhou, Henan 450001, China

found under unsaturated condition. This is because that Duong et al. (2013) controlled the global dry density of mixture ρ_d with varying f_v, inducing a varying dry density of fine soil fraction $\rho_{d\text{-}f}$ and thus a varying suction ψ, while Wang et al. (2018) and Su et al. (2021a) kept a constant $\rho_{d\text{-}f}$ with varying f_v, which resulted in a constant ψ at a given water content. In a general case, both f_v and ψ affected the permanent strain of fine/coarse soil mixture. From a practical point of view, it appears essential to develop a model of permanent strain for such mixtures, accounting for the combined effects of f_v and ψ.

Numerous studies reported that the permanent strain of soil mixture was mainly affected by the number of loading cycles N, stress state, coarse grain content f_v and suction ψ (or water content) (Li and Selig 1996; Puppala et al. 2005; Song and Ooi 2010; Gabr and Cameron 2013; Chen et al. 2019; Su et al. 2020a; Qi et al. 2020). Based on the experimental results, various empirical models were proposed to describe the variations of permanent strain with changes in either the loading cyles N (Barksdale 1972; Sweere 1990; Hornych et al. 1993), or the stress state (Shenton 1974; Lekarp and Dawson 1998). Gidel et al. (2001) studied the effects of N and stress level on the permanent strain of unbound granular material by multi-stage loading cyclic tests, and found that when the applied deviator stress σ_d exceeded the past maximum value, the permanent strain increased notably. Based on the experimental results, they developed a model of permanent strain under the combined effects of N and stress states. Wang et al. (2018) studied the effect of f_v on the permanent strain of fine/coarse soil mixture by multi-stage loading cyclic tests. They identified a characteristic coarse grain content $f_{v\text{-}cha}$, below which the permanent strain decreased quickly with increasing f_v, while beyond which the permanent strain decreased slowly. Su et al. (2020b) proposed a model describing such f_v effect. Trinh et al. (2012) studied the effect of water content on permanent strain of interlayer soil by large-scale cyclic triaxial tests and found that an increase of water content induced an increasing permanent strain. Based on the experimental results, they proposed a model allowing the effects of N, σ_d, and w to be accounted for. Azam et al. (2015) investigated the effects of water content and suction on the permanent strain of a mixture of clay masonry and concrete aggregate, and proposed different models for describing the variations of permanent strain with water content and suction, respectively. Jing et al. (2018) studied the effects of water content and fine soil content on the permanent strain of granular materials, and found that an increase of fine soil content led to an increasing permanent strain under saturated condition, but a decreasing permanent strain under unsaturated condition due to the contribution of suction. They proposed a model by substituting the effects of fine soil content and water content on permanent strain with that of suction.

However, the use of suction cannot fully reflect the effect of fine soil content (or coarse grain content) on permanent strain, in particular under saturated condition where suction is theoretically null when the osmotic suction is ignored. This indicated that both the effect of coarse grain content and that of matric suction should be accounted for. To date, no model has been proposed for describing the variations of permanent strain of soil mixture with changes in the number of loading cycles N, deviator stress σ_d, coarse grain content f_v and matric suction ψ.

In this study, based on the model proposed by Su et al. (2020b), a new fatigue model incorporating soil-water retention curve (SWRC) was developed. This model was validated using experimental data from literature, which included the authors' own data. A comparison between the proposed model and some representative existing models was made, allowing the performance of proposed model to be revealed in describing the variations of ε_1^p with N, σ_d, f_v and ψ.

Modelling background

Some investigators proposed empirical models for the description of ε_1^p variation with change in the number of loading cycles N. For instance, Hornych et al. (1993) studied the effect of N on ε_1^p for unbound granular materials, and proposed Eq. (1) for describing the variation of ε_1^p with N:

$$\varepsilon_1^p = f(N) = A \cdot [1 - (\frac{N}{100})^{-B}] \quad (1)$$

where A and B are model parameters. Eq. (1) has been commonly used to describe the effect of N on ε_1^p. This equation was also adopted in French standard (AFNOR 1995).

Gidel et al. (2001) studied the effects of N and stress state on ε_1^p for unbound granular materials, and extended Eq. (1) to the effect of stress state:

$$\varepsilon_1^p = g(p_{\max}, \sigma_d) \cdot a_1 \cdot \left[1 - \left(\frac{N}{100}\right)^{-B}\right] \quad (2)$$

with

$$g(p_{\max}, \sigma_d) = \varepsilon_1^{p_1} (\frac{l_{\max}}{p_a})^{n_1} \frac{1}{(m_1 + \frac{s_1}{p_{\max}} - \frac{\sigma_d}{p_{\max}})} \quad (3)$$

where $p_{\max} = (\sigma_1 + \sigma_2 + \sigma_3)/3$, σ_1, σ_2 and σ_3 are the three principal stresses; $l_{\max} = \sqrt{p_{\max}^2 + \sigma_d^2}$; $\varepsilon_1^{p_1}$, n_1, m_1, s_1, a_1 and B are model parameters; p_a is the atmospheric pressure.

Su et al. (2020b) incorporated the effect of f_v on permanent strain for fine/coarse soil mixtures, and proposed Eq. (4):

$$\varepsilon_1^p = k(f_v, \sigma_d) \cdot a_1 \cdot [1 - (\frac{N}{100})^{-B}] \tag{4}$$

with

$$k(f_v, \sigma_d) = \varepsilon_1^{p_0} \cdot [f_v^2 + b f_v + c] \cdot (\frac{\sigma_d}{p_a} + d) \tag{5}$$

where $\varepsilon_1^{p_0}$, b, c and d are model parameters.

Trinh et al. (2012) investigated the effect of water content on permanent strain for the interlayer soil by multi-stage loading cyclic tests, and developed Eq. (6) for describing the variations of permanent strain with loading cycles N, deviator stress σ_d and water content:

$$\varepsilon_1^p = t(w, \sigma_d) \cdot a_1 \cdot [1 - (\frac{N}{100})^{-B}] \tag{6}$$

with

$$t(w, \sigma_d) = \varepsilon_1^{p_2} \cdot (w + a_2) \cdot (\frac{\sigma_d}{p_a})^{b_2} \tag{7}$$

where $\varepsilon_1^{p_2}$, a_2 and b_2 are model parameters.

Azam et al. (2015) investigated the effect of water content on permanent strain for the mixture of clay masonry and concrete aggregate, and proposed Eq. (8) for the description of the variations of permanent strain under the combined effects of loading cycles N and a water content normalized by optimum moisture content w/w_{opt}:

$$\varepsilon_1^p = a_3 N^{b_3} (\frac{w}{w_{opt}})^{c_3} \tag{8}$$

where a_3, b_3 and c_3 are model parameters. Further, they modified Eq. (8) to obtain Eq. (9) by incorporating the effects of matric suction ψ and coarse grain content f_v:

$$\varepsilon_1^p = a_4 N^{b_4} \left(\frac{\psi+1}{p_a}\right)^{c_4} \left(\frac{\mathrm{DDR}}{1+\mathrm{wPI}+f_v}\right)^{d_4} \quad (9)$$

where a_4, b_4, c_4 and d_4 are model parameters; wPI is the weighted plasticity index, equal to PI × (percent passing 200 sieve/100); PI is the plasticity index (%); 200 sieve refers to 0.075 mm; DDR is the ratio of dry density to the maximum dry density corresponding to optimum moisture content.

Jing et al. (2018) revised Eqs. (1) – (3) by incorporating the effects of fine soil content f_c (the ratio of the mass of fine soil to that of mixture) and water content. Eq. (10) was then obtained:

$$\varepsilon_1^p = R\left[1 - \left(\frac{N}{100}\right)^{\left(\frac{k'}{w}+o'\cdot f_c\right)}\right] \cdot g(f_c, \sigma_d, w) \quad (10)$$

with

$$g(f_c, \sigma_d, w) = \left[a_5 \cdot \left(\frac{w}{k}\right)^{o\cdot {f_c}^u}\right] \cdot \left[\frac{l_{max}}{p_a}\right]^{n_5} \cdot \frac{1}{m_5 + \frac{s_5}{p_{max}} - \frac{\sigma_d}{p_{max}}} \quad (11)$$

where R, k', o', a_5, k, o, u, n_5, m_5 and s_5 are model parameters.

Furthermore, they obtained Eq. (12) by substituting the effects of f_c and w in Eq. (10) with that of suction ψ:

$$\varepsilon_1^p = T\left[1 - \left(\frac{N}{100}\right)^{e\cdot\ln\left(\frac{\psi}{\psi_a}\right)+f}\right] \cdot b_6 \cdot \left(\frac{\psi}{\psi^*}\right)^{d_6} \cdot \left(\frac{l_{max}}{p_a}\right)^{n_6} \cdot \frac{1}{m_6 + \frac{s_6}{p_{max}} - \frac{\sigma_d}{p_{max}}} \quad (12)$$

where ψ^* is the suction value corresponding to the intersection point of wetting and drying paths of SWRC; ψ_a = 100 kPa; T, e, f, b_6, d_6, n_6, m_6 and s_6 are model parameters.

Up to now, no model has been proposed to describe the permanent strain ε_1^p variations under the combined effects of the number of loading cycles N, deviator stress σ_d, coarse grain content f_v and matric suction ψ.

Proposition of a new model

Su et al. (2020b) proposed Eqs. (4) – (5) for the fine/coarse soil mixtures, allowing the description of permanent strain ε_1^p under the combined effects of the number of loading cycles

N, deviator stress σ_d and coarse grain content f_v. According to Eq. (8) (Azam et al. 2015), there was a power relationship between the permanent strain and the normalized water content w/w_{opt}. By adding w/w_{opt} as an independent term in Eq. (5) (Su et al. 2020b), Eq. (13) was obtained:

$$k(f_v, \sigma_d, w) = \varepsilon_1^{p_0} \cdot [f_v^2 + bf_v + c] \cdot (\frac{\sigma_d}{p_a} + d) \cdot (\frac{w}{w_{opt}})^{\beta_1} \quad (13)$$

where β_1 is a model parameter.

Assuming that the void ratio of fines is constant, the ratio of water content is equal to that of degree of saturation, as shown in Eq. (14):

$$\frac{w}{w_{opt}} = \frac{S_r}{S_{r-opt}} \quad (14)$$

where S_{r-opt} is the degree of saturation at optimum moisture content for the fines.

The van Genuchten (1980) model was adopted for describing soil-water retention curve (SWRC):

$$\frac{S_r - S_{r-r}}{1 - S_{r-r}} = [\frac{1}{1+(a\psi)^n}]^m \quad (15)$$

where S_{r-r} is the residual degree of saturation, assumed to zero in this study; *a*, *n*, *m* are model parameters.

Substituting Eq. (15) into Eq. (14) yields Eq. (16):

$$\frac{w}{w_{opt}} = [\frac{1+(a\psi_{opt})^n}{1+(a\psi)^n}]^m \quad (16)$$

where ψ_{opt} is the matric suction at optimum moisture content.

Substituting Eq. (16) into Eq. (13) leads to Eq. (17):

$$k(f_v, \sigma_d, \psi) = \varepsilon_1^{p_0} \cdot [f_v^2 + bf_v + c] \cdot (\frac{\sigma_d}{p_a} + d) \cdot [\frac{1+(a\psi_{opt})^n}{1+(a\psi)^n}]^{m \cdot \beta_1} \quad (17)$$

Finally, Eq. (18) was obtained for describing the variations of ε_1^p of soil mixture with changes in the number of loading cycles *N*, deviator stress σ_d, coarse grain content f_v and matric suction ψ:

$$\varepsilon_1^p = k(f_v, \sigma_d, \psi) \cdot a_1 \cdot [1 - (\frac{N}{100})^{-B}] \quad (18)$$

where $k(f_v, \sigma_d, \psi)$ was calculated by Eq. (17).

Validation of the proposed model

Table 1 shows the soil properties and SWRCs of fine/coarse soil mixture in different studies, including Su et al. (2021a, 2021b), Wang et al. (2018), Duong et al. (2013, 2014), Jing (2017) and Jing et al. (2018). In these studies, both unsaturated and saturated conditions were considered. Experimental results under saturated condition (ψ = 0) were used to determine the model parameters, while those under unsaturated condition were adopted to verify the proposed model with the parameters determined under saturated condition.

Su et al. (2021a) and Wang et al. (2018) studied the effects of f_v and ψ on the permanent strain of fine/coarse soil mixture. This mixture was compacted at $w_{opt\text{-}f}$ = 13.7% and $\rho_{dmax\text{-}f}$ = 1.82 Mg/m^3, corresponding to a matric suction ψ_{opt} = 739 kPa (Wang et al. 2018). With increasing f_v, the ρ_d of mixture increased (Table 1). The compacted specimen was then wetted to saturation (ψ = 0) or dried to S_r = 60% (ψ = 2882 kPa). Multi-stage loading cyclic triaxial tests were conducted. A series of deviator stresses σ_d (10, 15, 20, 25 and 30 kPa) were applied in sequence, with a number of loading cycles N = 90000 for each σ_d. Fig. 1 shows that the same SWRC was obtained for varying f_v = 0%, 20% and 35% (Su et al. 2021b). Fig. 2(a) shows a comparison between the measurements by Su et al. (2021a) and the calculations by the proposed Eq. (17) for the variations of end-stage ε_1^p with σ_d at ψ = 0, with parameters $\varepsilon_1^{p_0}$ = 2.911, b = -1.050, c = 0.360, d = -0.050 and β_1 = 10.774 (Table 2). Fig. 2(b) compares the variations of ε_1^p with N measured by Su et al. (2021a) and those calculated by the proposed Eq. (18) for ψ = 0 with parameters a_1 = 1.150 and B = 0.300 (Table 2). Figs. 3(a) – (b) show the measurements and the corresponding calculations by the proposed Eq. (18) with the parameters determined previously, for ψ = 739 and 2882 kPa, respectively. A good agreement was obtained ($R^2 \geq 0.92$ in Table 2), showing the performance of the proposed model.

Table 1. Soil properties and SWRCs of fine/coarse soil mixture in different studies

Reference	f_v (%)	ψ (kPa)	ψ_{opt} (kPa)	Fine soil fraction					Soil mixture		SWRC fitted by van Genuchten (1980) model			
				G_s	w_L (%)	I_p (%)	w_{opt-f} (%)	ρ_{dmax-f} (Mg/m^3)	S_r (%)	ρ_d (Mg/m^3)	S_{r-r} (%)	a	n	m
Su et al. (2021a , 2021b)	0	0							100	1.82				
	10									1.91				
	20									1.99				
	35									2.12				
	45									2.21				
Wang et al. (2018)	0	2882	739	2.68	32	20	13.7	1.82	60	1.82	0	$4.500*10^{-4}$	1.250	0.570
	0	739							78	1.82				
	5									1.86				
	10									1.91				
	20									1.99				
	35									2.12				
	45									2.21				
Duong et al. (2013, 2014)	50	0, 85 and 9792	900	2.67	40	11	N/A	N/A	100, 49 and 32	2.01		38.558	3.671	0.023
	56	0, 2 and 24	10						100, 49 and 32	2.01		14.627	0.500	0.396
Jing (2017) and Jing et al. (2018)	63	0, 99, 121 and 143	121	N/A					100, 81, 77 and 63	2.04		0.008	3.201	0.600
	70	0	75						100	2.04		0.011	2.066	0.518

Note: f_v represents the ratio of the volume of dry coarse grains to that of mixture (Su et al. 2021a). ψ and ψ_{opt} represents the matric suction at given w and w_{opt} respectively. G_s, w_L, I_P, w_{opt-f} and ρ_{dmax-f} represent the specific gravity, liquid limit, plasticity index, optimum water content and maximum dry density of fine soil, respectively. S_r and ρ_d represent the degree of saturation and dry density of soil mixture. S_{r-r} represents the residual degree of saturation of fine soil. *a, n, m* are constant parameters of van Genuchten (1980) model. N/A means data not available in the reference.

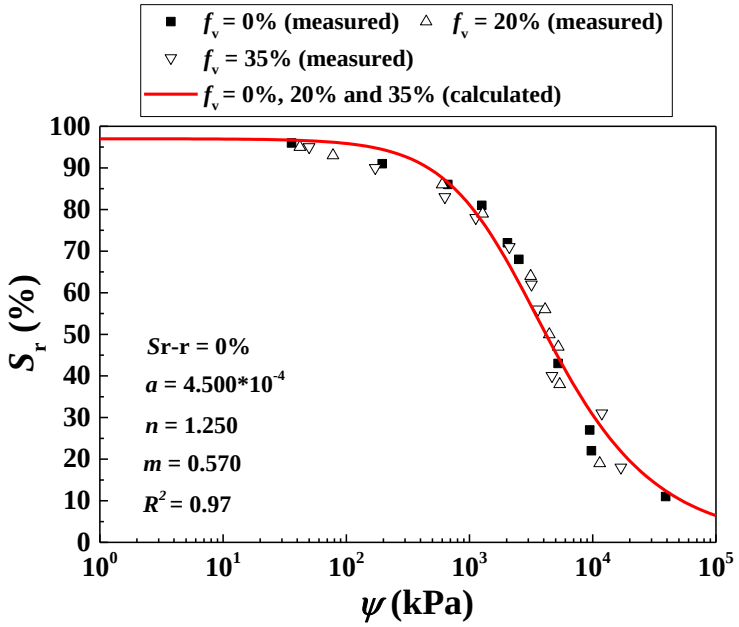

Fig. 1. Measured and calculated soil-water retention curves at varying f_v values (data from Su et al. 2021b)

Duong et al. (2013) investigated the permanent strain of interlayer soil under varying f_v and ψ. The soil mixture was kept at ρ_d = 2.01 Mg/m^3 (Table 1). ψ_{opt} was equal to 900 and 10 kPa for f_v = 50% and 56%, respectively. Large-scale cyclic triaxial tests were performed under multi-stage loadings. Fig. 4 presents the measured and calculated SWRCs for f_v = 50% and 56% using Eq. (15) (Duong et al. 2014). Fig. 5(a) shows the measured and calculated end-stage ε_1^p for f_v = 50% and 56% under ψ = 0 kPa, using Eq. (17) with parameters $\varepsilon_1^{p_0}$ = 2.887, b = -2.000, c = 0.819, d = -0.230 and β_1 = 3.330 (Table 2). Figs. 5(b) – (c) compare the variations of ε_1^p with N at ψ = 0, measured by Duong et al. (2013) and those calculated by the proposed Eq. (18) for f_v = 50% and 56%, respectively. Eq. (18) provides simulations with parameters a_1 = 1.165 and B = 0.338 (Table 2). Figs. 6(a) – (b) compare the measurements and the corresponding calculations by the proposed Eq. (18) with the parameters determined previously, for varying f_v, σ_d and ψ. Comparisons show a reasonably good agreement ($R^2 \geq 0.74$ in Table 2).

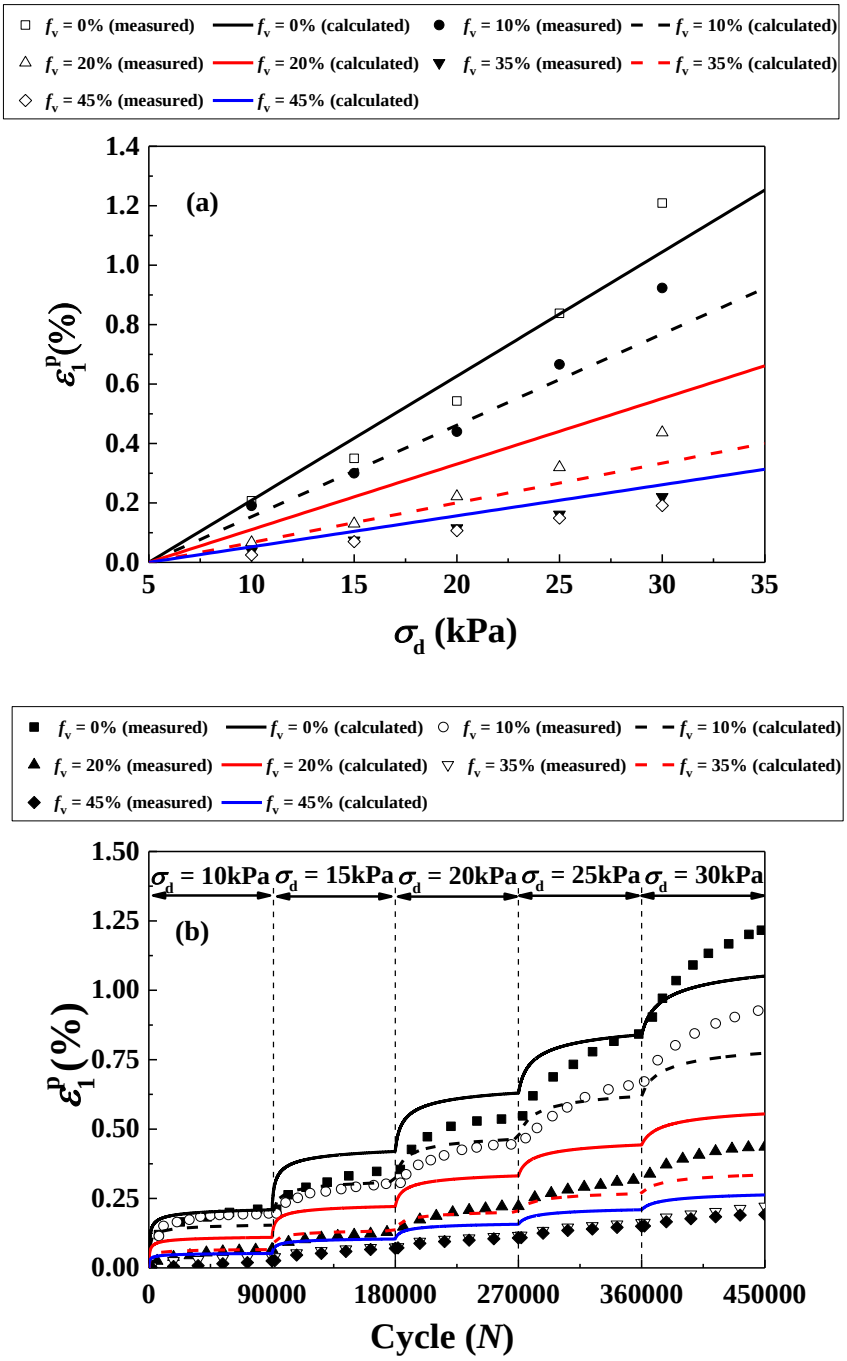

Fig. 2. Measured and calculated variations of (a) end-stage permanent strain with deviator stress and (b) permanent strain with loading cycle at ψ = 0 (data from Su et al. 2021a)

Table 2. Model parameters and coefficients of determination in different studies

Reference	f_v (%)	ψ (kPa)	$\varepsilon_1^{p_0}$	b	c	d	β_1	a_1	B	R^2
Su et al. (2021a)	0	0	2.911	-1.050	0.360	-0.050	10.774	1.150	0.300	0.94
	10									0.96
	20									0.94
	35									0.94
	45									0.98
Wang et al. (2018)	0	2882								0.92
	0	739								0.98
	5									0.97
	10									0.99
	20									0.98
	35									0.95
	45									0.94
Duong et al. (2013)	50	0	2.887	-2.000	0.819	-0.230	3.330	1.165	0.338	0.95
		85								0.96
		9792								0.93
		0								0.84
	56	2								0.85
		24								0.74
Jing et al. (2018)	63	0	0.345	-4.940	4.199	-0.135	6.619	1.200	0.380	0.99
		99								0.83
		121								0.88
		143								0.78
	70	0								0.98

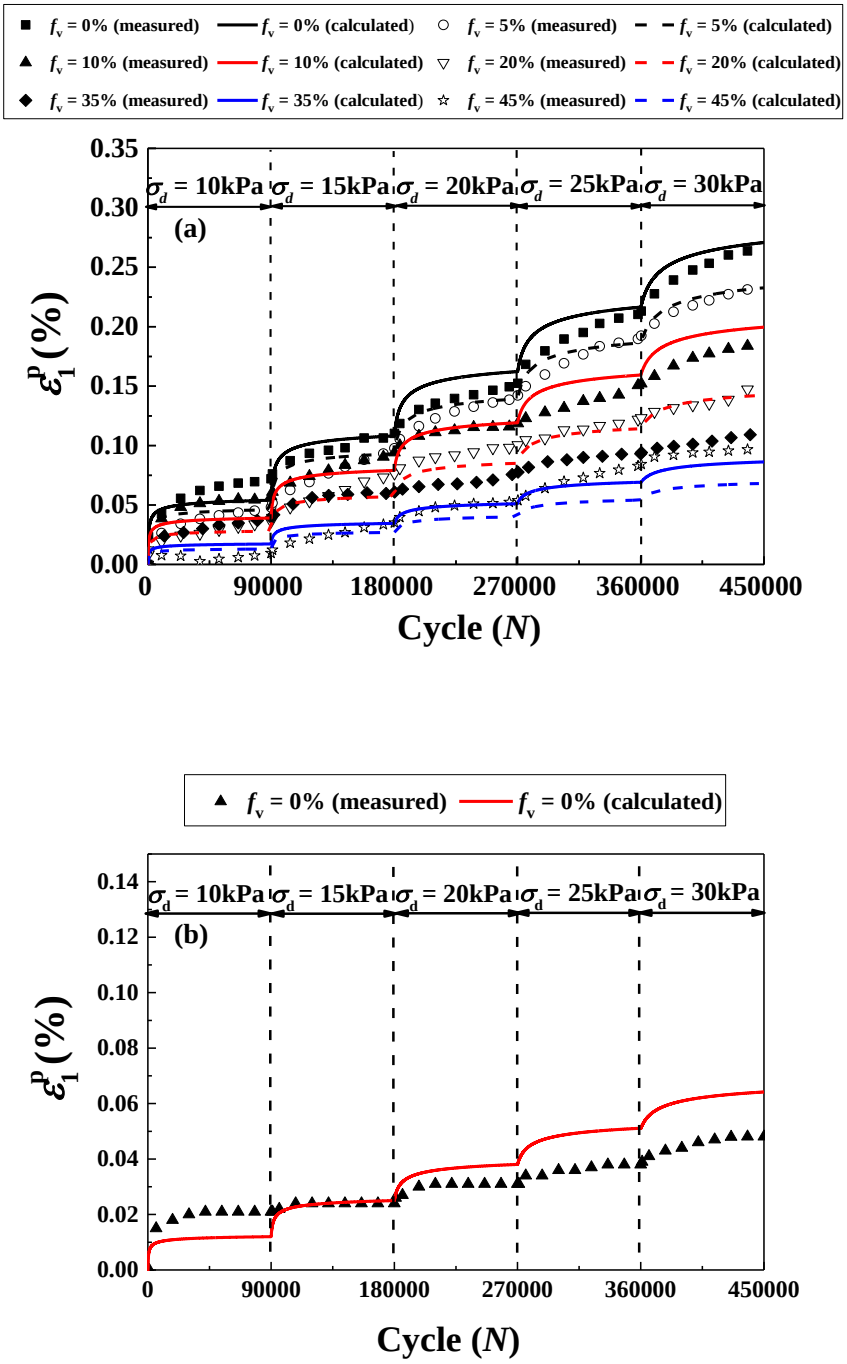

Fig. 3. Measured and calculated variations of permanent strain with loading cycle at different ψ values: (a) ψ = 739 kPa (data from Wang et al. 2018); (b) ψ = 2882 kPa (data from Su et al. 2021a)

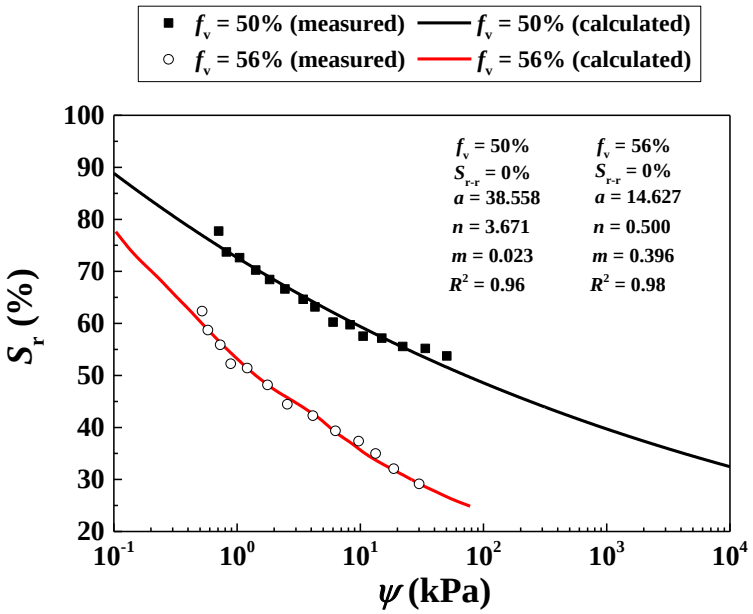

Fig. 4. Measured and calculated soil-water retention curves at varying f_v values (data from Duong et al. 2014)

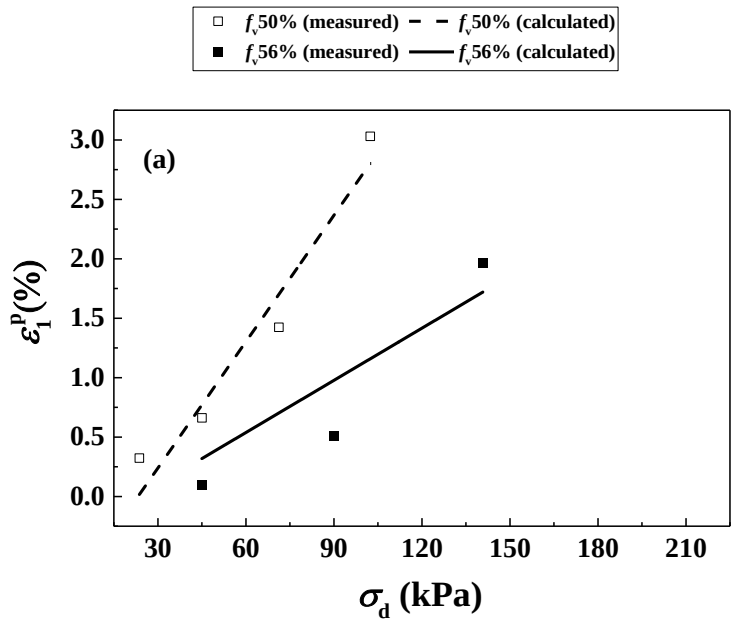

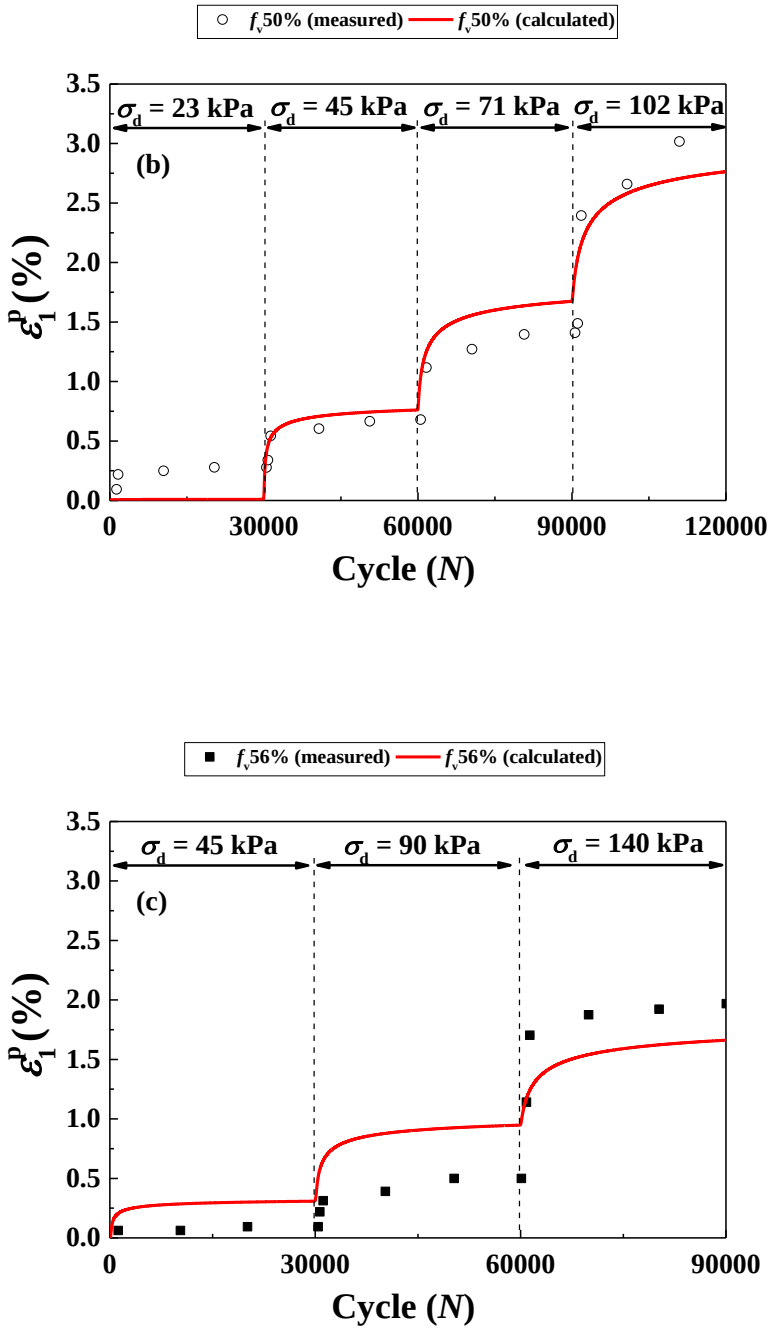

Fig. 5. Measured and calculated variations of (a) end-stage permanent strain with deviator stress and (b) - (c) permanent strain with loading cycle at ψ = 0 (data from Duong et al. 2013)

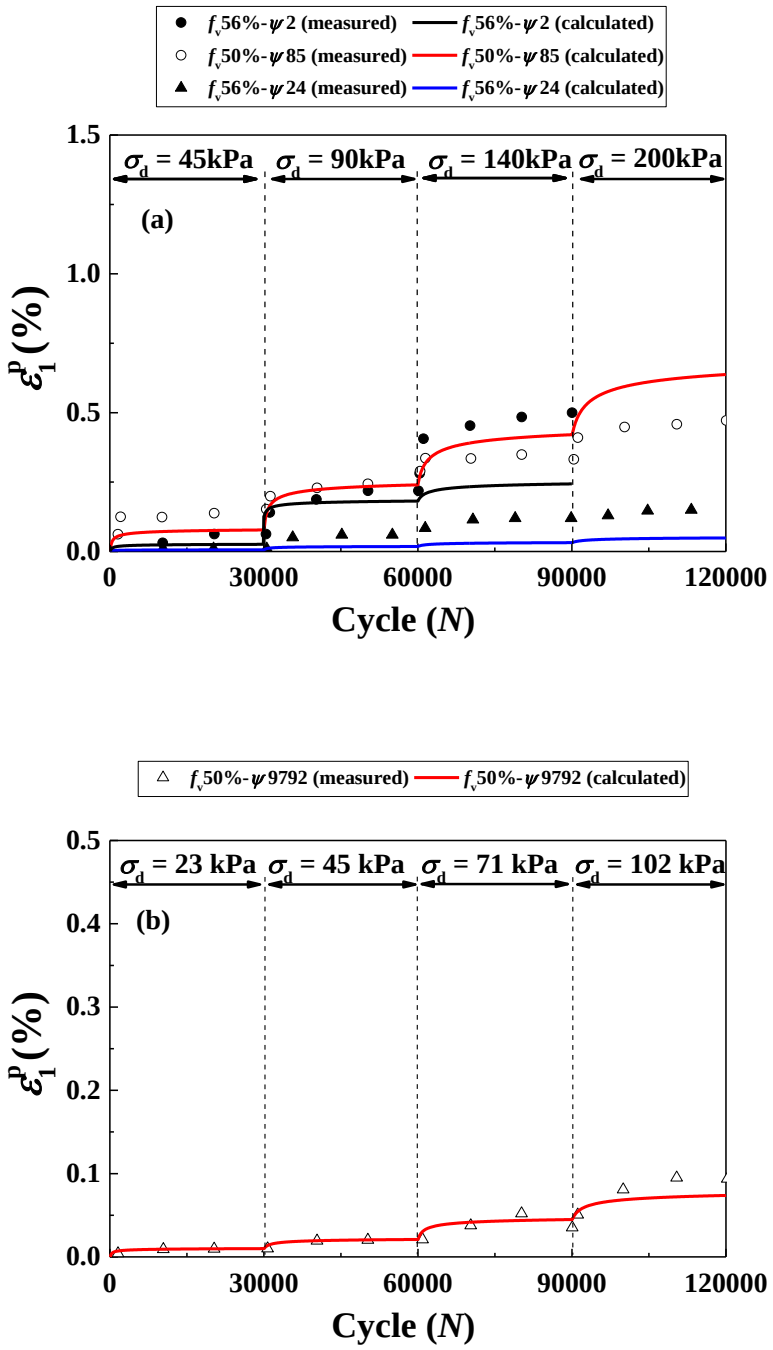

Fig. 6. Measured and calculated variations of permanent strain with loading cycle at varying f_v, σ_d and ψ (data from Dung et al. 2013)

Jing et al. (2018) investigated the effects of f_v and ψ on the permanent strain of granular materials. The soil mixture was controlled at a constant ρ_d = 2.04 Mg/m^3 for varying f_v and ψ. ψ_{opt} was found to be 121 and 75 kPa for f_v = 63% and 70%, respectively. Multi-stage loading cyclic triaxial tests were conducted, with a number of loading cycles N = 10000 for each stage. Fig. 7 shows the measured and calculated SWRCs for f_v = 63% and 70% using Eq. (15) (Jing

2017). Fig. 8(a) compares the end-stage ε_1^p at ψ = 0, measured by Jing et al. (2018) and those calculated by the proposed Eq. (17) for f_v = 63% and 70%, respectively. Figs. 8(b) – (c) show the comparisons of the variations of ε_1^p with N under ψ = 0 between the measurements by Jing et al. (2018) and calculations using the proposed Eq. (18) for f_v = 63% and 70%, respectively. The parameters in Eq. (18) were determined and presented in Table 2. Fig. 9 shows the predictions by Eq. (18) with the parameters determined previously, for f_v = 63% and varying ψ. A small difference between measurements and calculations was observed for the first three loading stages (σ_d = 40, 70 and 100), while a large difference for the fourth loading stage (σ_d = 140 kPa) appeared, especially in the case of ψ = 99 kPa.

Based on the shakedown theory (Werkmeister et al. 2001, 2004), Jing (2017) found that the permanent strain behavior for ψ = 99 kPa at σ_d = 140 kPa was classified as category B (plastic creep – failure at a large N). This implies that the proposed Eq. (18) can only well describe the permanent strain of category A (plastic shakedown – stabilization of permanent strain with increasing N), which was consistent with the model proposed by Trinh et al. (2012), Jing et al. (2018) and Su et al. (2020b). This explained the difference at the end of loading stages for f_v = 0% and 10% at ψ = 0 and σ_d = 30 kPa (Fig. 2(b)) and f_v = 50% at ψ = 0 kPa and σ_d = 102 kPa (Fig. 5(b)).

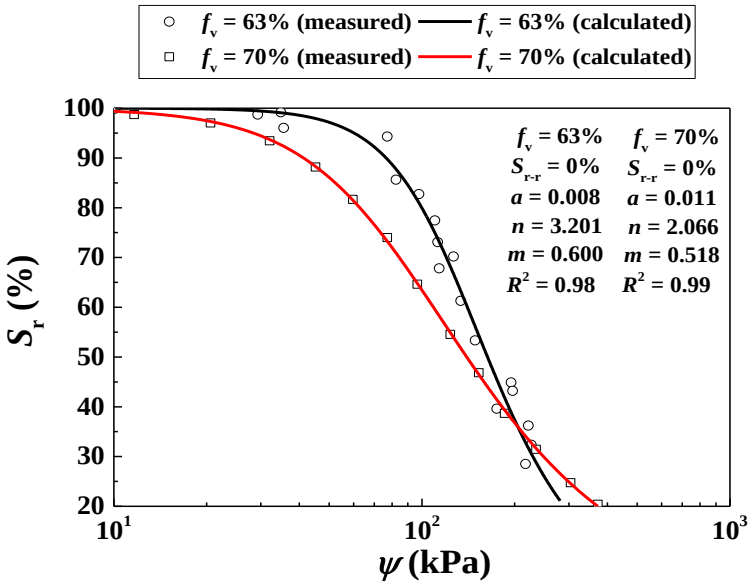

Fig. 7. Measured and calculated soil-water retention curves at varying f_v values (data from Jing 2017)

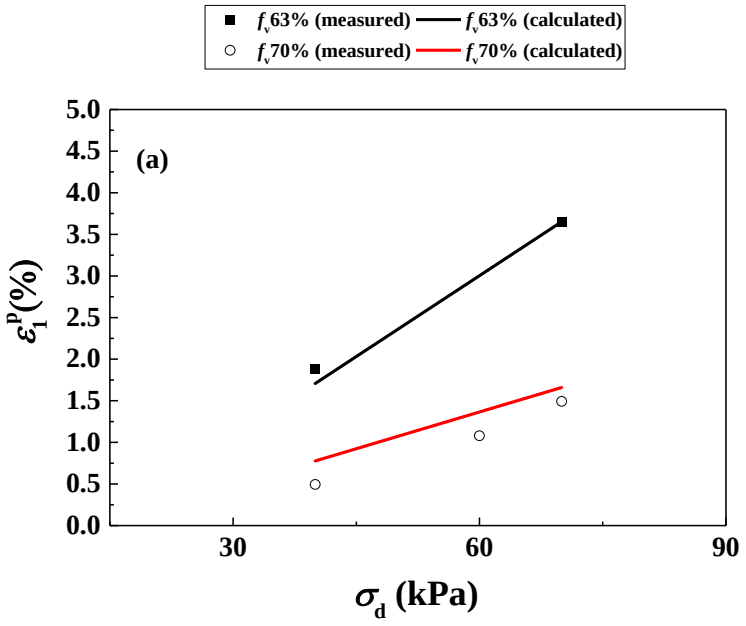
f_v63% (measured)
f_v63% (calculated)
f_v70% (measured)
f_v70% (calculated)
(a)
ε_1^p(%)
σ_d (kPa)

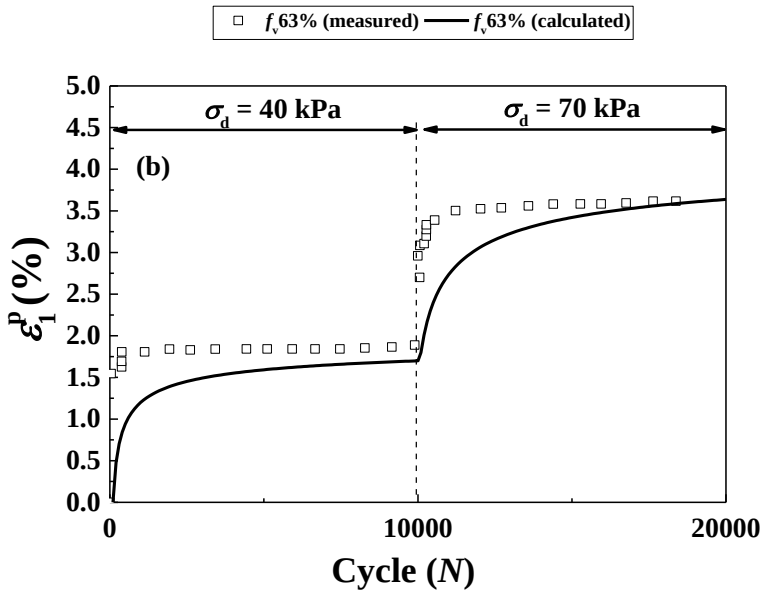
f_v63% (measured)
f_v63% (calculated)
σ_d = 40 kPa
σ_d = 70 kPa
(b)
ε_1^p(%)
Cycle (N)

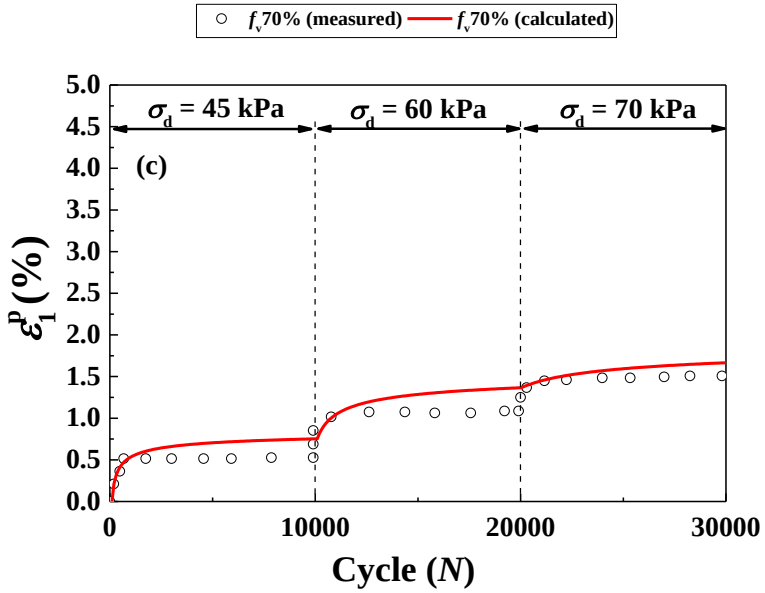

Fig. 8. Measured and calculated variations of (a) end-stage permanent strain with deviator stress and (b) - (c) permanent strain with loading cycle at ψ = 0 (data from Jing et al. 2018)

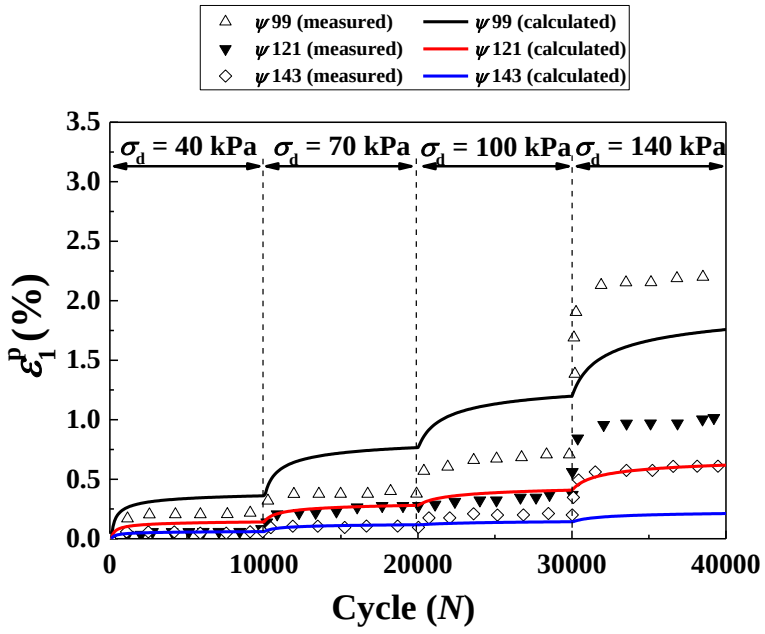

Fig. 9. Measured and calculated variations of permanent strain with loading cycle at f_v = 63% and varying ψ (data from Jing et al. 2018)

Comparisons between the proposed model and three representative existing models

To better illustrate the performance of the proposed model, a comparison with existing models was conducted. Three representative existing models were selected for this purpose (Table 3): Eq. (6) (Trinh et al. 2012) incorporating the effects of N, σ_d and w, Eq. (9) (Azam et al. 2015) incorporating the effects of N, f_v and ψ, and Eq. (10) (Jing et al. 2018) incorporating the effects of N, σ_d, f_c and w. Note that Eq. (12) incorporating the effects of N, σ_d and ψ was excluded for the comparison, because as mentioned before, the effect of ψ cannot reflect the effect of f_v on ε_1^p under saturated condition. For instance, an increase of f_v induced a decrease of ε_1^p in Fig. 2(b), while a constant ψ = 0 was kept. The experimental results in both the case of constant $\rho_{d\text{-}f}$ = 1.82 Mg/m^3 (Wang et al. 2018 and Su et al. 2021a in Table 1) and the case of constant ρ_d = 2.01 Mg/m^3 (Duong et al. 2013, Table 1) were chosen for the comparison between the proposed model (Eq. (18)) and the three representative existing models.

Fig. 10(a) compares the ε_1^p measured by Su et al. (2021a) with the calculated results by Eq. (6) for ψ = 0. The parameters in Eq. (6) took the values: $\varepsilon_1^{p_2}$= 1.296, a_2 = 3.403, b_2 = 1.696, a_1 = 1.150 and B = 0.360. Note that the same simulation curve must be obtained for varying f_v = 0 – 45% in Fig. 10(a), because Eq. (6) did not account for the effect of f_v. Figs. 10(b) – (c) show the comparisons between the measurements and the calculations by Eq. (6) with the parameters determined previously, for ψ = 739 and 2882 kPa, respectively. Compared with the simulations by the proposed model (Eq. (18)) in Figs. 2-3, Eq. (6) gave much less satisfactory results (Figs. 10(a) – (c)), with the coefficient of determination R^2 equal to 0.35, 0.57 and 0.37 for the cases of ψ = 0 (Fig. 10(a)), ψ = 739 kPa (Fig. 10(b)) and ψ = 2882 kPa (Fig. 10(c)), respectively. Because of this low performance, Eq. (6) was not further used for simulating the results of Duong et al. (2013).

Fig. 11(a) shows the comparisons of ε_1^p measured by Su et al. (2021a) and those calculated by Eq. (9) for ψ = 0. Eq. (9) gives the simulation results with parameters a_4 = 1.696*10^9, b_4 = 1.210, c_4 = -5.328 and d_4 = 25.305. Fig. 11(b) shows that poor simulations were provided by Eq. (9) with these parameters determined previously, for ψ = 739 kPa - the values of R^2 were smaller than 0.30 for varying f_v (Table 3). Similarly, Eq. (9) did not provide satisfactory simulations with the parameters determined previously, for ψ = 2882 kPa either. Because of this low performance, Eq. (9) was not further used to simulate the results of Duong et al. (2013).

Table 3. Model parameters and coefficients of determination of three representative existing models

Existing model/Parameter	Fine/coarse soil mixture (Su et al. 2021a;Wang et al.2018)											
	ψ = 0					ψ = 739						ψ = 2882
	f_v = 0%	f_v = 10%	f_v = 20%	f_v = 35%	f_v = 45%	f_v = 0%	f_v = 5%	f_v = 10%	f_v = 20%	f_v = 35%	f_v = 45%	f_v = 0%
Eq. (6) (Trinh et al. 2012)												
$\varepsilon_1^{p_2}$						1.296						
a_2						3.403						
b_2						1.696						
a_1						1.150						
B						0.360						
R^2			0.35					0.57				0.37
Eq. (9) (Azam et al. 2015)												
a_4						$1.696*10^9$						
b_4						1.210						
c_4						-5.328						
d_4						25.305						
R^2	0.94	0.96	0.76	0.69	0.76	0.12	0.30	0.15	0.17	0.14	0.22	/
Eq. (10) (Jing et al. 2018)												
a_5						0.172						
k						0.100						
o						4.908						
u						1.000						
n_5						1.000						
m_5						0.501						
s_5						21.269						
R						1.100						
k'						-0.010						
o'						-0.265						
R^2	0.98	0.78	0.97	0.98	0.91	0.70	0.74	0.68	0.61	0.79	0.86	0.22

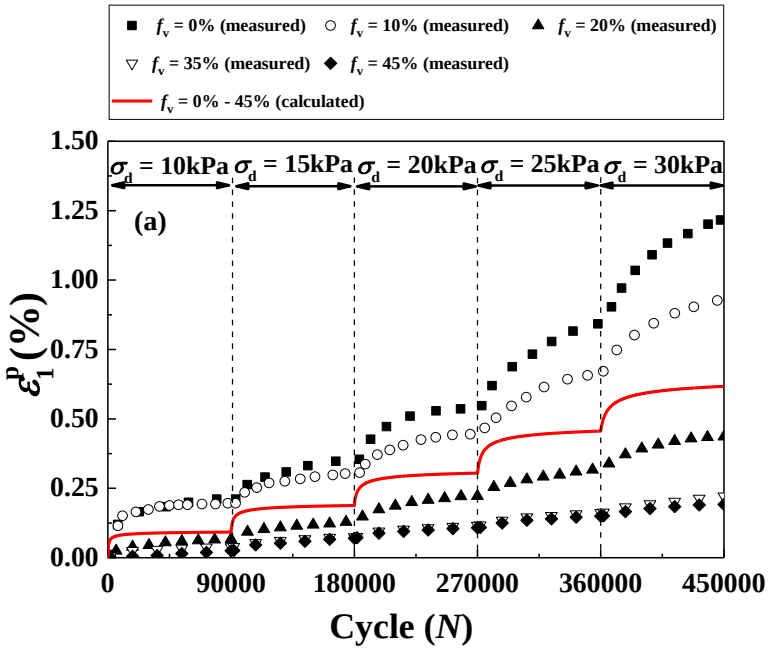
f_v = 0% (measured)
f_v = 10% (measured)
f_v = 20% (measured)
f_v = 35% (measured)
f_v = 45% (measured)
f_v = 0% - 45% (calculated)
σ_d = 10kPa
σ_d = 15kPa
σ_d = 20kPa
σ_d = 25kPa
σ_d = 30kPa
(a)
ε_1^p(%)
Cycle (N)

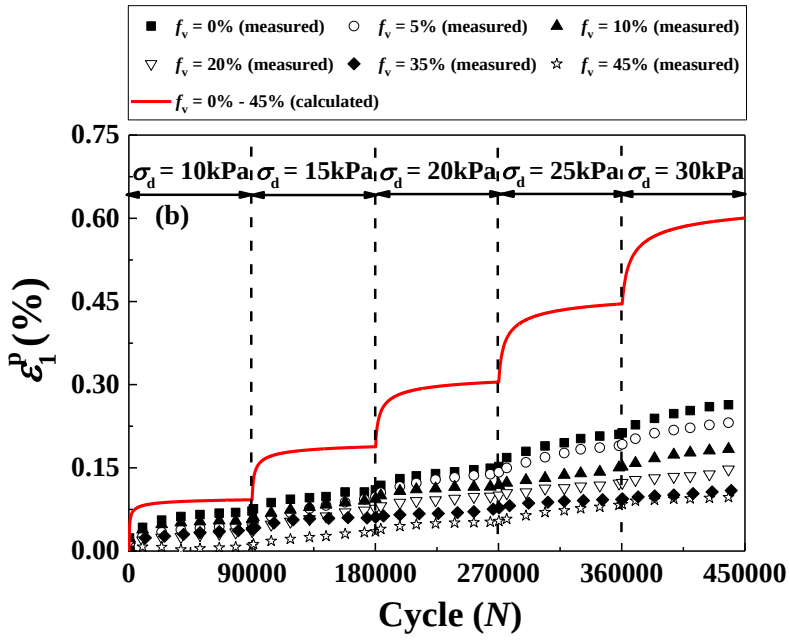
f_v = 0% (measured)
f_v = 5% (measured)
f_v = 10% (measured)
f_v = 20% (measured)
f_v = 35% (measured)
f_v = 45% (measured)
f_v = 0% - 45% (calculated)
σ_d = 10kPa
σ_d = 15kPa
σ_d = 20kPa
σ_d = 25kPa
σ_d = 30kPa
(b)
ε_1^p(%)
Cycle (N)

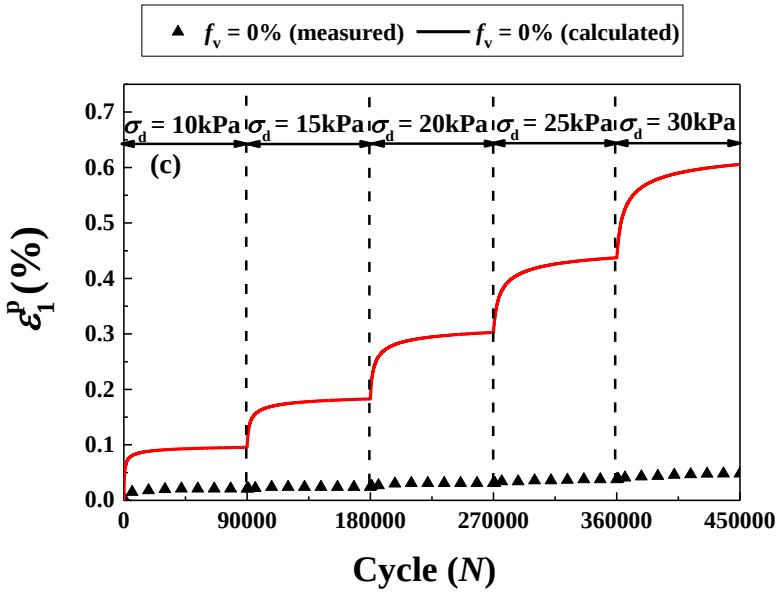

Fig. 10. Comparisons between the permanent strains measured by Su et al. (2021a) and Wang et al. (2018) and those calculated by Eq. (6) at varying ψ: (a) ψ = 0; (b) ψ = 739 kPa; (c) ψ = 2882 kPa

Fig. 12(a) compares the ε_1^p measured by Su et al. (2021a) and that calculated by Eq. (10) for ψ = 0. Eq. (10) provides the calculations with parameters a_5 = 0.172, k = 0.100, o = 4.908, u = 1.000, n_5 = 1.000, m_5 = 0.501, s_5 = 21.269, R = 1.100, k' = -0.010 and o' = -0.265. Note that the coarse grain contents by volume f_v = 0%, 5%, 10%, 20%, 35% and 45% corresponded to the fine soil contents by mass f_c = 52%, 50%, 49%, 45%, 40% and 35%, respectively. A good agreement was observed between the measurements and calculations for ψ = 0 (see the R^2 values for varying f_v in Table 3). This was because Eq. (10) (Jing et al. 2018) accounts for the effects of f_c, σ_d and N on ε_1^p under saturated condition (ψ = 0). Fig. 12(b) shows that the predictions provided by Eq. (10) with the parameters determined previously were larger than the measurements for ψ = 739 kPa. Compared with the predictions by the proposed model (Eq. (18)) in Fig. 3(a), Eq. (10) gave less satisfactory results (Fig. 12(b)): R^2 = 0.94 - 0.99 by Eq. (18) (Table 2), whilst R^2 = 0.61 - 0.86 by Eq. (10) (Table 3) for varying f_v. The similar phenomenon can be observed in Fig. 12(c) for the case of ψ = 2882 kPa.

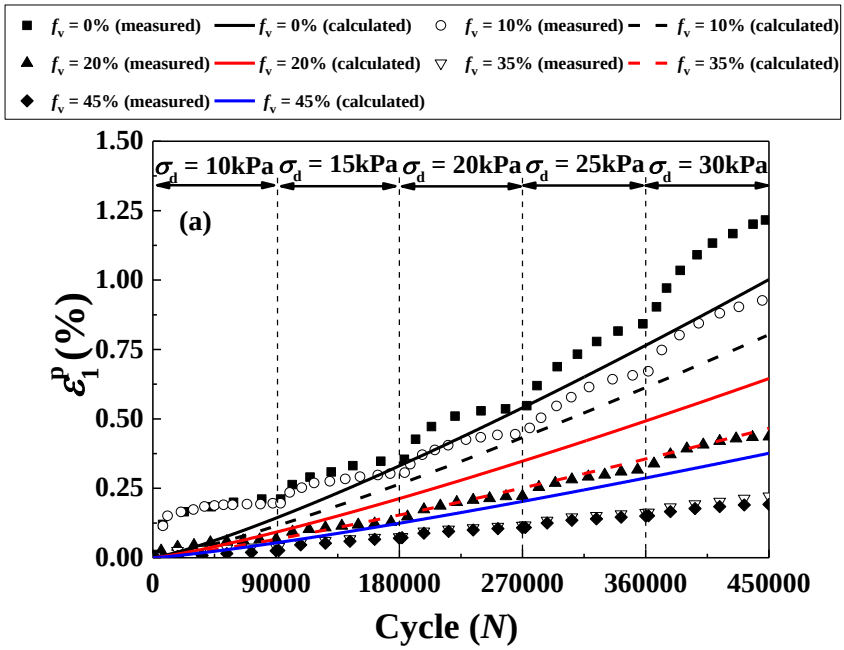

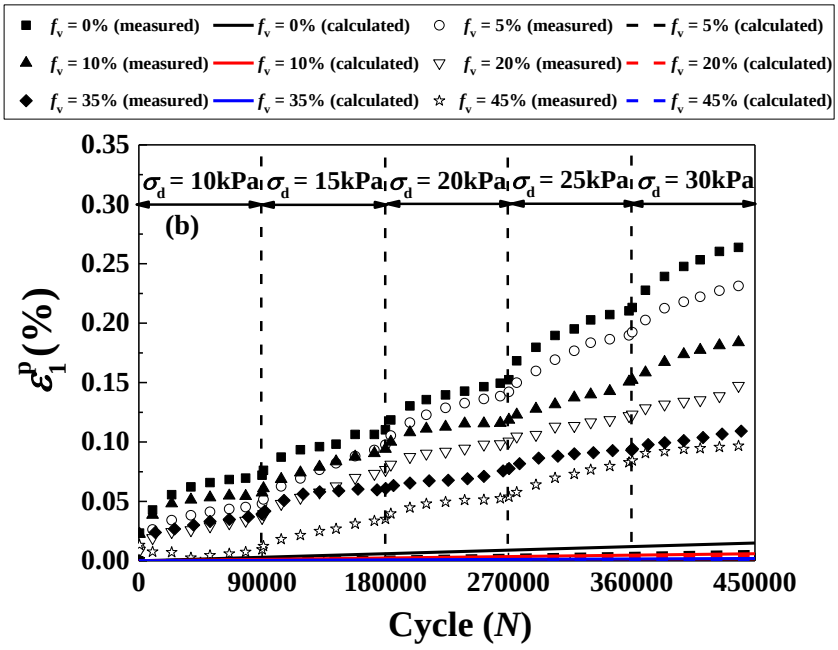

Fig. 11. Comparisons between the permanent strains measured by Su et al. (2021a) and Wang et al. (2018) and those calculated by Eq. (9) at varying ψ: (a) ψ = 0; (b) ψ = 739 kPa

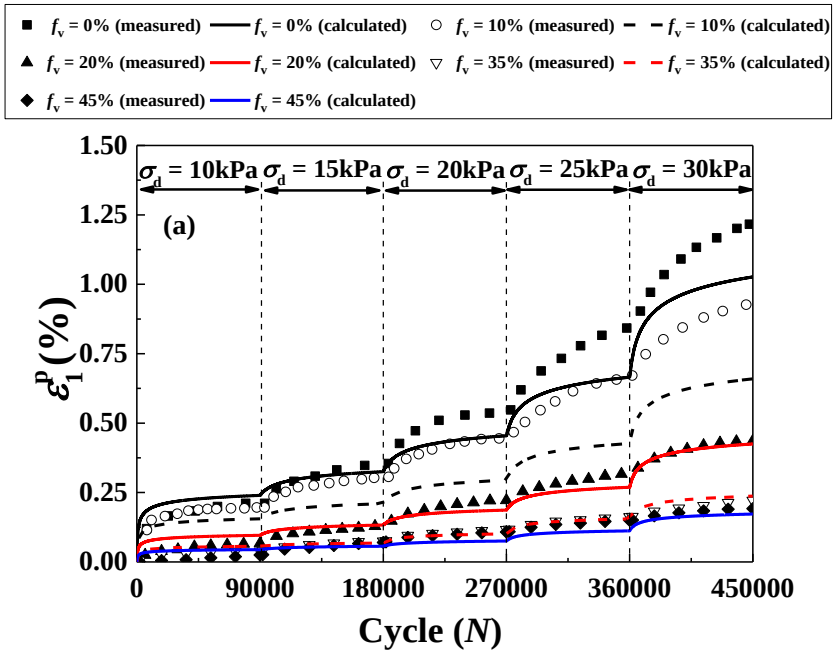
f_v = 0% (measured)
f_v = 0% (calculated)
f_v = 10% (measured)
f_v = 10% (calculated)
f_v = 20% (measured)
f_v = 20% (calculated)
f_v = 35% (measured)
f_v = 35% (calculated)
f_v = 45% (measured)
f_v = 45% (calculated)
σ_d = 10kPa
σ_d = 15kPa
σ_d = 20kPa
σ_d = 25kPa
σ_d = 30kPa
(a)
ε_1^p(%)
1.50
1.25
1.00
0.75
0.50
0.25
0.00
0
90000
180000
270000
360000
450000
Cycle (*N*)

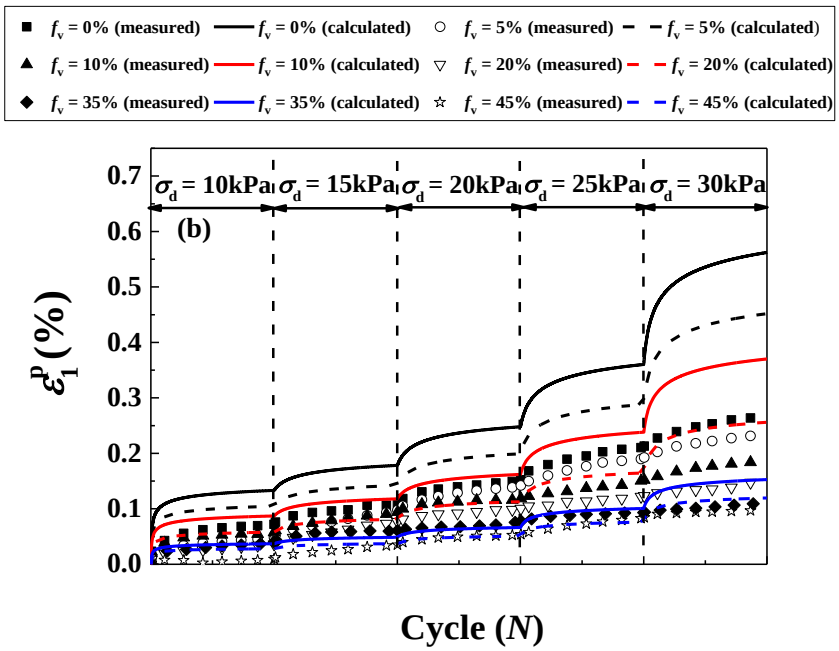
f_v = 0% (measured)
f_v = 0% (calculated)
f_v = 5% (measured)
f_v = 5% (calculated)
f_v = 10% (measured)
f_v = 10% (calculated)
f_v = 20% (measured)
f_v = 20% (calculated)
f_v = 35% (measured)
f_v = 35% (calculated)
f_v = 45% (measured)
f_v = 45% (calculated)
σ_d = 10kPa
σ_d = 15kPa
σ_d = 20kPa
σ_d = 25kPa
σ_d = 30kPa
(b)
ε_1^p(%)
0.7
0.6
0.5
0.4
0.3
0.2
0.1
0.0
Cycle (*N*)

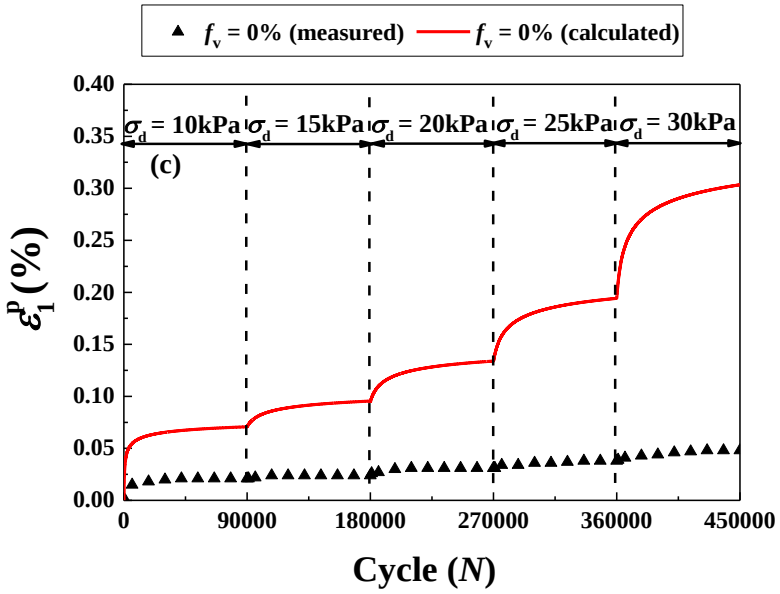

Fig. 12. Comparisons between the permanent strains measured by Su et al. (2021a) and Wang et al. (2018) and those calculated by Eq. (10) at varying ψ: (a) ψ = 0; (b) ψ = 739 kPa; (c) ψ = 2882 kPa

Figs. 13(a) - (b) show the comparisons of ε_1^p between the measurements by Duong et al. (2013) and the calculations by Eq. (10) for f_v = 50% and f_v = 56% at ψ = 0, respectively. The model parameters in Eq. (10) were presented in Table 4. The f_v = 50% and 56% corresponded to f_c = 33% and 27%, respectively. The comparisons show a good agreement (see the R^2 values for f_v = 50% and 56% at ψ = 0 in Table 4). Figs. 14(a) – (b) compare the measurements and the corresponding calculations by Eq. (10) with parameters shown in Table 4 for varying f_v, σ_d and ψ. Compared with description by the proposed Eq. (18) (Fig. 6), Eq. (10) provided less satisfactory results (Figs. 14(a) – (b)): R^2 = 0.74 - 0.96 by Eq. (18) (Table 2), whilst R^2 = 0.50 - 0.89 by Eq. (10) (Table 4) for varying f_v and ψ.

The difference between the proposed Eq. (18) and Eq. (10) was that Eq. (18) describes the variation of ε_1^p with ψ, while Eq. (10) describes the variation of ε_1^p with w. The comparisons made above show that Eq. (18) provides better predictions than Eq. (10) for both the case of constant $\rho_{d\text{-}f}$ (Su et al. 2021a and Wang et al. 2018 in Table 1) and the case of constant ρ_d (Duong et al. 2013, Table 1). For the latter case, a constant ρ_d = 2.01 Mg/m^3 of mixture was controlled by Duong et al. (2013) (Table 1), leading to a decrease of $\rho_{d\text{-}f}$ from 1.33 to 1.17 Mg/m^3 with an increase of f_v from 50% to 56%, thus a decrease of ψ (Su et al. 2021b). This contributed to an

increase of ε_1^p under unsaturated condition. For both the cases, the effect of $\rho_{\text{d-f}}$ on ε_1^p was rather reflected by ψ than by *w*. Thus, a better performance was obtained with the proposed Eq. (18) as compared to Eq. (10).

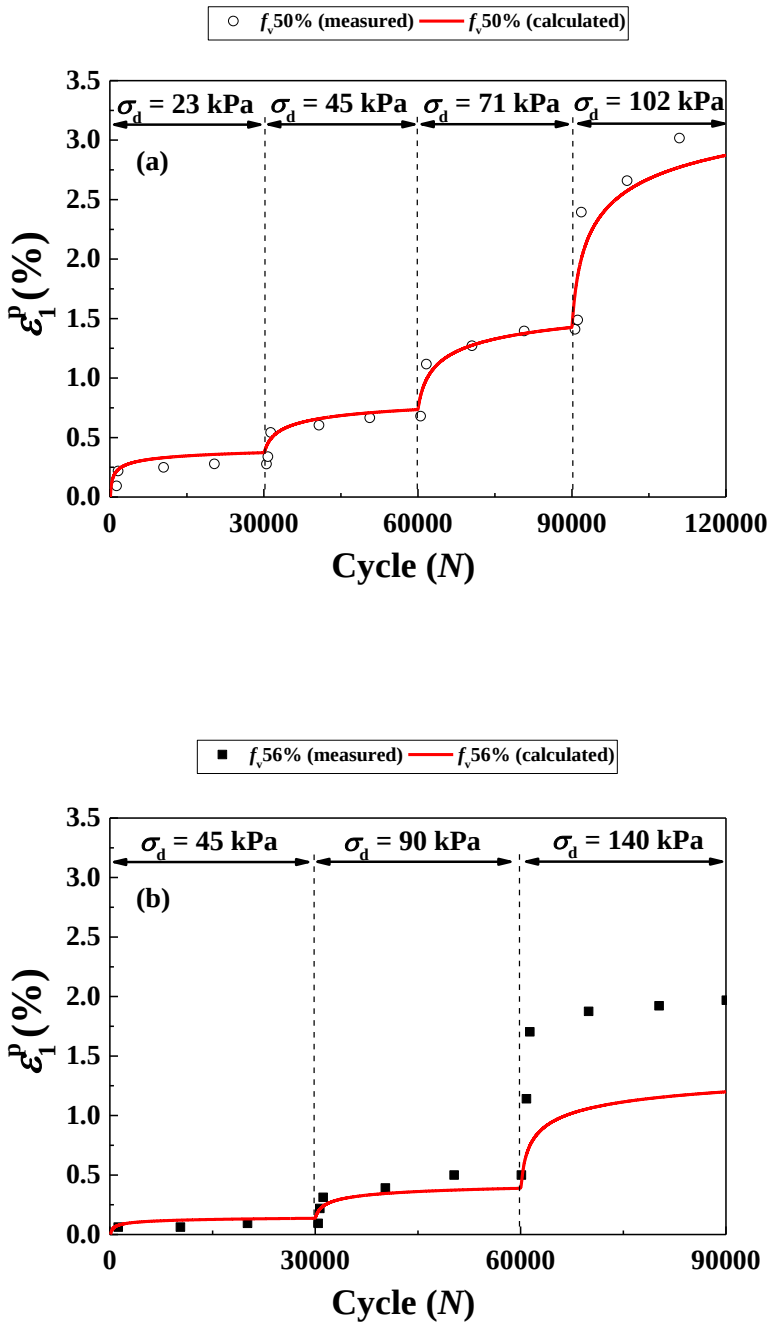

Fig. 13. Comparisons between the permanent strains measured by Duong et al. (2013) and those calculated by Eq. (10) at ψ = 0

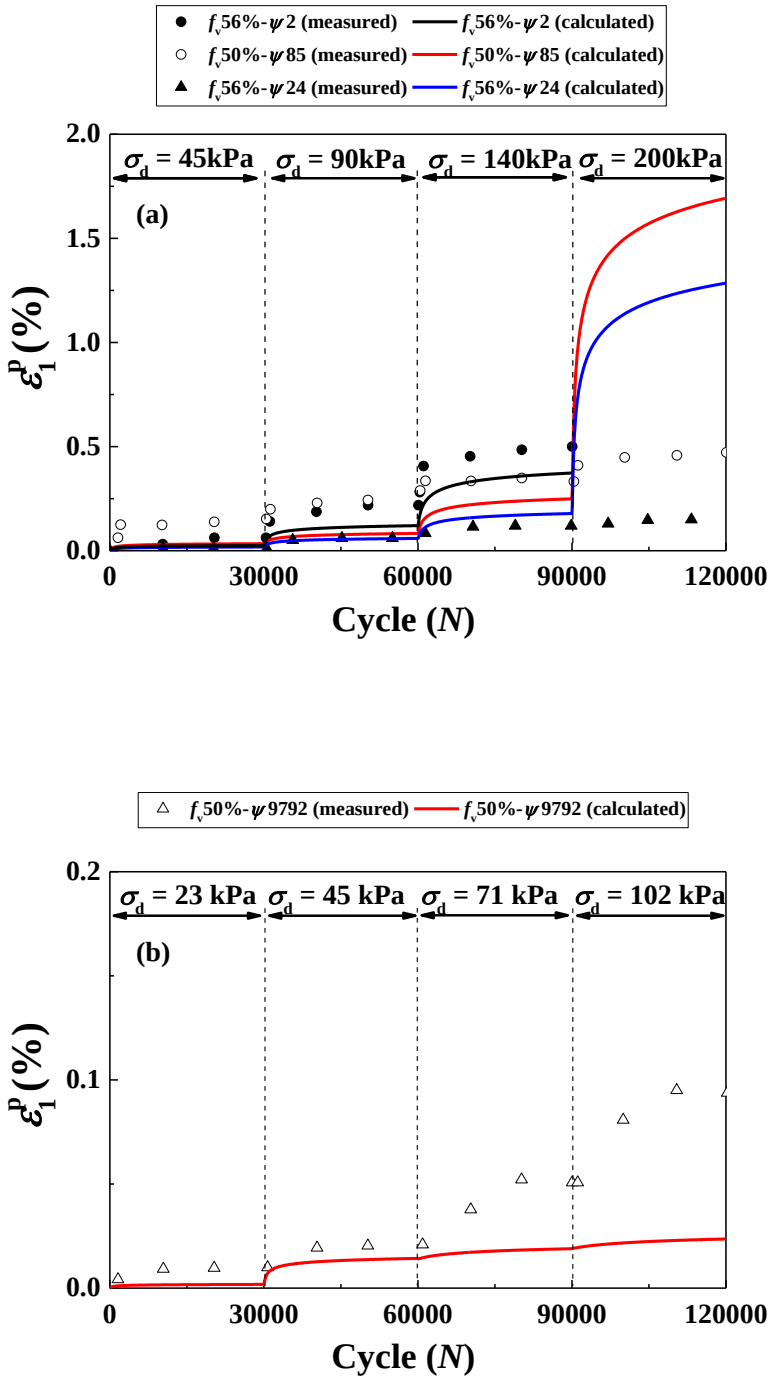

Fig. 14. Comparisons between the permanent strains measured by Duong et al. (2013) and those calculated by Eq. (10) at varying f_v, σ_d and ψ

Table 4. Model parameters in Eq. (10) and coefficients of determination for describing experimental results in Duong et al. (2013)

f_v (%)	ψ (kPa)	a_5	k	o	u	n_5	m_5	s_5	R	k'	o'	R^2
50	0	-0.909	0.068	1517.993	5.196	1.000	11.018	-920.000	1.350	-0.020	-0.230	0.97
	85											0.56
	9792											0.68
56	0											0.91
	2											0.89
	24											0.50

Summarizing, comparisons between the proposed Eq. (18) and the three representative existing models show that the proposed Eq. (18) which incorporated the suction effect through the water retention curve can better describe the variations of ε_1^p with N, σ_d, f_v and ψ under unsaturated and saturated conditions.

Conclusions

Based on the existing model proposed by Su et al. (2020b), a new model incorporating the soil-water retention curve (SWRC) was developed for fine/coarse soil mixture, allowing the effects of the number of loading cycles N, deviator stress σ_d, coarse grain content f_v and matric suction ψ to be accounted for. Several studies were selected from literature to verify the proposed model. The model parameters were determined by fitting the variations of ε_1^p with N, σ_d, f_v and ψ under saturated condition, and then used to predict the results under unsaturated condition. Good agreements were obtained between the measurements and the calculations, showing that the proposed model can well describe the variations of ε_1^p with N, σ_d, f_v and ψ in the case of plastic shakedown.

Comparisons between the proposed model (Eq. (18)) and three existing models (Eqs. (6), (9) and (10)) showed that Eq. (18) provides better simulations than Eqs. (6) and (9). This can be simply explained by the fact that Eq. (6) and Eq. (9) did not consider the effects of f_v and σ_d on ε_1^p, respectively. The difference between the proposed Eq. (18) and Eq. (10) was that Eq. (18) describes the variation of ε_1^p with ψ, while Eq. (10) describes the variation of ε_1^p with w. The comparisons show that Eq. (18) provides better simulations than Eq. (10) in both the case of constant $\rho_{d\text{-}f}$ (Su et al. 2021a and Wang et al. 2018 in Table 1) and the case of constant ρ_d

(Duong et al. 2013, Table 1). For the latter case, a constant ρ_d = 2.01 Mg/m^3 of mixture was controlled by Duong et al. (2013) (Table 1), leading to a decrease of $\rho_{d\text{-}f}$ from 1.33 to 1.17 Mg/m^3 with an increase of f_v from 50% to 56%, thus a decrease of ψ (Su et al. 2021b). For both cases, the effect of $\rho_{d\text{-}f}$ on ε_1^p was rather reflected by ψ than by w. Thus, a better performance could be obtained with the proposed Eq. (18) as compared to Eq. (10).

Acknowledgements

This work was supported by the China Scholarship Council (CSC) and Ecole des Ponts ParisTech.

References

AFNOR, 1995. NF P98-235-1—Test relating to pavements. Unbound granular materials. Part 1: Repeated Loading Triaxial Test.

Azam, A. M., Cameron, D. A., & Rahman, M. M. 2015. Permanent strain of unsaturated unbound granular materials from construction and demolition waste. Journal of Materials in Civil Engineering, 27(3), 04014125.

Barksdale, R. D. 1972. Laboratory evaluation of rutting in base course materials. In Presented at the Third International Conference on the Structural Design of Asphalt Pavements, Grosvenor House, Park Lane, London, England, Sept. 11-15, 1972. (Vol. 1, No. Proceeding).

Chen, W. B., Feng, W. Q., Yin, J. H., Borana, L., & Chen, R. P. 2019. Characterization of permanent axial strain of granular materials subjected to cyclic loading based on shakedown theory. Construction and Building Materials, 198, 751-761.

Duong, T. V., Tang, A. M., Cui, Y. J., Trinh, V. N., Dupla, J. C., Calon, N., ... & Robinet, A. 2013. Effects of fines and water contents on the mechanical behavior of interlayer soil in ancient railway sub-structure. Soils and foundations, 53(6), 868-878.

Duong, T. V., Cui, Y. J., Tang, A. M., Dupla, J. C., & Calon, N. 2014. Effect of fine particles on the hydraulic behavior of interlayer soil in railway substructure. Canadian geotechnical journal, 51(7), 735-746..

Gidel, G., Hornych, P., Breysse, D., & Denis, A. 2001. A new approach for investigating the permanent deformation behaviour of unbound granular material using the repeated loading triaxial apparatus. Bulletin des laboratoires des Ponts et Chaussées, (233).

Gabr, A. R., & Cameron, D. A. 2013. Permanent strain modeling of recycled concrete aggregate for unbound pavement construction. Journal of materials in civil engineering, 25(10), 1394-1402.

Hornych, P. 1993. Étude des déformations permanentes sous chargements répétés de trois graves non traitées. Bulletin de liaison des Laboratoires des Ponts et Chaussées, (184).

Jing, P. 2017. Experimental study and modelling of the elastoplastic behaviour of unbound granular materials under large number of cyclic loadings at various initial hydric states (Doctoral dissertation, Université de Strasbourg).

Jing, P., Nowamooz, H., & Chazallon, C. 2018. Permanent deformation behaviour of a granular material used in low-traffic pavements. Road Materials and Pavement Design, 19(2), 289-314.

Li, D., & Selig, E. T. 1996. Cumulative plastic deformation for fine-grained subgrade soils. Journal of geotechnical engineering, 122(12), 1006-1013.

Lekarp, F., & Dawson, A. 1998. Modelling permanent deformation behaviour of unbound granular materials. Construction and building materials, 12(1), 9-18.

Puppala, A. J., Chomtid, S., & Bhadriraju, V. 2005. Using repeated-load triaxial tests to evaluate plastic strain potentials in subgrade soils. Transportation research record, 1913(1), 86-98.

Qi, S., Cui, Y. J., Dupla, J. C., Chen, R. P., Wang, H. L., Su, Y., ... & Canou, J. 2020. Investigation of the parallel gradation method based on the response of track-bed materials under cyclic loadings. Transportation Geotechnics, 24, 100360.

Shenton, M. J. 1974. Deformation of railway ballast under repeated loading triaxial tests. Soil Mechanics Section, British Railways Research Departement, Derby, England.

Sweere, G.T.H. 1990. Unbound Granular Bases for Roads. PhD Thesis. Delft, Netherlands.

Song, Y., & Ooi, P. S. 2010. Interpretation of shakedown limit from multistage permanent deformation tests. Transportation research record, 2167(1), 72-82.

Su, Y., Cui, Y. J., Dupla, J. C., & Canou, J. 2020a. Investigation of the effect of water content on the mechanical behavior of track-bed materials under various coarse grain contents. Construction and Building Materials, 263, 120206.

Su, Y., Cui, Y. J., Dupla, J. C., Canou, J., & Qi, S. 2020b. A fatigue model for track-bed materials with consideration of the effect of coarse grain content. Transportation Geotechnics, 23, 100353.

Su, Y., Cui, Y. J., Dupla, J. C., & Canou, J. 2021a. Effect of water content on permanent deformation of fine/coarse soil mixtures with varying coarse grain contents and subjected to multi-stage cyclic loading. Submitted to Acta Geotechnica.

Su, Y., Cui, Y. J., Dupla, J. C., & Canou, J. 2021b. Soil-water retention behaviour of fine/coarse soil mixture with varying coarse grain contents and fine soil dry densities. Canadian Geotechnical Journal.

Trinh, V. N., Tang, A. M., Cui, Y. J., Dupla, J. C., Canou, J., Calon, N., ... & Schoen, O. 2012. Mechanical characterisation of the fouled ballast in ancient railway track substructure by large-scale triaxial tests. Soils and foundations, 52(3), 511-523.

van Genuchten, M. T. 1980. A closed-form equation for predicting the hydraulic conductivity of unsaturated soils. Soil science society of America journal, 44(5), 892-898.

Werkmeister, S., Dawson, A. R., & Wellner, F. 2001. Permanent deformation behavior of granular materials and the shakedown concept. Transportation Research Record, 1757(1), 75-81.

Werkmeister, S., Dawson, A. R., & Wellner, F. 2004. Pavement design model for unbound granular materials. Journal of Transportation Engineering, 130(5), 665-674.

Wang, H. L., Cui, Y. J., Lamas-Lopez, F., Dupla, J. C., Canou, J., Calon, N., & Chen, R. P. 2018. Permanent deformation of track-bed materials at various inclusion contents under large number of loading cycles. Journal of Geotechnical and Geoenvironmental Engineering, 144(8), 04018044.

Su, Y., Cui, Y. J., Dupla, J. C., & Canou, J. 2021. Submitted to Acta Geotechnica.

Modelling the suction- and deviator stress-dependent resilient modulus of unsaturated fine/coarse soil mixture by considering soil-water retention curve

Yu Su, Yu-Jun Cui, Jean-Claude Dupla, Jean Canou

Abstract: Experimental observations have shown that the resilient modulus M_r of fine/coarse soil mixture can be significantly affected by the coarse grain content f_v, deviator stress σ_d and matric suction ψ. In this study, a constitutive model incorporating the soil-water retention curve (SWRC) was proposed to describe the effects of ψ and σ_d on M_r. This model was then extended to the effect of f_v. The proposed model implied the resilient modulus at saturation condition ($M_{r\text{-}sat}$), the resilient modulus at optimum moisture content (OMC) condition ($M_{r\text{-}opt}$), the suction at OMC (ψ_{opt}) and the parameters related to SWRC. The model was validated using experimental data from five studies reported in literature. Comparisons with three representative existing models showed that the proposed model was capable to well describe the suction-dependent effect of deviator stress in the full range of suction, while the existing models gave satisfactory simulation results only in the low suction range. Indeed, experimental studies revealed that there was a threshold matric suction ψ_{th}, and with increasing σ_d, the M_r decreased when $\psi < \psi_{th}$, but increased when $\psi > \psi_{th}$. When $\psi < \psi_{th}$, all models gave good simulations. On the contrary, when $\psi > \psi_{th}$, only the proposed model gave good simulations, in particular when $\psi_{th} > \psi_{opt}$. This showed the performance of the proposed model in describing the variation of resilient modulus of unsaturated fine/coarse soil mixtures with changes in coarse grain content, deviator stress and matric suction.

Keywords: resilient modulus; constitutive model; matric suction; deviator stress; coarse grain content; soil-water retention curve

Introduction

An interlayer soil was naturally created in the French conventional rail tracks, corresponding to a mixture of ballast grains and subgrade fine soil. The in-situ investigation showed a decrease of ballast grain content over the depth of interlayer soil (Trinh 2011). The resilient modulus M_r, defined as the ratio of cyclic deviator stress to resilient strain, was adopted to characterize the stiffness of interlayer soil (Nie et al. 2020). Wang et al. (2017, 2018a, 2018b) and Qi et al. (2020a) studied the effects of coarse grain content f_v (the ratio of the volume of micro-ballast grains to that of mixture) and deviator stress σ_d on M_r of interlayer soil by cyclic triaxial tests under constant matric suction ψ. Figs. 1(a)-(b) show the grain size distribution curves of fine

Ecole des Ponts ParisTech, Laboratoire Navier/CERMES, 6 – 8 av. Blaise Pascal, Cité Descartes, Champs-sur-Marne, 77455 Marne – la – Vallée cedex 2, France

soil and micro-ballast, among which the micro-ballast was fabricated by a mixture of three coarse grains G 4-10, HN 2-4 and G 10-20 (see more details in Wang et al. 2017). The effect of ψ on the M_r of interlayer soil was further investigated by Su et al. (2021a) through multi-stage deviator stresses cyclic tests. Those experimental results indicated that the M_r of such fine/coarse soil mixture was significantly affected by coarse grain content f_v, matric suction ψ and deviator stress σ_d. From a practical point of view, it appears important to develop a constitutive model of M_r for the fine/coarse soil mixture, taking the combined effects of f_v, ψ and σ_d into consideration.

The effects of f_v, ψ and σ_d on M_r were addressed in numerous experimental studies and different models were proposed for that. Wang et al. (2017) and Cui et al. (2018) studied the effect of f_v on the M_r of fine/coarse soil mixture, and defined a characteristic coarse grain content $f_{v\text{-}cha}$ separating two fabric kinds for the mixtures: a fine matrix macrostructure at $f_v \leq f_{v\text{-}cha}$, and a coarse grain skeleton fabric at $f_v \geq f_{v\text{-}cha}$. They found that M_r increased slowly with increasing f_v at $f_v \leq f_{v\text{-}cha}$, while quickly at $f_v \geq f_{v\text{-}cha}$. No constitutive model has been developed for describing this phenomenon.

The effects of ψ and σ_d on M_r were generally investigated by multi-stage loadings cyclic triaxial tests (Gupta et al. 2007; Nowamooz et al. 2011). Gu et al. (2020) performed a series of large-scale cyclic triaxial tests on unbound granular materials, and found that the increase in both ψ and σ_d led to an increase of M_r. Ng et al. (2013) studied the effects of ψ and σ_d on the M_r of unsaturated subgrade soil by suction-controlled cyclic triaxial tests. The results showed that in a narrow range of ψ from 0 to 250 kPa, an increase of ψ induced an increase of M_r, and an increase of σ_d led to a reduction of M_r at a constant ψ. Yang et al. (2008) performed suction-controlled tests on residual mudstone soil with various deviator stresses σ_d. They reported that with increasing σ_d, the M_r decreased at low matric suctions (ψ = 50 and 150 kPa), while increased at a high matric suction (ψ = 450 kPa). Similarly, Su et al. (2021a) studied the effect of w on the M_r of fine/coarse soil mixture through multi-stage loadings cyclic triaxial tests. They found that an increase of w led to a decrease of M_r of soil mixture, due to the effect of ψ. Moreover, in the case of low ψ (smaller than or equal to ψ_{opt} at optimum moisture content OMC), the increase of σ_d resulted in a decrease of M_r, while in the case of high ψ (larger than ψ_{opt}), an opposite trend was observed. Han and Vanapalli (2015) investigated the effect of ψ on the M_r of unsaturated subgrade soil, and proposed a constitutive model incorporating the soil-water retention curve (SWRC). Oh et al. (2009) and Han and Vanapalli (2016a, 2016b) also

consider SWRC while modeling the effect of ψ on M_r. To date, there are no models for the description of M_r variation with changes in ψ and σ_d for unsaturated fine/coarse soil mixtures.

In this study, a constitutive model of M_r was proposed for unsaturated fine/coarse soil mixtures, accounting for the effects of ψ, σ_d, and f_v. Experimental data collected from literature including the authors' own data were used to validate the model. Comparisons between the proposed model and three representative existing models showed that the proposed model is capable to well describe the variations of M_r with changes in σ_d and f_v in the full range of ψ.

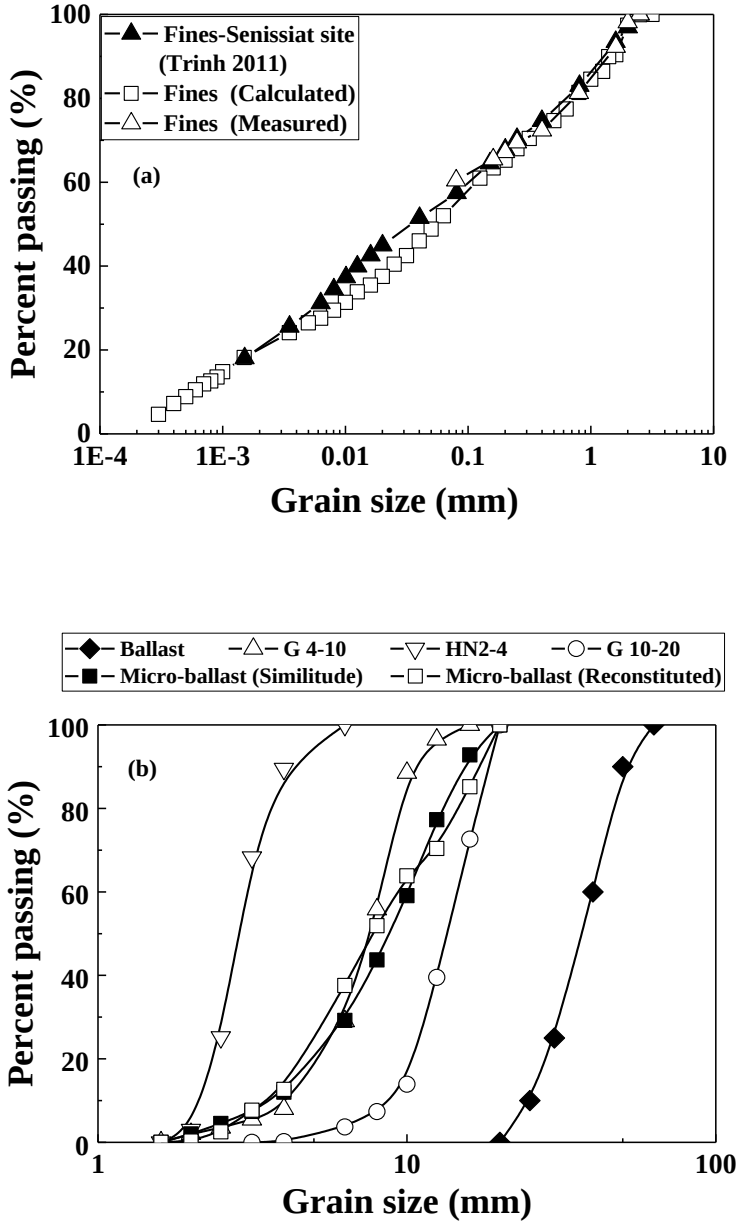

Fig. 1. Grain size distribution curves of (a) fine soil and (b) micro-ballast (after Wang et al. 2017)

Modelling background

Some investigators proposed empirical models to simulate the M_r - ψ relationship. For instance, Sawangsuriya et al. (2009) studied the effect of ψ on M_r with four compacted subgrade soils, and proposed Eqs. (1) - (2) by considering two reference M_r values at saturation condition and OMC condition- $M_{r\text{-}sat}$ and $M_{r\text{-}opt}$, respectively:

$$M_r/M_{r-sat} = -5.61 + 4.54\log(\psi) \quad (1)$$

$$M_r/M_{r-opt} = -0.24 + 0.25\log(\psi) \quad (2)$$

Ba et al. (2013) proposed Eq. (3) to estimate the variations of M_r of four compacted granular materials with respect to ψ using a resilient modulus ratio of M_r to the $M_{r\text{-}opt}$:

$$M_r/M_{r-opt} = 0.385 + 0.267\log(\psi) \quad (3)$$

These empirical models were simple and their parameters could be easily determined by regression analysis. However, since they were generally derived from limited experimental data, it appears difficult to be generalized to other materials.

The Mechanistic-Empirical Pavement Design Guide (MEPDG) (ARA, Inc., ERES Consultants Division. 2004) recommended the commonly used Eq. (4) to describe the variation of M_r with stress:

$$M_r = k_1 p_a \left(\frac{\theta_b}{p_a}\right)^{k_2} \left(\frac{\tau_{oct}}{p_a} + 1\right)^{k_3} \quad (4)$$

where θ_b is the bulk stress, equal to the sum of the three principal stresses σ_1, σ_2 and σ_3; τ_{oct} is the octahedral shear stress, equal to $\sqrt{2}/3(\sigma_1 - \sigma_3)$ in triaxial condition; p_a is the atmospheric pressure; k_1 , k_2 and k_3 are model parameters.

Liang et al. (2008) studied the effects of stress state and matric suction on the M_r of cohesive soil. They proposed Eq. (5) by incorporating ψ into the bulk stress of Eq. (4) using the Bishop's effective stress parameter χ:

$$M_r = k_4 p_a \left(\frac{\theta_b + \chi\psi}{p_a}\right)^{k_5} \left(\frac{\tau_{oct}}{p_a} + 1\right)^{k_6} \quad (5)$$

where k_4, k_5 and k_6 are model parameters.

Similarly, Heath et al. (2004) investigated the M_r of unsaturated granular materials, and developed Eq. (6) by modifying Eq. (4) using the Bishop's effective stress parameter χ:

$$M_r = k_7 p_a \left(\frac{\frac{\theta_b}{3} - u_a + \chi\psi}{p_a}\right)^{k_8} \left(\frac{\sigma_d}{p_a}\right)^{k_9} \quad (6)$$

where k_7, k_8 and k_9 are model parameters; u_a is the pore air pressure.

Gupta et al. (2007) and Khoury et al. (2013) modified Eq. (4) by adding ψ as an independent term, such as $A\psi^B$ in Eqs. (7) and (8) for subgrade soils:

$$M_r = k_{10} p_a \left(\frac{\theta_b - 3k_{11}}{p_a}\right)^{k_{12}} \left(\frac{\tau_{oct}}{p_a} + k_{13}\right)^{k_{14}} + A_1\psi^{B_1} \quad (7)$$

$$M_r = k_{15} p_a \left(\frac{\theta_b}{p_a}\right)^{k_{16}} \left(\frac{\tau_{oct}}{p_a} + k_{17}\right)^{k_{18}} + A_2\psi^{B_2} \quad (8)$$

where k_{10}–k_{18}, A_1, B_1, A_2 and B_2 are model parameters.

The MEPDG (ARA, Inc., ERES Consultants Division. 2004) adopted Eq. (9) to predict the variation of M_r with respect to the seasonal variation of water content in the field condition:

$$\log\left(\frac{M_r}{M_{r-opt}}\right) = a + \frac{b-a}{1+\exp[\ln\frac{-b}{a} + k_m \cdot (S_r - S_{r-opt})]} \quad (9)$$

where S_r is the degree of saturation; $M_{r\text{-}opt}$ and $S_{r\text{-}opt}$ are the resilient modulus and the degree of saturation at OMC, respectively; a and b are the minimum and maximum values of log ($M_r/M_{r\text{-}opt}$), respectively; k_m is a regression parameter. For fine-grained soil, a = -0.5934, b = 0.4 and k_m = 6.1324; for coarse-grained soil, a = -0.3123, b = 0.3 and k_m = 6.8157.

Han and Vanapalli (2015) proposed Eq. (10) for compacted subgrade fine soils, incorporating SWRC:

$$\frac{M_r - M_{r-sat}}{M_{r-opt} - M_{r-sat}} = \frac{\psi}{\psi_{opt}} \left(\frac{S_r}{S_{r-opt}}\right)^{\xi} \quad (10)$$

where ξ is the model parameter.

Summarizing, Table 1 presents a summary of model parameters for Eqs. (1) - (10).

Table 1. A summary of parameters for Eqs. (1) - (10)

Reference	Equation	Model parameters
Sawangsuriya et al. (2009)	(1)	ψ and $M_{r\text{-}sat}$
	(2)	ψ and $M_{r\text{-}opt}$
Ba et al. (2013)	(3)	ψ and $M_{r\text{-}opt}$
ARA, Inc., ERES Consultants Division. (2004)	(4)	θ_b, τ_{oct}, p_a, k_1, k_2 and k_3
Liang et al. (2008)	(5)	θ_b, τ_{oct}, p_a, χ,ψ, k_4, k_5 and k_6
Heath et al. (2004)	(6)	θ_b, p_a, χ,ψ,u_a, σ_d, k_7, k_8 and k_9
Gupta et al. (2007)	(7)	θ_b, τ_{oct}, p_a, ψ, k_{10}, k_{11}, k_{12}, k_{13}, A_1 and B_1
Khoury et al. (2013)	(8)	θ_b, τ_{oct}, p_a, ψ, k_{15}, k_{16}, k_{17}, k_{18}, A_2 and B_2
ARA, Inc., ERES Consultants Division. (2004)	(9)	S_r, $S_{r\text{-}opt}$, $M_{r\text{-}opt}$, a,b and k_m
Han and Vanapalli (2015)	(10)	S_r, $S_{r\text{-}opt}$, $M_{r\text{-}opt}$, $M_{r\text{-}sat}$ and ξ

Proposition of a new model

Proposing a model accounting for the effects of ψ and σ_d

Han and Vanapalli (2016b) reviewed the existing constitutive models of M_r with respect to ψ, and proposed a general form as follows:

$$M_r = M_{r-sat} + f(\psi),\ f(0) = 0 \tag{11}$$

where function $f(\psi)$ represents the contribution of ψ to M_r.

Referring to the existing models (e.g. Eq. (5) in Liang et al. 2008 and Eq. (6) in Heath et al. 2004), a factor $\chi\psi$ was adopted to reflect the effect of ψ on the M_r of unsaturated soils. As stated by Han and Vanapalli (2016a), using factor $\chi\psi$ induced a change of the role of suction ψ from a pore-scale stress to a macroscopic stress which contributed to the constitutive stress and hence the M_r of unsaturated soils. In this study, factor $\chi\psi$ was modified by considering (*i*) a power relationship of M_r - ψ in Eqs. (7) - (8) (Gupta et al. 2007 and Khoury et al. 2013) and (*ii*) a parameter χ equal to the effective degree of saturation S_r^e, which was defined as the ratio of $(S_r - S_{r-r})$ to $(1 - S_{r-r})$, where S_{r-r} is the residual degree of saturation (Alonso et al. 2010; Lu et al. 2010). Therefore, a new factor $\psi^B S_r^e$ was generated and Eq. (12) was obtained:

$$M_r = M_{r-sat} + A \cdot \psi^B \cdot S_r^e \tag{12}$$

where *A* and *B* are model parameters.

Substituting $M_{r\text{-}opt}$ and the corresponding ψ_{opt} and S_{r-opt}^e (the effective degree of saturation at OMC) into Eq. (12) yields Eq. (13):

$$M_{r-opt} = M_{r-sat} + A \cdot \psi_{opt}^B \cdot S_{r-opt}^e \tag{13}$$

Dividing Eq. (12) by Eq. (13) leads to the normalized Eq. (14) where parameter *A* vanishes:

$$\frac{M_r - M_{r-sat}}{M_{r-opt} - M_{r-sat}} = \left(\frac{\psi}{\psi_{opt}}\right)^B \cdot \frac{S_r^e}{S_{r-opt}^e} \tag{14}$$

Eq. (15) (Moossazadeh and Witczak 1981) was commonly used to characterize the effect of σ_d on M_r. Based on Eq. (15), Eq. (16) was proposed for relating σ_d to parameter *B* in Eq. (14):

$$M_r = k_{19}\left(\frac{\sigma_d}{p_a}\right)^{k_{20}} \tag{15}$$

$$B = l_1 \cdot \left(\frac{\sigma_d}{p_a}\right)^{l_2} \tag{16}$$

where k_{19}, k_{20}, l_1 and l_2 are model parameters.

The van Genuchten (1980) model was adopted for describing the SWRC:

$$S_r^e = \frac{S_r - S_{r-r}}{1 - S_{r-r}} = \left[\frac{1}{1+(a\psi)^n}\right]^m \tag{17}$$

where $S_{r\text{-}r}$ is the residual degree of saturation, assumed to be 0 in this study; a, n and m are model parameters.

Substituting Eqs. (16) and (17) into Eq. (14), Eq. (18) was obtained, which allowed prediction of the variation of M_r under the combined effects of ψ and σ_d:

$$\frac{M_r - M_{r-sat}}{M_{r-opt} - M_{r-sat}} = \left(\frac{\psi}{\psi_{opt}}\right)^{l_1 \cdot \left(\frac{\sigma_d}{p_a}\right)^{l_2}} \cdot \left[\frac{1+(a\psi_{opt})^n}{1+(a\psi)^n}\right]^m \quad (18)$$

Table 2 shows the properties of soils 1 - 5 tested by Wang et al. (2017) and Su et al. (2021a), with f_v varying from 0% to 45%. Fig. 2 shows that the same SWRC was obtained for f_v = 0%, 20% and 35% (Su et al. 2021b). This indicated that an increase of f_v led to a constant ψ under a given S_r when keeping the dry density of fine soil constant ($\rho_{dmax\text{-}f}$ = 1.82 Mg/m^3 in Table 2), as expected by Wang et al. (2017, 2018a, 2018b) and Qi et al. (2020a). Fig. 3 shows the comparisons between the measurements by Wang et al. (2017) and Su et al. (2021a) and the calculations by Eq. (18) for the variations of M_r with ψ under different deviator stresses σ_d and five f_v values. It can be observed from Fig. 3(a) that M_r increased with the increase of ψ under a constant σ_d, and a reasonably good agreement was obtained between the measurements and the calculations. Further examination showed that a threshold matric suction ψ_{th} could be identified, corresponding to the intersection of the curves of different deviators stresses (σ_d = 50, 100 and 200 kPa). When $\psi < \psi_{th}$, the M_r decreased with increasing σ_d, while an opposite trend was observed when $\psi > \psi_{th}$. In addition, the increase of σ_d led to a decrease of model parameter l_1, keeping parameter l_2 constant (equal to 1.000). The similar phenomenon was observed in Figs. 3(b) - (e) for f_v = 10% - 45%. It seems that the higher the ψ_{th}, the higher the coefficient of determination R^2 for soils 1-5. Overall, a good agreement was obtained between measurements and calculations, with the $R^2 \geq 0.90$. Figs. 3(a) - (e) indicate that an increase of f_v from 0% to 45% resulted in an increase of $M_{r\text{-}sat}$ from 11 to 85 MPa.

Table 2. Soil properties in Wang et al. (2017) and Su et al. (2021a)

Soil No.	f_v (%)	Fine soil fraction							Soil mixture	
		G_s	w_L (%)	w_p (%)	I_P (%)	$w_{opt\text{-}f}$ (%)	$\rho_{dmax\text{-}f}$ (Mg/m^3)	USCS classification	Compaction $w_{opt\text{-}f}$ (%)	ρ_d (Mg/m^3)
1	0									1.82
2	10									1.91
3	20	2.68	32	12	20	13.7	1.82	CL	13.7	1.99
4	35									2.12
5	45									2.21

Note: f_v represents the ratio of the volume of coarse grains to that of mixture (Su et al. 2021a). G_s, w_L, I_P, $w_{opt\text{-}f}$ and $\rho_{dmax\text{-}f}$ represent the specific gravity, liquid limit, plasticity index, optimum water content and maximum dry density of fine soil, respectively. $w_{opt\text{-}f}$ and $\rho_{dmax\text{-}f}$ were determined by standard Proctor compaction tests for soils 1-5. ρ_d represents the dry density of soil mixture sample. USCS refers to the unified soil classification system: CL, low-plasticity clay; CH, high-plasticity clay; MH, high-plasticity silt; ML, low-plasticity silt.

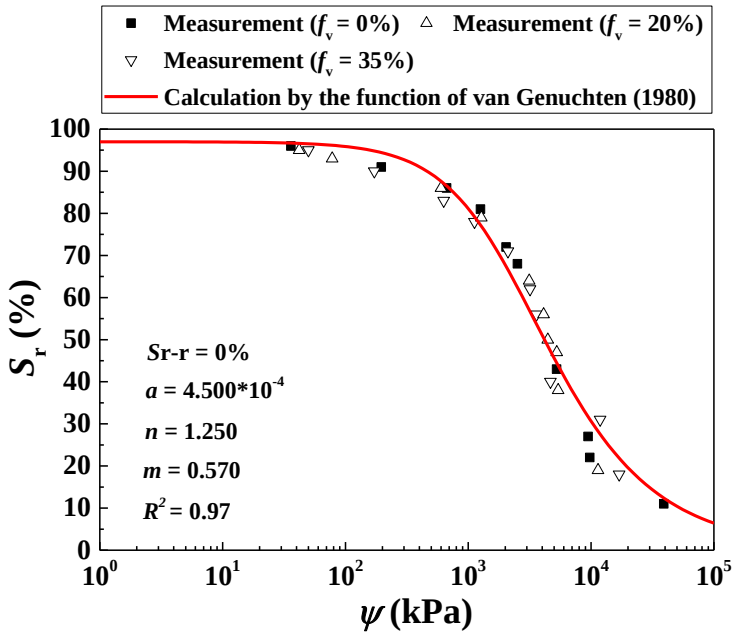

Fig. 2. Measured and calculated soil-water retention curves at varying f_v values for soils 1-5 (after Su et al. 2021b)

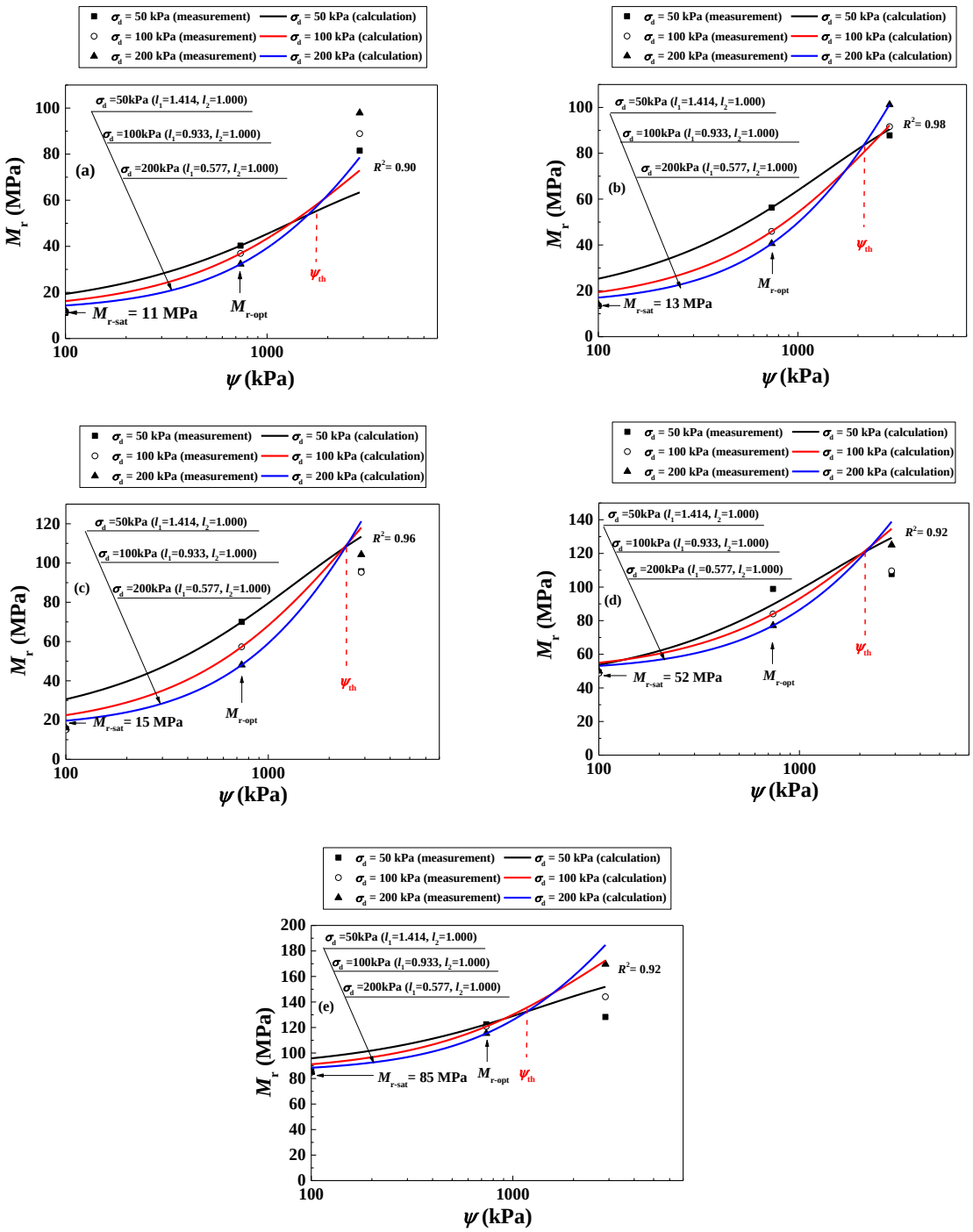

Fig. 3. Measured and calculated variations of M_r with ψ under varying σ_d for soils 1-5: (a) soil 1 at f_v = 0%; (b) soil 2 at f_v = 10%; (c) soil 3 at f_v = 20%; (d) soil 4 at f_v = 35%; (e) soil 5 at f_v = 45% (data from Wang et al. 2017 and Su et al. 2021a)

The M_r - σ_d relationship depended on the combined effects of the soil hardening in the loading process and the rebounding in the unloading process. When $\psi < \psi_{th}$, a matrix structure of fine soil was expected due to the effect of water hydration (Su et al. 2021c). On the contrary, the high ψ induced an aggregated fine soil microstructure (Cui and Delage 1996; Ng et al. 2017). Upon loading, an increase of σ_d contributed to the compression of fine matrix and the rearrangement of fine aggregates (Werkmeister et al. 2004). Thus, an increase of M_r is expected for both fabrics due to the hardening phenomenon. Conversely, in the unloading process, owing to the rebounding effect, the resilient strain increased, which resulted in a decrease of M_r. For the fine matrix fabric ($\psi < \psi_{th}$), due to its larger deformability, the effect of rebounding on M_r appeared to be more significant than the effect of hardening, leading to a decrease of M_r with increasing σ_d. By contrast, for the aggregated fabric ($\psi > \psi_{th}$), owing to its lower deformability, the rebounding effect was not as significant as the hardening effect. In this case, the M_r increased with increasing σ_d. This indicated that ψ_{th} could be considered as the threshold value between the fine matrix fabric (at $\psi < \psi_{th}$) and the fine aggregate fabric (at $\psi > \psi_{th}$). It appeared that ψ_{th} was slightly affected by the coarse grain content f_v. At f_v = 0% - 20%, a fine matrix macrostructure was obtained for soils 1 - 3, while at f_v = 35% - 45% the coarse grains were dominant for soils 4 - 5. With increasing f_v, the transition of these two fabrics contributed to a slight decrease of ψ_{th}, for that less fine soil was needed to be transferred from the fine matrix fabric to the fine aggregate fabric.

Fig. 4 shows the variations of M_r with f_v under varying ψ and a constant σ_d = 200 kPa for soils 1-5. Fig. 5 shows a linear variation of parameter l_1 with log (σ_d/p_a), leading to Eq. (19):

$$l_1 = \alpha_1 \log\left(\frac{\sigma_d}{p_a}\right) + \beta_1 \tag{19}$$

where α_1 and β_1 are model parameters. Eq. (19) allows the determination of the two parameters (α_1 = -1.390, β_1 = 0.967) with a regression coefficient R^2 = 0.99.

Substituting Eq. (19) into Eq. (18) yields Eq. (20):

$$\frac{M_r - M_{r-sat}}{M_{r-opt} - M_{r-sat}} = \left(\frac{\psi}{\psi_{opt}}\right)^{[\alpha_1 \log\left(\frac{\sigma_d}{p_a}\right)+\beta_1]\cdot\left(\frac{\sigma_d}{p_a}\right)} \cdot \left[\frac{1+(a\psi_{opt})^n}{1+(a\psi)^n}\right]^m \tag{20}$$

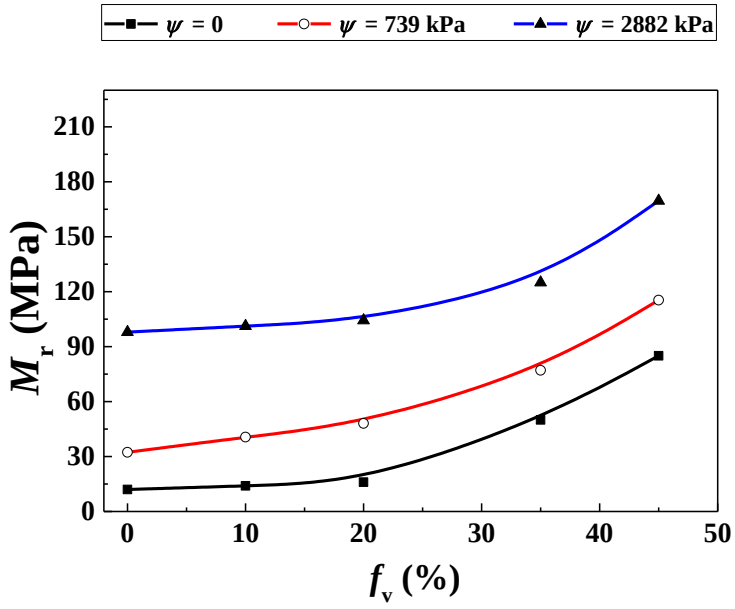

Fig. 4 Variations of M_r with f_v under varying ψ and a constant σ_d = 200 kPa for soils 1-5 (data from Wang et al. 2017 and Su et al. 2021a)

Extending the model to the effect of f_v

Fig. 6 shows the variation of $M_{r\text{-}sat}$ with f_v, measured by Su et al. (2021a) and Duong et al. (2016). Note that the same fine soil fraction was adopted by Su et al. (2021a) and Duong et al. (2016), while the micro-ballast was adopted by Su et al. (2021a) as a substitute of ballast adopted by Duong et al. (2016) following the parallel gradation method. The validity of this method was verified by Qi et al. (2020b). Since an increase of f_v led to a constant ψ under a given S_r (Fig. 2), the term $f(\psi)$ was independent of f_v in Eq. (11). Similarly, the whole term on the right-hand side of Eq. (20) was also independent of f_v. The effect f_v was reflected on the term $M_{r\text{-}sat}$ in Eqs. (11) and (20). It was found from Figs. 3(a) - (e) (Wang et al. 2017 and Su et al. 2021a) that an increase of f_v from 0% to 45% resulted in an increase of $M_{r\text{-}sat}$ from 11 to 85 MPa. This $M_{r\text{-}sat}$ - f_v relationship was expressed by Eq. (21):

$$M_{r-sat} = M_0 + \frac{M_1 - M_0}{1 + e^{k f_v + l}} \tag{21}$$

where M_0 and M_1 are the values of $M_{r\text{-}sat}$ at f_v = 0% and 100%, respectively; k and l are model parameters. Eq. (21) provides good simulations of $M_{r\text{-}sat}$ - f_v relationship measured by Duong et

al. (2016) and Su et al. (2021a) with R^2 = 0.97, using parameters M_0 = 11 MPa, M_1 = 200 MPa, k = -0.163 and l = 7.514.

It appears from Fig. 6 that the $M_{r\text{-}sat}$ - f_v curve could be divided into three zones with two critical f_v values: a fine matrix macrostructure zone at $f_v < f_{v1}$, a transition zone at $f_{v1} < f_v < f_{v2}$ and a coarse grain skeleton zone at $f_v > f_{v2}$. Vallejo and Mawby [36] studied the stiffness and shear strength of sand and clay mixture, and found $f_{v1} \approx 26\%$ and $f_{v2} \approx 56\%$. Cui et al. (2018a), Wang et al. (2018a) and Su et al. (2020) investigated the mechanical behavior of fine/coarse soil mixture subjected to monotonic and cyclic loadings, and defined a characteristic coarse grain content $f_{v\text{-}cha} \approx 25\% \sim 33\%$. They found that a fine matrix macrostructure was identified at $f_v \leq f_{v\text{-}cha}$. Obviously, the $f_{v\text{-}cha}$ identified corresponded to f_{v1}.

Summarizing, Eqs. (20) - (21) allow the determination of the variation of M_r under the combined effects of ψ, σ_d and f_v for the fine/coarse soil mixtures.

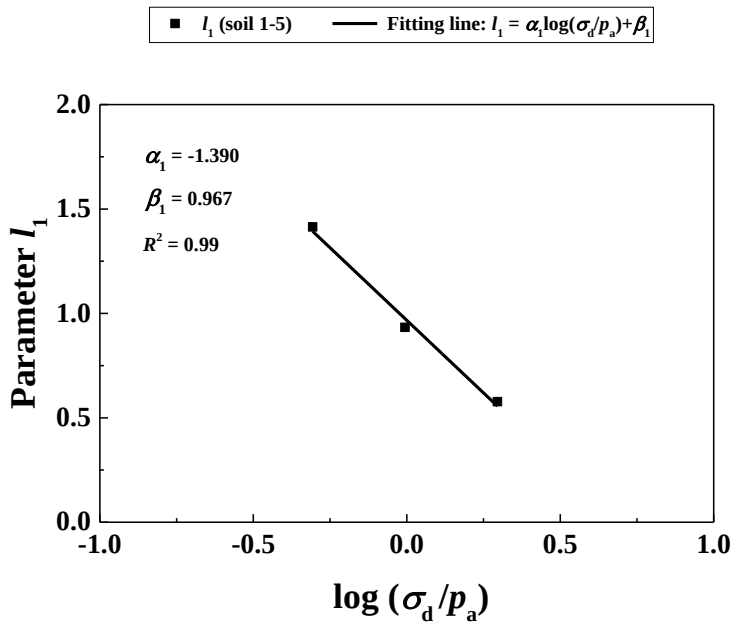

Fig. 5. Variation of parameter l_1 with log (σ_d/p_a) for soils 1-5

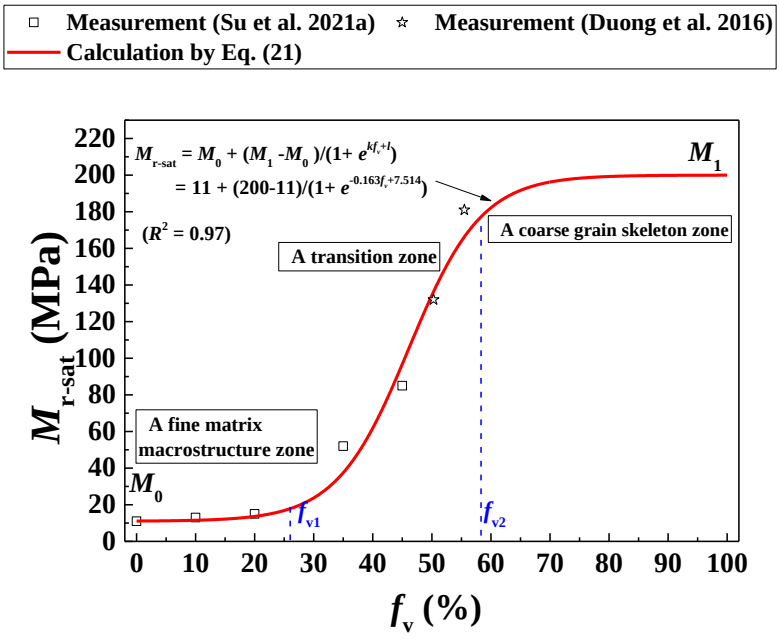

Fig. 6. Measured and calculated variation of $M_{r\text{-}sat}$ with f_v

Validation of the proposed model

Table 3 shows the properties of soils 6 - 12 compiled from five different studies. As f_v = 0% in these studies, Eq. (21) was simplified to Eq. (22):

$$M_{r-sat} = M_0 \quad (22)$$

Soils 6 - 12 were divided into two categories. Category I included soils 6 - 8 (Zaman and Khoury 2007), soil 9 (Gupta et al. 2007) and soil 10 (Ng et al. 2013), for which M_r decreased with increasing σ_d under a given ψ. The ψ values considered were supposed to be smaller than ψ_{th}. Category II included soils 11 - 12 (Yang et al. 2005, 2008), for which a value of ψ_{th} existed separating the ψ into two zones: with increasing σ_d, the M_r decreased at $\psi < \psi_{th}$ but increased at $\psi > \psi_{th}$. It is worth noting that ψ_{th} appeared soil type – dependent: smaller than ψ_{opt} for soils 11 - 12 (Yang et al. 2005, 2008) and larger than ψ_{opt} for soils 1 - 5 (Wang et al. 2017; Su et al. 2021a). The plastic limit w_p can be helpful in explaining this phenomenon. With respect to the findings of Delage et al. (1996), w_p was the threshold value between the fine matrix fabric and the fine aggregate fabric. For soils 1-5, the plastic limit w_p = 12% was smaller than $w_{opt\text{-}f}$ = 13.7% (Table 2), leading to $\psi_{th} > \psi_{opt}$. On the contrary, for soils 11-12, the w_p = 34% and 22% were larger than $w_{opt\text{-}f}$ = 18.1% and 16.8% respectively (Table 3), leading to $\psi_{th} < \psi_{opt}$.

Table 3. Soil properties in five different studies

Reference	Soil No.	f_v (%)	Fine soil fraction							Soil mixture	
			G_s	w_L (%)	w_p (%)	I_P (%)	w_{opt-f} (%)	ρ_{dmax-f} (Mg/m^3)	USCS classification	Compaction w (%)	ρ_d (Mg/m^3)
Zaman and Khoury (2007)	6	0	N/A	55	25	30	23.5	1.53	CH	19.5	
	7									23.5	1.53
	8									27.5	
Gupta et al. (2007)	9		2.75	28	17	11	13.5	1.79	CL	13.5	1.79
Ng et al. (2013)	10		2.73	43	29	14	16.3	1.76	ML	16.3	1.76
Yang et al. (2005)	11		2.71	54	34	20	18.1	1.76	MH	18.1	1.76
Yang et al. (2008)	12		2.67	37	22	15	16.8	1.77	CL	16.8	1.77

Note: w_{opt-f} and ρ_{dmax-f} were determined by standard Proctor compaction tests for soils 6-11, while modified Proctor compaction test for soils 12; N/A means data not available in the reference.

Zaman and Khoury (2007) studied the effects of compaction water content and matric suction on M_r for Burleson soil (soils 6, 7 and 8 in Table 3). In their study, the soils were compacted at w = 19.5% (optimum water content of fine soil w_{opt-f} - 4%), 23.5% (w_{opt-f}) and 27.5% (w_{opt-f} + 4%) respectively and at the same maximum dry density of soil ρ_{dmax-f} = 1.53 Mg/m^3. Cyclic triaxial tests were performed under a constant deviator stress σ_d = 28 kPa and a constant confining pressure σ_c = 41 kPa. The filter paper method was adopted to measure the matric suction ψ after completion of the cyclic tests. Fig. 7(a) shows the measured and calculated SWRCs for soils 6, 7 and 8 using Eq. (17) with the parameters shown in Table 4. The different SWRCs for soils 6, 7 and 8 were the consequences of their varying compaction water contents, as reported by Delage et al. (1996) and Vanapalli et al. (1999). Figs. 7(b) - (d) depict the variations of M_r with ψ under σ_d = 28 kPa for soils 6, 7 and 8 respectively. Eq. (20) calculated the variations of M_r with ψ for these three soils using parameter α_1 = 0 and β_1 = 2.891. Comparisons between the measurements and calculations showed a good agreement (R^2 = 0.95).

Table 4. Parameters of SWRCs for soils 1-12

Soil No.	$S_{r\text{-}r}$ (%)	a	n	m	R^2	SWRC type
1						
2						
3		$4.500*10^{-4}$	1.250	0.570	0.97	Drying SWRC
4						
5						
6		$1.770*10^{-3}$	1.540	0.126	0.91	
7	0	$6.500*10^{-8}$	0.662	70.750	0.95	Apparent SWRC
8		$3.200*10^{-4}$	1.624	0.306	0.89	
9		$1.656*10^{-4}$	0.769	1.049	0.99	
10		$1.120*10^{-6}$	0.688	243.330	0.99	Drying SWRC
11		0.034	2.747	0.021	0.98	
12		0.139	0.779	0.197	0.98	

Note: Drying SWRC was obtained by following a desaturation path; Apparent SWRC was obtained by the S_r - ψ relationships determined after cyclic tests.

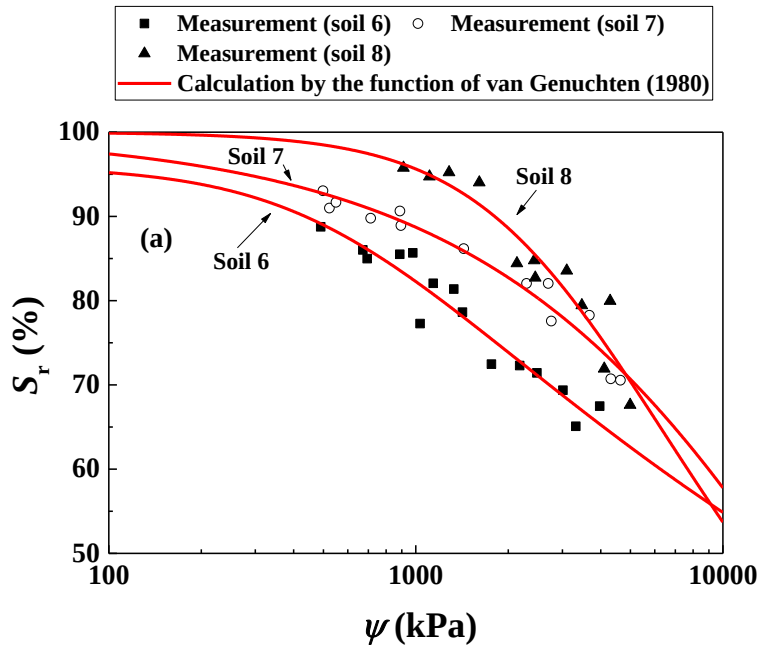
Measurement (soil 6)
Measurement (soil 7)
Measurement (soil 8)
Calculation by the function of van Genuchten (1980)
Soil 7
Soil 8
Soil 6
(a)
S_r (%)
ψ (kPa)

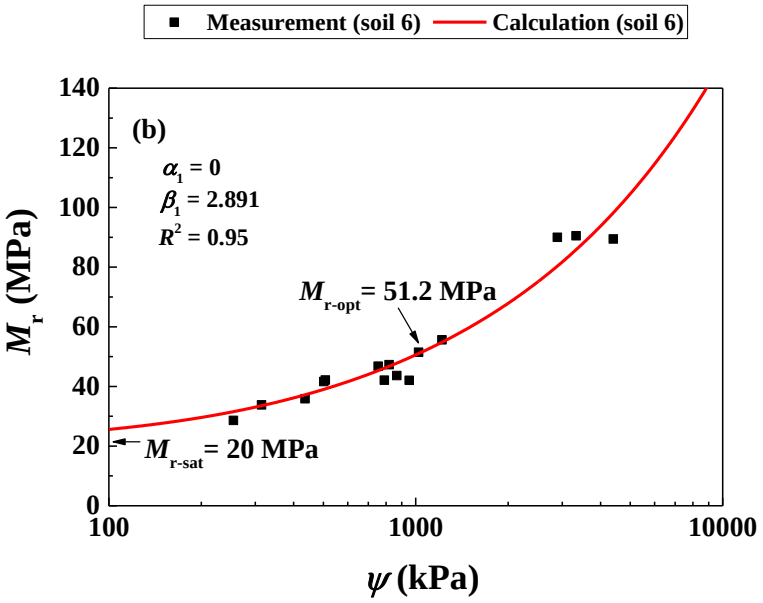
Measurement (soil 6)
Calculation (soil 6)
(b)
α_1 = 0
β_1 = 2.891
R^2 = 0.95
$M_{r\text{-}opt}$ = 51.2 MPa
$M_{r\text{-}sat}$ = 20 MPa
M_r (MPa)
ψ (kPa)

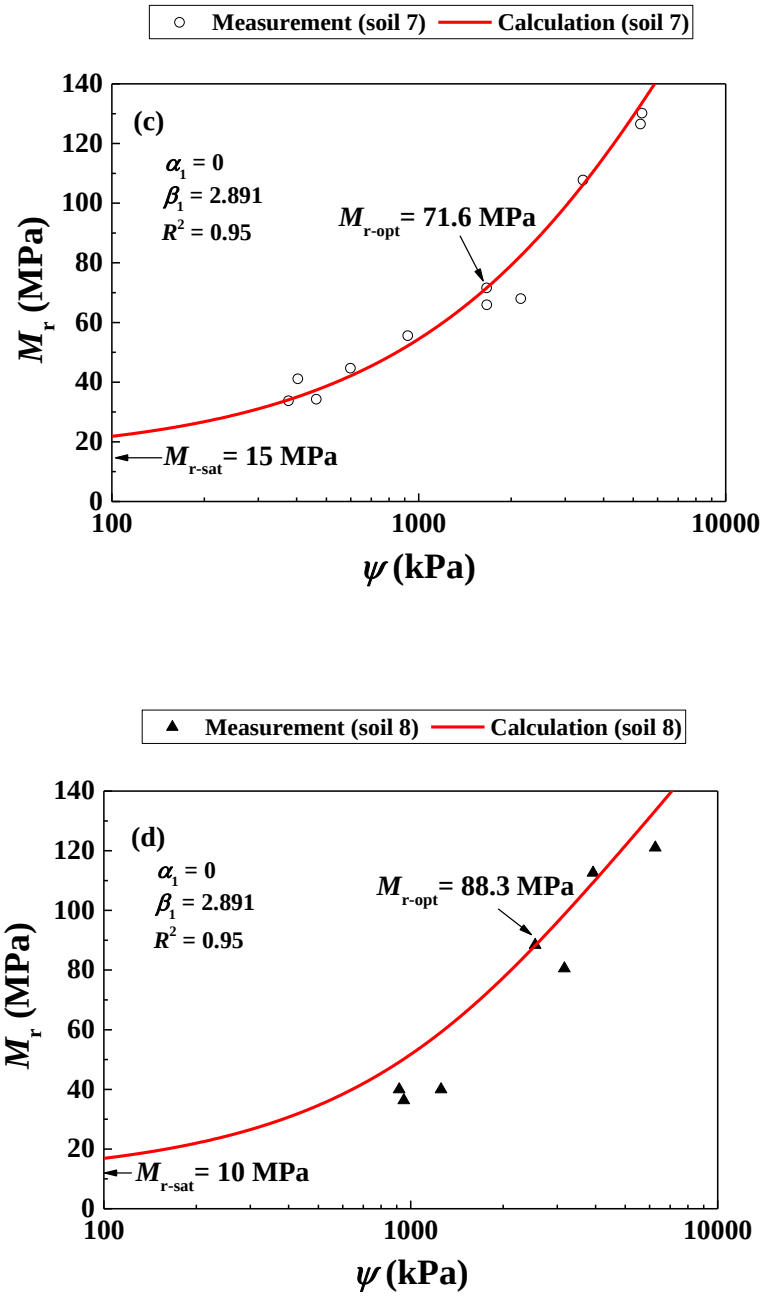

Fig. 7. Measured and calculated (a) SWRCs and (b)-(d) variations of M_r with ψ for soils 6-8 (data from Zaman and Khoury 2007)

Gupta et al. (2007) investigated the effects of ψ and σ_d on M_r of Duluth slope soil (soil 9 in Table 3). Soil 9 was compacted at $w_{opt\text{-}f}$ = 13.5% and $\rho_{dmax\text{-}f}$ = 1.79 Mg/m^3, defining a matric suction ψ_{opt} = 245 kPa, which was measured using a thermal dissipation sensor. The compacted soil was then subjected to a saturation process, followed by a drying process to different target suctions. Cyclic triaxial tests were performed for the M_r measurement, with axis- translation

technique and a thermal dissipation sensor adopted for suction control and measurement. A multi-stage loading with σ_d = 30, 50, 70 and 100 kPa was adopted under a constant σ_c = 14.5 kPa. Fig. 8(a) shows the measured and calculated SWRCs for soil 9 using Eq. (17). It appears from Fig. 8(b) that M_r increased with increasing ψ under a constant σ_d, and the increase of σ_d led to a decrease of M_r in the full measured ψ range. Eq. (20) provides the calculated results using parameters α_1 = -2.808 and β_1 = 1.046. Comparisons between the measurements and calculations showed a good agreement (R^2 = 0.98).

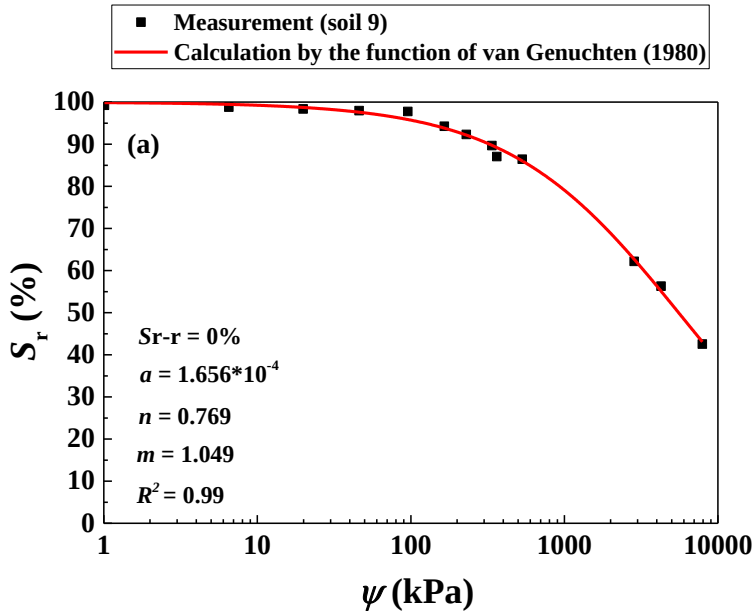

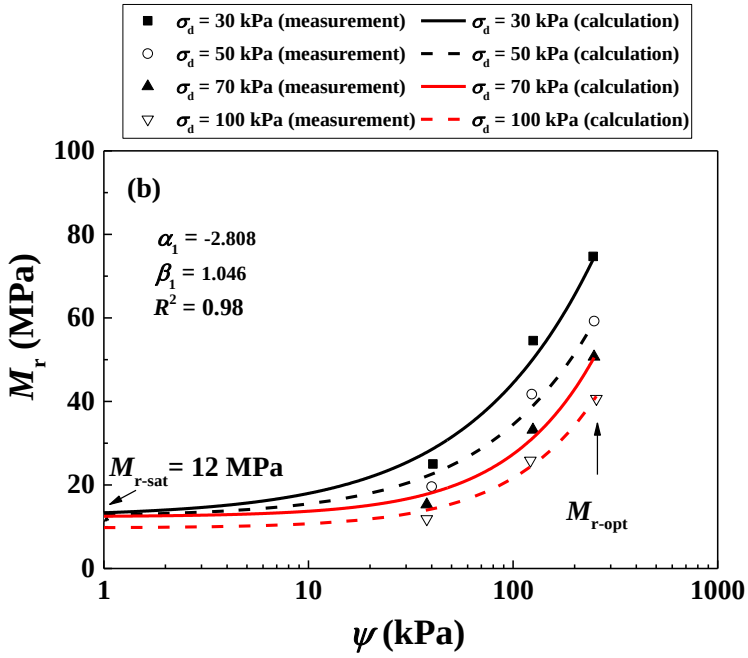

Fig. 8. Measured and calculated (a) SWRC and (b) variations of M_r with ψ for soil 9 (data from Gupta et al. 2007)

Ng et al. (2013) investigated the variations of M_r with ψ under varying σ_d for a completely decomposed tuff (soil 10 in Table 3). Soil 10 was compacted at $w_{opt\text{-}f}$ = 16.3% and $\rho_{dmax\text{-}f}$ = 1.76 Mg/m^3, and its corresponding ψ_{opt} = 95 kPa was measured by a suction probe. The compacted soil was then wetted or dried to different target suctions. Suction-controlled cyclic triaxial tests were performed under varying σ_d = 30, 40, 55 and 70 kPa and a constant σ_c = 30 kPa. Fig. 9(a) presents the measured and fitted SWRCs using Eq. (17). Fig. 9(b) depicts the variations of M_r with ψ under varying σ_d measured by Ng et al. (2013) and those calculated by Eq. (20) using α_1 = -4.126 and β_1 = 1.535. A good agreement was observed between the measurements and the calculations (R^2 = 0.96).

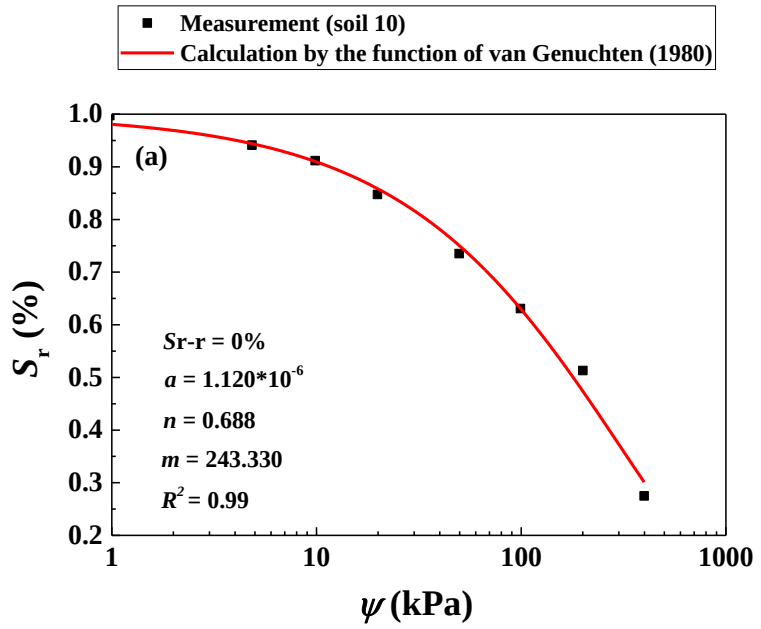

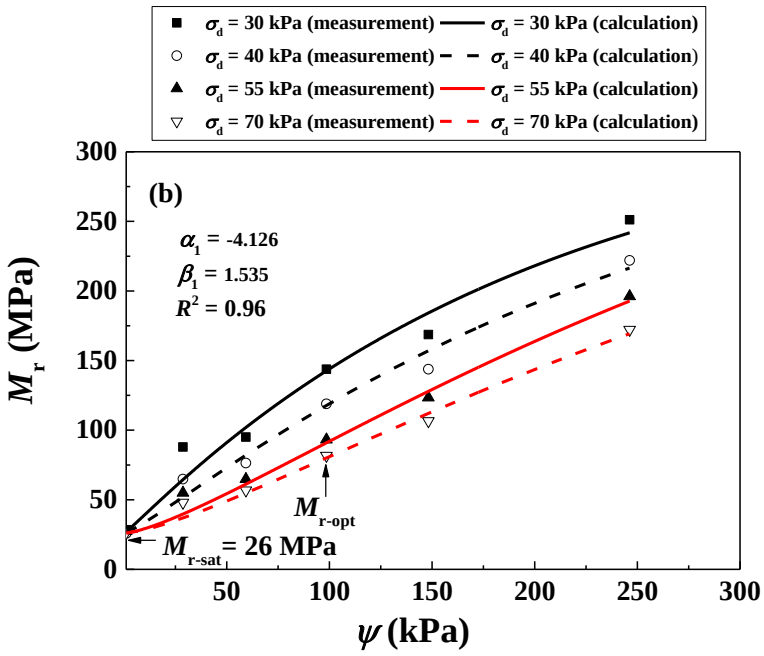

Fig. 9. Measured and calculated (a) SWRC and (b) variations of M_r with ψ for soil 10 (data from Ng et al. 2013)

Yang et al. (2005) studied the variations of M_r with ψ under varying σ_d for a compacted subgrade soil (soil 11 in Table 3). Soil 11 was compacted at $w_{opt\text{-}f}$ = 18.1% and $\rho_{dmax\text{-}f}$ = 1.76 Mg/m^3, with a matric suction ψ_{opt} = 5580 kPa measured using the filter paper method. The compacted soil was then wetted to higher water contents (lower suctions). Cyclic triaxial tests were performed under varying σ_d = 21, 34, 48, 69, 103 kPa and a constant σ_c = 21 kPa. After completion of the tests, the filter paper method was applied to measure the matric suction ψ. Fig. 10(a) shows the SWRCs measured by Yang et al. (2006) and fitted by Eq. (17). Fig. 10(b) compares the measured M_r at different ψ and σ_d values and the corresponding calculated M_r by Eq. (20) with parameters α_1 = -4.928 and β_1 = 0.681. A threshold matric suction ψ_{th} could be identified, separating the ψ into two zones with different effects of σ_d.

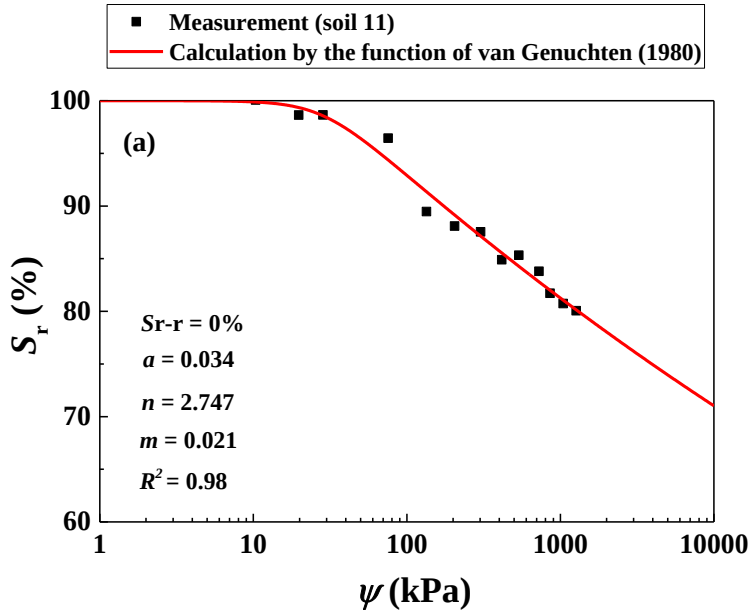

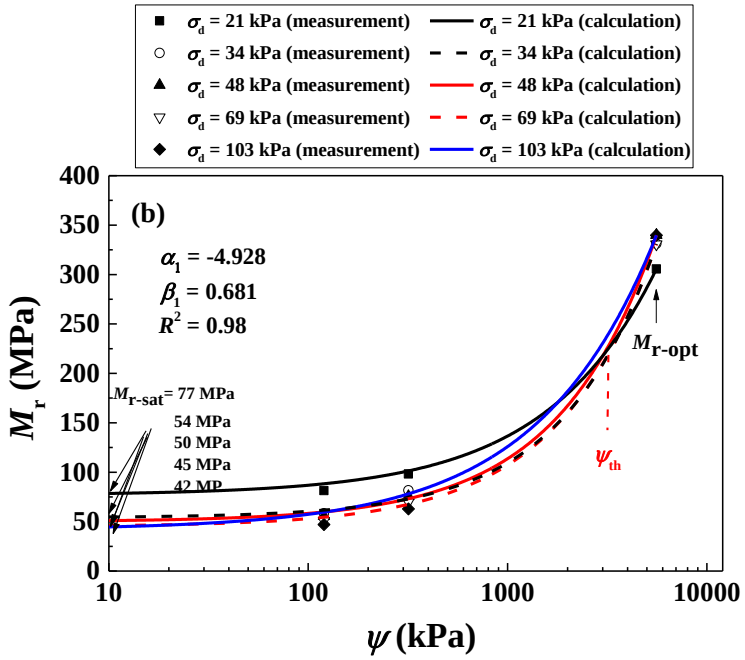

Fig. 10. Measured and calculated (a) SWRC (data from Yang et al. 2006) and (b) variations of M_r with ψ for soil 11 (data from Yang et al. 2005)

Yang et al. (2008) investigated the variations of M_r with ψ under varying σ_d for a compacted mudstone soil (soil 12 in Table 3). Soil 12 was compacted at $w_{opt\text{-}f}$ = 16.8% and $\rho_{dmax\text{-}f}$ = 1.77 Mg/m^3, defining a matric suction ψ_{opt} = 500 kPa which was measured by the filter paper method. It was then wetted to higher water contents (19.1%, 20.2% and 23.2%) to reach various suctions (450, 150 and 50 kPa respectively). Cyclic triaxial tests were performed with suction controlled by the axis-translation technique. Four deviator stresses σ_d = 34, 48, 69 and 103 kPa were applied in sequence under a constant σ_c = 21 kPa. Fig. 11(a) shows the measured and fitted SWRCs by Eq. (17). Fig. 11(b) depicts the variations of M_r with ψ under varying σ_d measured by Yang et al. (2008) and those calculated by Eq. (20) with parameters α_1 = -3.943 and β_1 = 1.606. A ψ_{th} was identified from Fig. 11(b), separating the ψ into two zones with different effects of σ_d, which was consistent with the observation in Fig. 10(b).

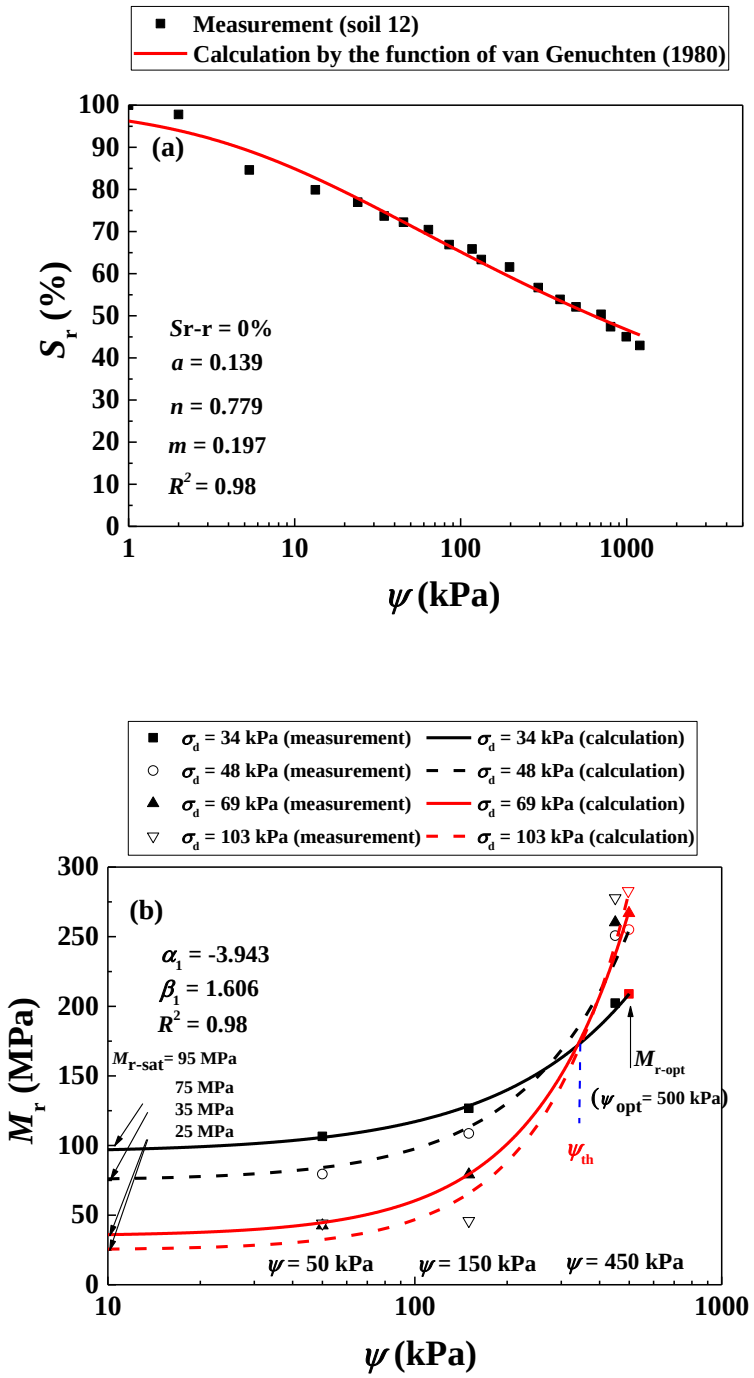

Fig. 11. Measured and calculated (a) SWRC and (b) variations of M_r with ψ for soil 12 (data from Yang et al. 2008)

Table 5 presents the values of model parameters α_1 and β_1 in the proposed Eq. (20) for soils 1-12, indicating that these parameters are dependent of soil studied. Fig. 12 shows the comparison between the measured and the calculated M_r values using Eq. (20) for soils 1-12 listed in Tables 2 and 3, illustrating that the proposed Eq. (20) provides satisfactory simulations with $R^2 = 0.98$.

Table 5. Values of model parameters in the proposed Eq. (20) for soils 1-12

Reference	Soil. No	α_1	β_1	R^2
Wang et al. (2017) and Su et al. (2021a)	1	-1.390	0.967	0.90
	2			0.98
	3			0.96
	4			0.92
	5			0.92
Zaman and Khoury (2007)	6	0	2.891	0.95
	7			0.95
	8			0.95
Gupta et al. (2007)	9	-2.808	1.046	0.98
Ng et al. (2013)	10	-4.126	1.535	0.96
Yang et al. (2005)	11	-4.928	0.681	0.98
Yang et al. (2008)	12	-3.943	1.606	0.98

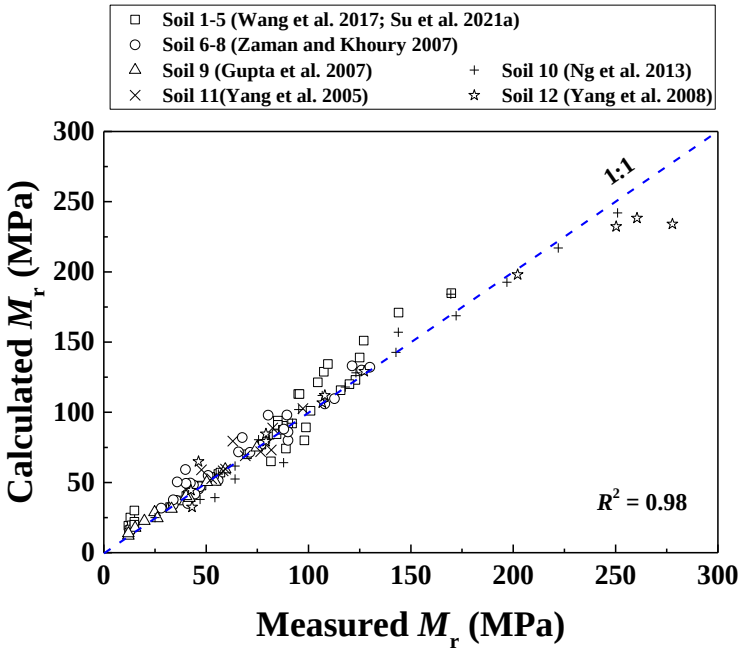

Fig. 12. Comparison between measured and calculated M_r values for soils 1-12

Comparison between the prosed model and representative existing models

To better illustrate the performance of the proposed model, a comparison was made with some representative existing models. According to Han and Vanapalli (2016b), the constitutive

models of M_r could be categorized into three groups: group A - empirical models (e.g. Eqs. (1) - (4) and (9)); group B - models incorporating ψ into deviator or mean stresses (e.g. Eqs. (5) - (6)); group C- models considering ψ as an independent term (e.g. Eqs. (7) - (8) and (10)). Three representative models were selected from these three groups: Eq. (9) (ARA, Inc., ERES Consultants Division. 2004), Eq. (5) (Liang et al. 2008) and Eq. (10) (Han and Vanapalli 2005) for groups A, B and C, respectively. Note that Eqs. (9) - (10) incorporated SWRC using Eq. (17). Three studies were adopted for the comparison among (Table 6): soil 10 (Ng et al. 2013) of category I ($\psi < \psi_{th}$), soil 12 (Yang et al. 2008) of category II ($\psi > \psi_{th}$ and $\psi_{th} < \psi_{opt}$) and soil 5 (Wang et al. 2017; Su et al. 2021a) of category II ($\psi > \psi_{th}$ and $\psi_{th} > \psi_{opt}$).

Fig. 13(a) shows the M_r measured by Ng et al. (2013) and that calculated by Eq. (9) using parameters a = -0.593, b = 0.400 and k_m = 6.132. A reasonably good agreement was obtained between the measurements and the calculations (R^2 = 0.94). The similar phenomenon was observed in Figs. 13(b) - (c): Eqs. (5) and (10) provided satisfactory simulations with parameters presented in Table 6 (R^2 = 0.97 and 0.92, respectively). This indicates that in the case of category I ($\psi < \psi_{th}$), all the three representative existing models as well as the proposed Eq. (20) can be used to describe the M_r variations.

Table 6. Model parameters for three representative existing models

Equation/ Parameter	Category I: $\psi < \psi_{th}$	Category II: $\psi > \psi_{th}$					
	Soil 10	$\psi_{th} < \psi_{opt}$ Soil 12	$\psi_{th} > \psi_{opt}$ Soil 1	Soil 2	Soil 3	Soil 4	Soil 5
Eq. (9)							
a	-0.593	-0.593					
b	0.400	0.400					
k_m	6.132	6.132			—		
R^2	0.94	0.72					
Eq. (5)							
k_4	0.453	0.513					
k_5	3.287	1.337					
k_6	-6.887	-1.303			—		
R^2	0.97	0.75					
Eq. (10)							
ξ	1.092	0.983	1.105	0.846	0.714	0.637	0.423
R^2	0.92	0.94	0.88	0.85	0.82	0.68	0.67

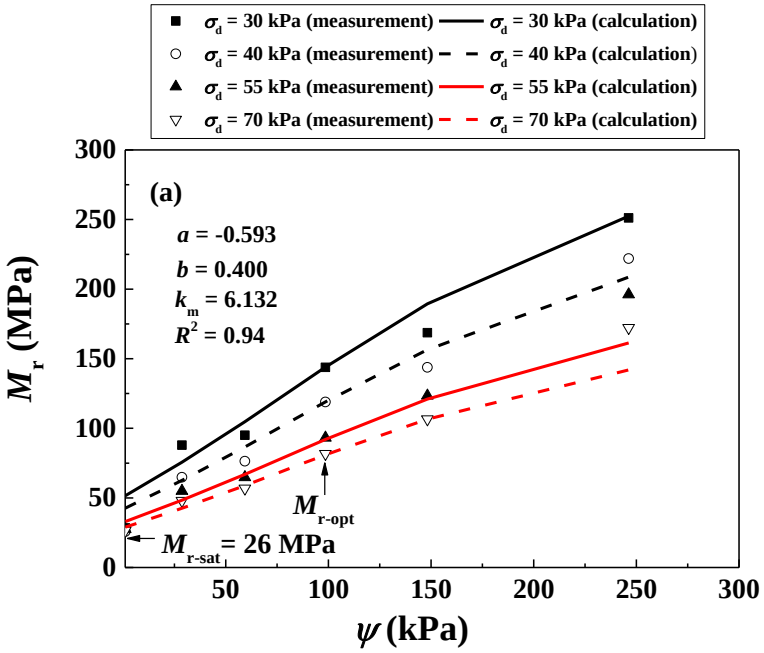

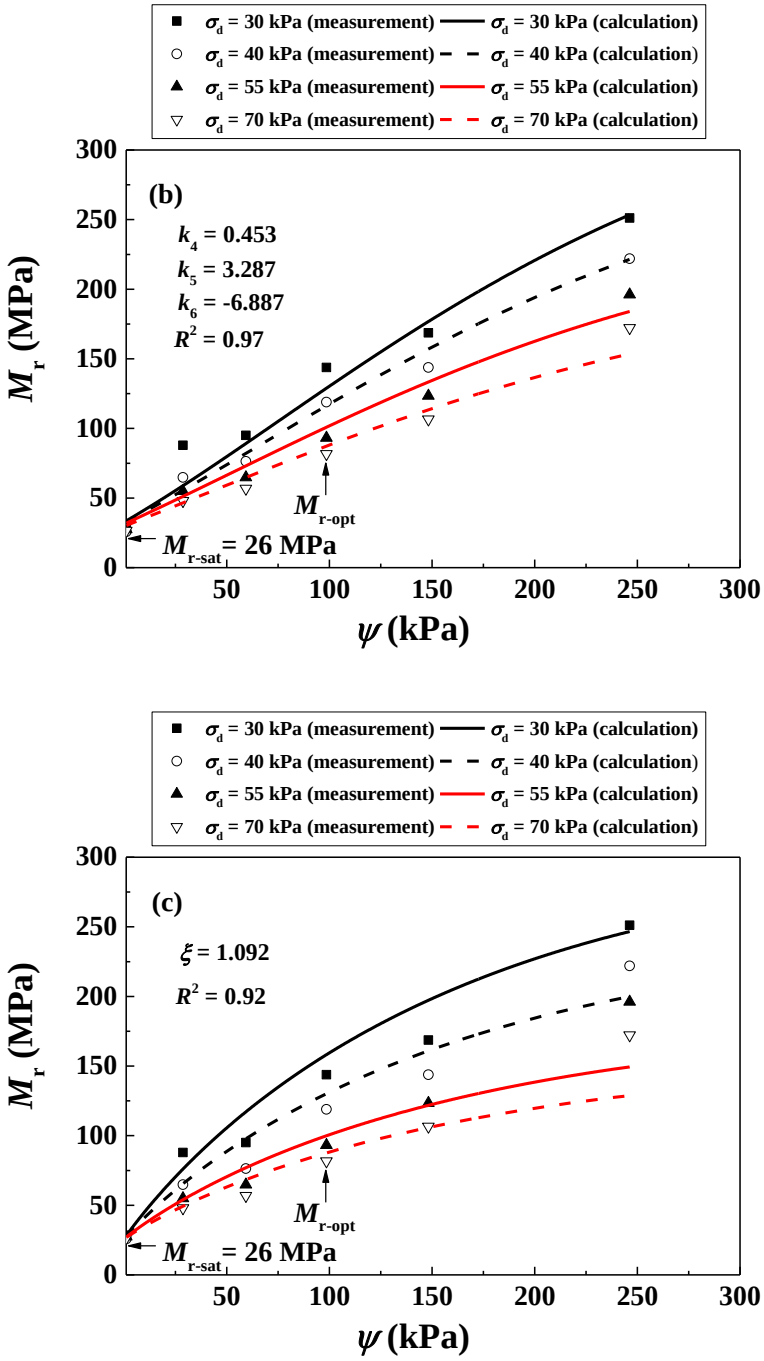

Fig. 13. Comparisons between the variations of M_r with ψ for soil 10 measured by Ng et al. (2013) and those calculated by: (a) Eq. (9) (ARA, Inc., ERES Consultants Division. 2004); (b) Eq. (5) (Liang et al. 2008); (c) Eq. (10) (Han and Vanapalli 2015)

Fig. 14(a) shows the M_r measured by Yang et al. (2008) and that calculated by Eq. (9). Compared with Eq. (20) (the proposed model), Eq. (9) provided less satisfactory simulations: R^2 = 0.72 for Eq. (9) against R^2 = 0.98 for Eq. (20) (see Fig. 11(b)). More importantly, the ψ_{th} cannot be reproduced by Eq. (9). The similar observations were made from Fig. 14(b) for Eq. (5). On the contrary, Fig. 14(c) shows good simulations by Eq. (10) with R^2 = 0.94 using parameter ξ = 0.983. Moreover, the ψ_{th} ($< \psi_{opt}$ = 500 kPa in Yang et al. 2008) was identified, separating the ψ into two zones with different effects of σ_d. This indicates that in the case of category II ($\psi > \psi_{th}$ and $\psi_{th} < \psi_{opt}$), among the three representative models, only Eq. (10) can be used describe the M_r variations.

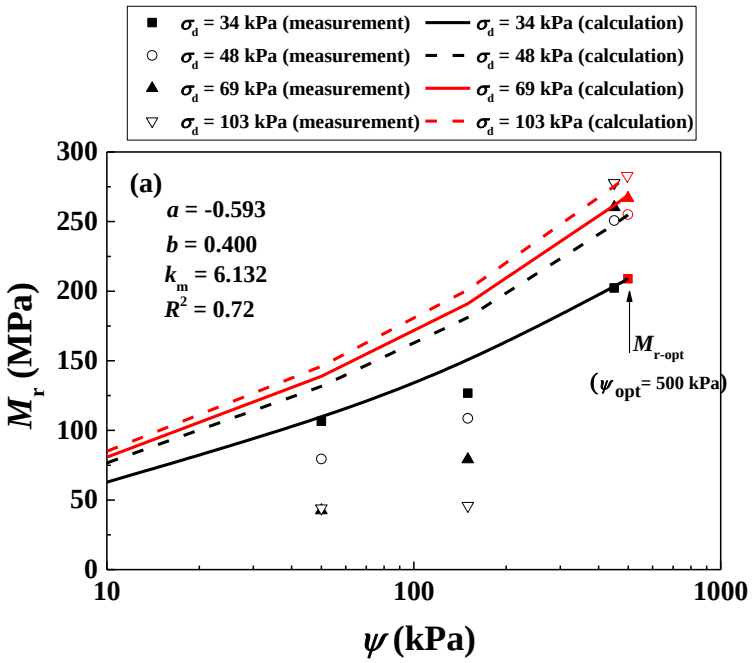

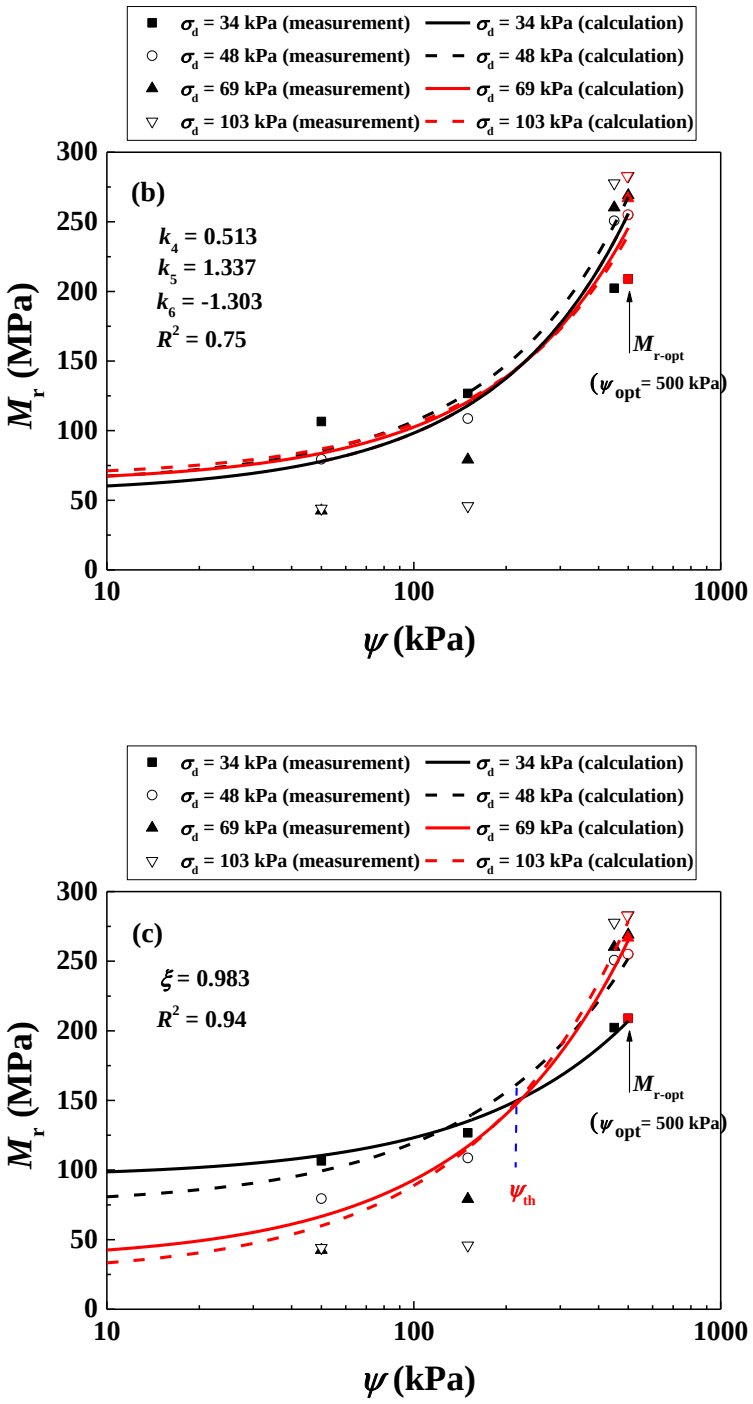

Fig. 14. Comparisons between the variations of M_r with ψ for soil 12 measured by Yang et al. (2008) and those calculated by: (a) Eq. (9) (ARA, Inc., ERES Consultants Division. 2004); (b) Eq. (5) (Liang et al. 2008); (c) Eq. (10) (Han and Vanapalli 2015)

Fig. 15 shows the comparisons between the M_r measured by Wang et al. (2017) and Su et al. (2021a) and that calculated by Eq. (10) for soils 1-5. Since Eqs. (5) and (9) cannot fit well for soil 12 of category II ($\psi_{th} < \psi_{opt}$, see details in Figs. 14(a) - (b)), they were excluded for soils 1-5 of category II ($\psi_{th} > \psi_{opt}$). Figs. 15(a) - (e) show that Eq. (10) provides simulation results with R^2 = 0.88, 0.85, 0.82, 0.68 and 0.67, smaller than R^2 = 0.90, 0.98, 0.96, 0.92 and 0.92 by the proposed Eq. (20) for soils 1-5 respectively. Moreover, the increase of σ_d led to a decrease of calculated M_r by Eq. (10) in the full ψ range, without identifying ψ_{th}. This indicated that Eq. (10) is not suitable for the case of category II ($\psi_{th} > \psi_{opt}$). This can be explained by the consideration of two reference M_r values- $M_{r\text{-}sat}$ and $M_{r\text{-}opt}$ in Eq. (10). Indeed, through such consideration, the variation of M_r from the saturated condition to the OMC condition (ψ varies from 0 to ψ_{opt}) is expected to be well depicted (see Fig. 14 (c)). However, when $\psi_{th} > \psi_{opt}$, the good description of Eq. (10) is no longer guaranteed (see Fig. 15).

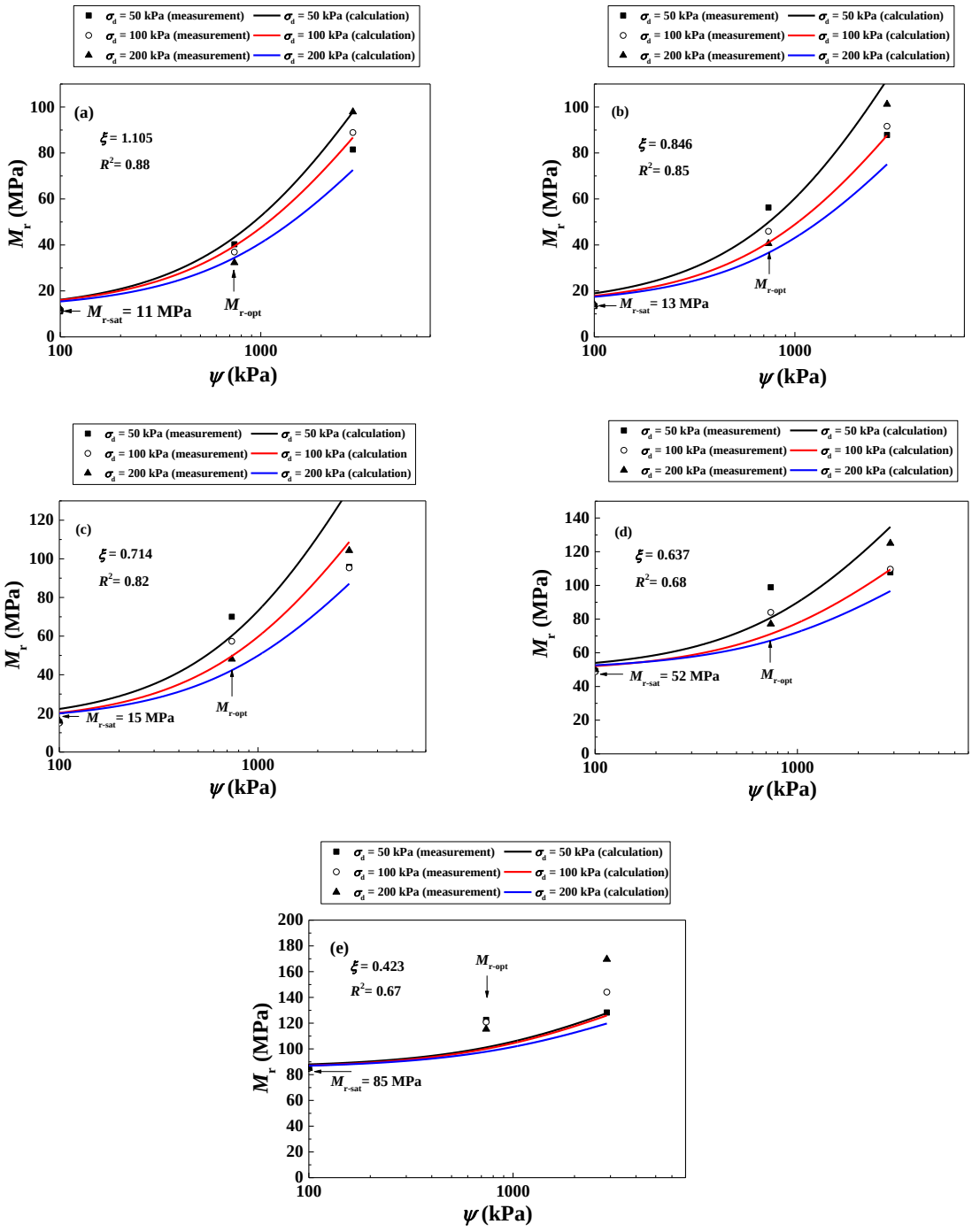

Fig. 15. Comparisons between the variations of M_r with ψ for soils 1 - 5 measured by Wang et al. (2017) and Su et al. (2021a) and those calculated by Eq. (10) (Han and Vanapalli 2015): (a) soil 1 at f_v = 0%; (b) soil 2 at f_v = 10%; (c) soil 3 at f_v = 20%; (d) soil 4 at f_v = 35%; (e) soil 5 at f_v = 45%

The comparison of different models indicates that the variation of M_r can be well described by Eqs. (9), (5) and (10) from group A, B and C for category I ($\psi < \psi_{th}$). For category II ($\psi_{th} < \psi_{opt}$), only Eq. (10) among the three representative models can give satisfactory description, while for category II ($\psi_{th} > \psi_{opt}$), even Eq. (10) fails. This leads to the conclusion that only the proposed Eq. (20) which incorporates the combined effects of σ_d and ψ on the M_r in the full range of suction can provide good description for both $\psi_{th} < \psi_{opt}$ and $\psi_{th} > \psi_{opt}$.

It is worth noting that as the existing models incorporating SWRC, such as Eq. (10) (Han and Vanapalli 2015), the hysteresis effect has not been accounted for. Further studies are needed to extend the proposed model to the hysteresis effect.

Conclusions

A constitutive model was proposed to describe the variation of resilient modulus M_r with matric suction ψ and deviator stress σ_d. This model was then extended to the effect of coarse grain content f_v based on the experimental data from Wang et al. (2017) and Su et al. (2021a) to describe the variation of M_r for unsaturated fine/coarse soil mixtures. The model incorporates soil-water retention curve (SWRC). The key parameters are the resilient modulus at saturated sate $M_{r\text{-}sat}$, the resilient modulus at optimum state $M_{r\text{-}opt}$, the matric suction at optimum state ψ_{opt}, soil parameters α_1 and β_1, as well as the parameters related to SWRC. The proposed model was validated using five different studies. A comparative study was also conducted between the proposed model and three representative existing models from literature. The following conclusions can be drawn:

The effect of σ_d on M_r was found to be highly dependent on ψ, with a threshold matric suction ψ_{th} separating ψ into two zones: with an increasing σ_d, the M_r decreased at $\psi < \psi_{th}$, while increased at $\psi > \psi_{th}$. Using the threshold matric suction $\psi_{th,}$ previous studies from literature could be divided into two categories: category I ($\psi < \psi_{th}$) and category II ($\psi > \psi_{th}$). For category I ($\psi < \psi_{th}$), the variation of M_r could be satisfactorily described by the three representative models. For category II ($\psi > \psi_{th}$), only Eq. (10) among the three representative models provided satisfactory simulations in the case of $\psi_{th} > \psi_{opt}$. However, in the case of $\psi_{th} < \psi_{opt}$, Eq. (10) failed also. Unlike the three representative models, the proposed model Eq. (20) could gave good results in the full ψ range. In addition, the effect of f_v was well incorporated using Eq. (21). Thus, the proposed model constitutes a helpful tool for describing

the variation of resilient modulus of unsaturated fine/coarse soil mixtures under the combined effects of deviator stress and suction

Acknowledgements

This work was supported by the China Scholarship Council (CSC) and Ecole des Ponts ParisTech.

References

ARA, Inc., ERES Consultants Division. 2004. Guide for mechanistic - empirical design of new and rehabilitated pavement structures. Final report, NCHRP Project 1-37A. Transportation Research Board, Washington, D.C.

Alonso, E. E., Pereira, J. M., Vaunat, J., & Olivella, S. 2010. A microstructurally based effective stress for unsaturated soils. Géotechnique, 60(12), 913-925.

Ba, M., Nokkaew, K., Fall, M., & Tinjum, J. M. 2013. Effect of matric suction on resilient modulus of compacted aggregate base courses. Geotechnical and Geological Engineering, 31(5), 1497-1510.

Cui, Y. J., & Delage, P. 1996. Yielding and plastic behaviour of an unsaturated compacted silt. Géotechnique, 46(2), 291-311.

Cui, Y. J. 2018. Mechanical behaviour of coarse grains/fines mixture under monotonic and cyclic loadings. Transportation Geotechnics, 17, 91-97.

Delage, P., Audiguier, M., Cui, Y.J. and Howat, M.D., 1996. Microstructure of a compacted silt. *Canadian Geotechnical Journal*, *33*(1), pp.150-158.

Duong, T. V., Cui, Y. J., Tang, A. M., Dupla, J. C., Canou, J., Calon, N., & Robinet, A. 2016. Effects of water and fines contents on the resilient modulus of the interlayer soil of railway substructure. Acta Geotechnica, 11(1), 51-59.

Gupta, S., Ranaivoson, A., Edil, T., Benson, C., & Sawangsuriya, A. 2007. Pavement design using unsaturated soil technology.

Heath, A. C., Pestana, J. M., Harvey, J. T., & Bejerano, M. O. 2004. Normalizing behavior of unsaturated granular pavement materials. Journal of Geotechnical and Geoenvironmental Engineering, 130(9), 896-904.

Han, Z., & Vanapalli, S. K. 2015. Model for predicting resilient modulus of unsaturated subgrade soil using soil-water characteristic curve. Canadian Geotechnical Journal, 52(10), 1605-1619.

Han, Z., & Vanapalli, S. K. 2016a. Stiffness and shear strength of unsaturated soils in relation to soil-water characteristic curve. Géotechnique, 66(8), 627-647.

Han, Z., & Vanapalli, S. K. 2016b. State-of-the-Art: Prediction of resilient modulus of unsaturated subgrade soils. International Journal of Geomechanics, 16(4), 04015104.

Khoury, N., Brooks, R., Boeni, S. Y., & Yada, D. 2013. Variation of resilient modulus, strength, and modulus of elasticity of stabilized soils with postcompaction moisture contents. Journal of Materials in Civil Engineering, 25(2), 160-166.

Liang, R. Y., Rabab'ah, S., & Khasawneh, M. 2008. Predicting moisture-dependent resilient modulus of cohesive soils using soil suction concept. Journal of Transportation Engineering, 134(1), 34-40.

Lu, N., Godt, J. W., & Wu, D. T. 2010. A closed-form equation for effective stress in unsaturated soil. Water Resources Research, 46(5).

Moossazadeh, J., & Witczak, M. W. 1981. Prediction of subgrade moduli for soil that exhibits nonlinear behavior. Transportation Research Record, (810).

Nowamooz, H., Chazallon, C., Arsenie, M. I., Hornych, P., & Masrouri, F. 2011. Unsaturated resilient behavior of a natural compacted sand. Computers and Geotechnics, 38(4), 491-503.

Ng, C. W. W., Zhou, C., Yuan, Q., & Xu, J. 2013. Resilient modulus of unsaturated subgrade soil: experimental and theoretical investigations. Canadian Geotechnical Journal, 50(2), 223-232.

Ng, C. W. W., Baghbanrezvan, S., Sadeghi, H., Zhou, C., & Jafarzadeh, F. 2017. Effect of specimen preparation techniques on dynamic properties of unsaturated fine-grained soil at high suctions. Canadian Geotechnical Journal, 54(9), 1310-1319.

Oh, W. T., Vanapalli, S. K., & Puppala, A. J. 2009. Semi-empirical model for the prediction of modulus of elasticity for unsaturated soils. Canadian Geotechnical Journal, 46(8), 903-914.

Qi, S., Cui, Y.J., Chen, R.P., Wang, H.L., Lamas-Lopez, F., Aimedieu, P., Dupla, J.C., Canou, J. and Saussine, G., 2020. Influence of grain size distribution of inclusions on the mechanical behaviours of track-bed materials. Géotechnique, 70(3), pp.238-247.

Sawangsuriya, A., Edil, T. B., & Benson, C. H. 2009. Effect of suction on resilient modulus of compacted fine-grained subgrade soils. Transportation research record, 2101(1), 82-87.

Su, Y., Cui, Y. J., Dupla, J. C., & Canou, J. 2020. Investigation of the effect of water content on the mechanical behavior of track-bed materials under various coarse grain contents. Construction and Building Materials, 263, 120206.

Su, Y., Cui, Y. J., Dupla, J. C., & Canou, J. 2021a. Effect of water content on resilient modulus and damping ratio of fine/coarse soil mixture with varying coarse grain contents. Transportation Geotechnics, 100452.

Su, Y., Cui, Y.J., Dupla, J.C., Canou, J., Qi, S., 2021b. Developing a sample preparation approach to study the mechanical behavior of unsaturated fine/coarse soil mixture. Geotechnical Testing Journal. https://doi.org/10.1520/GTJ20190450.

Trinh, V. N. 2011. Comportement hydromécanique des matériaux constitutifs de plateformes ferroviaires anciennes. PhD Thesis, Ecole Nationale des Ponts et Chaussées, Université Paris-Est.

Van Genuchten, M. T. 1980. A closed-form equation for predicting the hydraulic conductivity of unsaturated soils. Soil science society of America journal, 44(5), 892-898.

Vanapalli, S. K., Fredlund, D. G., & Pufahl, D. E. 1999. The influence of soil structure and stress history on the soil–water characteristics of a compacted till. Geotechnique, 49(2), 143-159.

Vallejo, L. E., & Mawby, R. 2000. Porosity influence on the shear strength of granular material–clay mixtures. Engineering Geology, 58(2), 125-136.

Werkmeister, S., Dawson, A. R., & Wellner, F. 2004. Pavement design model for unbound granular materials. Journal of Transportation Engineering, 130(5), 665-674.

Wang, H. L., Cui, Y. J., Lamas-Lopez, F., Dupla, J. C., Canou, J., Calon, N., & Chen, R. P. 2017. Effects of inclusion contents on resilient modulus and damping ratio of unsaturated track-bed materials. Canadian Geotechnical Journal, 54(12), 1672-1681.

Wang, H.L., Cui, Y.J., Lamas-Lopez, F., Calon, N., Saussine, G., Dupla, J.C., Canou, J., Aimedieu, P. and Chen, R.P., 2018a. Investigation on the mechanical behavior of track-bed materials at various contents of coarse grains. *Construction and Building Materials*, *164*, pp.228-237.

Wang, H.L., Cui, Y.J., Lamas-Lopez, F., Dupla, J.C., Canou, J., Calon, N., Saussine, G., Aimedieu, P. and Chen, R.P., 2018b. Permanent deformation of track-bed materials at various inclusion contents under large number of loading cycles. *Journal of Geotechnical and Geoenvironmental Engineering*, *144*(8), p.04018044.

Yang, S. R., Huang, W. H., & Tai, Y. T. 2005. Variation of resilient modulus with soil suction for compacted subgrade soils. Transportation Research Record, 1913(1), 99-106.

Yang, S. R., Kung, J. H., Huang, W. H., & Lin, H. D. 2006. Resilient modulus of unsaturated cohesive subgrade soils. Yantu Gongcheng Xuebao(Chinese Journal of Geotechnical Engineering), 28(2), 225-229.

Yang, S. R., Lin, H. D., Kung, J. H., & Huang, W. H. 2008. Suction-controlled laboratory test on resilient modulus of unsaturated compacted subgrade soils. Journal of Geotechnical and Geoenvironmental Engineering, 134(9), 1375-1384.

Zaman, M., & Khoury, N. 2007. Effect of soil suction and moisture on resilient modulus of subgrade soils in Oklahoma (No. ORA 125-6662).

CONCLUSIONS AND PERSPECTIVES

Conclusions

In the French conventional railway tracks, an interlayer was created by the interpenetration of ballast grains and subgrade fine soil. Considering the difficulty of obtaining intact interlayer soil from the field, the reconstituted soil mixture was adopted as a substitute in the laboratory. The water retention behavior of soil mixture was investigated under varying coarse grain contents and fine soil dry densities. Then, a sample preparation approach was developed, allowing the effect of microstructure of fine soil on the mechanical behavior of mixture to be minimized. Using this sample preparation approach, the mechanical behavior of mixture under monotonic and cyclic loadings was investigated. Factors such as water content, coarse grain content, stress state, loading cycles, etc, were considered. Finally, constitutive models were proposed for the permanent strain and resilient modulus of fine/coarse soil mixture, allowing the aforementioned factors to be accounted for.

Water retention behavior of soil mixture

The water retention behavior of soil mixture was investigated under varying coarse grain contents f_v and dry densities of fine soil $\rho_{d\text{-}f}$. The filter paper method was adopted to measure the matric suction ψ, and mercury intrusion porosimetry tests were performed for microstructure observation of fine soil.

Results showed that the drying soil-water retention curve (SWRC) of mixture was only dependent on $\rho_{d\text{-}f}$ and independent of f_v. When expressed in terms of gravimetric water content of fine soil versus matric suction, SWRC was significantly affected by $\rho_{d\text{-}f}$ at ψ < 715 kPa, while independent of $\rho_{d\text{-}f}$ at ψ > 715 kPa. This threshold matric suction corresponded to the delimiting pore diameter of microstructure, which separated micro-pores from macro-pores. This suggested that the SWRC in low ψ range (ψ < 715) was governed by macro-pores, while in high ψ range (ψ > 715) governed by micro-pores. When expressed in terms of the degree of saturation versus matric suction, the SWRC was affected by $\rho_{d\text{-}f}$ in the full ψ range, while independent of f_v. This help understand the observation of Duong et al. (2014) – the water retention capacity of mixture decreased with the increase of f_v: the dry density of mixture kept constant, resulted in a decrease of $\rho_{d\text{-}f}$ with increasing f_v and thus a decrease of water retention capacity.

Mechanical behavior of soil mixture under monotonic loading

The effect of microstructure of fine soil on the mechanical behavior of soil mixture was investigated. Two sample preparation approaches were compared: the first approach was to compact the mixture at optimum moisture content, then dry or wet to the target water content; the second approach was to directly compact the mixture at the target water content. Two coarse grain contents f_v (10% and 35%) and two target water contents (11% on the dry side of optimum and 16% on the wet side) were considered. The microstructure of fine soil was investigated using mercury intrusion porosimetry tests, and its effect on the overall mechanical behavior was examined by monotonic triaxial tests.

Results showed that in the case of the fine matrix macrostructure (f_v = 10%), a strong microstructure effect of fine soil on the overall mechanical behavior of mixture was identified. On the contrary, in the case of the coarse grain skeleton fabric (f_v = 35%), a very limited microstructure effect was observed. These findings can be helpful to minimize the effect of microstructure of fine soil on the overall mechanical behavior of mixture during sample preparation. In the case of fine matrix macrostructure, only the first sample preparation approach can be adopted for the mixture on the dry side of optimum, but both approaches can be adopted on the wet side. In the case of coarse grain skeleton, two approaches can be adopted, whatever the remolded water content.

The effect of water content on the mechanical behavior of mixture under varying coarse grain contents was investigated. Three water contents of fine soil w_f (17.6%, 10.6% and 7.0%) and five coarse grain contents f_v (0%, 10%, 20%, 35% and 45%) were considered. Results showed that variations of maximum deviator stress, elastic modulus, dilatancy angle and friction angle with f_v followed a bi-linear mode, defining a characteristic coarse grain content $f_{v\text{-}cha}$ for a given w_f: $f_{v\text{-}cha} \approx$ 25%, 29% and 33% for w_f = 17.6%, 10.6% and 7.0%, respectively. The $f_{v\text{-}cha}$ corresponded to a transition from a fine matrix macrostructure to a coarse grain skeleton fabric. The $f_{v\text{-}cha}$ increased with the decrease of w_f, which was explained by the shrinkage property of fine soil.

Mechanical behavior of soil mixture under cyclic loading

The effect of water content on permanent strain of soil mixture was investigated by cyclic triaxial tests. The dry density of fine soil $\rho_{d\text{-}f}$ kept constant for mixture with varying f_v. A multi-

stage loading procedure was applied, with a large number of loading cycles N = 90000 for each stage. Results showed that the decrease of water content led to a decrease of permanent strain owing to the increase of suction, and the increase of f_v led to a decrease of permanent strain owing to the reinforcement effect of coarse grains. These findings help understand the results of Duong et al. (2013): the dry density of mixture ρ_d kept constant, resulting in a decrease of $\rho_{d\text{-}f}$ with increasing f_v and thus a decrease of ψ. In this case, when the negative effect of decreasing ψ prevailed on the positive reinforcement effect of increasing f_v, the permanent strain increased with the increase of f_v.

The effect of water content on the resilient modulus and damping ratio of mixture with varying f_v was investigated by cyclic triaxial tests. A multi-stage loading procedure was applied, with a small number of loading cycles N = 100 for each stage. Results showed that increasing water content induced a decrease of resilient modulus owing to the decrease of suction, while an increase of damping ratio owing to the increase of soil viscosity. Through the variations of resilient modulus and damping ratio with f_v, the same $f_{v\text{-}cha}$ was identified at a given water content. It was found that the $f_{v\text{-}cha}$ increased with the decrease of water content, which was explained by the shrinkage property of fine soil. Comparisons of the values of $f_{v\text{-}cha}$ under cyclic and monotonic loadings showed that cyclic loading led to a slightly larger value than monotonic loading, evidencing the effect of cyclic loading on the soil fabric.

Constitutive models for soil mixture

A fatigue model of permanent strain of mixture was proposed, allowing the effects of coarse grain content f_v, deviator stress σ_d and loading cycles N to be accounted for. Results showed that the proposed model can well describe the permanent strain variations under the combined effects of aforementioned factors, in the case of plastic shakedown. This fatigue model was extended to the effect of ψ by incorporating soil-water retention curve. Different studies from literature were adopted to verify the proposed model. The model parameters were determined using experimental results under saturated condition, and then adopted to predict the results under unsaturated condition. A good agreement was obtained between the predictions and the measurements, showing the performance of the proposed model in describing the permanent strain variations under the combined effects of N, σ_d, f_v and ψ. Comparisons with existing models showed that the proposed model incorporating ψ provided better predictions of permanent strain than existing models considering w, for both the case of constant $\rho_{d\text{-}f}$ and the

case of constant ρ_d. This was explained by that the effect of $\rho_{d\text{-}f}$ on permanent strain was better reflected by ψ than by w.

A constitutive model incorporating soil-water retention curve was proposed for the resilient modulus of mixture, allowing the effects of ψ, σ_d and f_v to be accounted for. The model was validated using experimental results from literature. These experimental results revealed that a threshold matric suction existed. With increasing σ_d, resilient modulus decreased when ψ was smaller than the threshold value, but increased when ψ was larger than the threshold value. Comparisons with existing models showed that the proposed model can well describe this suction-dependent effect of σ_d on resilient modulus in the full ψ range, while existing model only gave satisfactory results in the low ψ range (smaller than the threshold value).

From a practical point of view, the experimental results obtained can be used in assessment of railway tracks mechanical degradation. Such mechanical degradation occurs when water content changes in the interlayer soil, because the mechanical behaviour of interlayer soil significantly varied with water content change. The models developed allowed the description of permanent deformation and resilient modulus, with changes in water content and coarse grain content. They constituted useful tools for evaluating the sensitivities of these mechanical behaviors with respect to changes in water content and coarse grain content. Once the sensitivity was identified, the corresponding measures can be applied to maintain or improve the mechanical performance of railway tracks. For instance, setting drainage systems in the railway tracks help alleviate the negative effect of water content on its mechanical behaviors.

Perspectives

This study allows better understanding the mechanical behavior of fine/coarse soil mixture and its corresponding constitutive models. In light of the findings, the following issues can be addressed in future studies:

The fatigue models for permanent strain of soil mixture could be implemented in a finite element code for numerically analysing the long-term behaviour of railway tracks under the combined effects of loading cycles, deviator stress, coarse grain content and matric suction.

The wetting-drying cycles can significantly affecte the microstructure of fine soil, and thus the mechanical behaviour of soil mixture. Thus, it is proposed to extend the study to the effect of wetting-drying cycles.

Basically, the effect of coarse grain content f_v on the hydraulic conductivity of mixture depended on two mechanisms: (i) the hydraulic conductivity decreases with the decrease of void ratio due to the increase of f_v; (ii) the hydraulic conductivity increases with the increase of the volume of macro-pores among coarse grains due to to the increase of f_v. This aspect deserves in-depth study because the track mechanical behaviour is fully coupled with the hydraulic behaviour through the variations of sucion or water content.

To better describe the mechanical behaviour in terms of shear strength and dilatancy, it is proposed to develop an elastoplastic model for the soil mixture under monotonic and cyclic loadings, allowing the consideration of the effects of suction and coarse grain content.

REFERENCES

AFNOR, 1995. NF P98-235-1—Test relating to pavements. Unbound granular materials. Part 1: Repeated Loading Triaxial Test.

AFNOR, 2004, NF EN 13286-7—Unbound and Hydraulically Bound Mixtures. Part 7: Cyclic Load Triaxial Test for Unbound Mixtures.

ASTM D5298-10. 2010. Standard test method for measurement of soil potential (suction) using filter paper. West Conshohocken, PA: ASTM International.

ASTM International. 2011. Standard Test Method for Consolidated Drained Triaxial Compression Test for Soils. ASTM D7181-11. West Conshohocken, PA: ASTM International approved July 1, 2011. https://doi.org/10.1520/D7181-11

ASTM International. 2012. Standard Test Methods for Laboratory Compaction Characteristics of Soil Using Standard Effort (12400 ft-lbf/ft3 (600 kN-m/m3)). ASTM D698-12. West Conshohocken, PA: ASTM International approved June 10, 2000. https://doi.org/10.1520/D0698-12

Ahmed, S., C. W. Lovell, & S. Diamond. 1974. Pore sizes and strength of compacted clay. Journal of the Geotechnical Engineering Division, ASCE, 100 (GT4): 407-425.

Alias La voie ferr´ee. 1984. Techniques de construction et d'entretien. 2nd Ed., Eyrolles.

ARA, Inc., ERES Consultants Division. 2004. Guide for mechanistic - empirical design of new and rehabilitated pavement structures. Final report, NCHRP Project 1-37A. Transportation Research Board, Washington, D.C.

Alonso, E. E., Pereira, J. M., Vaunat, J., & Olivella, S. 2010. A microstructurally based effective stress for unsaturated soils. Géotechnique, 60(12), 913-925.

Azam, A. M., Cameron, D. A., & Rahman, M. M. 2015. Permanent strain of unsaturated unbound granular materials from construction and demolition waste. Journal of Materials in Civil Engineering, 27(3), 04014125.

Ba, M., Nokkaew, K., Fall, M., & Tinjum, J. M. 2013. Effect of matric suction on resilient modulus of compacted aggregate base courses. Geotechnical and Geological Engineering, 31(5), 1497-1510.

Baetens, J. M., Verbist, K., Cornelis, W. M., Gabriels, D., and Soto, G. 2009. On the influence of coarse fragments on soil water retention. Water resources research, 45(7).

Barksdale, R. D. 1972. Laboratory evaluation of rutting in base course materials. In Presented at the Third International Conference on the Structural Design of Asphalt Pavements, Grosvenor House, Park Lane, London, England, Sept. 11-15, 1972. (Vol. 1, No. Proceeding).

Birle, E., D. Heyer and N. Vogt. 2008. Influence of the initial water content and dry density on the soil–water retention curve and the shrinkage behavior of a compacted clay. *Acta Geotechnica*, *3*(3), p.191. https://doi.org/10.1007/s11440-008-0059-y.

Bonaquist, R. F., & Witczak, M. W. 1997. A comprehensive constitutive model for granular materials in flexible pavement structures. In Eighth International Conference on Asphalt PavementsFederal Highway Administration (No. Volume I).

Brown, S. F., & Hyde, A. F. L. 1975. Significance of cyclic confining stress in repeated-load triaxial testing of granular material. Transportation research record, (537).

Caliendo, C. 2012. Local calibration and implementation of the mechanistic-empirical pavement design guide for flexible pavement design. Journal of Transportation Engineering, 138(3), 348-360.

Cary, C. E., & Zapata, C. E. 2011. Resilient modulus for unsaturated unbound materials. Road Materials and Pavement Design, 12(3), 615-638.

Chen, W. B., Feng, W. Q., Yin, J. H., Borana, L., & Chen, R. P. 2019. Characterization of permanent axial strain of granular materials subjected to cyclic loading based on shakedown theory. Construction and Building Materials, 198, 751-761.

Cui, Y. J., & Delage, P. 1996. Yeilding and plastic behaviour of an unsaturated compacted silt. Géotechnique, 46(2), 291-311.

Cui, Y. J., C. Loiseau, and P. Delage. 2002. Microstructure Changes of a Confined Swelling Soil Due to Suction Controlled Hydration. In Unsaturated Soils: Proceedings of the Third International Conference on Unsaturated Soils, UNSAT 2002, 10–13 March 2002, Recife, Brazil, Vol. 2, edited by J. F. T. Jucá, T. M. P. de Campos, and F. A. M. Marinho, 593–598. Lisse, the Netherlands: A. A. Balkema.

Cui, Y. J., Duong, T. V., Tang, A. M., Dupla, J. C., Calon, N., & Robinet, A. 2013. Investigation of the hydro-mechanical behaviour of fouled ballast. Journal of Zhejiang University Science A, 14(4), 244-255.

Cui, Y.J., F. Lamas-Lopez, V.N. Trinh, N. Calon, S.C. D'aguiar, J.C. Dupla, A.M. Tang, J. Canou, and A. Robinet. 2014. Investigation of interlayer soil behaviour by field monitoring. *Transportation Geotechnics*, *1*(3), pp.91-105. https://doi.org/10.1016/j.trgeo.2014.04.002.

Cui, Y. J. 2018. Mechanical behaviour of coarse grains/fines mixture under monotonic and cyclic loadings. Transportation Geotechnics, 17, 91-97.

de Frias Lopez, R., Silfwerbrand, J., Jelagin, D., & Birgisson, B. 2016. Force transmission and soil fabric of binary granular mixtures. Géotechnique, 66(7), 578-583.

Delage, P., Audiguier, M., Cui, Y.J. and Howat, M.D. 1996. Microstructure of a compacted silt. *Canadian Geotechnical Journal*, *33*(1), pp.150-158.

Delage, P., D. Marcial, Y.J. Cui, and X. Ruiz. 2006. Ageing effects in a compacted bentonite: a microstructure approach. *Géotechnique*, *56*(5), pp.291-304. https://doi.org/10.1680/geot.2006.56.5.291.

Diamond, S., 1970. Pore size distributions in clays. *Clays and clay minerals*, *18*(1), pp.7-23. https://doi.org/10.1346/CCMN.1970.0180103.

Doucet, F., & Doré, G. 2004. Module réversible et coefficient de poisson réversible des matériaux granulaires C-LTPP. In Proceedings of the 57th Canadian Geotechnical and 5th Joint IAH-CNC and CGS groundwater specialty conferences CD-Rom, Québec.

Duong, T. V., Tang, A. M., Cui, Y. J., Trinh, V. N., Dupla, J. C., Calon, N., ... & Robinet, A. 2013. Effects of fines and water contents on the mechanical behavior of interlayer soil in ancient railway sub-structure. Soils and foundations, 53(6), 868-878.

Duong, T. V., Cui, Y. J., Tang, A. M., Dupla, J. C., & Calon, N. 2014a. Effect of fine particles on the hydraulic behavior of interlayer soil in railway substructure. Canadian geotechnical journal, 51(7), 735-746.

Duong, T. V., Cui, Y. J., Tang, A. M., Dupla, J. C., Canou, J., Calon, N., & Robinet, A. 2014b. Investigating the mud pumping and interlayer creation phenomena in railway sub-structure. Engineering Geology, 171, 45-58.

Duong, T. V., Cui, Y. J., Tang, A. M., Dupla, J. C., Canou, J., Calon, N., & Robinet, A. 2016. Effects of water and fines contents on the resilient modulus of the interlayer soil of railway substructure. Acta Geotechnica, 11(1), 51-59.

Fiès, J. C., Louvigny, N. D. E., & Chanzy, A. 2002. The role of stones in soil water retention. European Journal of Soil Science, 53(1), 95-104.

Gabr, A. R., & Cameron, D. A. 2013. Permanent strain modeling of recycled concrete aggregate for unbound pavement construction. Journal of materials in civil engineering, 25(10), 1394-1402.

Gao, Y., Sun, D. 2017. Soil-water retention behavior of compacted soil with different densities over a wide suction range and its prediction. Computers and Geotechnics, 91(nov.):17-26.

Gargiulo, L., Mele, G., & Terribile, F. 2016. Effect of rock fragments on soil porosity: a laboratory experiment with two physically degraded soils. European Journal of Soil Science, 67(5), 597-604.

Gidel, G., Hornych, P., Breysse, D., & Denis, A. 2001. A new approach for investigating the permanent deformation behaviour of unbound granular material using the repeated loading triaxial apparatus. Bulletin des laboratoires des Ponts et Chaussées, (233).

Gupta, S., Ranaivoson, A., Edil, T., Benson, C., & Sawangsuriya, A. 2007. Pavement design using unsaturated soil technology.

Han, Z., & Vanapalli, S. K. 2015. Model for predicting resilient modulus of unsaturated subgrade soil using soil-water characteristic curve. Canadian Geotechnical Journal, 52(10), 1605-1619.

Han, Z., & Vanapalli, S. K. 2016a. Stiffness and shear strength of unsaturated soils in relation to soil-water characteristic curve. Géotechnique, 66(8), 627-647.

Han, Z., & Vanapalli, S. K. 2016b. State-of-the-Art: Prediction of resilient modulus of unsaturated subgrade soils. International Journal of Geomechanics, 16(4), 04015104.

Han, Z., & Vanapalli, S. K. 2016c. Relationship between resilient modulus and suction for compacted subgrade soils. Engineering geology, 211, 85-97.

Heath, A. C., Pestana, J. M., Harvey, J. T., & Bejerano, M. O. 2004. Normalizing behavior of unsaturated granular pavement materials. Journal of Geotechnical and Geoenvironmental Engineering, 130(9), 896-904.

Hornych, P. 1993. Étude des déformations permanentes sous chargements répétés de trois graves non traitées. Bulletin de liaison des Laboratoires des Ponts et Chaussées, (184).

Jibon, M., Mishra, D., & Kassem, E. 2020. Laboratory characterization of fine-grained soils for Pavement ME Design implementation in Idaho. Transportation Geotechnics, 25, 100395.

Jing, P. 2017. Experimental study and modelling of the elastoplastic behaviour of unbound granular materials under large number of cyclic loadings at various initial hydric states (Doctoral dissertation, Université de Strasbourg).

Jing, P., Nowamooz, H., & Chazallon, C. 2018. Permanent deformation behaviour of a granular material used in low-traffic pavements. Road Materials and Pavement Design, 19(2), 289-314.

Johnson, T. C. 1986. Frost action predictive techniques for roads and airfields: A comprehensive survey of research findings.

Khan, Z., El Naggar, M. H., & Cascante, G. 2011. Frequency dependent dynamic properties from resonant column and cyclic triaxial tests. Journal of the Franklin Institute, 348(7), 1363-1376.

Khasawneh, M. A., & Al-jamal, N. F. 2019. Modeling resilient modulus of fine-grained materials using different statistical techniques. Transportation Geotechnics, 21, 100263.

Khedr, S. 1985. Deformation characteristics of granular base course in flexible pavements. Transportation Research Record, 1043, 131-138.

Khoury, N., Brooks, R., & Khoury, C. 2009. Environmental influences on the engineering behavior of unsaturated undisturbed subgrade soils: Effect of soil suctions on resilient modulus. International Journal of Geotechnical Engineering, 3(2), 303-311.

Khoury, C. N., Khoury, N. N., & Miller, G. A. 2011. Effect of cyclic suction history (hydraulic hysteresis) on resilient modulus of unsaturated fine-grained soil. Transportation Research Record, 2232(1), 68-75.

Khoury, N., Brooks, R., Boeni, S. Y., & Yada, D. 2013. Variation of resilient modulus, strength, and modulus of elasticity of stabilized soils with postcompaction moisture contents. Journal of Materials in Civil Engineering, 25(2), 160-166.

Kim, H., Ganju, E., Tang, D., Prezzi, M., and Salgado, R. 2015. Matric suction measurements of compacted subgrade soils. Road Materials and Pavement Design, 16(2), 358-378.

Korkiala-Tanttu, L. 2005. A new material model for permanent deformations in pavements. In Proceedings of the international conferences on the bearing capacity of roads, railways and airfields.

Lamas-Lopez, F., d'Aguiar, S. C., Robinet, A., Cui, Y. J., Calon, N., Canou, J., ... & Tang, A. M. 2015. In-situ investigation of the behaviour of a French conventional railway platform. Proc., Transportation Research Board TRB 2015.

Lamas-Lopez, F. 2016. Field and laboratory investigation on the dynamic behavior of conventional railway track-bed materials in the context of traffic upgrade. PhD Thesis, Ecole Nationale des Ponts et Chaussées, Université Paris-Est.

Lashine, A. K., Brown, S. F., & Pell, P. S. 1971. Dynamic properties of soils. Department of Civil Engineering, University of Nottingham (England).

Lekarp, F., & Dawson, A. 1998. Modelling permanent deformation behaviour of unbound granular materials. Construction and building materials, 12(1), 9-18.

Leong, E.C., S. Tripathy, and H. Rahardjo. 2003. Total suction measurement of unsaturated soils with a device using the chilled-mirror dew-point technique. *Geotechnique*, *53*(2), pp.173-182. https://doi.org/10.1680/geot.2003.53.2.173.

Li, D., & Selig, E. T. 1996. Cumulative plastic deformation for fine-grained subgrade soils. Journal of geotechnical engineering, 122(12), 1006-1013.

Li, X. and L.M. Zhang. 2009. Characterization of dual-structure pore-size distribution of soil. *Canadian geotechnical journal*, *46*(2), pp.129-141. https://doi.org/10.1139/T08-110.

Liang, R. Y., Rabab'ah, S., & Khasawneh, M. 2008. Predicting moisture-dependent resilient modulus of cohesive soils using soil suction concept. Journal of Transportation Engineering, 134(1), 34-40.

Lin, S. Y., Lin, P. S., Luo, H. S., & Juang, C. H. 2000. Shear modulus and damping ratio characteristics of gravelly deposits. Canadian Geotechnical Journal, 37(3), 638-651.

Loach, S. C. 1987. Repeated loading of fine grained soils for pavement design (Doctoral dissertation, University of Nottingham).

Lu, N., Godt, J. W., & Wu, D. T. 2010. A closed-form equation for effective stress in unsaturated soil. Water Resources Research, 46(5).

Menq, F. Y. 2003. Dynamic properties of sandy and gravelly soils. Ph.D. thesis, The University of Texas at Austin.

Miao, L., S.L. Houston, Y. Cui, and J. Yuan. 2007. Relationship between soil structure and mechanical behavior for an expansive unsaturated clay. *Canadian Geotechnical Journal*, *44*(2), pp.126-137. https://doi.org/10.1139/t06-108.

Moossazadeh, J., & Witczak, M. W. 1981. Prediction of subgrade moduli for soil that exhibits nonlinear behavior. Transportation Research Record, (810).

Mousa, E., El-Badawy, S., & Azam, A. 2020. Evaluation of Reclaimed Asphalt Pavement as Base/Subbase Material in Egypt. Transportation Geotechnics, 100414.

Muñoz-Castelblanco, J. A., Pereira, J. M., Delage, P., and Cui, Y. J. 2010. Suction measurements on a natural unsaturated soil: A reappraisal of the filter paper method. In Unsaturated Soils-Proc. Fifth Int. Conf. on Unsaturated Soils (Vol. 1, pp. 707-712). CRC Press.

Ng, C. W. W., Zhou, C., Yuan, Q., & Xu, J. 2013. Resilient modulus of unsaturated subgrade soil: experimental and theoretical investigations. Canadian Geotechnical Journal, 50(2), 223-232.

Ng, C. W. W., Baghbanrezvan, S., Sadeghi, H., Zhou, C., & Jafarzadeh, F. 2017. Effect of specimen preparation techniques on dynamic properties of unsaturated fine-grained soil at high suctions. Canadian Geotechnical Journal, 54(9), 1310-1319.

Nowamooz, H., Chazallon, C., Arsenie, M. I., Hornych, P., & Masrouri, F. 2011. Unsaturated resilient behavior of a natural compacted sand. Computers and Geotechnics, 38(4), 491-503.

Oh, W. T., Vanapalli, S. K., & Puppala, A. J. 2009. Semi-empirical model for the prediction of modulus of elasticity for unsaturated soils. Canadian Geotechnical Journal, 46(8), 903-914.

Oh, J. H., Fernando, E. G., Holzschuher, C., & Horhota, D. 2012. Comparison of resilient modulus values for Florida flexible mechanistic-empirical pavement design. International Journal of Pavement Engineering, 13(5), 472-484.

Parreira, A. B., & Gonçalves, R. F. 2000. The influence of moisture content and soil suction on the resilient modulus of a lateritic subgrade soil. In ISRM International Symposium. International Society for Rock Mechanics and Rock Engineering.

Puppala, A. J., Chomtid, S., & Bhadriraju, V. 2005. Using repeated-load triaxial tests to evaluate plastic strain potentials in subgrade soils. Transportation research record, 1913(1), 86-98.

Qi, S., Cui, Y. J., Chen, R. P., Wang, H. L., Lamas-Lopez, F., Aimedieu, P., ... & Saussine, G. 2020a. Influence of grain size distribution of inclusions on the mechanical behaviours of track-bed materials. Géotechnique, 70(3), 238-247.

Qi, S., Cui, Y. J., Dupla, J. C., Chen, R. P., Wang, H. L., Su, Y., ... & Canou, J. 2020b. Investigation of the parallel gradation method based on the response of track-bed materials under cyclic loadings. Transportation Geotechnics, 100360.

Ravina, I., & Magier, J. 1984. Hydraulic conductivity and water retention of clay soils containing coarse fragments. Soil Science Society of America Journal, 48(4), 736-740.

Robinet. 2014. Investigating the mud pumping and interlayer creation phenomena in railway sub-structure. *Engineering geology*, *171*, pp.45-58. https://doi.org/10.1016/j.enggeo.2013.12.016.

Rollins, K. M., Evans, M. D., Diehl, N. B., & III, W. D. D. 1998. Shear modulus and damping relationships for gravels. Journal of Geotechnical and Geoenvironmental Engineering, 124(5), 396-405.

Romero, E., Gens, A., & Lloret, A. 1999. Water permeability, water retention and microstructure of unsaturated compacted Boom clay. Engineering Geology, 54(1-2), 117-127.

Romero, E., DELLA VECCHIA, G. A. B. R. I. E. L. E., and Jommi, C. 2011. An insight into the water retention properties of compacted clayey soils. Géotechnique, 61(4), 313-328.

Saba, S., Barnichon, J.D., Cui, Y.J., Tang, A.M., Delage, P. 2014. Microstructure and anisotropic swelling behaviour of compacted bentonite/sand mixture. Journal of Rock Mechanics and Geotechnical Engineering 6(2), 126-132.

Salager, S., Nuth, M., Ferrari, A., and Laloui, L. 2013. Investigation into water retention behaviour of deformable soils. Canadian Geotechnical Journal, 50(2), 200-208.

Sawangsuriya, A., Edil, T. B., & Benson, C. H. 2009. Effect of suction on resilient modulus of compacted fine-grained subgrade soils. Transportation research record, 2101(1), 82-87.

Seed, H. B., Chan, C. K., & Lee, C. E. 1962. Resilience characteristics of subgrade soils and their relation to fatigue failures in asphalt pavements. In International Conference on the Structural Design of Asphalt Pavements. SupplementUniversity of Michigan, Ann Arbor.

Seed, H. B., Wong, R. T., Idriss, I. M., & Tokimatsu, K. 1986. Moduli and damping factors for dynamic analyses of cohesionless soils. Journal of geotechnical engineering, 112(11), 1016-1032.

Seif El Dine, B., Dupla, J. C., Frank, R., Canou, J., & Kazan, Y. 2010. Mechanical characterization of matrix coarse-grained soils with a large-sized triaxial device. Canadian Geotechnical Journal, 47(4), 425-438.

Selig, E. T., & Waters, J. M. 1994. Track geotechnology and substructure management. Thomas Telford.

Shenton, M. J. 1974. Deformation of railway ballast under repeated loading triaxial tests. Soil Mechanics Section, British Railways Research Departement, Derby, England.

Simms, P. H., and Yanful, E. K. 2002. Predicting soil—Water characteristic curves of compacted plastic soils from measured pore-size distributions. Géotechnique, 52(4), 269-278.

Song, Y., & Ooi, P. S. 2010. Interpretation of shakedown limit from multistage permanent deformation tests. Transportation research record, 2167(1), 72-82.

Spomer, L. A. 1980. Prediction and Control of Porosity and Water Retention in Sand-Soil Mixtures for Drained Turf Sites 1. Agronomy Journal, 72(2), 361-362.

Stewart, H. E. 1982. The prediction of track performance under dynamic traffic loading. Ph.D. thesis, University of Massachusetts.

Su, Y., Cui, Y. J., Dupla, J. C., & Canou, J. 2020a. Investigation of the effect of water content on the mechanical behavior of track-bed materials under various coarse grain contents. Construction and Building Materials, 263, 120206.

Su, Y., Cui, Y. J., Dupla, J. C., Canou, J., & Qi, S. 2020b. A fatigue model for track-bed materials with consideration of the effect of coarse grain content. Transportation Geotechnics, 23, 100353.

Su, Y., Cui, Y. J., Dupla, J. C., Canou, J., & Qi, S. 2020c. Developing a Sample Preparation Approach to Study the Mechanical Behavior of Unsaturated Fine/Coarse Soil Mixture. Geotechnical Testing Journal, 44(4).

Su, Y., Cui, Y. J., Dupla, J. C., & Canou, J. 2021a. Effect of water content on resilient modulus and damping ratio of fine/coarse soil mixtures with varying coarse grain contents. Transportation Geotechnics, 26, 100452.

Su, Y., Cui, Y. J., Dupla, J. C., & Canou, J. 2021b. Effect of water content on permanent deformation of fine/coarse soil mixtures with varying coarse grain contents and subjected to multi-stage cyclic loading. Submitted to Acta Geotechnica.

Su, Y., Cui, Y. J., Dupla, J. C., & Canou, J. 2021c. Soil-water retention behaviour of fine/coarse soil mixture with varying coarse grain contents and fine soil dry densities. Canadian Geotechnical Journal.

Suiker, A.S.J., 2005. Static and cyclic triaxial testing of coarse-grained and fine-grained granular materials. Delft.

Sun, W. J., and Cui, Y. J. 2020. Determining the soil-water retention curve using mercury intrusion porosimetry test in consideration of soil volume change. Journal of Rock Mechanics and Geotechnical Engineering, 12(5), 1070-1079.

Sweere, G.T.H. 1990. Unbound Granular Bases for Roads. PhD Thesis. Delft, Netherlands.

Tao, M., Mohammad, L. N., Nazzal, M. D., Zhang, Z., & Wu, Z. 2010. Application of shakedown theory in characterizing traditional and recycled pavement base materials. Journal of Transportation Engineering, 136(3), 214-222.

Tennakoon, N., & Indraratna, B. 2014. Behaviour of clay-fouled ballast under cyclic loading. Géotechnique, 64(6), 502-506.

Thompson, M. R., & Robnett, Q. L. 1979. Resilient properties of subgrade soils. Transportation Engineering Journal of ASCE, 105(1), 71-89.

Trinh, V. N. 2011. Comportement hydromécanique des matériaux constitutifs de plateformes ferroviaires anciennes. PhD Thesis, Ecole Nationale des Ponts et Chaussées, Université Paris-Est.

Trinh, V. N., Tang, A. M., Cui, Y. J., Dupla, J. C., Canou, J., Calon, N., ... & Schoen, O. 2012. Mechanical characterisation of the fouled ballast in ancient railway track substructure by large-scale triaxial tests. Soils and foundations, 52(3), 511-523.

Vallejo, L. E., & Mawby, R. 2000. Porosity influence on the shear strength of granular material–clay mixtures. Engineering Geology, 58(2), 125-136.

Vallejo, L. E. 2001. Interpretation of the limits in shear strength in binary granular mixtures. Canadian Geotechnical Journal, 38(5), 1097-1104.

van Genuchten, M. T. 1980. A closed-form equation for predicting the hydraulic conductivity of unsaturated soils. Soil science society of America journal, 44(5), 892-898.

Vanapalli, S.K., D.G. Fredlund, D.E. Pufahl, and A.W. Clifton, 1996a. Model for the prediction of shear strength with respect to soil suction. *Canadian Geotechnical Journal*, *33*(3), pp.379-392. https://doi.org/10.1139/t96-060.

Vanapalli, S.K., D.G. Fredlund, D.E. Pufahl. 1996b. The relationship between the soil-water characteristic curve and the unsaturated shear strength of a compacted glacial till. *Geotechnical Testing Journal*, *19*(3), pp.259-268. https://doi.org/10.1520/GTJ10351J.

Vanapalli, S. K., Fredlund, D. G., & Pufahl, D. E. 1999. The influence of soil structure and stress history on the soil–water characteristics of a compacted till. Geotechnique, 49(2), 143-159.

Varandas, J.N., 2013. Long-Term Behaviour of Railway Transitions Under Dynamic Loading.

Vermeer, P. A. 1998. Non-associated Plasticity for Soils, Concrete and Rock. In Physics of Dry Granular Media, edited by H. J.Herrmann, J. P. Hovi, and S. Luding, 163–196. Dordrecht, the Netherlands: Springer. https://doi.org/10.1007/978-94-017-2653-5_10

Wan, Z., Bian, X., Li, S., Chen, Y., & Cui, Y. 2020. Remediation of mud pumping in ballastless high-speed railway using polyurethane chemical injection. Construction and Building Materials, 259, 120401.

Wang, H. L., Cui, Y. J., Lamas-Lopez, F., Dupla, J. C., Canou, J., Calon, N., ... and Chen, R. P. 2017. Effects of inclusion contents on resilient modulus and damping ratio of unsaturated track-bed materials. Canadian Geotechnical Journal, 54(12), 1672-1681.

Wang, H. L., Cui, Y. J., Lamas-Lopez, F., Calon, N., Saussine, G., Dupla, J. C., ... & Chen, R. P. 2018a. Investigation on the mechanical behavior of track-bed materials at various contents of coarse grains. Construction and Building Materials, 164, 228-237.

Wang, H.L., Cui, Y.J., Lamas-Lopez, F., Dupla, J.C., Canou, J., Calon, N., Saussine, G., Aimedieu, P. and Chen, R.P., 2018b. Permanent deformation of track-bed materials at various inclusion contents under large number of loading cycles. *Journal of Geotechnical and Geoenvironmental Engineering*, *144*(8), p.04018044.

Wang, H. L., Chen, R. P., Qi, S., Cheng, W., & Cui, Y. J. 2018c. Long-term performance of pile-supported ballastless track-bed at various water levels. Journal of Geotechnical and Geoenvironmental Engineering, 144(6), 04018035.

Wang, Q., Cui, Y. J., Tang, A. M., Xiang-Ling, L., and Wei-Min, Y. 2014. Time-and density-dependent microstructure features of compacted bentonite. Soils and Foundations, 54(4), 657-666.

Werkmeister, S., Dawson, A. R., & Wellner, F. 2001. Permanent deformation behavior of granular materials and the shakedown concept. Transportation Research Record, 1757(1), 75-81.

Werkmeister, S. 2004a. Permanent deformation behaviour of unbound granular materials in pavement constructions. Thesis dissertation, Fakultät Bauingenieurweser der Technischen Universität Dresden.

Werkmeister, S., Dawson, A. R., & Wellner, F. 2004b. Pavement design model for unbound granular materials. Journal of Transportation Engineering, 130(5), 665-674.

Yang, S. R., Huang, W. H., & Tai, Y. T. 2005. Variation of resilient modulus with soil suction for compacted subgrade soils. Transportation Research Record, 1913(1), 99-106.

Yang, S. R., Kung, J. H., Huang, W. H., & Lin, H. D. 2006. Resilient modulus of unsaturated cohesive subgrade soils. Yantu Gongcheng Xuebao(Chinese Journal of Geotechnical Engineering), 28(2), 225-229.

Yang, S. R., & Huang, W. H. 2007. Permanent deformation and critical stress of cohesive soil under repeated loading. Transportation research record, 2016(1), 23-30.

Yang, S. R., Lin, H. D., Kung, J. H., & Huang, W. H. 2008. Suction-controlled laboratory test on resilient modulus of unsaturated compacted subgrade soils. Journal of Geotechnical and Geoenvironmental Engineering, 134(9), 1375-1384.

Zaman, M., & Khoury, N. 2007. Effect of soil suction and moisture on resilient modulus of subgrade soils in Oklahoma (No. ORA 125-6662).

Zeng, Z., Cui, Y. J., Conil, N., and Talandier, J. 2020. Experimental study on the aeolotropic swelling behaviour of compacted bentonite/claystone mixture with axial/radial technological voids. Engineering Geology, 278, 105846.

Zhalehjoo, N., Tolooiyan, A., Mackay, R., & Bodin, D. 2018. The effect of instrumentation on the determination of the resilient modulus of unbound granular materials using advanced repeated load triaxial testing. Transportation Geotechnics, 14, 190-201.

Zhang, L.M. and Li, X., 2010. Microporosity structure of coarse granular soils. *Journal of Geotechnical and Geoenvironmental Engineering*, *136*(10), pp.1425-1436.

Zhang, T.W., Y.J. Cui, F. Lamas-Lopez, N. Calon, and S. Costa D'Aguiar. 2018a. Compacted soil behaviour through changes of density, suction, and stiffness of soils with remoulding water content. *Canadian Geotechnical Journal*, *55*(2), pp.182-190. https://doi.org/10.1139/cgj-2016-0628.

Zhang, F., Cui, Y. J., and Ye, W. M. 2018b. Distinguishing macro-and micro-pores for materials with different pore populations. Géotechnique Letters, 8(2), 102-110.

Zhao, H. F., Zhang, L. M., & Fredlund, D. G. 2013. Bimodal shear-strength behavior of unsaturated coarse-grained soils. Journal of geotechnical and geoenvironmental engineering, 139(12), 2070-2081.